Novel micromanipulation techniques in optical tweezers

A thesis submitted to the University of
St Andrews in application for the
degree of Doctor of Philosophy

by

Lynn Paterson

11th November 2003

Abstract

This thesis describes the use of novel techniques for the manipulation of microscopic particles in optical tweezers. Gaussian beams, Laguerre-Gaussian (LG) beams, Bessel beams and interference patterns have been used in this work to enhance optical trapping.

Stacking of multiple particles in a Gaussian beam is reported, as is the use of an LG beam for the enhanced axial trapping of silica spheres. Two dimensional arrays of glass rods and low refractive index particles have been created and manipulated, for the first time, in a pattern of linear fringes made by two interfering Gaussian beams. Interference patterns between a Gaussian beam and an LG beam were also generated, exhibiting spiral arms due to the helical wavefronts of the LG beam.

Two LG beams of opposite wavefront helicity were interfered to give a pattern of bright trapping spots arranged around a circumference which propagate without change in form. This allowed the assembly of three-dimensional structures by stacking particles in each of the trap sites of the pattern. These interference patterns, and therefore the three dimensional arrays of trapped particles, were rotated using the angular Doppler effect, a scheme which can induce a frequency shift of less than 1 Hertz to hundreds of Hertz.

The manipulation and microdissection of chromosomes was also performed using Gaussian beams, LG beams and 'non-diffracting' Bessel beams. Whole chromosomes or chromosomal fragments were enzymatically amplified in order to create fluorescent chromosome FISH probes for the detection of DNA inversions in chromatid break studies.

All these techniques have built upon and added to the optical toolkit, with applications in many fields of physics and biology.

Acknowledgements

First of all I would like to thank my supervisor Kishan Dholakia, for his endless enthusiasm and ideas and for the fantastic opportunity he provided me with just over three years ago. I would also like to thank my biology supervisor Peter Bryant for his guidance and ideas on all things concerning chromosomes. Many other people warrant thanks too, including group members past and present in both the physics department and at the Bute. Working in the altruistic atmosphere of Dholakia's dream team toward my PhD has been a great experience and I would like to thank every single member. Thanks especially go to Mike MacDonald who taught me a lot and was part of the team who went on the road with the optical rotator (knowledge is power!), Daniel (san) Rhodes who knows a lot of tricks, Vene (bye, now) and Tat for her taxi and her eagerness to get involved in biology collaborations, and also to David for proof reading this thesis. My thanks also extend to the other side of town to the E floor of the Bute. Michelle and Lindsay, Tina and Frank's group were always there to help or have a laugh with.

More personally I would like to thank Paul, my mum, dad and brother for their love, encouragement and support. This thesis is dedicated to you.

Abbreviations

ADE	Angular Doppler Effect
AOM	Acousto optical modulator
ATP	Adenosine triphosphate
CHO	Chinese Hamster Ovary
Cot	Concentration with time
DAPI	4',6-Diamidino-2-phenylindole
dATP	Deoxyadenosine triphosphate
dCTP	Deoxycytidine triphosphate
dGTP	Deoxyguanosine triphosphate
DNA	Deoxyribonucleic acid
dNTPs	Deoxynucleoside triphosphates
dUTP	Deoxyuridine 5'-triphosphate
DOP	Degenerate oligonucleotide primer
DOP-PCR	Degenerate oligonucleotide primed – polymerase chain reaction
dTTP	Deoxythymidine triphosphate
FACS	Fluorescent activated cell sorter
FFT	Fast Fourier Transform
FISH	Fluorescence *in situ* hybridisation
FITC	Fluorescein Isothiocyanate
IRS-PCR	Interdispersed Repetitive Sequence – Polymerase Chain Reaction
LA-PCR	Linker Adapter – Polymerase Chain Reaction
LCD	Liquid Crystal Device
LG	Laguerre-Gaussian
LPC	Laser Pressure Catapulting
NA	Numerical aperture
Nd: YAG	neodymium: yttrium-aluminium-garnet
Nd: YVO_4	neodymium: yttrium-vanadate
PCR	Polymerase Chain Reaction
PTK2	*Potorus tridactylous*- kidney cells
RNA	Ribonucleic acid
SLM	Spatial Light Modulator
TEM	Transverse Electromagnetic wave

Contents

1 Introduction 1
1.1 The origin of optical tweezers 1
1.2 Synopsis of thesis 3

2 Optical Micromanipulation 6
2.1 Introduction 6
2.2 Forces involved in optical tweezers 6
2.2.1 Mie and Rayleigh regimes 6
2.2.2 Interaction between light and Mie particles 7
2.2.3 Trapping Rayleigh particles 9
2.2.4 Trap efficiency 10
2.2.5 Trap stiffness 11
2.3 The Basic Optical Tweezers Set-Up 11
2.3.1 Requirements for optical tweezers 12
2.4 Novel laser beams in optical tweezers 16
2.4.1 Laguerre-Gaussian beams 16
2.4.2 'Non-diffracting' Bessel Beams 21
2.5 Optical Tweezers in biology 24
2.5.1 First biological applications of optical tweezers 24
2.5.2 Measuring motor protein forces 26
2.5.3 Measuring forces of DNA 29
2.5.4 Manipulation of chromosomes using optical tweezers 29
2.6 Summary 31

3 Stacking and alignment of particles in optical tweezers 39
3.1 Introduction 39
3.2 Linear arrays of spheres 39
3.3 Stacking spheres in a Gaussian beam 41
3.3.1 Stacking in standard tweezers 41
3.3.2 Stacking in inverted tweezers 43
3.4 Alignment of cylindrical particles 49
3.5 Discussion 51

4 Trapping in a Laguerre-Gaussian beam 53
4.1 Introduction 53
4.2 The use of Laguerre-Gaussian beams for trapping 54
4.2.1 Increasing axial trapping efficiency using LG beams 54
4.2.2 Axial and lateral trapping in inverted optical tweezers 56
4.3 Experiment for axial and lateral trapping efficiency measurements 57
4.4 Results of lateral and axial trapping using an $l = 1$ LG mode 58
4.4.1 Q values for lateral and axial trapping in an $l = 1$ LG beam 59
4.5 Discussion 60

5 Optical manipulation using interference fringes 63
5.1 Introduction 63
5.2 Interference fringes for trapping particles 64
5.3 Trapping arrays of high index spheres 66
5.4 Aligning and manipulating rod shaped particles 67
5.5 Low refractive index particles 71
5.5.1 Previous methods of trapping low-index spheres 73
5.5.2 Trapping Low-index particles 76
5.5.3 Trapping arrays of low-index and high index particles 79
5.6 Pattern propagation and manipulation 82
5.7 Discussion 83

6 Rotation of optically trapped particles in a revolving interference pattern 86
6.1 Introduction 86
6.2 Methods for the rotation of optically trapped particles 87
6.2.1 Asymmetric scattering force 87
6.2.2 Transfer of angular momentum 87
6.2.3 Rotation of shaped optical traps 90
6.3 Revolving interference patterns for the rotation of optically trapped particles 91
6.4 Spiral interference patterns 91
6.4.1 Experimental set-up 93
6.4.2 Achieving rotation of the spiral pattern 94
6.5 Analysis of interference patterns between a Gaussian beam and Laguerre-Gaussian beams 96
6.5.1 Gouy phase shifts and wavefront curvature 96
6.5.2 Aberrations in patterns due to misalignment 99
6.6 Results 100
6.7 Tilting glass slide to change optical path length 102
6.8 Discussion 109

7 Creating and rotating three dimensional structures using interference patterns between two Laguerre-Gaussian beams 114
7.1 Introduction 114
7.2 LG-LG interference patterns 114
7.2.1 Propagation of LG-LG interference patterns 117
7.2.2 Experimental set-up 118
7.3 The angular Doppler effect 119
7.3.1 Frequency shift arises due to conservation of energy and angular momentum 122
7.3.2 Optical beating between the two arms of the interferometer 123
7.4 Comparison of LG-LG patterns and LG-Gaussian beam patterns 125
7.5 Results 127
7.6 The alignment or rotation of trapped birefringent particles in a polarised, revolving interference pattern 131
7.6.1 Experimental setup 132

7.6.2 Spinning and orbiting of a birefringent particle in a circularly polarised, revolving light pattern 133
7.7 Discussion 136

8 Introduction to the generation of Fluorescent *in situ* Hybridisation (FISH) chromosome probes and their application to chromatid break studies 141
8.1 Introduction 141
8.2 Polymerase Chain Reaction 141
8.3 Previous methods of making whole chromosome or region specific FISH probes 143
8.3.1 DOP-PCR allows more general amplification 143
8.3.2 DOP-PCR of needle microdissected chromosomes 148
8.4 Laser microdissection 150
8.4.1 Commercially available laser capture microdissection tools 153
8.5 Mammalian DNA and chromosomes 155
8.5.1 Chromosome aberrations 156
8.5.2 Chromatid breaks 159
8.5.3 Chromatid breaks are formed by a single-event mechanism 162
8.6 The Signal Model 163
8.7 Methods to investigate the Signal Model 167
8.8 Summary 169

9 Investigation of various methods to isolate and amplify chromosomes and chromosomal fragments 174
9.1 Introduction 174
9.2 Cell lines and chromosomes 175
9.2.1 Cell lines used in experiments 175
9.2.2 Chromosome Preparation 176
9.3 Methods of isolation of whole chromosomes and chromosomal fragments ... 178
9.3.1 Isolating a single chromosome or chromosomal fragment using optical tweezers 178
9.3.2 Mechanical isolation of chromosomes (scraping off glass) 182
9.4 Generating a chromosome FISH probe from isolated chromosomal material 183
9.4.1 Degenerate Oligonucleotide Primed Polymerase Chain Reaction (DOP-PCR) 183
9.4.2 Fluorescent in situ hybridisation (FISH) techniques 186
9.4.3 Other methods used for the generation of chromosome FISH probes 189
9.5 Results of enzymatic amplification of isolated chromosomes and fragments to make chromosome FISH probes 191
9.5.1 DOP-PCR of a previously DOP-PCRed, needle microdissected, chromosome fragment 191
9.5.2 DOP-PCR of isolated chromosomes or fragments 192
9.5.3 DOP-PCR of optically levitated chromosomes 195
9.5.4 DOP-PCR following published protocols 199
9.5.5 A further DOP-PCR method 201
9.5.6 Linker Adaptor PCR 203

9.5.7 Genomiphi PCR 207
9.5.8 Whole cell paint probe hybridised to metaphases of another cell line ... 209
9.6 Attachment of streptavidin coated microspheres to chromosomes 210
9.6.1 Attaching microspheres to CHO chromosomes 211
9.6.2 Results of attaching microspheres to whole chromosomes 212
9.6.3 Optical micromanipulation of chromosomes with microspheres attached 215
9.7 Discussion 217

10 Final Conclusions 221
10.1 Summary of Thesis 221
10.2 Future work 223

Appendix A: DOP-PCR products protocols 225

A.1. Introduction 225
A.2. Review of DOP-PCR methods 225
A.2.1. Telenius et al. 1992a 225
A.2.2. Telenius et al. 1992b 226
A.2.3. Meltzer et al. 1992 227
A.2.4. Guan et al. 1993 228
A.2.5. Zimmer et al. 1997 229
A.2.6. Thalhammer et al. 1997 230
A.2.7. Masabada et al. 2003 231
A.2.7. Schermelleh et al. 1999 232

Appendix B: Materials 235

B.1. Reagents 235
B.1.1. Antibiotics 235
B.1.2. Chemicals 235
B.1.3. Enzymes 236
B.1.4. Other PCR/ ligation/ hybridisation reagents 236
B.1.5. Kits 237
B.2. Equipment 237
B.2.1. Centrifugation 237
B.2.2. Electrophoresis 237
B.2.3. Glassware 238
B.2.4. Microscopy 238
B.2.5. Plastic ware 238
B.2.6. Others 238
B.3. Formulation of frequently used solutions 239
B.3.1. Solutions for chromosome preparation 239
B.3.2. Collection buffers for PCR 239
B.3.3. Solutions for agarose gel 240
B.3.4. Solutions for FISH 240

B. 3.5. Solutions for washing slides after FISH 240
B.3.6. Blocking buffers used prior to labelling with avadin-Cy3 241

Appendix C: Publications and publicity 242

C.1. Publications 242
C.1.1. Publications (refereed) 242
C.1.2. Publications (not refereed) 243
C.2. Conference papers 243
C.2.1. Conference papers (refereed) 243
C.2.2. Conference papers (not refereed) 244
C.3. Publicity 245

List of Figures

2. Optical Micromanipulation

2.1: The Rayleigh and Mie regimes
2.2: Trapping forces
2.3: The basic setup for a single beam optical trap
2.4: The phasefronts of two modes, $l = 0$, with plane wavefronts, and $l = 3$ with helical wavefronts
2.5: Beam profiles of LG beams with various l and p indices
2.6: Formation of an $l = 1$ LG beam by passing a Gaussian beam through a computer generated hologram
2.7: Illuminating an axicon with a Gaussian beam produces a close approximation to a Bessel beam
2.8: The beam profile (left) and the radial intensity profile (right) of a zeroth-order Bessel beam
2.9: Measuring the force of kinesin (or dynein) as it moves along microtubules
2.10: Measuring the force of myosin as it moves along actin filaments

3. Stacking and alignment of particles in optical tweezers

3.1: Stacking in normal tweezers (beam coming into sample from above)
3.2: Experimental set-up with laser directed into sample cell from above
3.3: Maximum horizontal velocity of stacks of 1, 2 and 3 spheres trapped in a standard optical tweezers configuration
3.4: Stacking in inverted tweezers (beam coming into sample from below)
3.5: Experimental set-up with laser directed into sample cell from below
3.6: The assembly of a stack of six 5 μm silica spheres in an inverted geometry
3.7: Tilting of a stack of six 5 μm spheres as the laser beam is inclined, viewed from below in an inverted geometry
3.8: Maximum horizontal velocity of a stack of three 5 μm diameter silica spheres for increasing laser powers
3.9: Maximum horizontal velocity for stacks with various numbers of 5 μm diameter silica spheres at three different laser powers
3.10: Rod alignment and translation in an inverted optical trap
3.11: A 140 μm long rod falling from alignment

4. Trapping in a Laguerre-Gaussian beam

4.1: Lateral trapping results showing the power of the trap at the sample against the velocity reached before the particle fell out of the trap
4.2: Axial trapping results showing the power of the laser trap at the sample against the velocity reached before the particle fell out of the trap
Table 4.1 Q values for axial and lateral trapping with an $l = 1$ LG beam calculated using the power measured and the maximum speed of the trapped particles

Table 4.2 Ratios of trapping efficiency values calculated by various groups using 2 μm diameter spheres, with our calculated value for Q_{axial} taken as 1

5. Optical manipulation using interference fringes

5.1: Experimental set-up for interferometric optical tweezers
5.2: The two beams are directed separately through the x20 objective and for the fringe pattern at the focus inside the sample cell
5.3: One micron high-index silica spheres aligned in the bright fringes of an interference pattern between two Gaussian beams
5.4: Alignment of a 5 μm long glass rod (a-b), and tweezing in the x-direction (c-d)
5.5: Manipulating a 5 μm long glass rod by moving the whole beam spot and sweeping the fringes simultaneously
5.6: Alignment and manipulation in the x-y plane of a 20 μm long glass rod
5.7: Simultaneous alignment and manipulation of three 5 μm long rods
5.8: Ray optics for high- and low- index particles
5.9: Illustration of a low- and high-index particle simultaneously trapped in a Laguerre-Gaussian beam
5.10: Manipulation of a low-index sphere
5.11: Fringe spacing determines if the low index particle is repelled, trapped in two dimensions or trapped in one dimension
5.12: Manipulation of two low-index spheres in the dark fringes of an interference pattern between two Gaussian beams
5.13: Low- and high-index sphere array
5.14: Computer simulations of the pattern created by two interfering Gaussian beams and by making a reduced image of a Ronchi ruling

6. Rotation of optically trapped particles in a revolving interference pattern

6.1: Experimental interference patterns between: A. A Gaussian beam and an $l = 2$ Laguerre-Gaussian beam. B. A Gaussian beam and an $l = 3$ Laguerre-Gaussian beam
6.2: Phase fronts of an $l = 3$, $p = 0$ Laguerre-Gaussian beam and a plane wave and the intensity of the resulting interference pattern
6.3: Experimental set-up to use the interference pattern as an optical trap
6.4: A length of rope with three intertwined cords analogous to the phase fronts of an $l = 3$ beam
6.5: Interference pattern rotates slightly as it propagates due to the differences between the Gouy-phase shifts of the LG and Gaussian beam
6.6: Simulations of higher order interference patterns using a Gaussian and various LG beams
6.7: Simulations of misalignment between the LG and Gaussian beam
6.8: Rotation of three 1 μm diameter silica spheres in an $l = 3$ interference pattern
6.9: Rotation of three 5 μm diameter spheres in an $l = 3$ interference pattern

6.10: Rotation of micro objects in an $l = 2$ interference pattern
6.11: Simulation of the rotation of the interference pattern at a focus as the path length of one of the beams is changed
6.12: The parameters used for calculating the effect of tilting a glass plate in a laser beam
6.13: Number of rotations N of the spiral patterns (given in the legend) and displacement d of the beam as the glass plate is tilted
6.14: The number of rotations N of the spiral patterns and displacement d of the beam as the plate thickness is varied
6.15: The diamonds and squares show the number of rotations measured in an LG $l = 2$ interference pattern as a glass microscope slide and a glass coverslip are tilted from normal
6.16: The displacement d of an $l = 3$ interference pattern for various glass plate thicknesses t as the angle of the plate is tilted from normal
6.17: The displacement d for various values of N (given in legend) as the plate thickness t is varied for an $l = 3$ interference pattern

7. Creating and rotating three dimensional structures using interference patterns between two Laguerre-Gaussian beams

7.1: Patterns generated by interference between two Laguerre-Gaussian of opposite helicity
7.2: Propagation of the laser pattern
7.3: The experimental set up for creating LG-LG interference patterns
7.4: Adapted Mach-Zender interferometer for creating two co-propagating laser beams with a frequency shift between them of $2\Omega_{rot}$
7.5: The beat signal produced by interfering two Gaussian beams separated in frequency using the angular Doppler effect with fit
7.6: Fast Fourier transform of the beat signal shown in figure 7.5
7.7: Interference patterns which we have created and used to manipulate various particles
7.8: A group of four 1 μm diameter silica spheres that is tweezed and lifted vertically whilst simultaneously being rotated through the sample cell
7.9: The rotation of a cubic structure consisting of eight 1 μm diameter spheres
7.10: The same cubic structure is seen to collapse, revealing the eight constituent spheres as the trapping laser beam is blocked
7.11: The trapping of eight silica spheres in a four spot interference pattern (two spots stacked in each spot) to create a cubic structure
7.12: Structures that have been created and future possibilities
7.13: Microfabricated cogs created by Steve Neale at the University of St Andrews
7.14: Experimental set-up to use the polarisation of light and a rotating interference pattern together to spin birefringent particles
7.15: Fragment of mercury (I) chloride spins around its own axis in a clockwise direction (shown by changing direction of arrow) and orbits in the x-y plane of the sample in a clockwise direction (shown by circle) both at the same time
7.16: Rotating a birefringent particle in a linearly polarised light beam

7.17: Top panel from left to right then bottom panel from left to right shows four fragments of calcite (marked a, b, c and d) aligned in the bright spots of a $l = 2$, $l = -2$ interference pattern

8. Introduction to the generation of Fluorescent *in situ* Hybridisation (FISH) chromosome probes and their application to chromatid break studies

8.1: The polymerase chain reaction
8.2: Degenerate oligonucleotide primer and DOP-PCR
8.3: Levels of chromatin packaging in a mammalian metaphase chromosome
8.4: Chromosome type aberrations
8.5: Chromatid type aberrations
8.6: The breakage first model according to Bender et al. (1974)
8.7: The Revell exchange model (Revell, 1959)
8.8: Harlequin stained Chinese hamster chromosomes (using 5-bromo-2'-deoxyuridine [BrdU]).
8.9: The Signal Model (Bryant, 1998a)
8.10: Possible mechanisms for a colour-switch rearrangement
8.11: Non colour-switch break rearrangements (due to intra-chromatid breaks) can lead to excision of a chromatin ring (1) or genomic inversions (2, 3)
8.12: Method for creating narrow band chromosome FISH probes

9. Investigation of various methods to isolate and amplify chromosomes and chromosomal fragments

9.1: Overview of the ecdysone response system used to induce expression of I-SceI in mammalian cells
9.2: Tweezing of a CHO chromosome
9.3: Comparison of a DAPI stained chromosome under white light and illuminated by a 410 nm violet diode
9.4: Schematic of chromosome microdissection and manipulation system
9.5: Attachment of chromosome to coverslip using optical tweezers
9.6: Chromosome levitation
9.7: Chromosomes are scraped off a cover glass and resuspended in a small volume of water then transferred to PCR tube
9.8: Red region is paint probe generated by DOP-PCR of a microdissected chromosome
9.9: FISH slides of A. positive control, B. probe 1, C. probe 2, D. probe 3, E. probe 4, F. probe 5, G. negative control
9.10: In each FISH performed, the same region of chromosome was labelled in A. CHO metaphases and B. Muntjac metaphases
9.11: Typical DOP-PCR results. A. positive control, B. probe 1, C. probe 2, D. secondary negative control, E. primary negative control
9.12: Overview of PCR using linker adaptors
9.13: CHO metaphases labelled with a whole cell Muntjac paint probe
9.14: CHO whole cell paint probe hybridised to Muntjac chromosomes

9.15: A. Five 5 μm diameter spheres attached to a DAPI stained chromosome by incubating streptavadin coated microspheres to biotinylated chromosomes, B. A single 5 μm diameter sphere attached to a chromosome by hybridising probe-sphere conjugates with chromosomes
9.16: A. Many 1 μm spheres attached to chromosomes, B. Few 1 μm spheres attached to chromosomes, using the two methods described in the text
9.17: Many 1 μm streptavadin coated spheres attached to chromosomes after incubating them in excess with biotinylated chromosomes
9.18: Comparison of Gaussian and Bessel beam guiding
9.19: Guiding velocities of a 3 μm sphere, a 5 μm sphere and a chromosome in a Bessel beam
9.20: Chromosomal guiding velocities along a Bessel beam

1 Introduction

1.1 The origin of optical tweezers

Optical tweezers is a term used to describe the manipulation of microscopic objects using the force of focused laser light. A single laser beam focused to a diffraction limited spot can hold a transparent micro object in the region of highest light intensity due to the three dimensional intensity gradient of the light. The optical tweezers system has become a major tool in biological research over the last twenty years, as particles ranging from intracellular structures, such as chromosomes or motor proteins, to whole cells can be readily manipulated.

Laser light was discovered to have the ability to move particles in 1970 by Arthur Ashkin (Ashkin, 1970), who was based at Bell Telephone Laboratories in New Jersey. Microscopic silica spheres were accelerated along a horizontally directed TEM_{00} mode laser beam from an argon ion laser by the radiation pressure force of the beam. The particles were drawn into the beam axis by the transverse gradient force of the light and accelerated in the direction of beam propagation due to the scattering force of the light. It was also observed that bubbles (of lower refractive index than the surrounding medium) were repelled away from the centre of the beam as they were simultaneously accelerated in the direction of laser light by the radiation pressure force. Two opposing TEM_{00} beams were shown to trap spheres of high refractive index. Particles were drawn into the beam axis by the gradient force and accelerated to a stable equilibrium point between the foci of the two counter-propagating beams, where the particle was held in position by the opposing radiation pressure forces. The idea of using radiation pressure from laser beams was expanded to include the manipulation of atoms and molecules. It was hypothesised and subsequently shown that absorption and then spontaneous emission of resonant radiation striking the atom could provide a driving force, or pressure, in the direction of light propagation (Ashkin, 1987).

In 1971 the optical levitation trap for microscopic particles was used for the first time (Ashkin and Dziedzic, 1971). A focused TEM_{00} mode laser, directed upwards

was shown to support spheres against the downwards pull of gravity using radiation pressure force and to simultaneously hold the particle in the beam centre using the transverse gradient force. Such a levitation trap was used in 1985 to introduce particles into an alternating light beam trap (Ashkin and Dziedzic, 1985). Particles were trapped between the foci of the two counter-propagating beams without requiring any gradient force.

In 1986 a seminal paper entitled 'Observation of a single-beam gradient force optical trap for dielectric particles' (Ashkin et al., 1986) was published. Up until this point, optical traps used radiation pressure force from a laser beam to stably hold particles in the axial direction, either against a counter-propagating beam or against gravity, and the transverse gradient force held the particle in the centre of the Gaussian beam. In 1986, a single focused laser beam was used to stably trap, in three dimensions, particles ranging in diameter from 25 nm to 10 μm in diameter in water. This trapping was due to both the transverse and the axial gradient force exerted by the focused laser beam – a three dimensional intensity gradient. In the levitation traps the axial stability was dependent on the balance of the scattering force and gravity, but in the single beam gradient force traps the axial gradient force is so large that it dominates the axial stability. This type of single-beam gradient force trap, commonly known as optical tweezers, is now widely used, with applications ranging from investigating the angular momentum of light to measuring intracellular forces.

An optical tweezers system is a particularly useful tool for biological studies as the trapping process can be completely non-invasive and sterility of samples can be maintained. In addition, the trapping laser and associated optics can be readily incorporated into existing commercially available microscope systems.

The optical toolkit has evolved over the past two decades to include optical tweezers, optical scissors and optical spanners. During the course of my PhD the optical toolkit has been extended to include newly developed techniques for the enhanced optical manipulation of particles, the microdissection of chromosomes and the rotation of microscopic structures of silica spheres. These improvements of the optical toolkit have been realised primarily through the use of novel laser modes in optical trapping systems.

1.2 Synopsis of thesis

After this brief introduction, chapter two goes on to describe how optical tweezers work, the forces involved in micromanipulation and how to build an optical tweezers system. I will also introduce novel laser beams such as the Laguerre-Gaussian family of annular shaped beams and 'non-diffracting' Bessel beams which are used throughout my work and are discussed in other chapters. Following that, chapter three details the use of a Gaussian beam to create stacks of multiple particles and to align cylindrically shaped particles along the beam propagation axis. Chapter four is concerned with the use of a Laguerre-Gaussian beam for enhancing the axial trapping efficiency of silica spheres. In chapter five an experiment is described which uses parallel interference fringes created by interfering two Gaussian beams to align rod shaped particles and also to manipulate particles of lower-refractive index than the surrounding medium. This work was a precursor to that described in the next two chapters, which also describe the use of interference patterns for micromanipulation. Chapter six describes the creation and use of an interference pattern between a Laguerre-Gaussian beam and a Gaussian beam, and in chapter seven, the creation of an interference pattern between a Laguerre-Gaussian beam with its mirror image is discussed. These patterns can be used to trap particles but, importantly, in these two chapters, the trapped particles can be set into controlled rotation. Chapter seven is an extension of chapter six and uses an improved interference pattern where z-trapping and axial stacking of particles is possible. Chapter seven also introduces a technique developed during the course of my PhD called the angular Doppler effect. This technique is used to introduce a frequency shift between two interfering laser beams, sending the pattern into controlled, continuous rotation.

Chapter eight gives an introduction to the biological side of my work. Chromatid breaks that are induced by lesions in DNA are described as are the models which have been hypothesised to explain how these breaks come about, in particular the Signal model. The Signal model predicts that inversions, deletions and duplications

should occur in the region surrounding the break. We wish to detect such inversions by creating and using small fluorescent chromosome probes (FISH probes) and the method for generating such chromosome paint probes is discussed. Polymerase chain reaction (PCR), more specifically the degenerate oligonucleotide primed - polymerase chain reaction (DOP-PCR) is described. This is a method which uses a heat resistant enzyme to replicate DNA by cycling through certain temperatures which permit the denaturation of template DNA, the annealing of primers (short sequences of DNA which recognise the template DNA) and finally the extension of primers. This is repeated numerous times and results in many copies of the template DNA being synthesised which are used to make a fluorescent probe. Chapter nine describes experimental work using various optical techniques to isolate chromosomal material. The DNA is amplified by DOP-PCR and fluorescent probes are generated. Optical tweezers and scissors are used to isolate a whole chromosome or chromosomal fragments and in addition, novel laser modes are used in this work to enhance the quality of chromosome manipulation and microdissection. The thesis concludes with a summary of the work I have done and it's potential impact and a brief outline of potential investigations which may evolve from this. The appendices give further details of A, previous methods for amplification of chromosomal material, B, details of the materials I used for chromosome amplification and the generation of paint probes and C gives a list of publications, conference papers and publicity gained during my PhD.

In summary this thesis describes work which has led to enhancement of the optical toolkit by utilising novel laser modes for cutting, tweezing and rotating microscopic particles.

References

Ashkin A: **Acceleration and trapping of particles by radiation pressure.** *Physical Review Letters* 1970; **24**:156-159.

Ashkin A, Dziedzic , J. M.: **Optical levitation by radiation pressure.** *Applied physics letters* 1971; **19**:283-285.

Ashkin A, Dziedzic JM: **Observation of radiation-pressure trapping of particles by alternating light beams.** *Physical Review Letters* 1985; **54**:1245-1248.

Ashkin A, Dziedzic JM, Bjorkholm JE, Chu S: **Observation of a Single-Beam Gradient Force Optical Trap for Dielectric Particles.** *Optics Letters* 1986; **11**:288-290.

Ashkin A: **Laser Manipulation of Atoms.** *Nature* 1987; **330**:608-609.

2 Optical Micromanipulation

2.1 Introduction

A focused laser beam can stably hold a transparent microscopic object near the focus of the beam due to the three dimensional intensity gradient in that region. This chapter will firstly describe how particles are trapped in the region of highest light intensity. The efficiency and the stiffness of optical traps can be calculated and this is described, as are the specifications for constructing an optical tweezers system and the equipment required. Novel laser beams, which are used throughout my PhD and appear in later chapters, are introduced, as are the methods with which they can be generated. Finally, previous studies using optical tweezers on biological molecules and single cells are described.

2.2 Forces involved in optical tweezers

2.2.1 Mie and Rayleigh regimes

Understanding of the forces involved in optical tweezers can be elucidated by taking two approaches, one based on ray optics for particles in the Mie regime (where the diameter is large compared to wavelength, λ) and the other based on the electric field associated with the light for Rayleigh particles (diameter smaller than λ). Particles in the Rayleigh and Mie regimes compared to λ can be seen in figure 2.1.

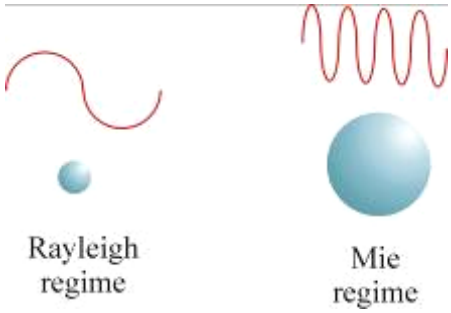

Figure 2.1: The Rayleigh and Mie regimes. In the Rayleigh regime the particle is much smaller than the wavelength of light and in the Mie regime the particle is larger than the wavelength of light.

2.2.2 Interaction between light and Mie particles

A ray optics approach is used to calculate forces acting on a particle with a diameter larger than the wavelength of laser light (the Mie regime). The effect of a laser beam on a transparent sphere can be modelled using a bundle of rays, in a similar manner to ray-tracing packages that are used for lens design, with each ray weighted according to its intensity. A photon of wavelength λ has a momentum $p = h/\lambda$ (or $\hbar k$) where h is Plank's constant, $\hbar$ is $h/2\pi$, and k is wave number. If an object causes light to change direction, for instance on reflection or refraction, the change in momentum of the light will exert an equal but opposite change of momentum on the object. This force exerted on an object is not large enough to move macroscopic objects however, the forces involved in the transfer of momentum from focused laser light to microscopic objects are of the order of picoNewtons and can move micron sized particles.

Within the Mie regime, if a transparent microscopic particle is situated within a gradient of light, the refraction of rays of differing intensity (due to the gradient) through the particle results in a change in total momentum of the exiting light beam, and hence a corresponding reaction force on the particle, which draws the particle into the region of highest light intensity of the beam (Figure 2.2). An equilibrium

position is reached and the particle is held in the centre of the beam as the rays of light passing through and exiting the particle are balanced with no overall change in momentum of the beam. This trapping force is due to the transverse gradient force which is a result of the Gaussian intensity distribution of the laser mode, however an axial gradient is also required in order to lift the particle and manipulate it in three dimensions.

Axial trapping in the z (vertical) direction, which results in a three dimensional trap or so-called optical tweezers, is a result of the axial gradient force which is created by the tight focusing of the laser beam. Off-axis rays come in at an angle towards the particle and gain momentum in the direction of beam propagation. This change in momentum leads to a force which pushes the sphere upwards against the direction of beam propagation towards the focal region of the beam resulting in a trapping force in the z-direction, and thus a three dimensional, optical trap. The equilibrium position is reached when the scattering force and gravity (which both act to push the sphere downwards) is balanced by the axial gradient force (which pushes the sphere upwards).

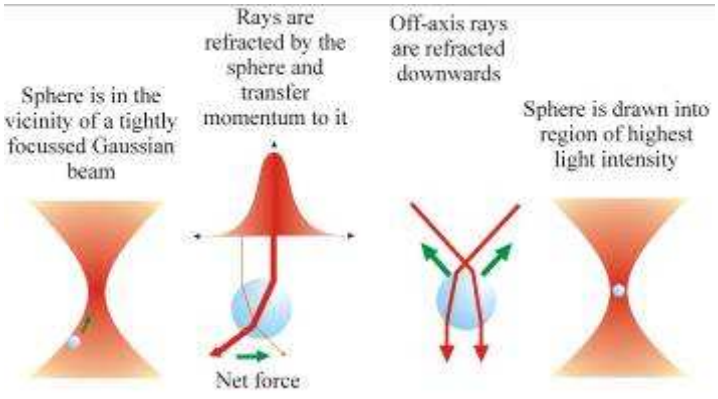

Figure 2.2: Trapping forces. The rays of a Gaussian beam are refracted as they pass through a particle of higher refractive index than the surrounding medium. The intensity gradient of the beam leads to the particle being drawn into the region of highest light intensity. Off axis rays contribute to axial trapping by being refracted in the direction of beam propagation. A force is exerted on the particle of equal but opposite size to the change of momentum of the light.

On axis rays are detrimental to the axial trapping ability of the tweezers when the laser beam is directed into the sample from above. The reflected (or backscattered) component of the on-axis rays gives rise to radiation pressure and exerts a force on the particle in the direction of beam propagation. This results in the particle being pushed downwards, away from the beam focus.

This scattering force is reduced when a certain type of beam called a Laguerre-Gaussian (or LG) beam is used. An LG beam, also known as an optical vortex has a dark centre which results in reduced radiation pressure working directly against the z-trapping, and as a result, has been shown to improve z-trapping (Simpson et al., 1998). Advanced trapping geometries such as these LG beams have led to many more exciting experiments, as beams can be tailored for trapping and manipulation, greatly extending the capabilities of optical tweezers, and will be described later in this chapter and in further chapters.

2.2.3 Trapping Rayleigh particles

For particles in the Rayleigh regime the ray optics approach is not sufficient to calculate forces as only a fraction of the wave has an effect on the particle. It is better to consider the force in terms of the electric field in the region of the trapped particle. When a polarisable particle is placed in an electric field it will develop an electric dipole moment in response to the light's electric field and is drawn up intensity gradients in the electric field towards the focus (if the polarisability is +ve, i.e. relative refractive index > 1). The energy of the system will be at a minimum when the particle moves to wherever the field is highest – which is at the focus.

Optically trapped particles discussed in this work (chromosomes, dielectric silica spheres etc.) lie primarily in the Mie regime, although some DNA particles and 1 μm diameter spheres have sizes comparable to the wavelength of the IR trapping light and are intermediate between the Mie and Rayleigh regime.

2.2.4 Trap efficiency

The force on a spherical particle of radius *r* can be calculated using the viscous drag exerted by moving the particle at a velocity *v* through a fluid of viscosity η(Stoke's law) when the particle is more than a few diameters away from the sample cell walls and is given by:

$$F_{stokes} = 6\pi\eta rv \qquad (2.1).$$

This is the maximum force that the optical trap can exert at the specified laser power and will typically be of the order of picoNewtons (Malagnino et al., 2002). The critical velocity of the trapped particle scales linearly with the laser power in the optical trap (as shown in eq. 2.2).

The trapping efficiency of any optical tweezers configuration is usually described in terms of a dimensionless parameter *Q*, the fraction of momentum transferred to the trapping force from the trapping laser beam, which is related to the force on the sphere, F_{stokes}, the power of the laser, *P*, and the refractive index of the surrounding medium, *n*, through the equation

$$F_{stokes} = \frac{nQP}{c} \qquad (2.2).$$

Possible values of *Q* range between 0 and 1. A *Q* value of 1 corresponds to all of the light beam's momentum being transferred to the particle. Optical tweezers configurations can be assessed experimentally to determine the *Q* values for trap efficiency in the lateral and axial directions. For optical forces acting on small dielectric particles *Q* values tend to be in the range 0.03 to 0.1 (Molloy and Padgett, 2002).

Within conventional optical tweezers Q_{axial} is usually an order of magnitude smaller than $Q_{lateral}$ (Simpson et al., 1996).

2.2.5 Trap stiffness

The displacement of the trapped object from the centre of the trap, under an applied viscous fluid force can be monitored using a position sensitive detector. This determines the spring (elastic) constant, in other words the stiffness of the optical trap. Optical tweezers stiffness can also be calculated from analysis of the thermal motion of the trapped object (Ishijima et al., 1991, Malagino et al., 2002). Trap stiffness tends to be in the range 0.001 to 1 pN nm^{-1} (Molloy and Padgett, 2002) depending on the application. Optical tweezers can also be placed under feedback control so that any particle movement out of equilibrium position can be immediately corrected by repositioning of the trap itself, so that the particle remains stationary within the trap. It is necessary to measure optical trap stiffness before investigating very low forces such as those in biological processes which are discussed later in this chapter. Biologists are mainly concerned with measuring trap stiffness so that molecular forces can be measured, whereas physicists are more interested in the *Q* value of an optical trap (efficiency), which can be calculated both theoretically and experimentally. In chapter four we calculate the *Q* value of an optical trap experimentally by measuring the maximum velocity that a trapped particle can be dragged through a viscous medium.

2.3 The Basic Optical Tweezers Set-Up

Optical tweezers have become commercially available in recent years; however a system can be readily built by someone with experience in building optical systems. As part of my research a portable optical tweezers system was built and exhibited at the Royal Society Summer 2002 exhibition in London and at the BBC's Tomorrow's World Road show in London and Glasgow also in the summer of 2002. The requirements for a successful single beam optical trap are detailed below.

2.3.1 Requirements for optical tweezers

It is important that the particle to be trapped is somewhat transparent to the laser light as absorption of the light can result in heating and therefore optical damage ('opticution'- a term coined by Ashkin) of the tweezed sample. This is especially true in biology, where visible light is heavily absorbed by pigments that are found naturally in biological specimens. For tweezing biological material near infrared laser light (700-1300 nm) is often chosen because visible light is absorbed by the pigments within the material and far infrared is absorbed by water. In addition, microscope objectives are not efficient when wavelengths in the far infrared are used. Lasers commonly used in optical tweezing include the Nd: YAG (neodymium: yttrium-aluminium-garnet) at 1064 nm, Nd: YLF (neodymium: yttrium-lithium-fluoride) at 1047 nm and Nd :YVO_4 (neodymium: yttrium-vanadate) also at 1064 nm. The Ti: Al_2O_3 (titanium sapphire) laser is tunable from 695-1100 nm. Diode lasers which operate at wavelengths of 700-1300 nm are a less expensive alternative but powers can be low and the laser mode may be non-circular. Highest powers are achieved from 800-900 nm diodes, and some come with corrected non-circular beams and astigmatism. A single focused laser beam can trap a particle using approximately 10 mW of power if certain criteria are met, but in general traps use from around 10 mW to 1 W of optical power. A laser for optical trapping of biological particles should operate in a continuous wave (cw) fashion, as pulsed lasers will damage specimens due to their high energy in space and time. The intensity at a one micron diffraction limited spot of a typical cw trapping laser operating at around 100 mW is 10^7 W/cm^2, where as for mode locked and Q-switched lasers, very high intensities in the order of GW/cm^2 are generated (Neuman et al., 1999). Proposed mechanisms for photodamage include transient local heating (Liu et al., 1996), two-photon absorption (Koenig et al., 1995, 1996, 1998) and photochemical processes leading to the creation of reactive chemical species (Liu et al. 1996). Neuman et al. characterised photodamage in *E.coli* by tethering the cells via their flagellum to a microscope slide and observing how the optical trap affected the natural rotation of the cell (Neuman et al., 1999). The least damaging

wavelength was found to be 970 nm, followed closely by 830 nm. Damage occurred when the trapping laser was operating at 870 nm and also at 930 nm. All experiments were performed at the same power level. The wavelength which cause minimum and maximum damage agree with data determined by Laing et al. when they determined the cloning efficiency of CHO cells which had been trapped in various wavelengths of laser light (Laing et al., 1996). The results of Neuman et al. show a linear relationship between sensitivity and power. This suggests that a single-photon mechanism leads to photodamage but the spectrum of damage does not resemble the absorption of water or oxygen of *E.coli* in suspension. The shape of the spectral features suggests that light is absorbed by one or more specific photopigments. The similarity between the wavelength dependence of photodamage seen in *E.coli* and CHO cells indicates that there may be a common basis for damage in both prokaryotic and eukaryotic systems, perhaps a ubiquitous intracellular chromophore. It was also shown that oxygen is critical in the photodamage pathway as aerobic and anaerobic experiments were performed with much less damage occurring in the anaerobic system. In general, there are two regimes for photodamage. One at very high peak intensities generated by mode-locked and Q-switched lasers (GW/cm^2) where two-photon processes dominate and another at lower intensities encountered in cw traps (MW/cm^2) where single photon events prevail.

Another important factor to consider when using optical tweezers is the profile of the laser beam. TEM_{00} mode Gaussian beams are the most commonly used in optical tweezers systems. The irradiance of a Gaussian beam decreases exponentially towards the edges of the beam and thus provides the transverse optical gradient required to trap particles in a three dimensional optical trap.

Stable three dimensional trapping is achieved in a focused laser beam if the gradient force is large enough to overcome the scattering force. This is achieved by using a high numerical aperture (NA) microscope objective lens, which creates steep gradients due to the angle at which the off-axis rays come into the sample. The numerical aperture equals the refractive index of the immersion fluid, *n* (air, water or

oil), multiplied by the sine of the half angle of opening of the focused light. Angles of opening can be up to 140° with high numerical apertures having values of 1.00-1.40.

The maximum numerical aperture is therefore determined by *n*, the refractive index of the medium immediately following the objective. For air, this is one and for oil immersion microscopes, which require a drop of index matching fluid between the sample and the objective lens, the index of refraction can be up to 1.4. Therefore oil immersion microscopes and index matching fluid are often used in optical tweezers devices however, the use of a high numerical aperture is limited by total internal reflection at the glass water interface.

2.3.1.1 Equipment

We have established that for an efficient optical tweezers device we need

- Non-damaging wavelength
- High NA (oil immersion) objective
- Index matching fluid

The laser chosen should have a good Gaussian profile and a wavelength which is not absorbed by the specimen to be tweezed. A telescope may be used to collimate the beam and make it the correct diameter for filling the rear aperture of the microscope objective. Before entering the microscope objective aperture, the beam is passed through another pair of lenses in a 1:1 telescope to allow conjugate images to be formed between the beam steering mirror and the back focal plane of the microscope objective. A dichroic mirror placed at 45º directs the incident laser beam into the microscope objective but allows white light to pass through and an image to be formed on the charged coupled device (CCD) camera which can be viewed on a monitor and recorded on a video recorder. Incoherent illumination of the sample is provided from below the sample cell by a 35 W halogen reflector.

The back aperture of the objective should be slightly overfilled so that the full numerical aperture is used to ensure maximum off-axis rays and the creation of a

steep z-direction intensity gradient. The objective has a high numerical aperture which gives a tightly focused trapping beam. A x100 objective is commonly used to give the smallest possible spot size. Using a less powerful objective (x60 or x20) would give a larger spot size at the focus, so the power of the laser is spread over a greater surface and the trap strength is lessened and furthermore, these objectives are usually air, not oil immersion microscope lenses.

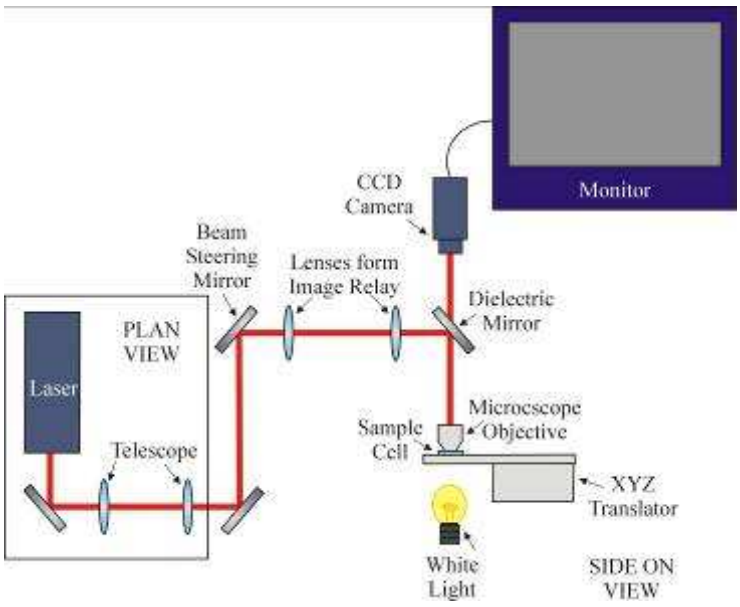

Figure 2.3: The basic setup for a single beam optical trap.

Sample cells are created using a microscope slide or a 22 x 50 mm coverslip as a base, typically an 80 μm deep, 1cm wide vinyl spacer as a well and a small coverslip on top. A drop of index matching fluid is placed on top if required for the objective. The sample is placed on a xyz translation stage and, if the beam entering the objective in collimated, the focus of the beam is coincident with the image plane where the particles lie. Collimation of the beam as it enters the microscope objective is determined by the positions of the conjugate lenses in the second telescope. The beam can be moved in the sample by changing the angle of the beam steering mirror, or the sample can be moved by translating the xyz on which the sample stage is located.

2.4 Novel laser beams in optical tweezers

In recent years optical tweezers set-ups have evolved from using a single Gaussian beam for trapping to presently using a wide range of advanced laser beam geometries to trap particles. Beams can now be tailored for a particular experiment, and as a consequence the capabilities of optical tweezers have been greatly extended.

In the following section, novel laser beams which have played an essential part of my PhD are presented. The Laguerre-Gaussian family of laser modes are introduced and are discussed further in later chapters where they are used to create novel interference patterns, to improve axial trapping efficiencies and to make cuts in chromosomes. 'Non-diffracting' Bessel beams are also introduced here, and appear later in this thesis when they are used to transport chromosomes and silica spheres attached to chromosomes. These beams have led to the enhancement of the optical toolkit which now includes optical tweezers, scissors and spanners. Beams can now be tailor made to fit their application, be it in biology, colloid physics, microfluidics or atomic physics.

2.4.1 Laguerre-Gaussian beams

Laguerre-Gaussian (LG) beams are a family of circularly symmetric modes usually denoted LG_p^l where l and p are two integer indices that describe the mode. The index l is the azimuthal index and refers to the number of complete (2π) phase cycles around the circumference of the mode, whereas $p + 1$ gives the number of radial nodes in the mode profile. Figure 2.4 shows the wave fronts of an $l = 0$, $p = 0$ LG beam consisting of plane wave fronts and of an $l = 3$, $p = 0$ LG beam with three intertwined helices of phase. Figure 2.5 shows LG beams of various l and p indices.

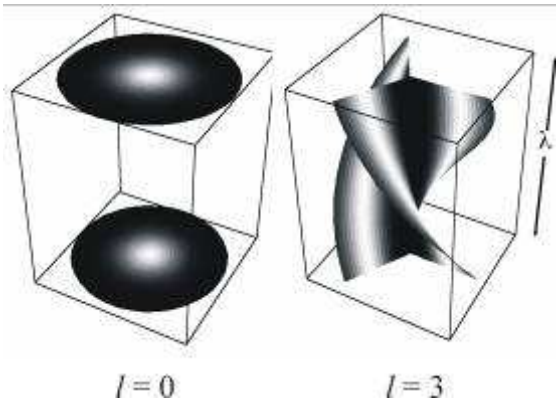

Figure 2.4: The phasefronts of two modes, $l = 0$, with plane wavefronts, and $l = 3$ with helical wavefronts. The phasefronts of an $l = 3$ LG beam is as a triple start helix.

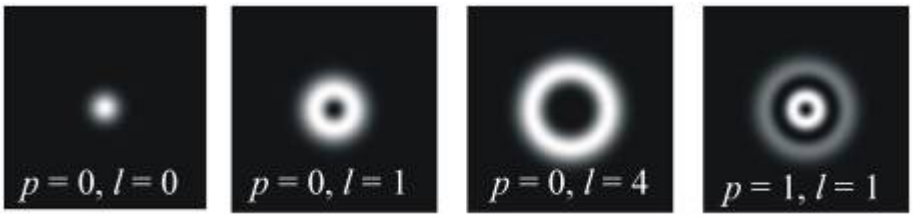

Figure 2.5: Beam profiles of LG beams with various l and p indices. $p = 0$ has one radial node and $p = 1$ has two radial nodes. $l = 0$ LG beams have plane wavefronts, $l = 1$ has one cycle of phase around the mode circumference and $l = 4$ has four complete (2π) phase cycles.

LG modes with $l \neq 0$ are interesting as they have an azimuthal phase that gives rise to helical wavefronts and thus a well defined orbital angular momentum of $l\hbar$ per photon. This is in addition to any spin angular momentum (of $\pm\hbar$ per photon) that the light may posses due to its state of polarisation. These beams are also termed optical vortices (Gahagan and Swartzlander, 1996) owing to the phase singularity within the intensity profile of the beam due to destructive interference.

The full mode description of a Laguerre-Gaussian beam is given by

$$E\left(LG_p^l\right) \propto \exp\left[\frac{-ikr^2 z}{2\left(z_R^2+z^2\right)}\right]\exp\left[\frac{-r^2}{\omega(z)^2}\right]\exp\left[-i\left(2p+|l|+1\right)\arctan\left(\frac{z}{z_R}\right)\right]\times \exp[-il\phi]\times\left(\frac{r\sqrt{2}}{\omega(z)}\right)^{|l|} L_p^{|l|}\left(\frac{2r^2}{\omega(z)^2}\right) \quad (2.3).$$

z is the distance from the beam waist, z_R is the Rayleigh range, k is the wave number, $\omega(z)$ is the radius at which the Gaussian term falls to 1/e of its on-axis value, r is the radius and $L_p^{|l|}$ is the generalised Laguerre polynomial (Beijersbergen et al., 1993).

2.4.1.1 Generation of Laguerre-Gaussian beams

Several methods exist for generating LG beams including the use of a spiral phase plate (Beijersbergen et al., 1994) or the direct formation of the beam inside a laser resonator (Oron, Davidson et al, 2000, Oron, Blit et al, 2000). However, the most practical methods are the use of a mode converter to transform a higher-order Hermite-Gaussian beam into an LG beam (Beijersbergen et al., 1993) and the use of holographic elements (Gahagan and Swartzlander, 1996, Clifford et al., 1998, Dufresne et al., 2001, Mogensen and Gluckstad, 2000, Heckenberg et al., 1992). The mode converter results in a pure LG beam but the holographic method is more versatile in that one only has to illuminate the hologram with a TEM_{00} mode and conversion efficiencies in excess of 75% are possible. A hologram is simply a recording of a diffraction pattern between an electromagnetic field of interest and a reference field. For holographic generation of an LG mode, the diffraction pattern takes the form of a forked diffraction grating with l dislocations. This results in a screw phase dislocation on the beam axis that gives us the characteristic phase structure of these beams with an azimuthal index of l.

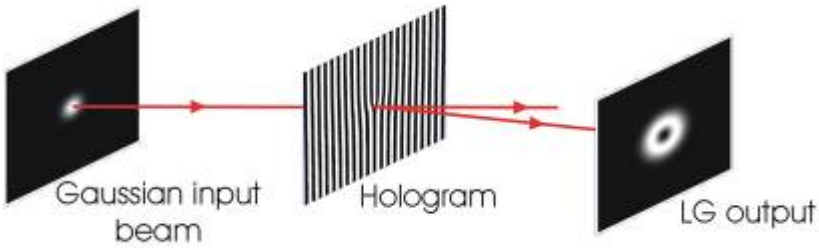

Figure 2.6: Formation of an l = 1 LG beam by passing a Gaussian beam through a computer generated hologram.

To tweeze using an LG mode, the annular ring of the collimated laser beam should match the size of the rear aperture of the objective lens. This ensures that most of the energy in the LG mode goes into off-axis rays as the beam is focused, which are essential for z-trapping.

Laguerre-Gaussian beams can also be generated using spatial light modulators (SLMs) (Curtis et al., 2002). The SLM consists of a number of birefringent liquid crystals (pixels) and the value (amplitude or phase) of each pixel can be changed to sculpt any light beam which hits the SLM surface. Holograms can be displayed on the SLM screen and specific light potentials can be tailored according to amplitude and phase information given by the orientation of the liquid crystals in the SLM screen, and the light beam reflected off the SLM can be imaged at any distance using lenses. The SLM has a number of advantages over computer generated holograms. The holograms generated by the SLM do not have to be microfabricated and they can be iteratively corrected to optimise trapping. In addition, SLMs allow dynamic control of optical potentials so that a sequence of holograms displayed on the screen can result in a dynamic optical trap which is not possible using a computer generated, microfabricated hologram.

2.4.1.2 Improved axial trapping

Laguerre-Gaussian beams have reduced on-axis intensity, so when this family of beams are used for trapping there is no backscattered component in the centre of the trap. In a single beam Gaussian trap the light which is scattered results in a radiation pressure force which works in the opposite direction to the axial gradient force, so is detrimental to z-trapping. LG beams can increase axial trapping efficiency due to the reduced radiation pressure force because of less on axis intensity, and also due to more off axis intensity in these beams (Simpson et al, 1998, Simpson et al., 1996) and as a result lower powers can be used to achieve z-trapping when using an LG beam in place of a Gaussian beam. Also, lower numerical apertures may also be used when using substituting an LG beam for a Gaussian beam which is advantageous when longer working distances are required.

2.4.1.3 Particle rotation using Laguerre-Gaussian beams

LG beams have a well defined orbital angular momentum of $l\hbar$ per photon as a result of the azimuthal phase of the beam and this orbital angular momentum is distinct from spin angular momentum associated with polarisation of photons. Angular momentum of light can be transferred to objects by absorption of the light. Microscopic particles which are partly absorbing as well as partly transparent can be made to rotate in a Laguerre-Gaussian optical trap (Friese et al., 1996).

2.4.1.4 Trapping of metallic and low-index particles in a Laguerre-Gaussian beam

Objects with a lower index of refraction than the surrounding medium such as bubbles are usually repelled from an optical trap because they are drawn into the region of lower light intensity along gradient of light intensity and particles which are highly reflecting such as metallic particles are also repelled from a trap due to radiation pressure. However LG beams have been used to successfully trap these

families of particles. In the case of highly reflecting particles, optical vortex beams such as those of the LG family can be used to trap the particle in the dark centre of the beam (Sasaki et al., 1992). The particle reflects light from the annular ring and the scattering force which is exerted on the particle from all around holds it stably in a trap. Similarly, low-index particles can be held in the zero intensity region of an LG beam as the particle is repelled from all around by light from the annular ring (Gahagan and Swartzlander, 1998). The bubble is held slightly below the focus of the LG beam as it is buoyant and the distance it is held from the focus depends on many parameters, including the diameter of the bubble and the power of the laser.

2.4.2 'Non-diffracting' Bessel Beams

All real beams, no matter how well collimated they are, spread out (diverge) as they propagate. The TEM_{00} mode Gaussian beam doubles its cross sectional area after propagating a distance of z_R away from the focus, also known as the Rayleigh range, where

$$z_R = \pi D_0^2 / 4\lambda \qquad (2.4),$$

and D_0 is the beam waist diameter.

There are beams, however, called Bessel beams, that are 'diffraction free'. A Bessel beam is so called because the variation of its intensity follows the mathematical pattern known as a zero-order Bessel function.

2.4.2.1 Generation of a Bessel beam

A Bessel beam can be practically realised by illuminating a conical shaped optical element, called an axicon, with a Gaussian beam (Arlt et al., 2001).

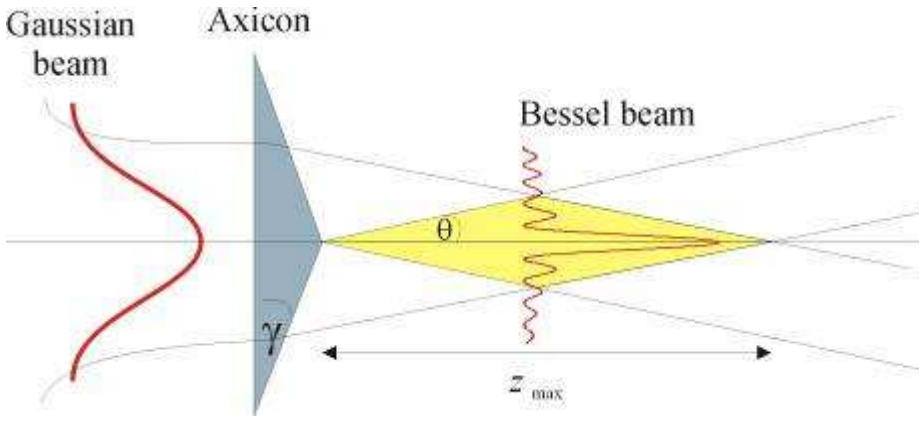

Figure 2.7: Illuminating an axicon with a Gaussian beam produces a close approximation to a Bessel beam.

The beam produced is a close approximation to a Bessel beam over a characteristic propagation distance. The central maximum propagates for several Rayleigh ranges without much divergence, and thus approximates a rod of light, or a focal line rather than a focal spot.

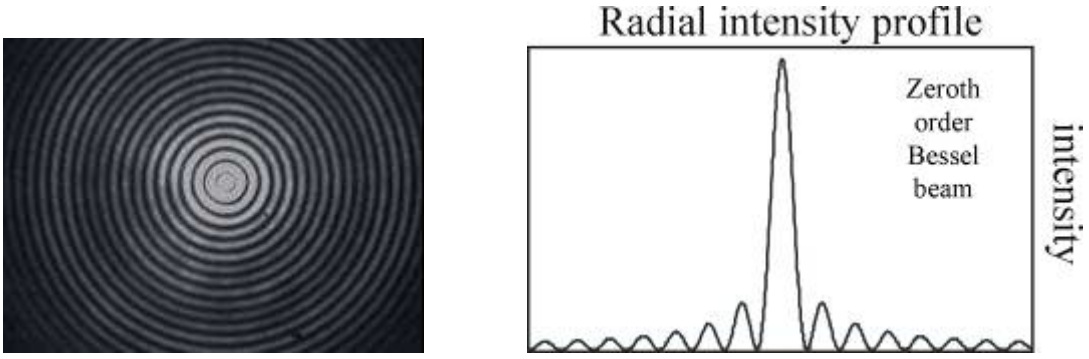

Figure 2.8: The beam profile (left) and the radial intensity profile (right) of a zeroth-order Bessel beam.

The Bessel beam is in fact an interference pattern, in which the outer rings of the Bessel beam act to replenish the central maximum and prevent it from spreading. This replenishment also allows the Bessel beam to reconstruct itself if it is blocked (Bouchal et al., 1998).

Bessel beams can also be created using holograms or spatial light modulators (SLMs) (Davis et al., 1993), which offer the possibility of creating arrays of Bessel beams in any desired pattern, or dynamic arrays of Bessel beams.

Bessel beams can be used as two dimensional optical tweezers with no confining forces in the direction of beam propagation and so do not offer any strong axial trapping. Bessel tweezers can be created in several geometries. Standard tweezers are in a downwards direction and push any trapped samples down towards the bottom surface via radiation pressure. Inverted tweezers come from below the sample and are used to levitate, align, stack and guide particles (O'Neil et al., 2001), again using radiation pressure in the direction of beam propagation. Horizontal Bessel tweezers can also be used to transport particles horizontally across a sample cell. Telescopic optics before the axicon allows us to vary the propagation length of the Bessel beam. A variable magnification telescopic system is placed after the axicon which allows the size of the central maximum to be changed. Axicons with different angles are also available to vary the Bessel beam parameters. Higher-order Bessel beams have also been created by illuminating an axicon with a Laguerre-Gaussian beam (Arlt and Dholakia, 2000). These beams have a dark central core which propagates in free space without any spreading due to diffraction, whereas the zeroth-order beam has a bright central maximum. These higher-order Bessel beams may find applications in coupling cold atoms into optical atomic guides because of the extended distances involved compared to LG beams (Arlt et al., 2000).

2.4.2.2 Stacking particles and transport of particles using a Bessel beam

The 'non -diffracting' nature of the Bessel beam means that that the line of focus is well suited for aligning long rod-like particles and also for stacking particles along the beam (Arlt et al., 2001). Arlt et al. showed nine spheres of 5 μm diameter stacked one above the other and this chain of particles can be manipulated as a whole. Laser guiding (transport) of 1 μm spheres over a distance of 1 mm was also observed in a Bessel beam which is a distance over 10 times the Rayleigh range for a

comparable Gaussian beam. This optical transport of particles to predetermined destinations may have applications in biological fields such as tissue engineering, as laser guided transport of hepatocytes onto a matrix has already been shown (Odde and Renn, 1999).

2.5 Optical Tweezers in biology

Optical tweezers have had widespread application in biological studies as they offer non-invasive, precise micromanipulation of a specimen in a closed, entirely sterile environment. Before optical tweezers, lasers were used as a tool in the field of biology to cut holes in the membranes of cells or organelles through which genes can be introduced. Chromosomes could also be cut *in vitro* and *in vivo*, however any manipulation involved the use of a fine glass rod until optical tweezers were developed. Since the late 1980s a huge variety of cells and intracellular structures have been trapped and manipulated using optical tweezers.

2.5.1 First biological applications of optical tweezers

The first paper which reported the use of optical tweezers for manipulating biological objects appeared in Science in 1987 (Ashkin and Dziedzic, 1987). Bacteria and viruses were trapped using an argon laser at a wavelength of 514 nm, however this visible laser light caused substantial damage to the particles even at very low powers. A second paper that year in Nature by the same authors described the use of an IR laser to trap and manipulate a variety of living cells and organelles (Ashkin et al., 1987). A Nd: YAG laser of wavelength 1064 nm was used in the studies and the authors found that the IR laser did not cause any visible damage to the cells when the argon laser at 514 nm did cause damage. Many cells and single celled organisms are transparent at infrared wavelengths so light is refracted through the object without being absorbed. The paper shows *E.coli* bacteria reproducing while trapped in the laser beam and the rod-like bacteria were seen to align vertically in the laser in the direction of beam. It was also shown that one bacterium could be

moved from one sample to another fresh sample by tweezing the particle into a hollow glass fibre attached to the top of the sample cell. The fibre could be removed along with the top coverslip of the sample cell, cleaned and dried while the bacterium stayed inside the fibre, then the whole structure could be placed on a fresh sample and the bacterium manipulated out. Two beams were also used with the bacteria to hold the rod-like structure at either end and the cell could be oriented at will by moving the two beams.

Yeast cells were seen to reproduce in the trap by budding, and powers from 5-80 mW were used without damaging the cells. Human red blood cells were trapped and it was found that the haemoglobin did not absorb as much at 1064 nm as it did at 514 nm which resulted in less damage. Powers from 4-40 mW could be used and at 80 mW the cells became less flexible indicating that damage was occurring. Unspecified organelles of 1 μm diameter inside Spirogyra were trapped and less damage occurred due to the lower absorption of chlorophyll at the IR wavelength. Protozoa and organelles within protozoa were also trapped and 160 mW could be used in this case without any damage to the sample. An organelle was held in the trap while the cell moved slowly out of the beam and the restrained particle is seen to finally collide with the cell wall at the rear of the advancing protozoan. Subsequently the protozoan pulls the organelle free of the trap with a snap, almost back to its original position. The authors state that ‘observations such as these are clearly giving information on the viscosity and elastic properties of the cytoplasm in the region of the trapped organelle’ and suggest that ‘to manipulate organelles within the interior of a living cell without damaging the cell wall is probably unique to the optical manipulation technique’. These initial studies were made on material that was large enough to manipulate directly using optical tweezers, such as whole cells and organelles. However, more recently studies have been made on much smaller particles such as proteins and DNA and rather than manipulating the objects directly, experimenters use ‘handles’ with which to indirectly manipulate material. In my work we have for the first time to our knowledge attached microsphere handles onto whole chromosomes, in order to facilitate optical micromanipulation and this is reported in chapter nine. Chromosomes are larger than proteins and can also be

manipulated directly however optical tweezers can trap silica spheres much more readily and efficiently as they are less scattering than chromosomes.

2.5.2 Measuring motor protein forces

Proteins are usually less than 25 nm in diameter and cannot be manipulated directly. Until optical tweezers became widely used in the field of biology, much of what was known about the mechanical properties of proteins and all other biological material was determined by testing of bulk material as individual molecules could not be tested. It could not be determined if individual molecules undergo a conformational change gradually, either smoothly or in small steps or if such structural changes occur rapidly in one huge step. Forces induced by optical tweezers are of the order of picoNewtons (pN), the same as the strength of forces that exist within living cells. Since the publication of Ashkin's first paper on the optical manipulation of biological particles, there have been many studies of mechanical and kinetic properties of single macromolecules using optical tweezers as a force transducer.

In order to use optical tweezers to measure biological forces, a position detector is required to measure the position of the trapped objects. The sensor is calibrated and the stiffness of the optical trap can be calculated (by analysis of thermal motion and/or by application of known viscous drag forces). The position of the microsphere 'handles' in the optical trap can be determined using a four-quadrant photosensor, either using conventional imaging or interferometry.

Optical tweezers have been used to study cellular mechanisms at the molecular level by measuring the forces created by motor proteins such as microtubule-based dynein (Shingyoji et al., 1998), kinesin (Svoboda et al., 1993, Schnitzer and Block, 1997), and the molecular basis of muscle contraction has been explored by investigation the actin-based motor protein myosin (Finer et al., 1994). In all these experiments microspheres have been attached to the proteins of interest and used as 'handles'.

These molecular motors move along linear substrates so are called linear motors and can be divided into two subsections. 'Porters' are processive enzymes, such as

kinesin, which walk along their filament, often carrying a cargo contained in a vesicle, without diffusing away. 'Rowers' are non-processive enzymes which produce just a single tug on the filament and then dissociate, such as myosin in muscle.

A seminal paper on the measurement of motor forces using optical tweezers was published in 1993 by Svoboda et al. (Svoboda et al., 1993). Discrete nanometer scale steps and picoNewton forces of kinesin, a molecular motor which carries vesicles of neurotransmitter along microtubules, were measured. A kinesin molecule was attached to a microsphere 'handle' and was held in optical tweezers and brought close to a microtubule which was fixed to a microscope slide. When they interacted, the kinesin molecule pulled the bead (its cargo) along the microtubule track. The position of the sphere was monitored using a four-quadrant detector and discrete 8 nm steps taken by the kinesin molecule were identified. It was determined that each step was a result of the protein using one ATP molecule of cellular energy. The experimental methods for measuring the forces these molecules exert on microfilaments are illustrated in figures 2.9 (for microtubule based motors dynein and kinesin) and 2.10 (for myosin).

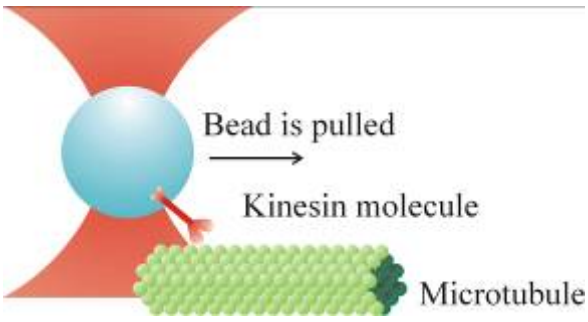

Figure 2.9: Measuring the force of kinesin (or dynein) as it moves along microtubules. The molecule kinesin is attached to a sphere which is held in an optical trap. When kinesin moves along microtubules, which are attached to the surface of a coverslip, the sphere is moved in the trap. (Svoboda et al., 1993 – not to scale)

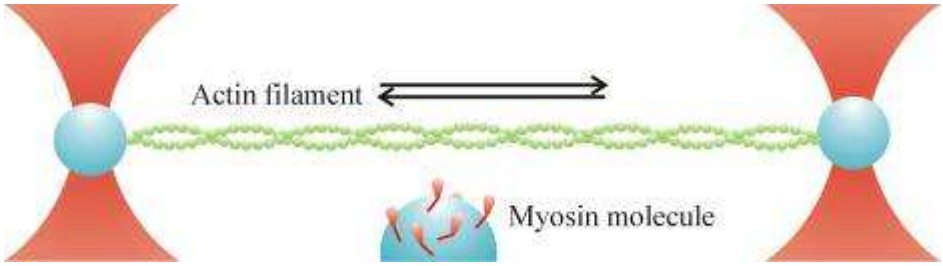

Figure 2.10: Measuring the force of myosin as it moves along actin filaments. Microspheres held in optical traps act as handles on either end of an actin filament. When a myosin molecule, which is attached to a fixed sphere, moves along the actin it pulls at the filament which in turn moves the spheres in the traps. Measurements of the forces of this motor protein can therefore be made (Finer et al., 1994 – not to scale).

The force of single myosin molecule pulling against an actin filament was determined by Finer et al. (Finer et al., 1994) by attaching polystyrene spheres, which act as a handles, to both ends of an actin filament and using optical tweezers to hold the spheres in place. Another sphere fixed to a surface is coated in single myosin molecules and when the head of the myosin molecule strokes against the actin filament and pulls the bead slightly out of the trap the motion was measured by monitoring the position of one of the trapped beads using a photodiode. The motion forces of these motor proteins have been determined to be in the range between 1 and 3 pN per binding site. RNA polymerase, a molecular motor capable of moving through thousands of basepairs without detaching from the DNA template, has also been investigated and was found capable of generating at least 14 pN of force (Yin et al., 1995, Wang et al. 1998). All of these aforementioned molecular motors use chemical energy available in the cell to perform mechanical work.

There exist another group of motor proteins that rotate (rotary motors) which are found in membranes and are driven by the flow of ions across transmembrane electrochemical gradients. One such rotary motor is the bacterial flagellar motor which Steven Block and others have studied. They made the first calibrated measurements of the stiffness of bacterial flagellum (Block et al., 1989) and since

then Berry and Berg (Berry and Berg, 1997, Ryu et al., 2000) have made a more detailed study of the forward and reverse rotation of the bacterial flagella rotary motor protein. F_1-ATPase is another rotary motor which is a part of ATP synthase and it rotates relative to the rest of the molecule in the presence of ATP (Noji et al., 1997, Yasuda et al. 1998).

2.5.3 Measuring forces of DNA

Steve Chu and his group have manipulated single DNA molecules by attaching polystyrene spheres to the ends of a DNA molecule, and measured its elasticity by pulling apart the two spheres and stretching the molecule using optical tweezers (Chu, 1991). It is hoped that this type of system may also be used to examine the motion of enzymes along the DNA and to investigate gene expression and repair. Carlos Bustamante and his group have investigated elastic responses of single and double stranded DNA molecules after overstretching and they found that conformational changes follow overstretching and may play a significant role in DNA recombination (Smith et al., 1996).

Cell sorting for making cell patterns for drug screening (Zahn et al., 1999), studies of membrane tension (Raucher et al., 1999) and mobility of membrane proteins (Raucher and Sheetz, 2000), measuring the rigidity of microtubules (Sako et al., 1998), and the elasticity of the cytoplasm (Tomishigie et al., 1998) and cell membrane (Ashkin and Dziedzic, 1989) and bringing together immune cells and their target cells under the microscope (Eriksson et al., 1999) are examples of some of the many other biological applications of optical tweezers.

2.5.4 Manipulation of chromosomes using optical tweezers

In order to make fluorescent chromosomal FISH probes as part of my work, we have manipulated and microdissected chromosomes in suspension. This work is described in more detail in chapters eight and nine however it is worth noting that

Michael Berns' group carried out groundbreaking work on the manipulation of chromosomes. In the early 1990's the group used optical tweezers to manipulate chromosomes inside living cells to investigate cell division, particularly the mitotic spindle of living cells (Berns et al., 1989, Laing et al., 1991, Laing et al., 1993, Laing et al., 1994). The cells used were PTK2 (*Potorus tridactylous*- kidney cells from the male kangaroo rat) which have a flat morphology and the chromosomes along with other mitotic structures are clearly visible. Cells with late moving metaphase chromosomes were used for experiments (cells in which one chromosome was located between the spindle pole and the metaphase plate when the rest of the chromosomes had aligned on the metaphase plate). Chromosome movement during cell division was studied by applying optical forces to chromosomes (Berns et al., 1989) and it was observed that the chromosomes would move in the direction opposite to the applied 'trapping' force, and that these chromosomes moved at 10-20 times their normal velocity of 2 μm/minute. It is thought that mitotic motors sense the force applied by the optical trap and in response shorten the microtubules on the opposite side of the chromosome pulling it towards the pole (depolymerisation of the microtubule). Similar results had been previously observed with tension applied to chromosomes using microneedles. The increased velocity was explained as the mitotic motor sensing the opposing force due to the optical trap and being stimulated into a high rate of activity, so when the chromosome was pulled out of the trap there was much less of an opposing force. The chromosomes stopped moving at the metaphase plate and did not continue moving to the opposite pole because the chromosome had moved substantially out of the optical gradient and normal microtubule and spindle dynamics dominated and cells went on to divide normally. It is not thought that the optical trap destroyed the microtubule attachments to the chromosomes at the points of laser focus, because when the attachments are destroyed, the chromosomes do not stop at the metaphase plate and are pulled all the way to the opposite spindle pole. A pair of chromatids could also be held in an optical trap at the initiation of anaphase and held motionless while the other chromatids separated and moved into their respective daughter cells, and the maximum force that the mitotic spindle can exert on a single chromosome can be

measured. Monosomic and trisomic cells can also be created for cell genetic studies (Berns et al., 1989). The group also used 'optical scissors' to microdissect chromosomes in vivo at different stages of metaphase in combination with optical tweezers to hold the microdissected fragments. Cells used were PTK2 cells (Laing et al., 1991) as before and Newt Lung cells (Laing et al., 1993) because they have large chromosomes and mitotic spindle, and the cells remain flat during mitosis. Newt cells also have the advantage of having a large area between the intermediate filament (IMF) cage and the mitotic spindle whereas in other cells the cage is in close proximity to the spindle. This permits the chromosome fragments to be manipulated outside of the spindle when previously they were caged by the intermediate filaments surrounding the spindle. The dissecting laser was a pulsed, frequency doubled Nd: YAG at a wavelength of 532 nm, and the laser tweezers was a continuous wave Nd: YAG operating at a wavelength of 1064 nm. It was shown that an optical trap could move and cut chromosome fragments outside of the mitotic spindle of newt pneumocytes when previously, in other cell lines this could not be achieved due to the close proximity of the IMF cage.

Lasers were first used to microdissect chromosomes in the 1980s and a paper by Monajembashi et al. (Monajembashi et al., 1986) reported using diffraction rings to cut a chromosome into nine pieces each of 0.5 μm thickness. Pulses of ultraviolet light, 20 ns in length were used and resulted in energy densities of 10^{14} W/cm^2. A more detailed analysis of previous investigations into chromosome manipulation and microdissection using coherent light sources can be found in chapter eight.

In the general field of biology optical techniques have much to offer, with optical tweezers being an important and essential tool in many biology disciplines and with the development of tailored beams and dynamic traps, optical tweezers hold great promise.

2.6 Summary

The potential impact of optical tweezers on the fields of biotechnology and also in the construction and driving of optically driven micro machines has been realised in

recent years. My three years of research at St Andrews University within the optical trapping group has played a part in this, with both the manipulation of chromosomes and the assembly of three-dimensional structures in an optical trap and their subsequent manipulation and rotation. The entire thesis concerns the use of beams such as Laguerre-Gaussian beams, interference patterns and Bessel beams to enhance the ability of optical tweezers to manipulate microscopic particles, with the exception of the following chapter which describes the use of a single Gaussian beam optical trap to stack multiple particles and also to align long cylindrical particles in the beam axis.

References

Arlt J, Hitomi T, Dholakia K: **Atom guiding along Laguerre-Gaussian and Bessel light beams.** *Applied Physics B-Lasers and Optics* 2000; **71**:549-554.

Arlt J, Garces-Chavez V, Sibbett W, Dholakia K: **Optical micromanipulation using a Bessel light beam.** *Optics Communications* 2001; **197**:239-245.

Arlt J, Dholakia K: **Generation of high-order Bessel beams by use of an axicon.** *Optics Communications* 2000; **177**:297-301.

Ashkin A, Dziedzic JM, Yamane T: **Optical trapping and manipulation of single cells using infrared-laser beams.** *Nature* 1987; **330**:769-771.

Ashkin A: **Optical trapping and manipulation of viruses and bacteria.** *Science* 1987; **235**:1517-1520.

Ashkin A, Dziedzic JM: **Internal cell manipulation using infrared laser traps.** *Proceedings of the National Academy of Sciences* 1989; **86**:7914-7918.

Beijersbergen MW, Allen L, Vanderveen H, Woerdman JP: **Astigmatic Laser Mode Converters and Transfer of Orbital Angular-Momentum.** *Optics Communications* 1993; **96**:123-132.

Beijersbergen MW, Coerwinkel RPC, Kristensen M, Woerdman JP: **Helical-Wave-Front Laser-Beams Produced with a Spiral Phaseplate.** *Optics Communications* 1994; **112**:321-327.

Block SM, Blair DF, Berg HC: **Compliance of bacterial flagella measured with optical tweezers.** *Nature* 1989; **338**:514-518.

Berns MW, Wright WH, Tromberg BJ, Profeta GA, Andrews JJ: **Use of a laser-induced optical force trap to study chromosome movement on the mitotic spindle.** *Proceedings of the National Academy of Sciences* 1989; **86**:4539-4543.

Berry RM, Berg HC: **Absence of a barrier to backwards rotation of the bacterial flagellar motor demonstrated with optical tweezers.** *Proceedings of the National Academy of Sciences* 1997; **94**:14433-14437.

Bouchal, Z., J. Wagner & M. Chlup. **Self-reconstruction of a distorted nondiffracting beam.** *Optics Communications* 1998; **151**: 207-211.

Chu S: **Laser manipulation of atoms and particles.** *Science* 1991; **253**:861-866.

Clifford MA, Arlt J, Courtial J, Dholakia K: **High-order Laguerre-Gaussian laser modes for studies of cold atoms.** *Optics Communications* 1998; **156**:300-306.

Curtis JE, Koss BA, Grier DG: **Dynamic holographic optical tweezers.** *Optics Communications* 2002; **207**:169-175.

Davis JA, Guertin J, Cottrell DM: **Diffraction-free beams generated with programmable spatial light modulators.** *Applied Optics* 1993; **32**:6368-6370.

Dufresne ER, Spalding GC, Dearing MT, Sheets SA, Grier DG: **Computer-generated holographic optical tweezer arrays.** *Review of Scientific Instruments* 2001; **72**:1810-1816.

Eriksson M, Leitz G, Fallman E, Axner O, Ryan JC, Nakamura MC, Sentman CL: **Inhibitory receptors alter natural killer cell interactions with target cells yet allow simultaneous killing of susceptible targets.** *Journal of Experimental Medicine* 1999; **190**:1005-1012.

Finer JT, Simmons RM, Spudich JA: **Single myosin molecule mechanics: piconewton forces and nanometre steps.** *Nature* 1994; **368**:113-119.

Friese MEJ, Enger J, RubinszteinDunlop H, Heckenberg NR: **Optical angular-momentum transfer to trapped absorbing particles.** *Physical Review A* 1996; **54**:1593-1596.

Gahagan KT, Swartzlander GA: **Optical vortex trapping of particles.** *Optics Letters* 1996; **21**:827-829.

Gahagan KT, Swartzlander GA: **Trapping of low-index microparticles in an optical vortex.** *Journal of the Optical Society of America B-Optical Physics* 1998; **15**:524-534.

Heckenberg NR, McDuff R, Smith CP, Rubinsztein-Dunlop H, Wegener MJ: **Laser beams with phase singularities.** *Optical and Quantum Electronics* 1992; **24**:S951-S962.

Ishijima A, Doi T, Sakurada K, Yanagida T: **Sub-piconewton force fluctuations of actomyosin *invitro*.** *Nature* 1991; **352**: 301-306.

Koenig K, Liang H, Berns MW, Tromberg BJ: **Cell damage by near-infrared laser beams.** *Nature* 1995; **377**:20-21.

Koenig K, Liang H, Berns MW, Tromberg BJ: **Cell damage in near-infrared multimode optical traps as a result of multiphoton absorption.** *Optics Letters* 1996; **21**:1090-1092.

Koenig K: **Laser tweezers are sources of two-photon excitation.** *Cellular and Molecular Biology* 1998; **44**:721-733.

Laing H, Wright WH, He W, Berns MW: **Micromanipulation of mitotic chromosomes in PTK2 cells using laser-induced optical forces ('optical tweezers').** *Experimental Cell Research* 1991; **197**:21-35.

Laing H, Wright WH, Cheng S, He W, Berns MW: **Micromanipulation of chromosomes in PTK2 cells using laser microsurgery (optical scalpel) in combination with laser-induced optical forces (optical tweezers).** *Experimental Cell Research* 1993; **204**:110-120.

Laing H, Wright WH, Rieder CL, Salmon ED, Profeta G, Andrews J, Liu Y, Sonek GJ, Berns MW: **Direct movement of chromosome arms and fragments in mitotic newt lung cells using optical scissors and optical tweezers.** *Experimental Cell Research* 1994; **213**:308-312.

Laing H, Vu KT, Krishnan P, Trang TC, Shin D, Kimel S, Berns MW: **Wavelength dependence of cell cloning efficiency after optical trapping.** *Biophysical Journal* 1996; **70**:1529-1533.

Lui Y, Sonek GJ, Berns MW, Tromberg BJ: **Physiological monitoring of optically trapped cells; assessing the effects of confinement by 1064-nm laser tweezers during microfluorometry.** *Biophysical Journal* 1996; **71**:2158-2167.

Malagnino N, Pesce G, Sasso A, Arimondo E: **Measurements of trapping efficiency and stiffness in optical tweezers.** *Optics Communications* 2002; **214**:15-24.

Mogensen PC, Gluckstad J: **Dynamic array generation and pattern formation for optical tweezers.** *Optics Communications* 2000; **175**:75-81.

Molloy JE, Padgett M: **Light, action: optical tweezers.** ***Contemporary Physics*** 2002; **43**:241-258.

Monajembashi S, Cremer C, Cremer T, Wolfrum J, Greulich KO: **Microdissection of human chromosomes by a laser microbeam.** ***Experimental Cell Research*** 1986; **167**:262-265.

Neuman KC, Chadd EH, Liou GF, Bergman K, Block SM: **Characterization of photodamage to Escherichia coli in optical traps.** ***Biophysical Journal*** 1999; **77**:2856-2863.

Noji H, Yasuda R, Yoshida M, Kinosita Jr K: **Direct observation of the rotation of F_1-ATPase.** *Nature* 1997; **386**:299-302.

Odde DJ, Renn MJ: **Laser-guided direct writing for applications in biotechnology.** *Trends in biotechnology* 1999; **17**:385-389.

O'Neill AT, Padgett MJ: **Axial and lateral trapping efficiency of Laguerre-Gaussian modes in inverted optical tweezers.** *Optics Communications* 2001; **193**:45-50.

Oron R, Blit S, Davidson N, Friesem AA, Bomzon Z, Hasman E: **The formation of laser beams with pure azimuthal or radial polarization.** *Applied Physics Letters* 2000; **77**:3322-3324.

Oron R, Davidson N, Friesem AA, Hasman F: **Efficient formation of pure helical laser beams.** *Optics Communications* 2000; **182**:205-208.

Raucher D, Sheetz MP: **Membrane expansion increases endocytosis rate during mitosis.** *Journal of Cell Biology* 1999; **144**:497-506.

Raucher D, Sheetz MP: **Cell spreading and lamellipodial extension rate during mitosis.** *Journal of Cell Biology* 2000; **148**:127-136.

Ryu WS, Berry RM, Berg HC: **Torque-generating units of the flagellar motor of *Escherichia coli* have a high duty ratio.** *Nature* 2000; **403**:444-451.

Sako Y, Nagafuchi A, Tsukita S, Takeichi M, Kusumi A: **Cytoplasmic regulation of the movement of E-cadherin on the free cell surface as studied by optical tweezers and single particle tracking: Corralling and tethering by the membrane skeleton.** *Journal of Cell Biology* 1998; **140**:1227-1240.

Sasaki K, Koshioka M, Misawa H, Kitamura N, Masuhara H: **Optical Trapping of a Metal-Particle and a Water Droplet by a Scanning Laser-Beam.** *Applied Physics Letters* 1992; **60**:807-809.

Schnitzer MJ, Block SM: **Kinesin hydrolyses one ATP per 8-nm step.** *Nature* 1997; **388**:386-388.

Shingyoji C, Higuchi H, Yoshimura M, Katayama E, Yanagida T: **Dynein arms are oscillating force generators.** *Nature* 1998; **393**:711-714.

Simpson NB, Allen L, Padgett MJ: **Optical tweezers and optical spanners with Laguerre-Gaussian modes.** *Journal of Modern Optics* 1996; **43**:2485-2491.

Simpson NB, McGloin D, Dholakia K, Allen L, Padgett MJ: **Optical tweezers with increased axial trapping efficiency.** *Journal of Modern Optics* 1998; **45**:1943-1949.

Smith SB, Cui Y, Bustamante C: **Overstretching B-DNA: The elastic response of individual double-stranded and single-stranded DNA molecules.** *Science* 1996; **271**:795-799.

Svoboda K, Schmidt CF, Schnapp BJ, Block SM: **Direct observation of kinesin stepping by optical trapping interferometry.** *Nature* 1993; **365**:721-727.

Tomishigie M, Sako Y, Kusumi A: **Regulation mechanism of the lateral diffusion of band 3 in erythrocyte membranes by the membrane skeleton.** *Journal of Cell Biology* 1998; **142**:989-1000.

Wang MD, Schnitzer MJ, Yin H, Landick R, Gelles J, Block SM: **Force and velocity measured for single molecules of RNA polymerase.** *Science* 1998; **282**:902-907.

Yasuda R, Noji H, Kinosita Jr K, Yoshida M: **F_1-ATPase is a highly efficient molecular motor that rotates with discrete 120 steps.** *Cell* 1998; **93**:1117-1124.

Yin H, Wang MD, Svoboda K, Landick R, Block SM, Gelles J: **Transcription against an applied force.** *Science* 1995; **270**:1653-1657.

Zahn M, Renken J, Seeger S: **Fluorimetric multiparameter cell assay at the single cell level fabricated by optical tweezers.** *FEBS Letters* 1999; **443**:337-340.

3 Stacking and alignment of particles in optical tweezers

3.1 Introduction

When more than one particle is trapped at the focus of a laser beam, the beam profile is altered by the first particle that the rays encounter. All other particles present in the trap will interact with this modified beam profile. The theoretical techniques used to model and predict the behaviour of a single spherical particle in various regions of the laser beam fail when more than one particle is present or when the particle is irregularly shaped. Stacking of particles and the creation of ordered horizontally or vertically aligned arrays has been observed in a few configurations by several groups in recent years and is not only limited to single beam optical traps. This chapter describes how multiple particles can be stacked along the beam propagation axis and we have shown the stacking of particles in a standard and an inverted optical tweezers configuration and report on the stability of these trapped stacks. We also show the alignment of cylindrically trapped particles along the axis of beam propagation.

3.2 Linear arrays of spheres

The dynamic behaviour of single and multiple spheres in the trap region of a focused laser beam has been theoretically predicted by Gauthier and Ashman (Gauthier and Ashman, 1998) using a sophisticated optical trapping program which they have developed. The dynamic behaviour of one to four spherical particles in the optical trap is computed using an enhanced ray optics theoretical approach. In a two sphere system, one sphere is pulled into the beam while the other is pushed out and falls due to gravity. The falling sphere is quickly drawn back into the beam axis due to the diffracting beam and rises again until it contacts the top sphere and a stable trap with the two spheres stacked, is created. The theoretical dynamics of a triangular three sphere configuration whose plane is perpendicular and centred on the beam

propagation axis and a four sphere rectangular configuration is also described. In both cases one sphere is drawn into alignment with the beam's central propagation axis and the others are pushed down, but are eventually drawn back into the beam when they encounter the diverging beam, and rise into contact with the sphere above. Multiple spheres in a single beam optical trap tend to evolve into a configuration linearly aligned with the laser beams propagation axis.

Several groups have reported the creation of one dimensional arrays of particles in novel optical traps. Stacking of a small number of particles in a Bessel beam has been observed and the manipulation of the chain of particles as a whole has been performed (Arlt, 2001). It was reported by Zemanek and co-workers in 1999 that a number of micro-objects from 0.3 – 15 μm in diameter could be collected in a vertical line along the optical axis of a Gaussian standing wave and moved together within the sample (Zemaneck, 1999). The standing wave traps were produced by the interference of incoming and reflected Gaussian beams under a microscope objective. A particle in the vicinity of the beam waist (near the reflective slide) feels a strong axial gradient force caused by the steep intensity gradients between the nodes and antinodes of the standing wave. The interference of two counter-propagating beams results in a number of particle equilibrium positions (standing wave traps) that are located at the standing wave antinodes and are separated axially by $\lambda/2$. It is possible to manipulate in three dimensions particles trapped in these sites however, in the same setup but using a single beam, three dimensional trapping of the same particles was not possible. One-dimensional arrays of regularly spaced particles have been observed in a potential well created by two counter-propagating beams (Tatarkova, 2002). The light forces are thought to act to optically bind matter and microscopic particles may be organised to study 'optical molecules' or self assembly of matter. Linear arrays of trapped particles could be of great importance in colloid physics, for example to study binary colloid suspensions (Crocker, 1999).

3.3 Stacking spheres in a Gaussian beam

The work reported in this chapter was carried out by Lynn Paterson and Michael MacDonald. Experimentally we have observed controlled stacking of large numbers of particles in optical tweezers using a single Gaussian beam. The mechanism for creating particle stacks depends on whether the trapping laser propagates in the direction of gravity (standard tweezers) or against gravity (inverted tweezers). High refractive index silica particles in water tend to sink to the bottom of the sample cell, so they must be lifted in order to build stacks.

3.3.1 Stacking in standard tweezers

To create a stack of spheres in standard tweezers, a sphere must be lifted off the bottom of the sample cell by z-trapping and moved over a second sphere which is trapped below the initial sphere. Both spheres can be tweezed in three dimensions because of the refocusing ability of the first sphere, with the second sphere directly below the first sphere. These first two spheres can be lifted up and manoeuvred over the top of a third sphere which will be two dimensionally trapped at the bottom of the cell by the light coming through the top two spheres. At this stage there is a stack of three spheres which can be manipulated in two dimensions. This mechanism for creating a stack of particles in standard optical tweezers geometry can be seen in figure 3.1.

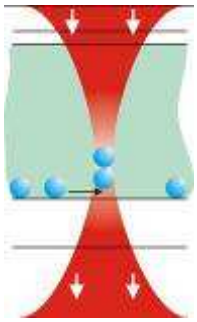

Figure 3.1: Stacking in normal tweezers (beam coming into sample from above).

This stack of three spheres can be lifted off the bottom of the sample cell and manoeuvred over a fourth sphere but the refocusing that tweezed the second sphere in three dimensions is not available to the third sphere, however there is a capillary force that can lead to a slight cohesion of the spheres within the stack. By z-trapping the top spheres, the stack of three spheres can be lifted off the bottom of the sample cell due to the cohesion of the stack and placed over a fourth sphere. This leads to a stack of four spheres being produced which can be manipulated in 2 dimensions. This was performed with an approximate power of 400 mW. The experimental set-up used to observe the stacking of 5 μm diameter dielectric spheres using a laser incident from above the sample is shown in figure 3.2.

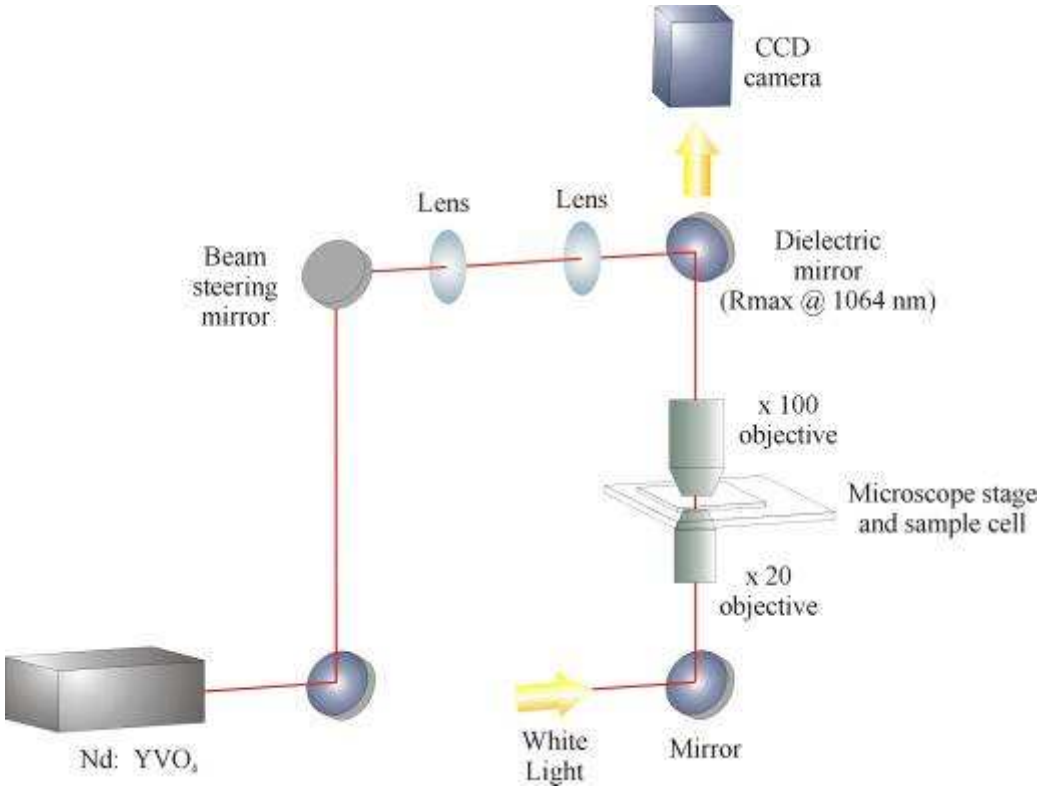

Figure 3.2: Experimental set-up with laser directed into sample cell from above.

The largest stacks formed consisted of four 5 μm diameter spheres. The horizontal speeds at which the spheres fell out of stacks of 1, 2 and 3 spheres in size is shown in figure 3.3.

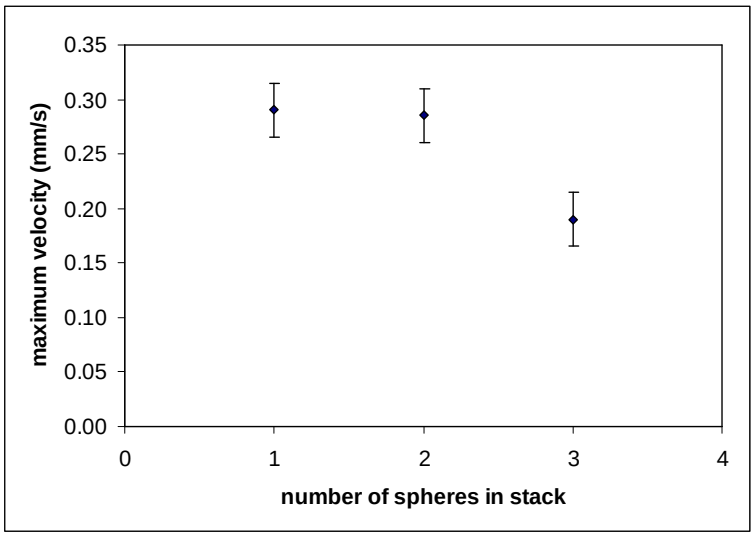

Figure 3.3: Maximum horizontal velocity of stacks of 1, 2 and 3 spheres trapped in a standard optical tweezers configuration.

There is very little change in stability of the stacks of one or two spheres but the stack of three spheres is more difficult to create in the trap, and the figure 3.3 shows that the stack is less stable than one or two spheres, and collapses at a lower velocity.

3.3.2 Stacking in inverted tweezers

In the inverted optical tweezers geometry, in which the trapping beam comes into the sample cell from below, the laser is focused at the top of the sample cell in such a way that it forms a cone, the widest cross section of which is at the bottom of the sample cell. Dielectric spheres are captured and guided upward within the cone to the focal region of the laser beam at the top of the sample cell, and the particles align

in a vertical stack. The mechanism by which the stack is formed by a laser focused from below a sample cell is illustrated in figure 3.4.

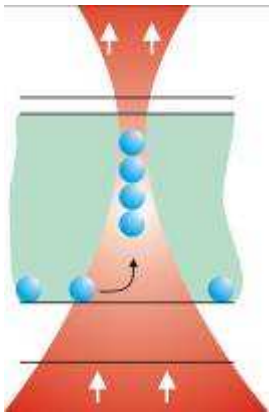

Figure 3.4: Stacking in inverted tweezers (beam coming into sample from below).

Stacking from below does not depend on the ability to 3 dimensionally tweeze particles. When the laser beam is moved under a sphere, the sphere is pushed up to the top of the sample cell (levitated) by the radiation pressure of the laser. This sphere defines the top of the stack and all subsequent spheres lie underneath this sphere. By moving the trapped sphere over a second sphere on the bottom surface of the sample cell the second sphere is guided by the cone of the laser, up underneath the first sphere to form a stack of two spheres. This process can be repeated numerous times to form a stack, the height of which is initially limited only by the height of the sample cell or the stability of the stack when it is moved to pick up further spheres. Eventually the stack height will also be limited by the Rayleigh range of the laser focus and the working distance of the microscope objective. This method of trapping resulted in stacks of up to sixteen spheres being created (the largest created in this work). The experimental set-up used to observe stacking with a laser focused from below a sample cell is shown in figure 3.5.

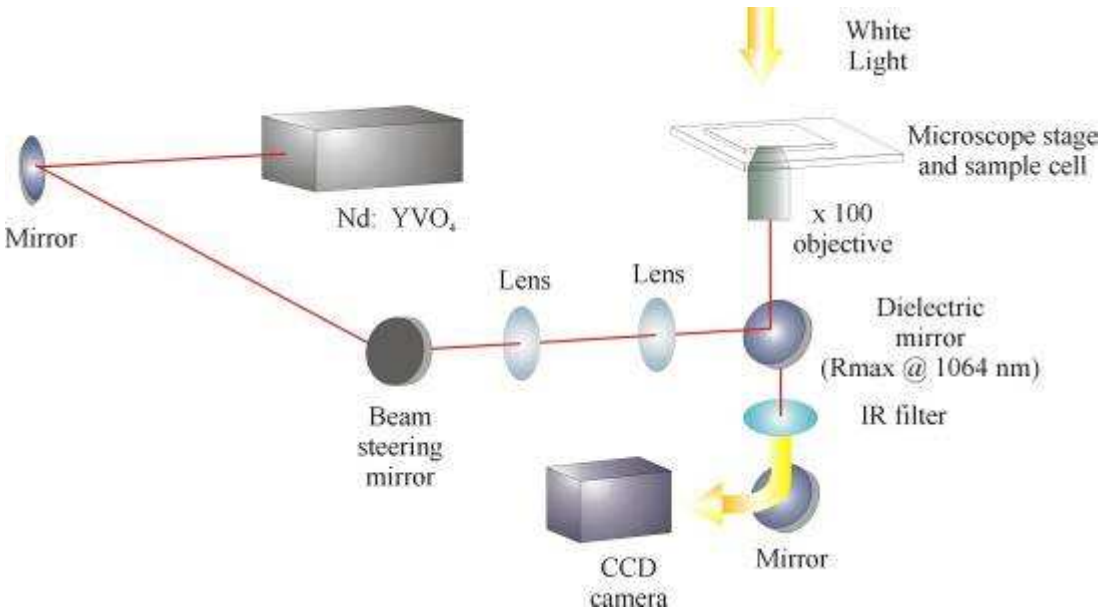

Figure 3.5: Experimental set-up with laser directed into sample cell from below.

The stack height in both geometries is limited by the divergence of the laser beam and the working distance of the microscope objective. Our experimental optical tweezers geometry uses a Nd: YVO_4 laser, operating at 1064 nm, directed through a x100 microscope objective. In the inverted geometry, we have stacked as many as 16 spheres (5 μm in diameter) and have moved the chain as a whole across the sample slide. Figure 3.6 shows the assembly of a stack of six 5 μm diameter silica spheres.

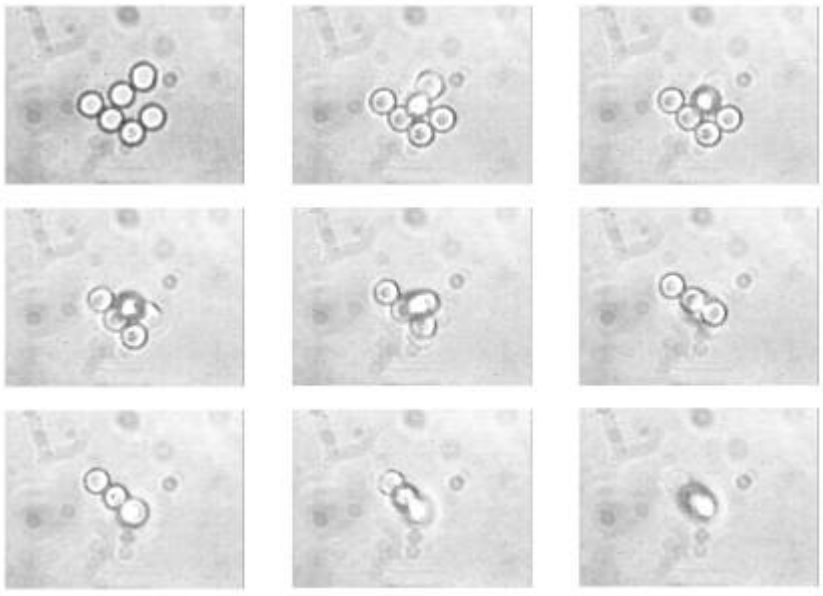

Figure 3.6: The assembly of a stack of six 5 μm silica spheres in an inverted geometry.

By tilting the tweezing laser beam, it is possible to incline stacks of spheres and this can be seen in figure 3.7. A stack of six spheres can be held at an angle of 30° to vertical, along the axis of beam propagation. This tilting will result in a change in the forces exerted on the stack of spheres, so maximum velocity of the stack and the *Q* value of the trap at an angle will be altered.

Figure 3.7: Tilting of a stack of six 5 μm spheres as the laser beam is inclined, viewed from below in an inverted geometry.

The stability of the stacks (a measurement of the maximum velocity of the stack before it collapses in the trap) with increasing power showed linear behaviour as illustrated by figure 3.8.

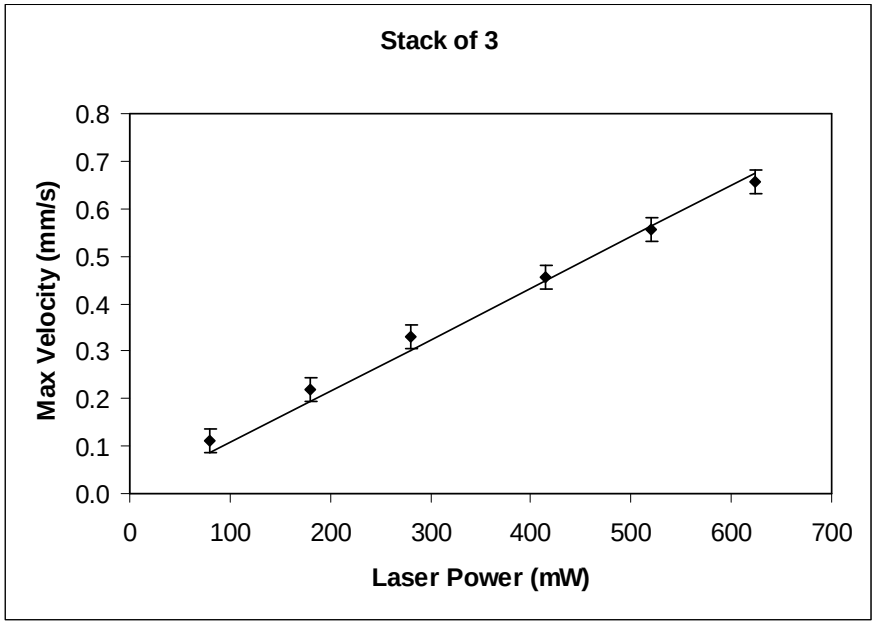

Figure 3.8: Maximum horizontal velocity of a stack of three 5 μm diameter silica spheres for increasing laser powers.

Figure 3.8 shows a very close fit to the points can be made with a straight line passing through the origin. This behaviour might be expected to continue until a point at which the intensity of the laser is too great at the focus such that heating of the spheres or the sample medium results in damage.

The relationship between power, P and velocity, v is linear and is given by

$$nQP = 6\pi\eta rvc \qquad (3.1),$$

where n is the refractive index of the medium, Q is trap efficiency, η is the viscosity of the medium, r the radius of the trapped particle and c the speed of light in a vacuum.

The stability of the stack can be quantified by its maximum velocity before one or more spheres fall out of line. The results of such measurements for three different

power levels and for various numbers of spheres in the stack in an inverted geometry are shown in figure 3.9. Importantly, in these results the stack velocities were measured when the top sphere of the stack was in very close proximity to the top surface of the sample chamber, so there was a definite surface interaction which should be considered.

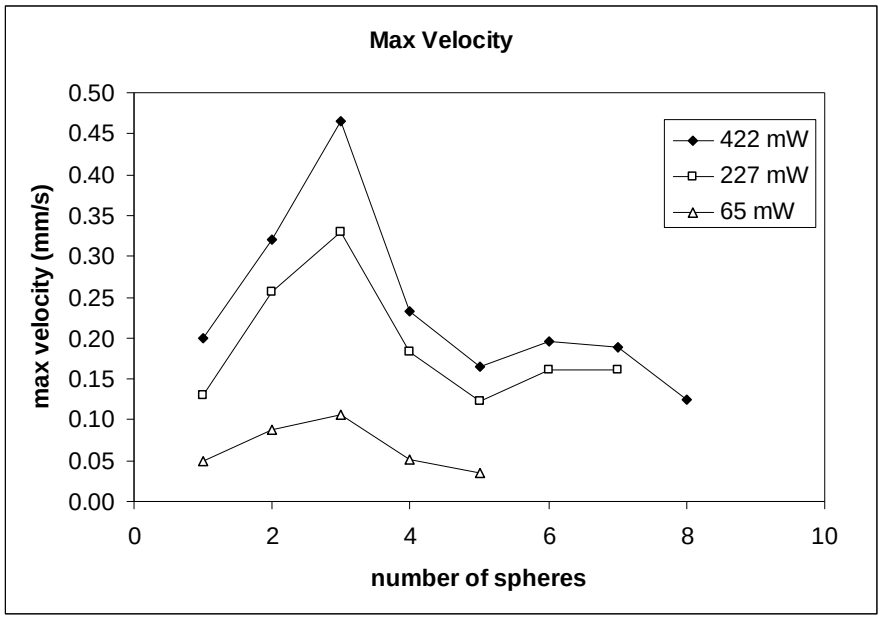

Figure 3.9: Maximum horizontal velocity for stacks with various numbers of 5 μm diameter silica spheres at three different laser powers.

The most notable aspect of the above figure is the increase in stability of the stack between 1- and 3-sphere stacks with a stack of three being the most stable even compared to a single tweezed sphere. It is also notable that the stability starts to level off with increasingly large stacks.

As with stacking from above, there is a sphere-sphere interaction due to capillary force, seen when translating a stack that sticks together. The top sphere which is held in the beam focus stays firmly in the centre of the laser but the other spheres drag out behind the top sphere so that the stack resembles a string of beads. There is also an interaction between the stack and the surface of the sample cell. The top

sphere is held at the very top of the sample chamber, and this closeness to a surface as well as sphere-sphere interactions may somehow cause a stack of two spheres to be trapped more stably than a single sphere and a stack of three to be more stable than two in this geometry. Although this behaviour is difficult to explain it is of interest and this technique may be used as a probe to inform us about surface interactions.

3.4 Alignment of cylindrical particles

Gauthier and co workers, as well as predicting the stacking of multiple spheres in optical tweezers, predicted, and experimentally confirmed the optical trapping properties of cylindrical objects (Gauthier et al., 1999). In a standard set up the beam can be used to manipulate the cylinder (or rod) by steering the beam towards the ends of the rod and dragging the rod along the sample plane. In an inverted set up it was shown that the central axis of a trapped rod should align with the propagation axis of the laser beam such that the longest dimension (diagonal) of the rod closely aligns with the laser axis.

We have also experimentally observed similar results in both a standard and inverted set up. The following results were observed in an inverted set up. Figure 3.10 shows a 5 μm long rod aligning with the beam propagation axis (3.10A-B) and being translated across the sample plane, maintaining its alignment with the beam axis (3.10B-D). The beam is then blocked and the rod slowly collapses from its alignment (3.10E-H).

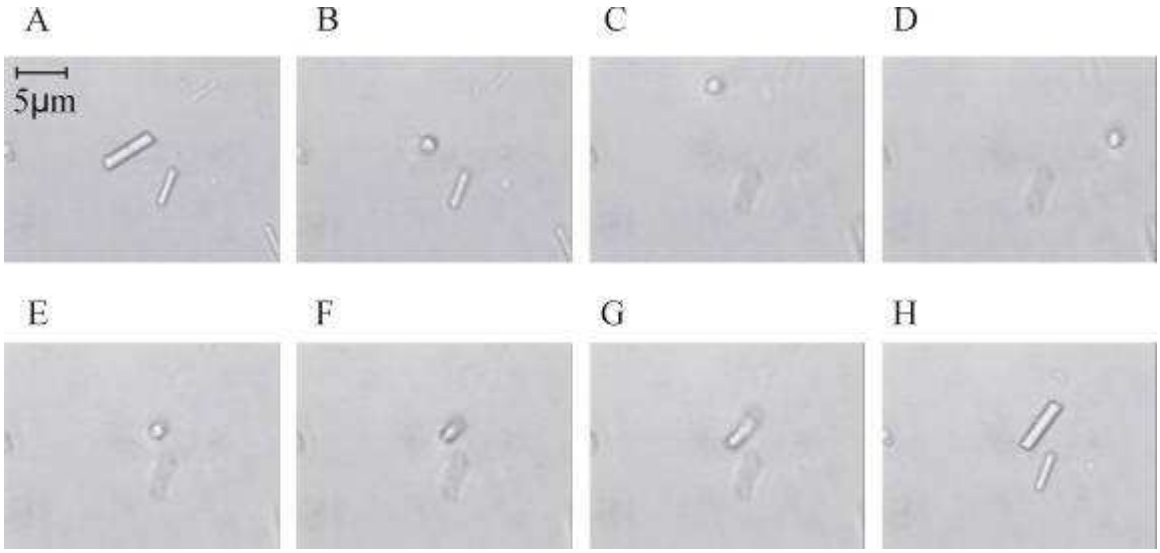

Figure 3.10: Rod alignment and translation in an inverted optical trap.

The longest rod which was manipulated into partial alignment with the beam propagation axis was 250 µm long. It could not be fully aligned because the depth of the sample chamber was not large enough. Figure 3.11A shows an aligned 140 µm long rod and in the following frames the rod can be seen to fall from alignment as the beam is blocked, with only one end in view.

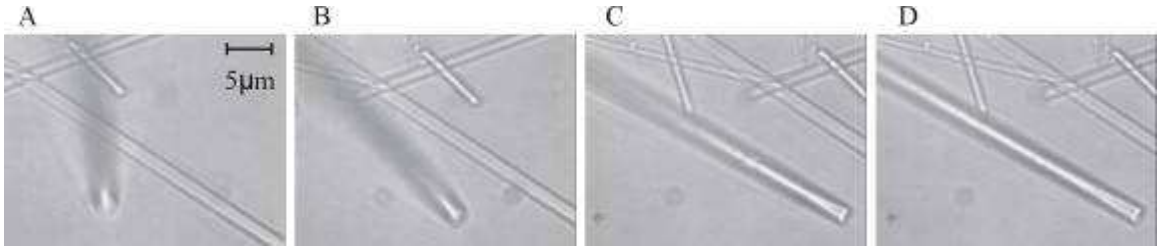

Figure 3.11: A 140 µm long rod falling from alignment.

In summary, if the trapping beam is directed into the sample from above the rods can be ‘dragged’ across the sample plane by bringing the beam close to one end of the rod, but they cannot be aligned in the direction of beam propagation. In an inverted

set up where the beam comes into the sample from below, rods can be aligned with the beam propagation axis and manipulated in the x-y plane.

3.5 Discussion

The stacking of large numbers of spheres and the alignment of long cylindrical shaped particles in an inverted optical tweezers will have implications in the construction of extensive three dimensional microscopic structures. The linear arrays of spheres which we have created may assist investigations into interactions between colloidal particles or act as probes with which to investigate surface interactions with trapped particles.

References

Arlt J, Garces-Chavez V, Sibbett W, Dholakia K: **Optical micromanipulation using a Bessel light beam.** *Optics Communications* 2001; **197**:239-245.

Crocker JC, Matteo JA, Dinsmore AD, Yodh AG: **Entropic attraction and repulsion in binary colloids probed with a line optical tweezer.** *Physical Review Letters* 1999; **82**:4352-4355.

Gauthier RC, Ashman M: **Simulated dynamic behaviour of single and multiple spheres in the trap region of focused laser beams.** *Applied Optics* 1998; **37**:6421-6431.

Gauthier RC, Ashman M, Grover CP: **Experimental confirmation of the optical-trapping properties of cylindrical objects.** *Applied Optics* 1999; **38**:4861-4869.

Tatarkova SA, Carruthers AE, Dholakia K: **One-dimensional optically bound arrays of microscopic particles.** *Physical Review Letters* 2002; **89**:article no. 283901.

Zemanek P, Jonas A, Sramek L, Liska M: **Optical trapping of nanoparticles and microparticles by a Gaussian standing wave.** *Optics Letters* 1999; **24**:1448-1450.

4 Trapping in a Laguerre-Gaussian beam

4.1 Introduction

The trapping efficiency of optical tweezers was described in chapter 2. It is usually described in terms of a dimensionless parameter Q which is related to the force on the sphere, F_{escape}. This force can be approximated as the Stoke's Drag, F_{Stokes}.

$$F_{escape} = \frac{nQP}{c} \quad (4.1).$$

$$F_{escape} \approx F_{Stokes} = 6\pi\eta r v \quad (4.2),$$

where P is the power of the laser, n is the refractive index of the medium, η is the viscosity of the medium, r is the radius of the spherical particle and v is the velocity of the particle as it travels through the medium, or the velocity of the fluid flow against the particle.

F_{escape} of a trap is calculated by measuring the critical velocity of particles of radius r in the trap. The maximum force that an optical trap can exert is of the order of picoNewtons and from that the Q value of the optical trap can be calculated.

Q has a value between 0 and 1, and represents the fraction of momentum nP/c carried by the laser beam converted into the trapping force (Malagnino et al., 2002). In the Mie regime, when the rays from the trapping beam strike the sphere a fraction of the momentum is reflected and the remainder is transmitted to the sphere.

In this chapter Q values for the axial and lateral trapping of 2 μm diameter spheres in a Laguerre Gaussian beam are reported and the results are compared to the results of other groups.

4.2 The use of Laguerre-Gaussian beams for trapping

4.2.1 Increasing axial trapping efficiency using LG beams

Within conventional optical tweezers Q_{axial} is usually a magnitude of order smaller than $Q_{lateral}$ (Felgner et al., 1995). Increasing axial trapping efficiency as a means of improving the overall performance of tweezers has been investigated by several groups. Particles in a trap escape from, or fall out of the bottom of the trap, so increasing z-stiffness increases F_{escape}. Simpson et al. (Simpson et al., 1996) developed a computer model for modelling trapping forces in optical tweezers. The axial trapping forces arising from a laser operating in the fundamental mode was compared with higher-order Laguerre-Gaussian modes. The axial trapping force for an 8 μm diameter sphere in LG modes of l = 0, 1, 2 and 4 (with p = 0) were presented. As the azimuthal index l is increased the radius of the beam increases and the thickness of the ring decreases. It was found that the higher-order LG modes produce an axial trapping force several times that of the fundamental, with the axial trapping force of an l = 4 LG mode being four times that of the fundamental. This enhanced axial trapping force is due to the reduction of on-axis rays. On-axis rays are not refracted as they pass straight through a sphere so they do not contribute a trapping force, but reflected on-axis rays apply radiation pressure on the sphere and a corresponding force, the scattering force, acts in the propagation direction of the beam. This force is in the same direction as gravity in the standard tweezers geometry. An equilibrium position is reached when the gradient force balances the scattering force and the force of gravity. Using a beam with reduced on-axis intensity, such as an LG beam, means that the scattering force opposing the axial trapping gradient force is greatly reduced. Higher-order LG beams produce a greater axial trapping force per unit power than the fundamental mode and consequently less laser power is needed to overcome gravity. It is not clear if Laguerre-Gaussian beams can also improve lateral trapping with Sato and Inaba (Sato and Inaba, 1996) predicting but being unable to show experimentally that the lateral trapping force improves if an LG beam is used instead of a Gaussian TEM_{00} beam. Others (O'Neil

et al., 2001) believe that there is no improvement in lateral trapping efficiency when a Laguerre-Gaussian beam is used. Enhanced axial trapping by use of Laguerre-Gaussian modes may enable tweezing of delicate biological samples at lower laser power, thereby avoiding optical destruction of the sample. Alternatively, if the laser power is constant, higher order LG beams can produce the same trapping powers using an objective lens of lower numerical aperture. Lowering the NA of an objective increases its working distance which is useful for many applications. Freise et al. (Friese et al., 1996) measured fluctuations in the backscattered light of trapping LG beams and inferred that the use of these beams can increase the axial force of the trap. Simpson et al. followed up this work by demonstrating that axial trapping in optical tweezers is improved by using a Laguerre-Gaussian mode as the trapping beam (Simpson et al., 1998). The axial trapping efficiencies produced by optical tweezers using a TEM_{00} fundamental mode and a Laguerre-Gaussian mode with an index of $l = 3$ are compared by measuring the threshold laser power required to achieve axial trapping of silica spheres between 1 and 5 μm in diameter suspended in water. The minimum force required to hold a particle of density ρ_s and diameter d in medium of density ρ_m against gravity g and thermal motion, is given by

$$F_{\min} = \frac{\pi}{6}(\rho_s - \rho_m)d^3 g + \frac{2kT}{d} \qquad (4.3),$$

where T is the ambient temperature and k is Boltzmann's constant. The second term in this equation relates to the force required to suppress the thermal motion of the sphere and is calculated assuming a trap with a radius equal to the size of the sphere. The gradient force produced by the focused laser beam has to be large enough to overcome both this force and the force due to the backscattered light.

The following equation relating Q_{axial} to the measured minimum power P_{min} required for successful trapping was used by Simpson et al. in this work,

$$Q_{axial} = \frac{c}{n_m P_{\min}}\left(\frac{\pi}{6}(\rho_s - \rho_m)d^3 g + \frac{2kT}{d}\right) \qquad (4.4).$$

Twenty measurements were taken for each combination of laser mode and sphere size, and for the TEM_{00} mode the measured values for Q_{axial} were in agreement with those of Felgner et al. (Felgner et al., 1995). However, the efficiency falls by

approximately one order of magnitude at a depth of 70 μm below the coverslip and it is suggested here and elsewhere that this is due to additional imaging aberrations introduced by increased thickness of fluid, leading to a reduction in the field gradient near the focus and a corresponding decrease in the trapping force. For 5 μm diameter spheres, which are significantly larger than the diameter of the laser mode, the use of an $l = 3$ LG mode resulted in the axial trapping efficiency being improved by a factor of two, when measured at both near the top and near the bottom of the sample cell. Little or no improvement was observed when l was increased further, however this was expected as most of the power in the $l = 3$ beam was already at the limit of the numerical aperture of the objective lens.

For smaller spheres (1 and 2 μm diameter) axial trapping was improved near the top of the cell, where aberrations are less, by a factor of two, however, at the bottom of the sample cell optical tweezers using the Laguerre-Gaussian mode exhibit reduced axial trapping efficiency. This can be explained as the diameter of the spheres in this case was comparable with the region of zero on axis intensity in the mode. The aberrations at large cell depths mean that the form of the LG mode may not be sufficiently maintained to trap such small particles on the beam axis.

4.2.2 Axial and lateral trapping in inverted optical tweezers

O'Neil et al. measured axial and trapping forces in an inverted geometry (O'Neil et al., 2001) as more applications, in biomedicine for example, use inverted tweezers in which the trapping beam is directed upwards to the underside of the sample cell. Computer generated holograms were used to produce $l = 2$ and $l = 3$ modes and the undiffracted zero order beam was used as the TEM_{00} Gaussian beam. Particles used were 1.1, 2 and 5 μm diameter silica spheres suspended in water. Trapping efficiency was calculated by measuring the maximum speed at which particles could be moved and relating that to the calculated drag force F_{Stokes} acting on particles moving through the viscous fluid and equating this to equation 4.1.

The force acting on the particle due to gravity and scattering is small compared to the drag force so can be ignored here. The measured *Q* values of the group using the fundamental, Gaussian TEM_{00} mode fall within the range reported by other groups. Laguerre-Gaussian modes improve axial trapping but do not noticeably alter the lateral trapping efficiency. The improvement in axial trapping is only realised when the 2 and 5 μm diameter spheres are used, for 1.1 μm diameter spheres the LG beam is less effective, due to the small size of the spheres not interacting with the whole cross section of the beam, with an $l = 3$ beam performing worse than an $l = 2$ beam. The group calculated *Q* values for rays at different numerical apertures by applying Snell's law at the sphere-fluid interface and found that off-axis rays provide significantly greater axial trapping than on-axis rays, but all rays provide similar levels of lateral trapping. In summary, for spheres that are larger than the focused beam size, the use of a high-order Laguerre-Gaussian mode improves the axial trapping efficiency of optical tweezers but there is no improvement in lateral trapping.

4.3 Experiment for axial and lateral trapping efficiency measurements

A standard tweezers set up was used to measure the axial and lateral trapping efficiencies of an $l = 1$ LG beam. The laser used to produce the trapping beam was a 1.5 W Nd: YAG laser with a wavelength of 1064 nm. To create the LG mode, the beam was passed through a computer generated hologram with the first order diffracted beam having an azimuthal index of 1. The beam is passed through conjugate lenses before being directed into the objective, slightly overfilling the back aperture to ensure off axis rays come in at a wide angle for maximum axial trapping efficiency. 2 μm silica spheres suspended in water are sealed in a sample chamber consisting of a 100 μm deep well on a microscope slide with a coverslip placed on top. The sample is placed on a xyz translation stage which can be manipulated using a programmable motion controller (Newport) so that speed, acceleration and distances can be defined and easily repeated.

For our measurements, spheres are picked up from the bottom surface of the sample chamber by focusing slightly below the sphere then slowly lifting it 20 μm from the surface. The particle is repeatedly moved from side to side for lateral trapping measurements or up and down for axial measurements. The maximum speed that a particle can be manipulated without falling out of the trap is measured, and this is repeated with ten different spheres. The drag force acting on the particles moving through the viscous fluid is calculated using the measured maximum velocity (eq. 4.2). The drag force and the laser power at the sample are then used in equation 4.1 to calculate the *Q* value. We estimate that the microscope objective transmits 50% of 1064 nm wavelength light and measure the power immediately before the beam goes into the rear aperture of the objective.

4.4 Results of lateral and axial trapping using an $l = 1$ LG mode

Lateral trapping efficiency was measured and calculated by Paul Prentice and axial trapping experiments and calculations were performed by Lynn Paterson.

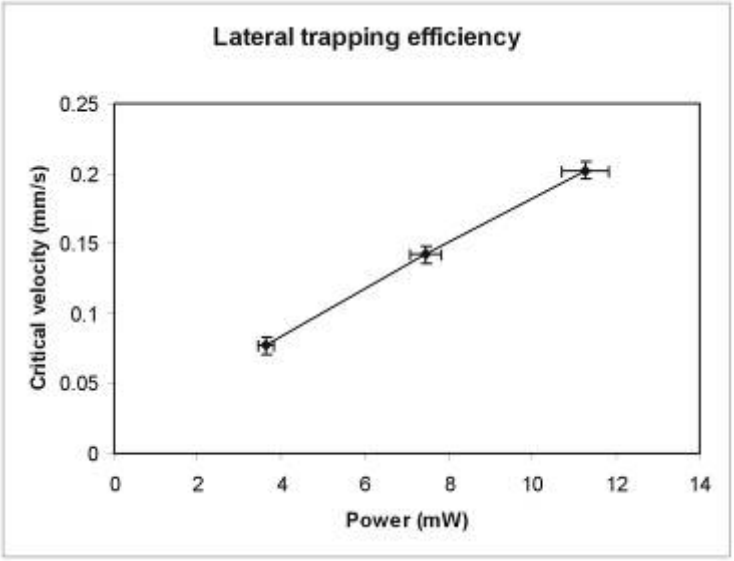

Figure 4.1: Lateral trapping results showing the power of the trap at the sample against the horizontal velocity reached before the particle fell out of the trap.

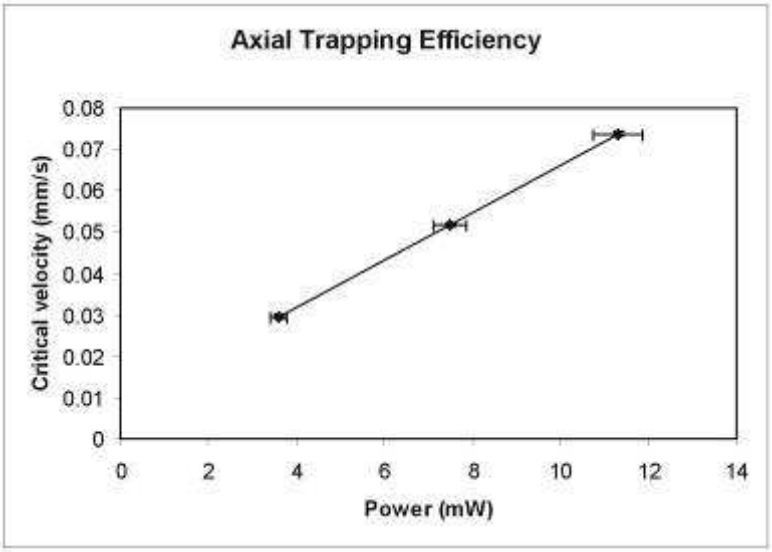

Figure 4.2: Axial trapping results showing the power of the laser trap at the sample against the vertical velocity reached before the particle fell out of the trap.

In both these graphs the error in the y-axis is taken from the measured critical velocities (the maximum value minus the minimum value divided by the number of measurements) and the error in the x-axis is an estimated percentage error (5%) of the measured power.

4.4.1 Q values for lateral and axial trapping in an l = 1 LG beam

Using equation 4.2, F_{Stokes} can be calculated for lateral and trapping results, using the values viscosity of water η = 1 x 10^3 $kgm^{-1}s^{-1}$, diameter of particle d = 2 μm and the measured velocity, v for different powers used.

Substituting this into equation 4.1 we can calculate the Q value of the trap using laser power, P, speed of light, c = 3 x 10^8 ms^{-1} and the refractive index of water n = 1.33.

P/mW	v axial (m/s)	v lateral (m/s)	F-axial drag (N)	F-lateral drag (N)	Q-axial	Q-lateral
3.6	2.96E-05	7.70E-05	5.58E-13	1.45E-12	0.035	0.091
7.5	5.18E-05	1.42E-04	9.76E-13	2.68E-12	0.029	0.081
11.3	7.38E-05	2.02E-04	1.39E-12	3.81E-12	0.028	0.076
					0.031	0.082
				error	0.002	0.005

Table 4.1: *Q* values for axial and lateral trapping with an $l = 1$ LG beam calculated using the power measured and the maximum speed of the trapped particles.

The final value for *Q* is the average of the values for the three powers used in the experiment, which is 0.031 ± 0.002 for trapping in the axial direction and 0.082 ± 0.005 for lateral trapping with an $l = 1$ Laguerre-Gaussian mode. The error has been calculated by taking the minimum *Q* value from the maximum *Q* value and dividing by three (the number of values for *Q* that we have calculated).

4.5 Discussion

As mentioned previously, Q_{axial} in standard optical tweezers using a TEM_{00} mode is usually an order of magnitude smaller than $Q_{lateral}$. In our work, using an $l = 1$ LG beam in a standard configuration, the value of Q_{axial} is still much less that $Q_{lateral}$ but the gap between the sizes of the two trapping forces has been reduced. This is due to the reduction of on-axis rays which are present in a Gaussian beam but not in LG beams and results in the loss of scattering force which acts in addition to the force of gravity in standard TEM_{00} optical tweezers against the axial trapping force.

Table 4.2 shows how the *Q* values calculated by other groups compare, as a ratio, to our calculated value for axial and lateral trapping with an $l = 1$ LG beam. Trapped particles were all 2 μm in diameter, however the refractive index of the particles and the microscope objectives used differ between the groups. Comparing *Q* values within one experiment is more useful than between experiments performed by different groups.

Author	TEM00		*l* =1		*l* = 2		*l* = 3	
	Qaxial	Qlateral	Qaxial	Qlateral	Qaxial	Qlateral	Qaxial	Qlateral
Felgner (2)	0.19	2.74						
		6.77						
	0.65	4.52						
	2							
Simpson (5)	2.13						3.23	
	0.28						0.13	
O'Neil (6)	1.94	2.18			3.02	2.24	4.69	1.87
Malagnino (1)		1.41						
		1.93						
Paterson			1	2.65				

Table 4.2: Ratios of trapping efficiency values calculated by various groups using 2 μm diameter spheres, with our calculated value for Q_{axial} taken as 1.

O'Neil et al (O'Neil et al., 2001) found that the Q value for lateral trapping in inverted tweezers did not change when using different modes however axial trapping efficiency did improve for spheres of 2 μm in diameter (and also for 5 μm diameter spheres but not as much, but axial trapping did not improve for 1.1 μm spheres). Our calculated value for $Q_{lateral}$ is higher than O'Neil et al. however our axial value is not as large, but that can be easily explained. Their setup was inverted so there would be some scattering force present acting against gravity (although much less when the LG beams were used). We also use an l = 1 beam which is predicted to not give as strong an axial trapping force as higher l, which they use. We can conclude by saying that in most standard optical tweezers, lateral trapping is an order of magnitude stronger than axial trapping with a TEM_{00} mode (Felgner et al., 1995) and with an l = 1 LG mode this difference in trapping force between Q_{axial} and $Q_{lateral}$ is reduced by increasing the value of Q_{axial}.

References

Felgner H, Muller O, Schliwa M: **Calibration of Light Forces in Optical Tweezers.** *Applied Optics* 1995; **34**:977-982.

Friese MEJ, Rubinsztein-Dunlop H, Heckenberg NR, Dearden EW: **Determination of the force constant of a single-beam gradient trap by measurement of backscattered light.** *Applied Optics* 1996; **35**:7112-7116.

Malagnino N, Pesce G, Sasso A, Arimondo E: **Measurements of trapping efficiency and stiffness in optical tweezers.** *Optics Communications* 2002; **214**:15-24.

O'Neill AT, Padgett MJ: **Axial and lateral trapping efficiency of Laguerre-Gaussian modes in inverted optical tweezers.** *Optics Communications* 2001; **193**:45-50.

Sato S, Inaba H: **Optical trapping and manipulation of microscopic particles and biological cells by laser beams.** *Optical and Quantum Electronics* 1996; **28**:1-16.

Simpson NB, Allen L, Padgett MJ: **Optical tweezers and optical spanners with Laguerre-Gaussian modes.** *Journal of Modern Optics* 1996; **43**:2485-2491.

Simpson NB, McGloin D, Dholakia K, Allen L, Padgett MJ: **Optical tweezers with increased axial trapping efficiency.** *Journal of Modern Optics* 1998; **45**:1943-1949.

5 Optical manipulation using interference fringes

5.1 Introduction

Particles of various shapes can be trapped in optical tweezers however when rod shaped particles, for example *E.coli* bacteria or glass rods (see Chapter 3), are trapped they tend to align in the direction of beam propagation (along the z-axis) (Ashkin et al., 1987). Gauthier et al. showed the alignment of cylindrical glass particles in an inverted optical tweezers configuration (Gauthier et al., 1999). If more than one spherical particle is trapped they often are observed to stack one above the other in the direction of beam propagation. Gauthier and Ashman have also predicted that stacking of spherical particles will occur in an optical trap along the axis of beam propagation (Gauthier and Ashman, 1998) and this has been discussed in chapter three also. Michael MacDonald and I have investigated novel ways in which to trap rod-like particles, which may include many biological specimens such as chromosomes, microtubules and rod shaped bacteria, in the x-y plane without the particle aligning in the z-direction. We can also trap arrays of high refractive index spheres in the x-y plane without stacking of the particles occurring. This is achieved using a pattern of interference fringes created at the focus of two interfering Gaussian beams. The particles can be manipulated by either moving the beam spot as a whole or by changing the path length in one of the arms of the interferometer so that the fringes are translated within the beam spot. In addition the pattern can be used to trap particles of low refractive index within the dark fringes. Particles of lower refractive index than the surrounding medium (such as bubbles) are repelled from the laser beam and travel down the light intensity gradient toward the region of lowest intensity, so this is a novel way to trap these particles (or highly reflective particles which are also repelled from the region of highest light intensity).

5.2 Interference fringes for trapping particles

Interference fringes for optical manipulation of low-index particles, rod-like particles and arrays of high- and/or low- index particles were created by interfering two plane wave Gaussian beams using a Mach-Zender interferometer. The experimental set up is illustrated below in figure 5.1.

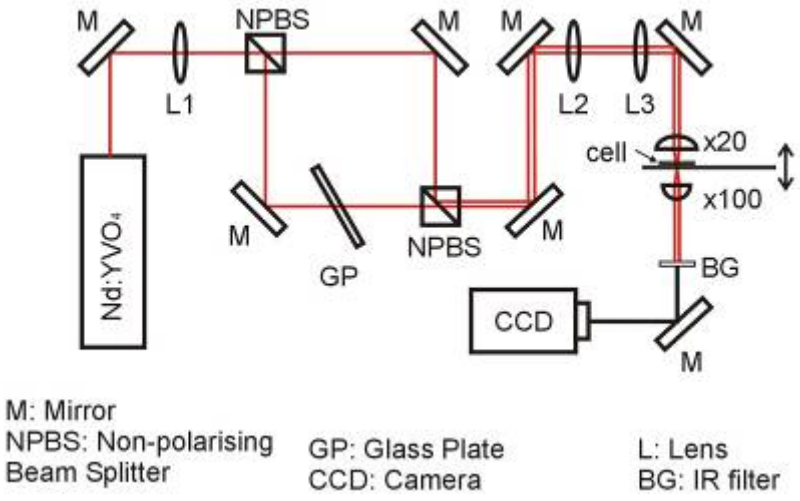

Figure 5.1: Experimental set-up for interferometric optical tweezers.

The interference fringes used for optical manipulation were produced as follows: The 500 mW collimated (by lens L1 = 750 mm) output from an Nd: YVO_4 (λ = 1064 nm) laser was split by a Mach-Zender interferometer. The beams were not recombined at the second beam splitter in the bottom right hand corner of the interferometer, but left slightly separated (and parallel to each other) until they reached the focus of the x20 microscope objective. The pattern could be moved around the sample by use of the beam steering mirror (the mirror which comes before the two lenses L2 and L3). Two lenses (L2 = 150 mm and L3 = 100 mm) form an image relay that gives a conjugate image of the spot on the beam steering mirror at the back focal plane of the x20 microscope objective. This image relay allowed the two beams to be moved without being clipped by the back aperture of

the x20 objective. These lenses could be used to obtain the desired spot size and collimation of the beam at the rear aperture of the objective. Tweezing was also demonstrated by the translation of the microscope stage on an xyz translation stage such that the sample would move relative to the focused spot.

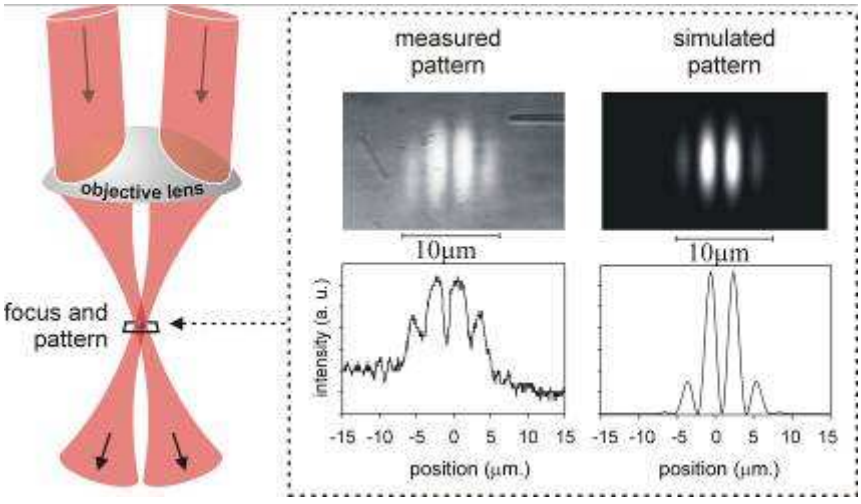

Figure 5.2: The two beams are directed separately through the x20 objective and for the fringe pattern at the focus inside the sample cell. The actual pattern and the ideal pattern (Mathematica simulation by Jochen Arlt) are shown.

Figure 5.2 shows how the two beams combine to form fringes, and the actual and ideal patterns made by the two beams at their focus. The two beams are sent into the back of the x20 objective in parallel but separated and the interference pattern is focused on the same plane in which the particles to be manipulated are situated. The fringe spacing was varied by adjusting the position of the mirror in the bottom left hand corner of the interferometer thereby varying the distance between the two parallel beams as they enter the back aperture of the microscope objective. Adjusting the separation of the beams changed the angle at which they came through the objective and hence changed the pitch of the pattern.

The interference fringes could be swept across the beam spot without the beam itself moving by inducing a change in the optical path length of one of the interfering Gaussian beams. This was achieved by tilting a glass plate in one of the arms of the

interferometer. As the plate was tilted in the beam, the optical path length was changed. This action resulted in a phase shift between the two beams and manifests itself as the fringes sweeping across the beam spot. In addition the complete pattern could easily be moved by tilting the beam steering mirror or by shifting the translation stage.

5.3 Trapping arrays of high index spheres

Initially, multiple 1 μm diameter high refractive index silica spheres were aligned in the interference pattern. The spheres are located at the bottom of the sample cell as they sink due to gravity, and they are arranged into lines in the x-y plane along the bright fringes and could be easily manipulated as whole chains. The aligned spheres could be swept across the pattern by scanning the fringes or they could be moved around the sample cell using the steering mirror to move the whole beam spot without losing their alignment to the bright fringes of the pattern. Figure 5.3 shows 1 μm diameter spheres trapped in the fringes and swept across the beam spot.

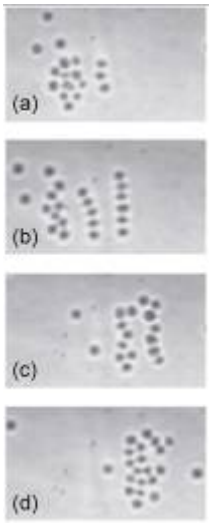

Figure 5.3: One micron high-index silica spheres aligned in the bright fringes of an interference pattern between two Gaussian beams. The fringes are scanned from left

to right and the trapped particles follow the fringes and are collected at the right hand side of the beam spot (d).

If many spheres were swept to the edge of the pattern of fringes, they would bounce back in as the bright fringes approached the edge of the pattern because they are attracted back into the outermost bright fringe, and they keep striking back as long as the fringes keep on sweeping. As many as ten spheres would align in each fringe with the spheres being aligned more regularly and trapped more strongly when the width of the fringes was 1.5 – 3 μm.

5.4 Aligning and manipulating rod shaped particles

The ability to manipulate rod-like particles is of particular use in biology, where many such structures exist, for example chromosomes, microtubules and certain species of bacteria. Tailored patterns such as our interference fringes could perhaps be used to align and sort chromosomes or deliver them in ordered, aligned patterns to a substrate for analysis. For example in fluorescent *in situ* hybridisation experiments metaphase chromosomes are often overlapping and it is difficult to resolve which chromosomes have been labelled.

In our experiments we have used microscopic sized glass rods (made in house by our glass blower, Fritz Akerboom) which range in length from around 2 μm to 250 μm and in diameter from 1 μm to 5 μm. Figure 5.4 shows a single 5μm long, 1 μm wide glass rod suspended in water aligning with a bright fringe and being tweezed in the x-direction by moving the beam spot using the beam steering mirror.

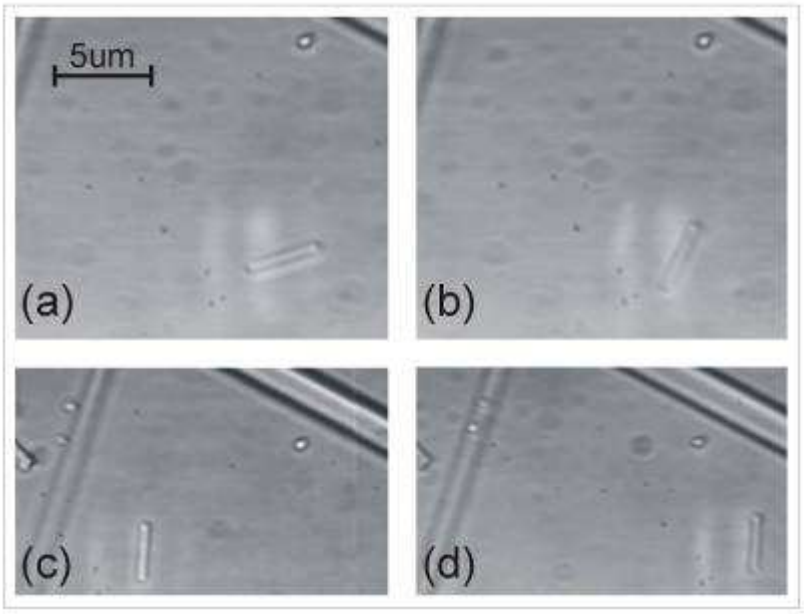

Figure 5.4: Alignment of a 5 μm long glass rod (a-b), and tweezing in the x-direction (c-d).

The same glass rod can be seen in figure 5.5 trapped in a bright fringe which is both tweezed and swept across the beam spot simultaneously. The sample stage was translated in the x direction, moving the whole sample relative to the beam spot, and the fringes in the beam spot were swept across its diameter by tilting a glass plate, situated in one arm of the interferometer.

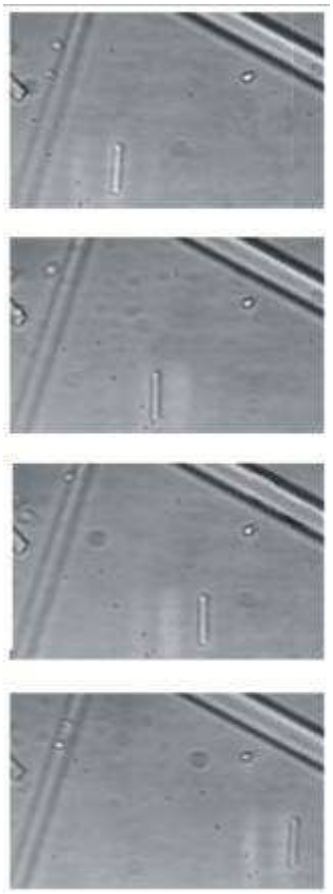

Figure 5.5: Manipulating a 5 μm long glass rod by moving the whole beam spot and sweeping the fringes simultaneously.

The smallest rod that could be aligned in this manner was approximately 1.5 μm in length. We have aligned a rod 250 μm in length in an inverted Gaussian beam optical tweezer along the direction of beam propagation (see chapter 4) however the longest rod we could align in the x-y plane in this pattern was 30 μm. The upper limit to the size of the rods aligned was governed by the available power.

We aligned a 20 μm long rod and then manipulated it by scanning the fringes of the pattern. This can be seen in figure 5.6, with A-C showing the gradual alignment (smaller rods align much more rapidly) of the rod and D-E shows the sweeping of the fringes and the trapped rod from left to right and back again.

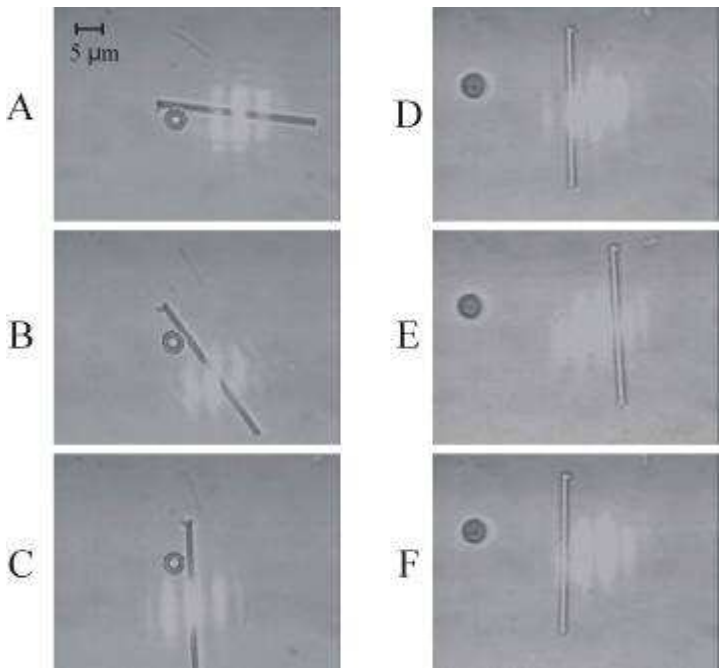

Figure 5.6: Alignment and manipulation in the x-y plane of a 20 µm long glass rod.

The interference pattern was also used to trap three short rods of around 5 µm in length in each of the bright fringes and this is shown in figure 5.7. The interference pattern with the rods beginning to align can be seen in 5.7A and the rod on the right hand side can be seen to jump from the right most bright fringe to the slightly brighter one to the left of it in 5.7B and C. The group of three rods is then translated to the right (5.7D) and then towards the sphere located at the top of the picture (5.7E).

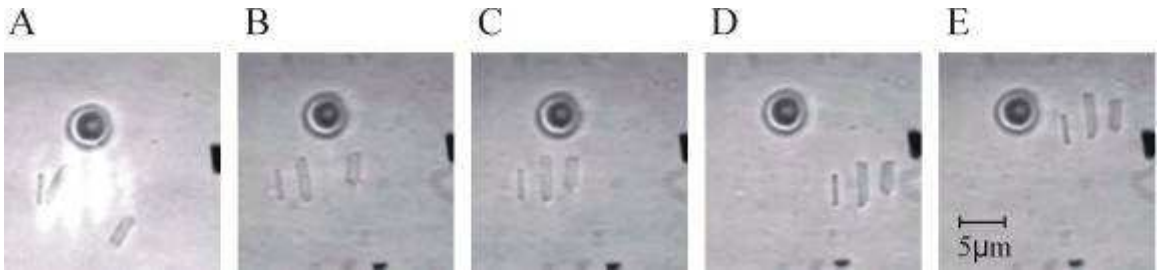

Figure 5.7: Simultaneous alignment and manipulation of three 5 µm long rods.

Tweezing and alignment of rods was achieved at a power of 120 mW, although alignment could be achieved at powers as low as 30 mW. The same interference pattern was also used to trap and manipulate particles of lower refractive index than their surrounding medium by holding the 'bubbles' in the dark regions between bright fringes of the pattern. Low- index particles are drawn into regions of low light intensity in a similar manner to the way high index particles are drawn into the regions of high intensity. The following section describes the trapping of low refractive index particles.

5.5 Low refractive index particles

There has been recent interest in the trapping of particles of lower refractive index (n_p) compared to their surrounding medium (n_m) (Gahagan and Swartzlander, 1998) as these can be, for example, air bubbles in any medium such as water or oil. In a typical Gaussian single beam optical trap, such as that used to trap high index particles, more light is refracted through the particle away from the region of highest light intensity (figure 5.8A) so the particle is forced into the region of highest light intensity. On the other hand, if a low index particle is in the vicinity of a focused laser beam the transverse component of the force exerted on the particle tends to push the low index particle out of the beam towards lower intensity regions (figure 5.8B), the opposite of what happens to high-index particles.

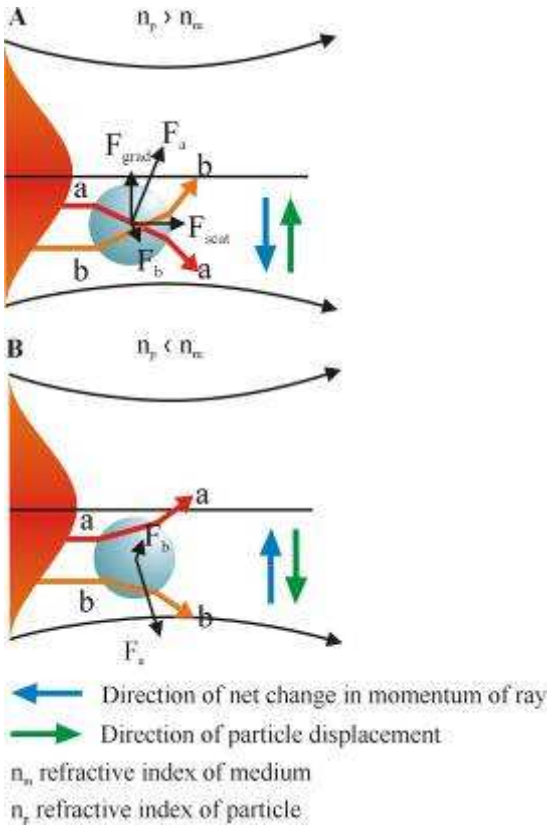

Figure 5.8: Ray optics for high- and low- index particles. A. The refraction of light from a Gaussian beam through an object with a higher refractive index than the surrounding medium ($n_p > n_m$) results in the particle being drawn into the region of highest light intensity. B. An object with lower refractive index than its surroundings ($n_p < n_m$) is pushed out of the beam.

Micro bubbles in a medium of higher refractive index have been trapped using a Gaussian beam in conjunction with the fluid force of the ethanol medium (Lu et al., 2000). The medium is heated non-uniformly by absorbing some of the laser radiation and as a result convection occurs in the medium in the region of the laser beam, symmetric with the beam axis. This convection of the medium acts as a micro fountain which can be used to assist in trapping of the micro bubble. Without the fluid force, the laser beam alone could not trap the bubble thus the fluid force and the light pressure force act together as a hybrid trap for bubbles. In contrast with the light pressure force, the transverse fluid force is centripetal and tends to draw the

micro-bubble into the light beam. The bubbles can be trapped either at the rim of the beam if the beam is focused above the bubble and the bubble diameter is smaller than the beam spot or in the centre of the beam if the focus is very close to the bubble. If the beam is travelling upward through the sample the bubble will float on the surface of the liquid because of the buoyancy force, the axial light pressure force and the axial fluid force all point upwards. If the beam is directed down into the sample, the axial light pressure force points downwards and can overcome the buoyancy force and the axial fluid force so pushes the micro bubble into the medium until an equilibrium position is reached. Particles with a high reflection coefficient at the wavelength of an incident laser beam such as metallic particles also experience the repulsive force analogous to those with a lower refractive index than the surrounding medium. Low-index particles are of interest in many areas of science and engineering in which the properties and effects of bubbles are investigated, for example in the food, drink, drug and petroleum industries where low-index particles might be bubbles of air in water or bubbles of water in oil. Multiphase emulsions contain low- and high-index 'particles' and these could be investigated if there was a technique to trap both low- and high-index particles simultaneously. An emerging technique for gene transfection, called sonoporation, uses the properties of cavitating bubbles (air filled protein bubbles) to create transient pores in the membrane of cells through which DNA can get into the cell. The properties and dynamics of these bubbles may be explored if one could hold them in a trap or manipulate them in three dimensions.

5.5.1 Previous methods of trapping low-index spheres

Schemes which have already proven useful for trapping and manipulating low-index particles include the use of a hybrid trap mentioned above which uses the optical force of a Gaussian beam and the fountain-like fluid force caused by convection of the heated medium (Lu et al., 2000) or a scanning Gaussian beam (Sasaki et al., 1992), in which a Gaussian beam, orbiting at ~25Hz, cages a metal particle in water

or a water droplet in liquid paraffin due to repulsive forces from all directions confining the particle or bubble in one place. The circular scanning of the laser creates a potential well and if the repetitive scan rate of the laser beam is faster than particle diffusion, the particle or droplet will be confined in the time-averaged potential well. Axial trapping of low-index particles can occur using a TEM_{00} non-scanning laser if the objects are fabricated into ring-like shapes (Higurashi et al., 1995). When the laser light is focused near the centre of the object radiation pressure exerts a force on the inner walls of these objects. Incident laser light strikes the inner wall and exits from the bottom. The ring shaped object acts as a weak positive lens and the object is pulled towards the laser focal point. If the object is displaced axially in the direction of the incident light, the divergence of the resulting refracted light increases so that the net force is once again directed towards the laser focal point. Transverse trapping occurs because the total radiation pressure exerted on the inner wall of the object is directed towards the laser beam axis. If the object moves laterally, it experiences increased repulsive radiation pressure towards the laser beam axis, driving it back towards the centre. Another method is to use an optical vortex beam (Gahagan and Swartzlander, 1996, Gahagan and Swartzlander, 1998), either the TEM_{01}* mode of a laser or a beam produced using a computer-generated hologram. Optical vortex beams can trap individual low-index particles in the dark core of the optical vortex at a point located on the optical axis at a distance of 2 to 3 times the particle radius before the beam focus. The location of the trapped particle and the trapping efficiency depends on several parameters, such as the width of the vortex core, the NA of the focusing objective, and the relative refractive index between the particle and the medium (Gahagan and Swartzlander, 1996). These optical vortices can also trap a high index sphere simultaneously in the axial direction near the focus of the beam (Gahagan and Swartzlander, 1998). This permits the ability to produce arrays of trapped high- and low-index spheres or manipulate them simultaneously in the horizontal plane.

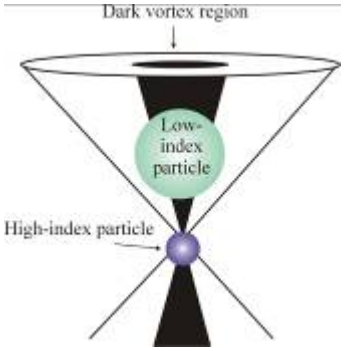

Figure 5.9: Illustration of a low- and high-index particle simultaneously trapped in a Laguerre-Gaussian beam. Adapted from Gahagan, K. T. and G. A. Swartzlander (1999). "Simultaneous trapping of low-index and high-index microparticles observed with an optical-vortex trap." Journal of the Optical Society of America B-Optical Physics 16(4): 533-537.

The low index particle is trapped before the focus in the dark region of the beam and the high index particle is located below the low-index particle at the region of highest light intensity. The authors found that near the top of the sample cell the high-index particle was more stably trapped than the low index one because the low index particle scatters 20% of the light and only slightly reduces the trapping efficiency for the high-index particle because the large angle rays are not scattered so they can go on to focus and trap the high-index particle. Deeper in the sample chamber, aberrations caused by the glass- water interface cause non paraxial rays to focus closer to the coverslip than paraxial rays. This astigmatism is minimal when the beam is focused just below the coverslip and the gradient forces on a trapped high-index particle are optimal, but lower in the sample chamber the non paraxial rays converge at points above the focal plane. In addition, at this depth some paraxial rays will be scattered by the low index particle, further weakening the high index particle trap. In our work, Michael MacDonald and I have trapped low index spheres in a Laguerre-Gaussian beam however the particle is always trapped in the vortex region below the focus. This is because the spheres are buoyant and settle at the top of the sample cell. The repulsive force surrounding the sphere from the conical shaped vortex from above pushes the sphere down from the surface of the

sample chamber and it reaches an equilibrium position when the scattering and refractive radiation pressure balances buoyancy.

We have developed a novel method for trapping low index particles which is based on work carried out in 1997 by Chiou et al. (Chiou et al., 1997) which used bright fringes of an interference pattern between two Gaussian beams to trap high index particles. Once a particle was trapped in a bright fringe within the two beam interference pattern the pattern of fringes, and therefore the particle could be moved in a direction normal to the fringes themselves within the laser spot by sweeping the fringes via the translation of a mirror in a Michelson interferometer. The number and size of fringes in the beam spot could be changed by adjusting the spatial separation of the two parallel incident beams. By adjusting the separation of the beams, the angle at which the two beams exit the microscope objective and interfere with each other is altered, thus the pitch of the pattern can be changed. Another method for creating a similar pattern of bright fringes was to project a reduced image of a Ronchi ruling at the focal plane of the microscope objective. The ruling (250 line-pairs per inch, reported in the publication) was illuminated with a single beam and the fringes were shifted by translating the Ronchi ruling perpendicular to the direction of beam propagation and perpendicular to the rulings themselves. During the course of my research the use of interference fringes to manipulate rod-like particles in the bright fringes of the pattern, low-index particles in the dark fringes and arrays of high- and low- index particles in the light and dark fringes respectively has been demonstrated for the first time (MacDonald et al., 2001).

5.5.2 Trapping Low-index particles

Low-index spheres (hollow glass spheres) were first repelled from the beam by slowly moving the pattern from the side towards the sphere. This showed that they were indeed low-index particles as high-index particles would become trapped in the bright region. As mentioned above, optical vortex beams, which consist of a ring of light with a dark centre, can trap low-index particles. Contained within a set of

bright interference fringes is a set of dark interference fringes that can be used to attract low-index (or highly reflective) particles. The particles are trapped in a similar fashion to optical vortex trapping or, indeed the use of a scanning Gaussian beam by surrounding the particle in a dark region with light. We would expect low-index spheres to align with the dark fringes of an interference pattern similar to the high index particles aligning in the bright fringes in figure 5.3. A 4 μm hollow glass sphere was trapped in the dark region between the bright fringes by blocking the beam until it was positioned over the sphere. Although the fringes were brighter in the centre of the spot due to the Gaussian amplitude profile of the interfering beams this increased brightness did not lead to a trapped hollow sphere falling out along the line of a dark fringe. This was because the spheres that were being trapped were slightly larger than the width of the dark fringes, leading to rings of light that were centred on the spheres. These rings can be seen in Figure 5.10 and are as a result of scattering and diffraction of light by the edges of the sphere. This scattering and diffraction led to a confinement of the sphere between the dark fringes in a manner similar to the trapping of low-index particles in a Laguerre-Gaussian beam (Gahagan and Swartzlander, 1996, Gahagan and Swartzlander, 1998) or in a scanning Gaussian beam (Sasaki et al., 1992) by repelling the particle from all around, in the x-y plane. An additional, although much weaker, contribution to this confinement was the Airy rings produced by the optics of the system.

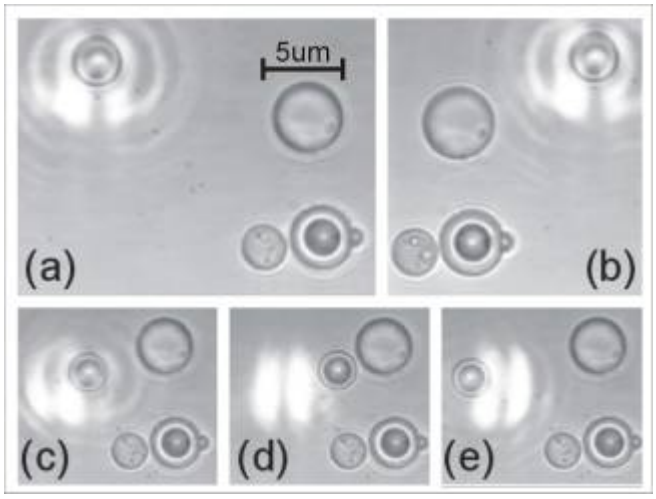

Figure 5.10: Manipulation of a low-index sphere. Tweezing in the x-direction (a-b), tilting of the glass slide causes the fringes to be swept to the right and then back to the left of the beam spot. The trapped, low-index sphere follows the movement of the fringes (c-e).

A hollow (air filled) glass sphere could be manipulated in the x and y directions (Figure 5.10 (a-c)) with tweezing strongest in the direction perpendicular to the fringes. Tweezing in the direction parallel to the fringes was also possible due to the diffraction effects described above, however, if spheres did not overlap with the bright fringes they would fall out of the trap when tweezed in the that direction. Figure 5.10 (c-e) shows the sphere being swept across the beam spot to the right, then back to the left, by changing the path length of one of the beams using the tilting glass plate in one of the arms of the interferometer. Sweeping of the fringes led to the sphere's being pushed to the side of the pattern just as it did with solid spheres, but in this case the hollow spheres bounced back into the pattern as dark fringes approached the edge of the spot (again as if attracted to the dark areas). For small hollow spheres (< 2 μm) the ratio of shell thickness to diameter is large so they no longer behave as low-index particles and are attracted to bright fringes, as solid high refractive index spheres are. However, a large hollow structure (> 10 μm) fails to detect the structure of the pattern and acts as if the beam is homogenous and the particle is repelled (figure 5.11). This behaviour can be overcome if the spacing of

the fringes in the pattern is changed, which can be implemented by changing the separation of the parallel beams that are directed into the microscope objective.

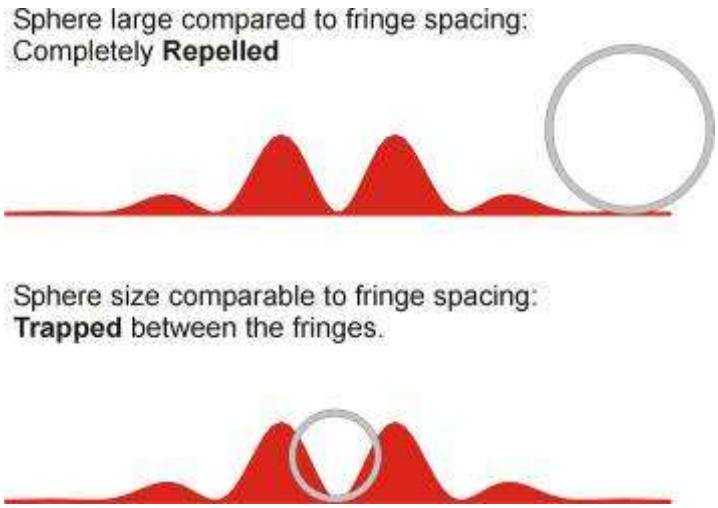

Figure 5.11: Fringe spacing determines if the low index particle is repelled, trapped in two dimensions or trapped in one dimension.

If the low index particle is smaller than the spacing of the dark fringes it will be trapped in the x-direction but will fall out of the trap when it is translated in the y-direction as the rings created by scattering (which add to trapping strength in the y direction) are not created. It is also necessary that the refractive index of the centre of the hollow sphere be less than $n = 1.33$ when the sphere is in water. The hollow sphere filled with air ($n = 1$) that is shown in figure 5.10 had a low enough shell thickness/ diameter ratio to behave as a normal low-index particle, as demonstrated by its repulsion from the pattern if the beam approached it slowly from the side on which the beam would push the sphere away instead of tweezing it.

5.5.3 Trapping arrays of low-index and high index particles

In the same manner as multiple high index particles will be drawn into the bright fringes, multiple low refractive index particles are expected to be drawn into the dark

fringes of the pattern. In this way arrays of low-index spheres can be made for the first time, where the negative image of any beam that was used to obtain an array of high-index particles can be used to reproduce the same pattern with low-index particles.

This ability was demonstrated by the alignment of two hollow spheres in adjacent dark fringes and their manipulation in unison as shown in figure 5.12.

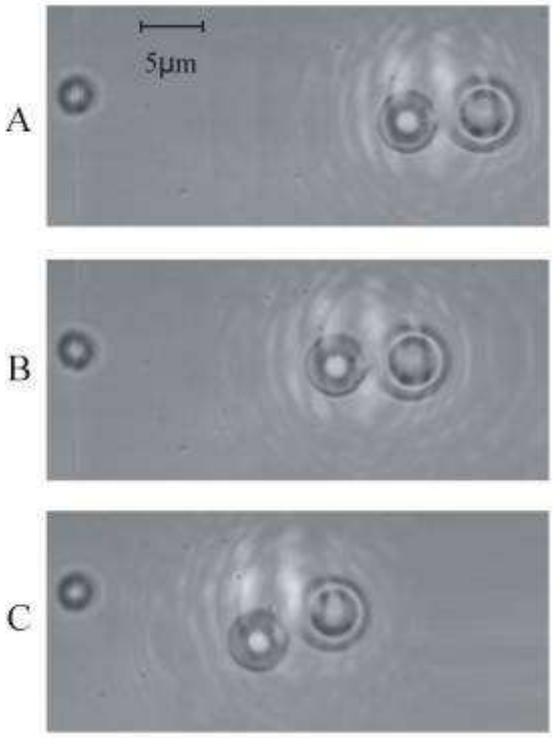

Figure 5.12: Manipulation of two low-index spheres in the dark fringes of an interference pattern between two Gaussian beams.

The two low refractive index spheres are each in a dark fringe of the interference pattern. The pattern is translated in the y direction past another sphere which is stationary. Both spheres overlap into the adjacent bright fringes and scattered light from the bright fringes which they impinge on create bright circles centred on the spheres themselves. This assists trapping and allows the spheres to be manipulated in the y-direction without falling through the trap. The two spheres are too large to

remain aligned with each other in the x-direction and it can be seen in 5.12C that the smaller of the two spheres has been slightly pushed out of position.

A single high-index sphere was also aligned in the centre of a bright fringe with hollow spheres trapped in dark fringes, one on either side of it, forming a line of three particles which can be manipulated in the x and y directions and can be seen in figure 5.13 manipulated past a stationary sphere.

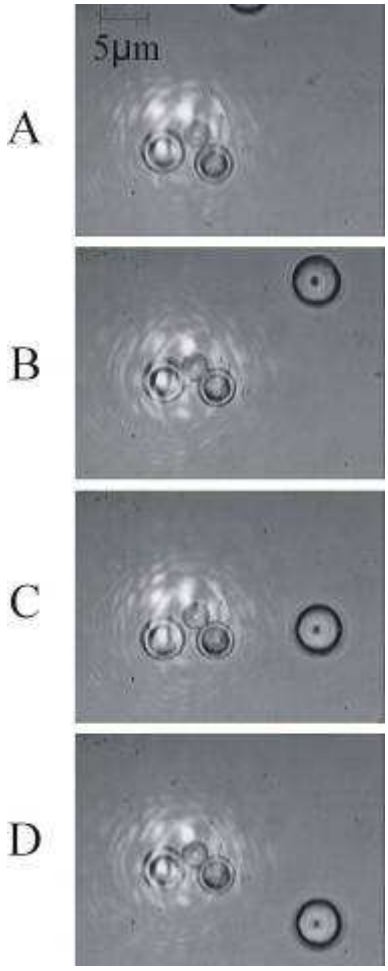

Figure 5.13: Low- and high-index sphere array. The high-index sphere is trapped in the bright fringe in the middle, low-index spheres are on either side in the dark fringes.

In this case the buoyant low-index particles are pushed down to the focal plane as the high-index particles by radiation pressure. High-index glass rods and low-index spheres were also aligned and manipulated simultaneously in the x-y plane which to our knowledge is not possible using an optical vortex beam (although it may be possible to align and manipulate a hollow sphere and a very short rod in the direction of beam propagation as in figure 5.9).

The power is obtained from the total of the two beams measured at the back of the x20 objective. Z-trapping was not achieved using this technique as a x20 objective had to be used to ensure a large spot size, hence the beam was not tightly enough focused to create the steep optical gradient required for a true, three-dimensional optical trap.

5.6 Pattern propagation and manipulation

A similar pattern of these fringes may be produced by imaging a Ronchi ruling into the sample however the pattern created by imaging an aperture will diffract and the form will quickly change as it propagates away from the focus due to interference within the diffracting pattern. Interference between the two Gaussian beams results in the pattern maintaining its intensity form over a much larger propagation distance. The pattern produced by the two interfering Gaussian beams propagates for more that 50 μm without changing form, however the pattern produced by imaging a Ronchi ruling is distorted only 15 μm after the focus, which could cause problems if z-trapping is required. Figure 5.14 shows Mathematica simulations of the propagation of an interference pattern and an imaged Ronchi ruling and the differences can be clearly seen.

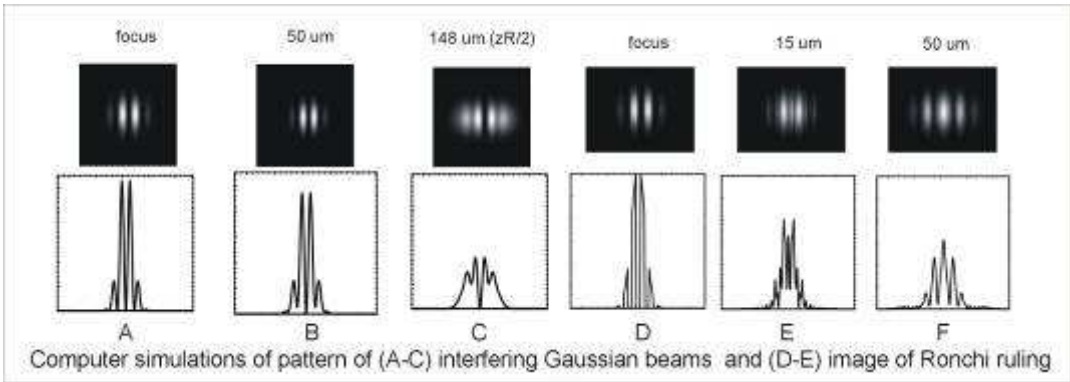

Figure 5.14: Mathematica simulations (by Jochen Arlt) of the pattern created by two interfering Gaussian beams and by making a reduced image of a Ronchi ruling. The interference pattern keeps its shape over 50 μm away from the focus (A-C), but the pattern created by imaging a Ronchi ruling does not propagate and becomes distorted at only 15 μm away from the focus (D-E).

5.7 Discussion

An interference pattern between two plane wave Gaussian beams of bright and dark fringes enables the generation of arrays of high-index, elongated and/or low-index particles to be created and manipulated in the horizontal plane for the first time. Importantly this can be easily implemented by splitting a Gaussian beam in two and interfering the two resulting beams at the focus of a microscope objective. The size and number of the fringes within the pattern can be readily adjusted and the fringes can be moved normal to themselves within the beam spot by changing the optical path length of one of the beam. We achieve this by simply tilting a glass plate in one of the arms of the interferometer. A drawback of this technique is that high- and low- refractive index particles cannot be independently manipulated using this technique.

In our work two dimensional trapping was achieved as the beam spot we needed was too large to allow sufficient tight focusing of the beam for three dimensional trapping. However, as the intensity form of the interference pattern propagates over

a large distance it may be possible to z-trap using a scheme such as this if the required spot size is smaller and a higher numerical aperture can be used.
This method may lead to the creation of two dimensional arrays of low refractive index particles such as bubbles, or to the construction of mixed phase arrays of high- and low-refractive index particles. Arrays of rod shaped particles can also be created such as groups of aligned glass cylinders for the construction of micro machines and in addition the technique could be extended to chromosome sorting for cytogenetic applications.

References

Ashkin A, Dziedzic JM, Yamane T: **Optical Trapping and Manipulation of Single Cells Using Infrared Laser Beams.** *Nature* 1987; **330**:769-771.

Chiou AE, Wang W, Sonek GJ, Hong J, Berns MW: **Interferometric optical tweezers.** *Optics Communications* 1997; **133**:7-10.

Gahagan KT, Swartzlander GA: **Optical vortex trapping of particles.** *Optics Letters* 1996; **21**:827-829.

Gahagan KT, Swartzlander GA: **Trapping of low-index microparticles in an optical vortex.** *Journal of the Optical Society of America B-Optical Physics* 1998; **15**:524-534.

Gahagan KT, Swartzlander GA: **Simultaneous trapping of low-index and high-index microparticles observed with an optical-vortex trap.** *Journal of the Optical Society of America B-Optical Physics* 1999; **16**:533-537.

Gauthier RC, Ashman M: **Simulated dynamic behaviour of single and multiple spheres in the trap region of focused laser beams.** *Applied Optics* 1998; **37**:6421-6431.

Gauthier RC, Ashman M, Grover CP: **Experimental confirmation of the optical-trapping properties of cylindrical objects.** *Applied Optics* 1999; **38**:4861-4869.

Higurashi E, Ohguchi O, Ukita H: **Optical Trapping of Low-Refractive-Index Microfabricated Objects Using Radiation Pressure Exerted on Their Inner Walls.** *Optics Letters* 1995; **20**:1931-1933.

Lu BL, Li YQ, Ni H, Wang YZ: **Laser-induced hybrid trap for micro-bubbles.** *Applied Physics B-Lasers and Optics* 2000; **71**:801-805.

MacDonald MP, Paterson L, Sibbett W, Dholakia K, Bryant PE: **Trapping and manipulation of low-index particles in a two-dimensional interferometric optical trap.** *Optics Letters* 2001; **26**:863-865.

Sasaki K, Koshioka M, Misawa H, Kitamura N, Masuhara H: **Optical Trapping of a Metal-Particle and a Water Droplet by a Scanning Laser-Beam.** *Applied Physics Letters* 1992; **60**:807-809.

6 Rotation of optically trapped particles in a revolving interference pattern

6.1 Introduction

The ability to controllably rotate microscopic particles in optical tweezers adds another level of manipulation to the translational motion already possible in a single beam optical trap. Particles can be made to spin in an optical trap by using three fundamental techniques. In the first of these general methods of rotation, radiation pressure exerted on a trapped particle due to an asymmetric scattering force can result in a torque on the particle which drives the rotation of the particle (Higurashi et al., 1994, Galadja., 2002a and 2002b). Secondly, angular momentum can be transferred to an absorbing particle (Friese et al., 1996; Simpson et al., 1997). Spin angular momentum can also be transferred to a birefringent particle (Friese et al., 1998; Moothoo et al., 2001) which makes it rotate or a birefringent particle in linearly polarised light can be rotated by rotating the direction of linear polarisation (Higurashi et al., 1998b). In addition, orbital angular momentum can be transferred by scattering from a trapped particle (O'Neil and Padgett, 2000; O'Neil et al., 2002a) and particle will orbit as opposed to spin around its own axis. Finally, a trapped particle can be rotated by using a moving trap, so that the particle will follow the motion of the trap as it is continually drawn to the region of highest intensity (Sato et al., 1991; O'Neil and Padgett, 2002).

These rotating particles could be used to drive micromachine elements such as micropumps and microstirrers for microfluidic devices, or used as instruments to measure torsional properties of objects such as biological polymers or to measure the viscosity of microscopic volumes, for example inside cells. The optical rotator has now joined optical tweezers and optical scissors in the optical tool kit and offers a further degree of non-contact control of trapped particles.

In previous chapters we have discussed the use of Gaussian beam and Laguerre-Gaussian beams for trapping of particles and also the use of an interference pattern between two Gaussian beams for aligning and manipulating rod-like particles and

arrays of low refractive index particles in the sample plane. This chapter describes the creation of a spiral shaped interference pattern between a Gaussian beam and a Laguerre-Gaussian. The pattern can be set into rotation and therefore induce the rotation of particles trapped within the pattern. Rotation using this method does not rely on intrinsic properties of the particle, merely the ability to be trapped. Previous methods used for particle rotation and their limitations are described in more detail below. The remainder of the chapter describes the generation, analysis and rotation of the interference patterns we have created including trapping results.

6.2 Methods for the rotation of optically trapped particles

6.2.1 Asymmetric scattering force

The scattering of light from the laser beam by a particle results in a force which can exert a torque on the particle and drive it into rotation, analogous to wind driving a windmill (Higurashi et al., 1994; Higurashi et al., 1997; Higurashi et al., 1998a; Galajda and Ormos, 2001; Galajda et al., 2002a; Galajda et al., 2002b; Omori et al., 1999; Luo et al., 2000). In this method the rotation of the particle is not a result of angular momentum transfer from the light to the particle, rather it is due to the radiation pressure, which acts on the particle, not being rotationally symmetric with respect to the beam axis. This lack of rotationally symmetric radiation pressure is due to the trapped particles having been microfabricated with an anisotropic shape (propeller or cog shaped). Microfabricated gear structures have also been designed and rotated due to a torque exerted by the scattering force in a dual counter-propagating beam trap (Gauthier et al., 2001).

6.2.2 Transfer of angular momentum

Light is known to possess both spin and orbital angular momentum. Spin angular momentum comes about due to the polarisation state of the photons in the beam.

Circularly polarised light possesses spin angular momentum of $\pm\sigma\hbar$ per photon, with σ= -1, +1 for right and left circularly polarised light, respectively. Orbital angular momentum comes from the helical form of the wavefronts of the beam. Laguerre-Gaussian (LG) beams possess orbital angular momentum of $l\hbar$ per photon due to the azimuthal phase of these beams (l is the azimuthal index of the beam). LG beams with $l \neq 0$ have a helical phase structure and as such, the Poynting vector follows a corkscrew-like path (Allen et al., 1992). The spin and orbital angular momentum of a light beam can be added to give the total angular momentum of $(l + \sigma)\hbar$ per photon.

6.2.2.1 Absorption

Absorption of beams possessing spin and/or orbital angular momentum by a trapped particle results in the transfer of angular momentum to the particle, and as a result the particle will rotate. For example, an absorptive ceramic or metal oxide particle trapped in the dark central region of a Laguerre-Gaussian beam was set into rotation in the same direction as the sense of the helical beam and it reversed direction of rotation when the helicity of the beam was reversed (He et al., 1995). The speed of particle rotation in this study was between 1 and 10 Hz depending on the size and shape of the objects and the laser beam used was linearly polarised so the rotation originated from the orbital angular momentum associated with the helical wave-front structure. Rotation frequency of absorptive particles trapped in an LG beam can be increased or decreased by changing the polarisation of the trapping LG beam as spin angular momentum is introduced into the light (Friese et al., 1996; Simpson et al., 1997). Orbital angular momentum is distinct from spin angular momentum but both can be transferred to particles by absorption.

A trapped particle will rotate faster if the beam is changed from linearly to circularly polarised with spin of the same sense as the helicity of the LG mode and slower if the beam is changed to a circular polarisation with spin of the opposite sense to that of the helicity. This mechanism to rotate micro objects has been dubbed the optical spanner (Simpson et al., 1996). Weakly absorbing dielectric particles such as BG38

glass and Teflon spheres were held in a three dimensional trap and were seen to rotate while being simultaneously manipulated in three dimensions. The usefulness of this method for rotating particles depends on the particle being transparent enough to allow tweezing to occur and also being suitably absorbent to allow angular momentum to be transferred, thus has limitations. Another method to rotate trapped birefringent particles using intrinsic angular momentum is described next.

6.2.2.2 Birefringence

Circularly polarised light possesses spin angular momentum of $\pm\sigma\hbar$ per photon. In 1936, Beth observed a torque on a suspended birefringent quartz wave-plate caused by a change in polarisation of the transmitted circularly polarised light (Beth, 1936). This torque caused by the passage of circularly polarised light through a birefringent material has been observed at the microscopic level when birefringent particles, that have been trapped using optical tweezers with a polarised light beam, spin around their axis (Friese et al., 1998; Moothoo et al., 2001).

A birefringent particle, for instance calcite, has two principle indices of refraction and it is the difference between these refractive indices that gives the birefringence. The ordinary and extraordinary rays of a light beam each see a different refractive index of the particle and undergo a relative phase shift on passage through the birefringent material. This may result in a change of angular momentum carried by the beam as the rays exit the particle and due to conservation of momentum a corresponding torque will be exerted on the birefringent particle.

Irregular samples of crushed calcite can be rotated at rates of a few hundred hertz using this scheme (Friese et al., 1998).

In linearly polarised light a birefringent particle will align with the axis of polarisation (Higurashi et al., 1998b; Higurashi et al., 1999). The half-wave plate used to create the linearly polarised light can be rotated in the beam axis thus rotating the angle of vibration of the electric field and any particle trapped in the beam.

Circularly polarised light can be used for the continuous rotation of trapped birefringent particles or linearly polarised light can be used for the controlled alignment of birefringent particles. This method of making particles rotate also has limitations as it depends on birefringence of the trapped particle and many particles used in optical tweezers, such as biological specimens, are not birefringent.

6.2.2.3 Scattering

The transfer of angular momentum by absorption or birefringence as described above results in the particle trapped in the beam axis rotating around its own axis. The transfer of orbital angular momentum by scattering has been shown to induce reflective, 2 μm diameter silver particles trapped in the annular ring of an LG beam to orbit around the ring circumference (O'Neil and Padgett, 2000). When a Dove prism is placed in the beam to change the sense of the helical wavefronts, the azimuthal scattering force is reversed resulting in a change of rotation direction. It was also shown that a transparent dielectric sphere trapped off-axis in the bright ring of an LG beam rotated around the ring circumference (O'Neil et al., 2002a). This was also attributed to the transfer of orbital angular momentum by scattering of the beam.

Orbiting around the circumference of the LG beam is distinct from the rotation of particles around their axis but both mechanisms are of interest in the study of the nature of angular momentum of light. However, for the continuous controlled rotation of particles these techniques have several drawbacks, such as the reliance on intrinsic particle properties and rotation rate is not readily controlled.

6.2.3 Rotation of shaped optical traps

The final category of methods with which to induce particle rotation in optical tweezers relies on the particle continuously realigning itself with a moving gradient force optical trap. Apertures have been used to shape the trapping beam in order to

assist the particles to align. Rotation of the aperture in the laser cavity (Sato et al., 1991) or in the beam axis (O'Neil et al., 2002b) results in the trapped particle (red blood cells (Sato et al., 1991) or two silica spheres (O'Neil et al., 2002b)) following the rotation of the imaged aperture. Similarly, a laser with an elliptically shaped output mode could be rotated in order to spin any particle trapped at the beam focus (Sato and Inaba, 1996) or a higher-order mode laser beam (TEM_{0n}, n = 2 or 3) (Sato, 1991). Spatial light modulators can be used to create dynamic traps that may rotate particles in any plane (Bingelyte, 2003). In theory any shaped optical trap that can be rotated can lead to the rotation of a particle or group of particles trapped in the pattern.

6.3 Revolving interference patterns for the rotation of optically trapped particles

As part of my PhD, a system has been developed with which to controllably rotate optically trapped objects in a spiral interference pattern between a TEM_{00} Gaussian beam and a Laguerre-Gaussian beam (Paterson et al., 2001; MacDonald, 2002). Objects are trapped in the spiral arms of the interference pattern and the whole pattern can be rotated by changing the optical path length of one of the interfering beams. Particles trapped in the beam follow the rotation of the pattern as they are continuously drawn into the region of highest light intensity of the moving interference pattern due to the gradient force of light. This method does not depend on particles having an anisotropic shape or on the particles being absorptive or birefringent. It solely relies on the ability of the particle to be trapped (in other words being partially transparent to the trapping wavelength). The work reported in this chapter was performed by Lynn Paterson and Michael MacDonald.

6.4 Spiral interference patterns

Interference between a Gaussian beam and a Laguerre-Gaussian beam results in a pattern which has a number of bright spiral arms due to constructive interference between the two beams. The number of spiral arms is given by the azimuthal index *l*

of the LG beam. The azimuthal index l is the number of 2π cycles of phase around the circumference of the mode, and beams with $l \neq 0$ are annular with l helices of phase. When an LG beam is interfered with a Gaussian, the azimuthal phase variation of the pattern will be transformed into an azimuthal intensity variation, resulting in a pattern with l spiral arms. A beam with $l = 2$ (and $p = 0$) possesses a phase structure of two intertwined helices and the resulting interference pattern has two spiral arms and an $l = 3$ LG beam consists of three intertwined helices of phase and the resulting pattern has three spiral arms. The spiral interference patterns between a TEM_{00} mode Gaussian beam and either an $l = 2$ and an $l = 3$ LG beam are shown in figure 6.1.

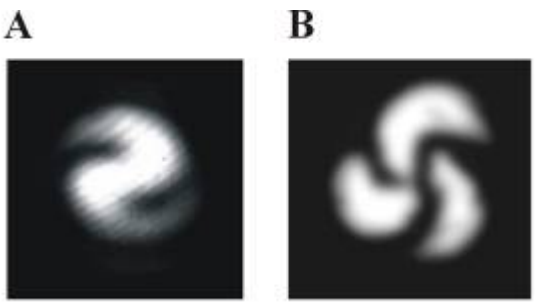

Figure 6.1: Experimental interference patterns between: A. A Gaussian beam and an $l = 2$ Laguerre-Gaussian beam. B. A Gaussian beam and an $l = 3$ Laguerre-Gaussian beam.

A helix of phase in an LG beam of index l will repeat every $l\lambda$. In our work we only use beams with index $p = 0$, single ringed LG beams. The resulting interference pattern between an LG beam and a Gaussian beam propagates without significantly changing its form in space or time as shown in figure 6.2.

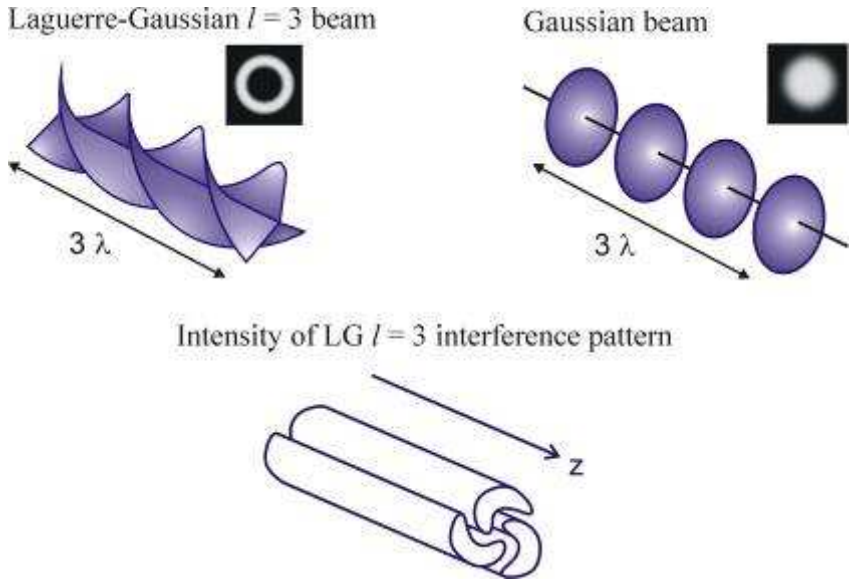

Figure 6.2: Phase fronts of an $l = 3$, $p = 0$ Laguerre-Gaussian beam and a plane wave and the intensity of the resulting interference pattern.

6.4.1 Experimental set-up

The experimental set up to create the spiral interference pattern is illustrated in figure 6.3. A neodymium yttrium vanadate (Nd: YVO_4) laser (1064 nm, 300 mW) is directed through an in-house manufactured holographic element that yielded a first order LG beam with 30% efficiency. The first order LG beam is interfered with the zeroth order straight-through beam from the hologram to generate the spiral interference pattern.

The pattern is guided through the optical system and a schematic of the arrangement is shown below, with two lenses creating an image relay between the beam steering mirror and the back aperture of either a x40 or x100 microscope objective. The pattern is focused into a sample which is placed on an xyz translation stage. Typically around 1-13 mW of laser light was incident on our trapped structures. A charge-coupled device (CCD) camera was placed above the dielectric mirror for observation purposes when the x100 objective was used for tweezing and illumination of the sample was from below, however when the x40 was used for

tweezing, a CCD camera was placed below the sample, viewing through a x100 objective, with illumination from above.

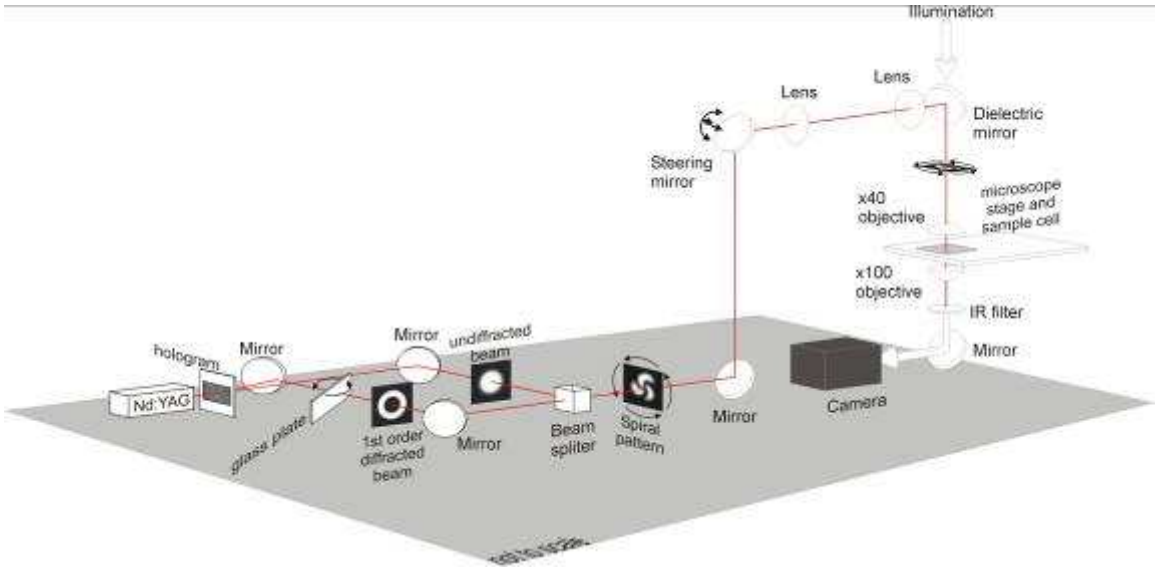

Figure 6.3: Experimental set-up to use the interference pattern as an optical trap.

6.4.2 Achieving rotation of the spiral pattern

The interference pattern can be set into motion, with the pattern rotating around the beam axis, by displacing the two interfering beams either through a change in the relative longitudinal (axial) phase of the two beams or by creating a frequency difference between the two beams. The frequency of one of the beams can be shifted by as little as a few Hertz, through the use of two acousto-optic modulators (one to step the frequency up and the other to shift it down). This will cause the pattern to rotate continuously at a rate directly related to the beat frequency between the two beams. Through control of the frequency shift between the two beams the sense and speed of rotation may be accurately controlled, making this technique most suited to the situation where continuous or high repetition rate rotation is desired.

Control of the relative longitudinal phase between the LG and Gaussian beams can be achieved by manipulating the path length in one arm of the interferometer using for example: the piezo-electric activation of a mirror in the interferometer, the rotation of a radial phase plate in one arm of the interferometer, with the aid of an LCD phase actuator or simply through the tilting of a glass plate. In our work we used the tilting of a glass plate in one arm of the interferometer to change the optical path length of that beam in order to rotate the pattern.

An analogy of the rotation of the pattern is the cutting of a piece of thick rope consisting of l intertwined cords of different colours. If this rope is cut and viewed end on the end of each cord (spiral arm) can be seen (figure 6.4). The intertwined cords represent the helices of phase and the ends of the cords represent the spiral arms, as the azimuthal variation between the two beams has been converted to an intensity variation. As the position of the cut is moved along the rope, the cords viewed end on can be seen to rotate around the rope axis. In our work, altering the path length of one of the beams is analogous to moving the rope with respect to the site where the cutting takes place.

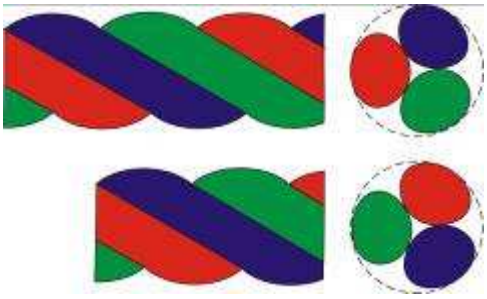

Figure 6.4: A length of rope with three intertwined cords analogous to the phase fronts of an $l = 3$ beam. The ends of the cords show how the spiral arms of the interference pattern rotate around the axis as the path length of one of the arms in the interferometer is changed (when the rope is shortened).

6.5 Analysis of interference patterns between a Gaussian beam and Laguerre-Gaussian beams

The intensity forms resulting from the interference of a Gaussian beam and an LG beam are simulated on computer to reveal how the interference patterns change in form as they propagate through a focus. The spiral sense of the arms in the interference pattern determined by the wavefront curvature of the laser light and the slight rotation in space of the pattern due to the Gouy phase shift as the beam propagates are investigated. We also consider how various misalignments between the two interfering beams affect the interference pattern at the beam focus and hence the trapping and rotating ability of the pattern.

6.5.1 Gouy phase shifts and wavefront curvature

As mentioned in Chapter 2 the full mode description for a Laguerre-Gaussian beam is given by:

$$E\left(LG_p^l\right) \propto \exp\left[\frac{-ikr^2 z}{2\left(z_R^2+z^2\right)}\right]\exp\left[\frac{-r^2}{\omega(z)^2}\right]\exp\left[-i\left(2p+|l|+1\right)\arctan\left(\frac{z}{z_R}\right)\right]\times \exp[-il\phi]\times\left(\frac{r\sqrt{2}}{\omega(z)}\right)^{|l|} L_p^{|l|}\left(\frac{2r^2}{\omega(z)^2}\right) \quad (6.1),$$

where z is the distance from the beam waist, z_R is the Rayleigh range, k is the wave number, ω is the Gaussian beam waist, r is the radius and $L_p^{|l|}$ is the generalised Laguerre polynomial.

The term $\Phi_{Guoy}^{LG} = \left(2p+|l|+1\right)\arctan\left(\frac{z}{z_R}\right)$ is the Gouy-phase shift which gives the difference of the phasefronts near the focus from that of a spherical wave. The matching mode description for a fundamental Gaussian beam is given by the above equation for LG modes with $l = 0$ and $p = 0$, hence the Gouy phase shift is simply $\arctan(z/z_R)$. This shows us that both the curvature of the wavefronts of the LG and Gaussian beams and their Gouy-phase shifts will be different. As mentioned

previously when an LG beam and a Gaussian beam are interfered the azimuthal phase variation of the LG beam is transformed into an azimuthal intensity variation with *l* nodes.

A simulation (by Michael MacDonald) of the pattern produced by interfering a Gaussian beam and an LG beam of azimuthal index $l = 3$ as the pattern propagates through a focus is shown in figure 6.5 for the case of the Gaussian waist being double that of the LG beam ($\omega_g = 2\omega_{lg}$) but both of equal amplitude, and for when the amplitude of the Gaussian beam is half that of the Laguerre-Gaussian ($A_g = 0.5A_{lg}$) but the beam waists are of equal size.

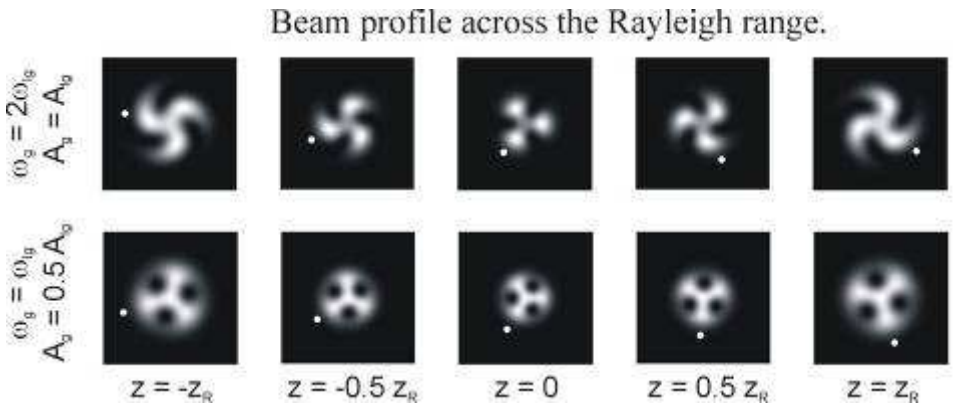

Figure 6.5: Interference pattern rotates slightly as it propagates due to the differences between the Gouy-phase shifts of the LG and Gaussian beam. The pattern is spiral shaped due to the difference in wavefront curvature between the two interfering beams.

Discrete trapping sites are not created when $\omega_0^G = \omega_0^{LG}$ however, it can be seen that when $\omega_0^G = 2\omega_0^{LG}$ the pattern does have trapping sites which are not spiral in shape but three connected spots at the focus which evolve into spirals as the beam propagates away from the focus. The spiral shape is a result of the mismatch between the curvatures of the LG and Gaussian wavefronts. The interference pattern will always have a spiral shape unless the wavefronts of the two beams have the same curvature, such as at a focus, in which case the pattern will look like *l* intense

spots of light. This can be seen above where the pattern reduces to a set of three spots at the focus. The spiral pattern rotates slightly as it propagates through the focus and this is due to the differences between the Gouy-phase shifts Φ_{Guoy} of the LG and Gaussian beams. The white dot in the figure indicates the rotation of the pattern due to the different Gouy-phase shifts of an LG and a Gaussian beam. A further effect is the reversal of the sense of the spiral as it passes through the focus. This is due to the reversal of the curvature of the wavefronts and does not affect the sense of rotation of the spiral due to the Gouy-phase shift mismatch.

The formation of discrete trapping sites at the focus when the Gaussian waist is double that of the LG waist occurs because the Gaussian beam is at its most plane. The spiral arms do not occur as there is very little curvature of the wavefronts at the beam focus. We have simulated patterns which may be created by interfering Gaussian beams higher order LG beams (figure 6.6). The use of higher order LG beams of differing azimuthal index in interference patterns offers the prospect of trapping and rotating different shaped objects and groups of objects.

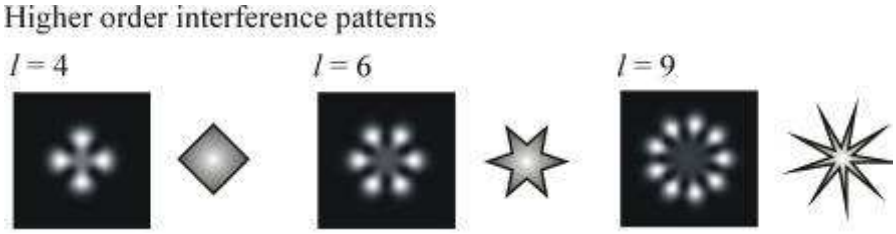

Figure 6.6: Mathematica simulations of higher order interference patterns (by Michael MacDonald) using a Gaussian and various LG beams. The Gaussian is interfered with an $l = 4$ LG beam to rotate a square or cuboidal structure, and $l = 6$ or 9 to rotate star shaped structures, or microfabricated microscopic cogs.

The propagation of the beams in figure 6.5 show the slight rotation of the pattern in space due to the difference in Gouy phase shift of the two interfering beam. This makes the alignment of multiple particles in the spiral arms along the beam propagation axis or z-trapping difficult to achieve. Eliminating the difference in

Gouy phase shift between the two interfering beams will improve the chances of stacking or z-trapping in the bright arms (or spots) as they will propagate without the slight rotation in space and this is achieved in the following chapter.

6.5.2 Aberrations in patterns due to misalignment

For practical applications, simulations of the interference patterns were made to discover how resilient they would be to misalignment. The beams have been displaced in three different ways, in one simulation the beam sizes are changed, in another the relative focal point between the two beams are changed and finally the beams are transversely displaced.

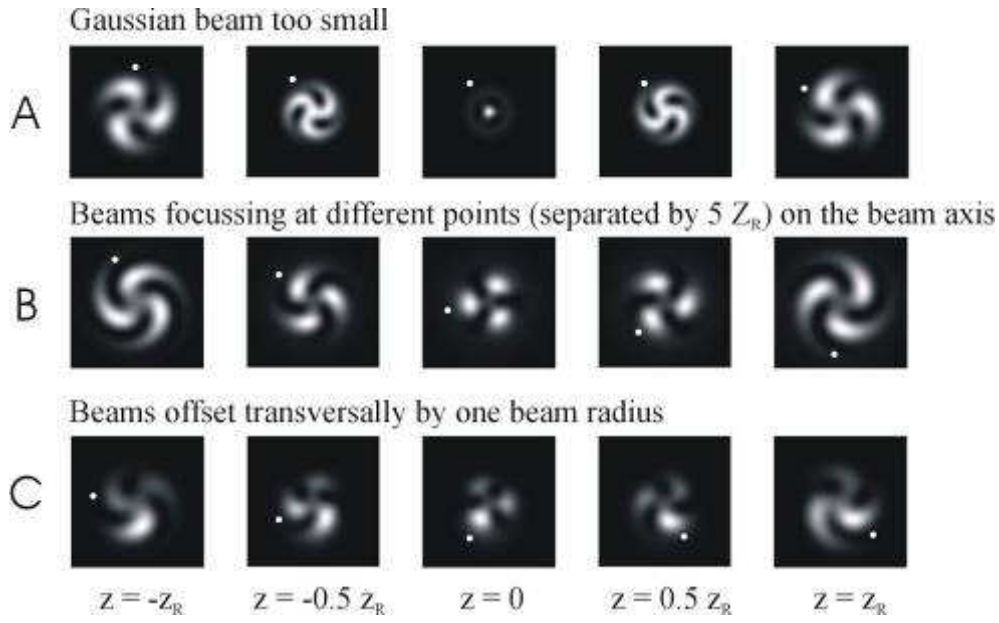

Figure 6.7: Mathematica simulations (by Michael MacDonald) of misalignment between the LG and Gaussian beam.

In figure 6.7A the Gaussian beam has half the beam waist ω_0 of the LG beam which makes it difficult to resolve the pattern at the focus as the focused Gaussian beam actually fits inside the dark centre of the focused LG beam. Figure 6.7B shows the

effect of the Gaussian beam coming to a focus earlier than the LG beam by $5z_R$ (Rayleigh range of the LG beam) which is not detrimental to the overall pattern, and figure 6.7C shows the effect of a transverse misalignment of the beams by a whole LG beam radius ω_0. This results in part of the beam having a higher intensity than the rest of the beam, which would mean that the optical trapping and rotation would be much less efficient than when the beams are co-linear.

6.6 Results

The experimental setup shown in figure 6.3 was used to trap and rotate transparent microscopic objects in an interference pattern between a Gaussian beam and either an $l = 2$ Laguerre-Gaussian beam or an $l = 3$ LG beam. A glass plate is placed in one arm of the interferometer to induce pattern rotation by tilting it, therefore varying the optical path length of the beam. A x40 microscope objective was used to obtain the $l = 3$ results and a x100 objective was used in the $l = 2$ rotation experiments. Using a x40 increased the size of the beam profile compared to using a x100 objective.

The optical gradient force in each of the spiral arms was used to trap particles in each arm and rotation of the pattern resulted in the particles revolving with it. The rotation of trapped 1 μm diameter silica spheres in an $l = 3$ interference pattern can be seen in figure 6.8 with an arrow tracking the motion of one of the three spheres.

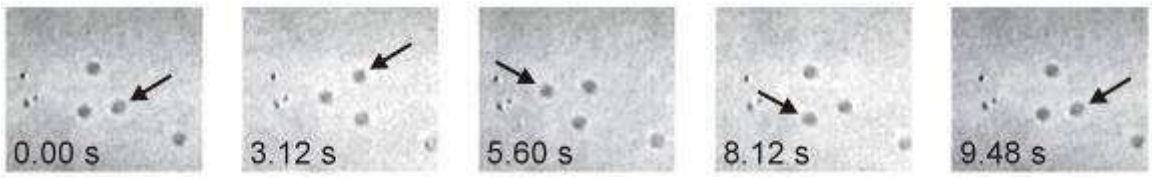

Figure 6.8: Rotation of three 1 μm diameter silica spheres in an $l = 3$ interference pattern. One of the spheres is tracked with an arrow.

Figure 6.9 shows the same pattern used to rotate larger spheres of 5 μm diameter. The slight deformity in one of the spheres indicated by the arrow allows us to view the degree of rotation of the structure.

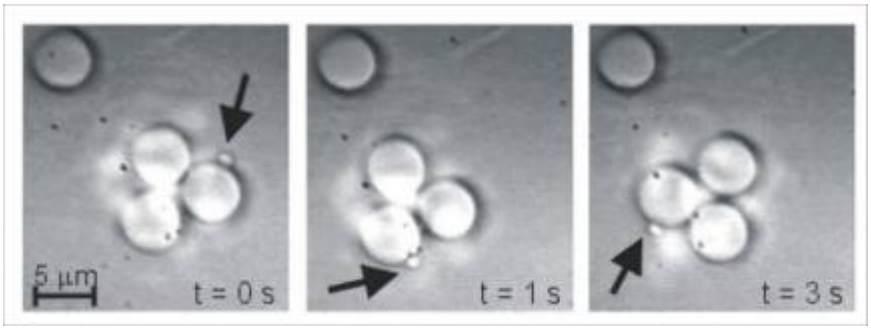

Figure 6.9: Rotation of three 5 μm diameter spheres in an l = 3 interference pattern.

The two spiral arms of an l = 2 interference pattern were used to trap and rotate two 1 μm diameter silica spheres at a rate of 7 Hz as shown in figure 6.10A. The minimum optical power required to rotate the 1 μm spheres is 1 mW.

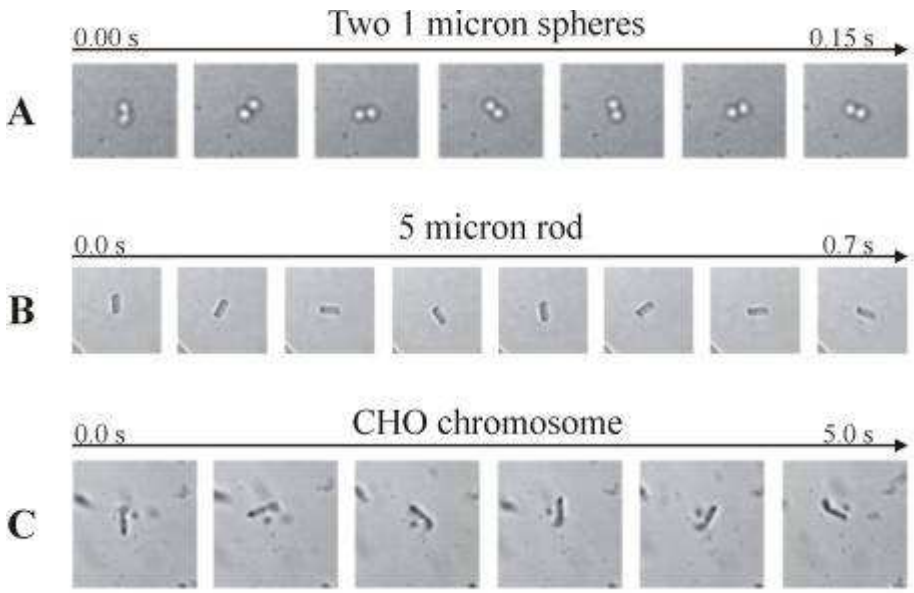

Figure 6.10: Rotation of micro objects in an $l = 2$ interference pattern. A. Two 1 μm diameter silica spheres, B. A 5 μm long glass rod, C. A 7 μm long Chinese Hamster Ovary (CHO) chromosome.

Two 1 μm diameter silica spheres can be seen to rotate around each other in figure 6.10A and a tweezed 5 μm long glass rod can be seen to be rotated between the frames of figure 6.10B. This constitutes an all-optical microstirrer and may have potential to operate as micro pumps and valves in optically driven micromachines and motors or alignment of particles using this technique may have applications in the lock-and-key assembly of all-optically created microstructures. The rotation of a Chinese hamster ovary (CHO) chromosome is also demonstrated in figure 6.10C with the axis of the spiral interference pattern over the centromere of the chromosome. This may be useful if such a chromosome or another biological specimen has to be aligned correctly prior to laser microdissection.

In these experiments we have typically achieved rotation rates in excess of 5 Hz which were limited by the amount of optical power in the interference pattern at the sample plane (~13 mW). The use of optimised components would readily lead to rotation rates of tens to hundreds of Hertz. In the following section we analyse the use of a tilting glass plate to induce pattern rotation to discover the optimal parameters when this method is used.

6.7 Tilting glass slide to change optical path length

Going back to figure 6.2 it can be seen that a change of path length in one arm of the interferometer by λ x l will cause a full rotation of 360° of the pattern. By using the tilting of a glass slide in one of the interfering beams we can readily change the sense of rotation of the pattern by reducing the path length of one arm of the interferometer instead of increasing it and as a result we have a very simple way of controlling both the sense and rate of rotation of our interference pattern.

Figure 6.11 shows a simulation of the rotation of an l = 3 interference pattern by tilting a glass plate of 1 mm thickness in one arm of the interferometer through various angles given by Φ, with the white dot following the rotation of the pattern. The beams are of equal amplitude ($A_g = A_{lg}$) and the Gaussian waist is double that of the Laguerre-Gaussian beam ($\omega_g = 2\omega_{lg}$).

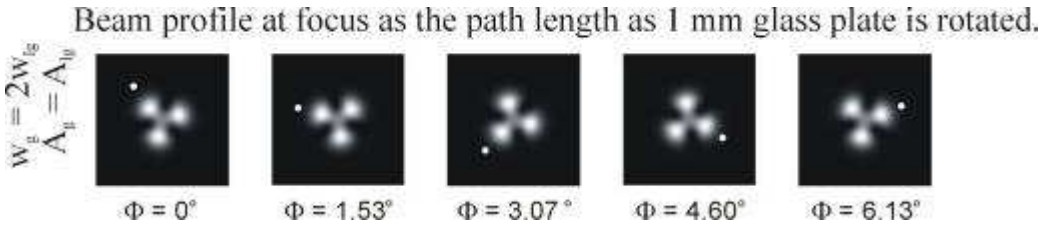

Figure 6.11: Simulation of the rotation of the interference pattern at a focus as the path length of one of the beams is changed. The white dot indicates anti-clockwise rotation.

The necessary parameters for calculating the effect of tilting the glass plate are shown in figure 6.12.

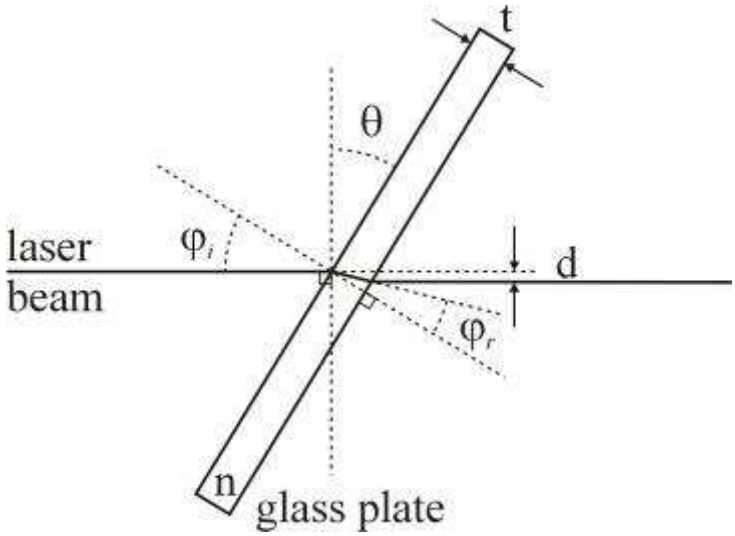

Figure 6.12: The parameters used for calculating the effect of tilting a glass plate in a laser beam. n = refractive index of glass plate, d = beam displacement, t = plate thickness, $\theta = \varphi_i$ = angle of incidence, φ_r = angle of refraction.

The following equations were derived by Michael MacDonald. The change in path length Δ produced by a tilt angle θ ($\theta = \varphi_i$) in the glass plate is given by equation 6.2:

$$\Delta = t\left[n\left(\frac{1}{\cos\varphi_r} - 1\right) + 1 - \frac{\cos(\theta - \varphi_r)}{\cos\varphi_r}\right] \qquad (6.2).$$

Applying Snell's Law, it is possible to determine φ_r and hence the number of rotations N produced in the spiral interference pattern from equation 6.3.

$$N = \frac{\Delta}{l\lambda} \qquad (6.3),$$

where l again is the azimuthal index of the LG beam and λ is the wavelength. For the purposes of accurate alignment of the beam it is more useful to express rotation as an angle in radians: $\alpha = 2\pi N$. There is a resultant displacement d in the beam which can be found from equation 6.4,

$$d = t\frac{\sin(\theta - \varphi_r)}{\cos\varphi_r} \qquad (6.4),$$

although there is no angular deflection so long as sides of the plate are parallel. It is clear that both the number of rotations the glass plate can induce in the spiral and the resultant deflection of the beam are proportional to the plate thickness t. This means that the ratio N/d is always the same for a given tilt angle. The number of rotations of different patterns and the lateral displacement of the beam as the glass plate is tilted from normal ($\theta = 0$) are shown in figure 6.13.

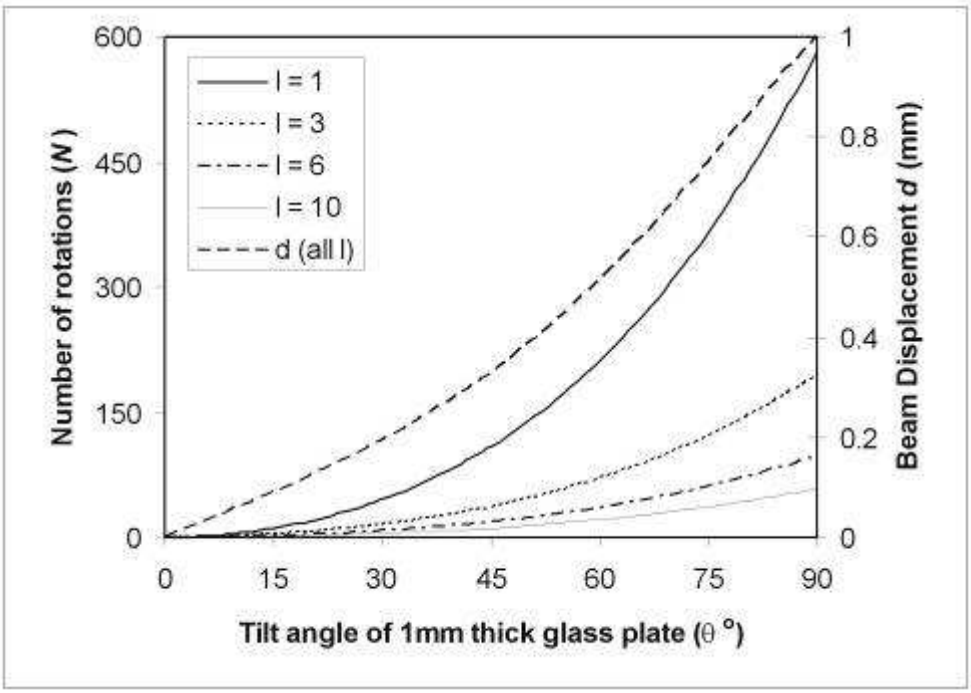

Figure 6.13: Number of rotations *N* of the spiral patterns (given in the legend) and displacement *d* of the beam as the glass plate is tilted. Patterns with a lower *l* rotate more times for a given tilt angle than higher *l* indices, but the larger the tilt of the glass plate, the larger the displacement of the beam.

It can be seen from figure 6.14 that the number of rotations for a given pattern will increase as plate thickness increases, however a thicker plate also results in a larger lateral displacement of the beam.

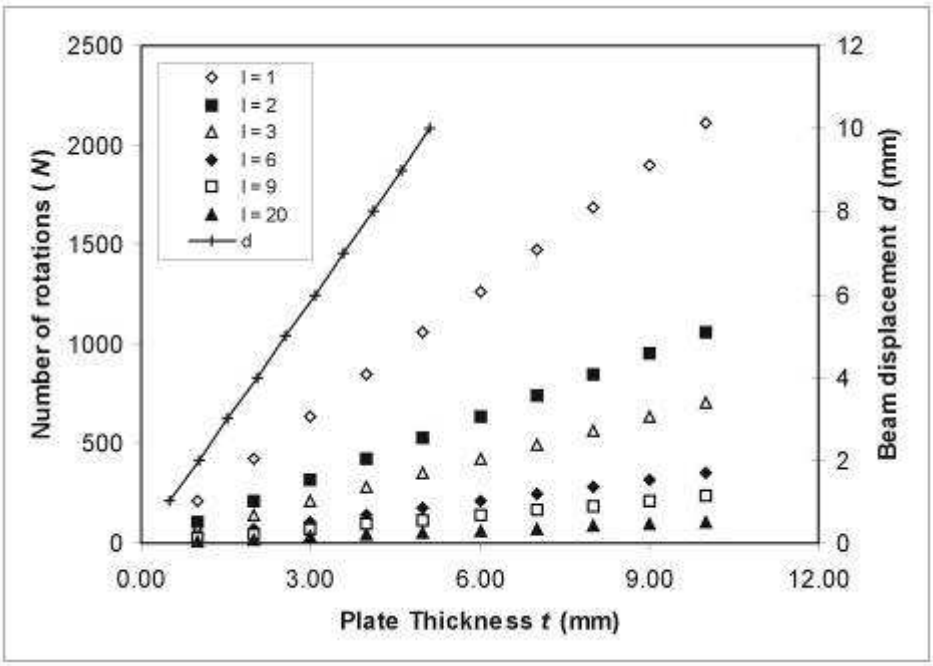

Figure 6.14: The number of rotations N of the spiral patterns and displacement d of the beam as the plate thickness is varied. In each case the plate is tilted 60° from normal. More rotations are possible if a thicker plate is used but displacement of the beam increases.

The rotations achieved in an $l = 2$ interference pattern from tilting a glass microscope slide (approximately 1 mm thick) and cover glass (approximately 0.1 mm thick) are shown in figure 6.15 where we see very good agreement with theory.

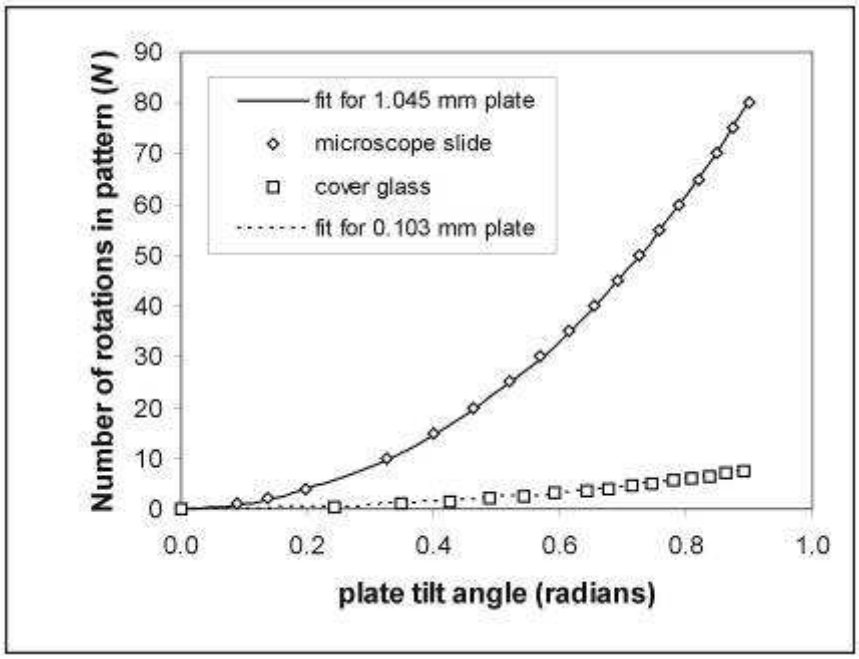

Figure 6.15: The diamonds and squares show the number of rotations measured in an LG $l = 2$ interference pattern as a glass microscope slide and a glass coverslip are tilted from normal. The line curves show equation 6.3 for a glass plate of thickness t = 1.04 mm and cover glass t = 0.103 mm.

One full rotation of the $l = 3$ spiral is shown in figure 6.11 as a result of tilting the glass plate through 6.13° from the normal. Since the displacement d is not proportional to the number of rotations N, the displacement that results from a given number of rotations will be different depending on what tilt angle the glass plate has as a starting angle. In practice the smallest displacement possible should be sought and this is found when tilting the glass plate from normal ($\theta = 0°$).

It is clear that the number of rotations achievable is greater for a thicker plate but that the possible displacement is also larger. Figure 6.16 shows the displacement of the beam when various thicknesses of glass plate are used and tilted through various angles of rotation.

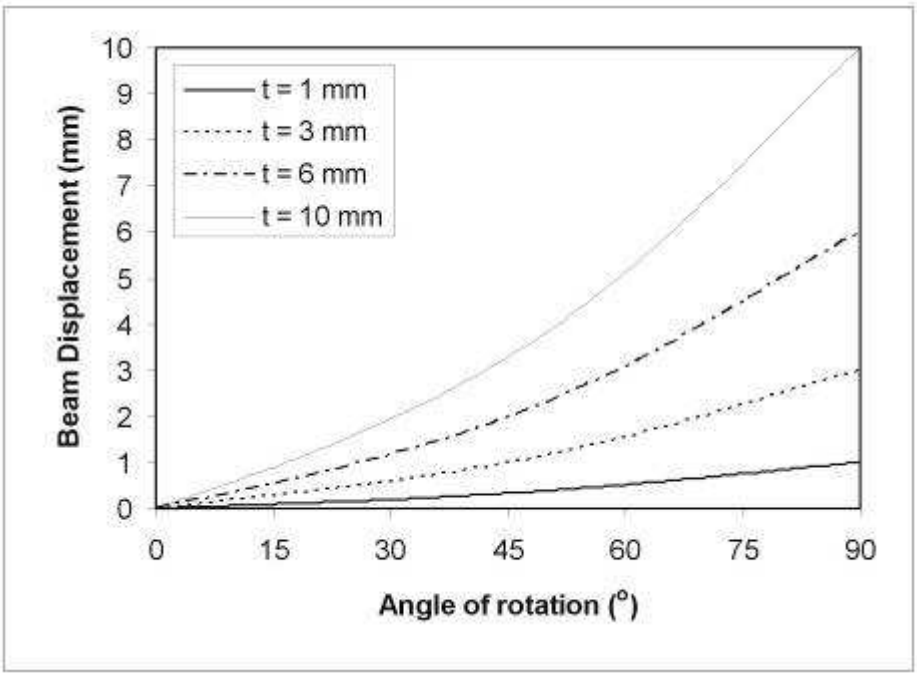

Figure 6.16: The displacement d (mm) of an $l = 3$ interference pattern for various glass plate thicknesses t (mm) as the angle of the plate is tilted from normal.

A further consideration is that a thick plate requires a smaller angle of rotation to create the same number of rotations as a thin plate but for a given maximum desired number of rotations it is always best to take the thinnest plate available to avoid undue displacement of the beam. This is illustrated in figure 6.17 which shows continually increasing values of displacement d with plate thickness t for the $l = 3$ interference pattern when the plate is tilted from the normal. It can also be seen that the displacement becomes very large if high numbers of rotations are made.

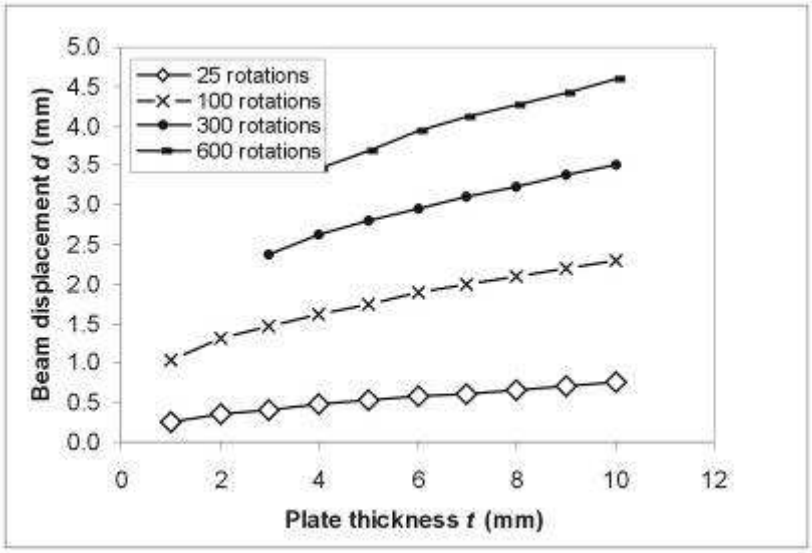

Figure 6.17: The displacement d (mm) for various values of N (number of full rotations of pattern around optic axis -given in legend) as the plate thickness t (mm) is varied for an $l = 3$ interference pattern.

In summary the use of a glass plate to produce the rotation in the interference pattern (and trapped particles) is most suitable when the number of rotations required is limited. If a maximum required number of rotations are known, then the thinnest plate that can achieve this number of rotations should be used to limit beam displacement. If continuous rotation of the pattern is necessary then another approach may be required such as the use of two AOMs.

6.8 Discussion

Rotation of optically trapped particles in a revolving interference pattern does not depend on intrinsic properties such as anisotropic shape, birefringence or absorption of the trapping wavelength but relies only on the particles ability to be tweezed by the gradient force of the focused laser beam. In addition, our method of inducing rotation in the interference pattern by tilting a glass plate in one arm of the interferometer means that the sense of rotation and rate of rotation of the pattern can be easily controlled by varying the sense and rate of tilting of the glass plate. The

pattern changes slightly in form as it propagates due to the mismatch of wavefront curvature of the beam and the Gouy phase shift between the two beams but in general the intensity pattern maintains its spiral shape except at the beam waist where the pattern focuses down to a set of spots rather than spiral arms. This is attributed to the Gaussian wavefront which become planar when focused. The fact that the beam is an interference pattern and propagates without huge change in form leads us to the possibility of z-trapping, or stacking in rotating interference patterns. The possibility of more stable trapping is especially true if the Gouy phase shift difference could be deleted and if the curvature of the Gaussian wavefronts was eliminated. The following chapter explores another family of interference patterns in which this is possible and z-trapping is achieved.

References

Allen L, Beijersbergen MW, Spreeuw RJC, Woerdman JP: **Orbital Angular-Momentum of Light and the Transformation of Laguerre-Gaussian Laser Modes.** *Physical Review A* 1992; **45**:8185-8189.

Beth RA: **Mechanical detection and measurement of the angular momentum of light.** *Physical Review* 1936; **50**:115-125.

Bingelyte V, Leach J, Courtial J, Padgett MJ: **Optically controlled three-dimensional rotation of microscopic objects.** *Applied Physics Letters* 2003; **82**:829-831.

Friese MEJ, Enger J, RubinszteinDunlop H, Heckenberg NR: **Optical angular-momentum transfer to trapped absorbing particles.** *Physical Review A* 1996; **54**:1593-1596.

Friese MEJ, Nieminen TA, Heckenberg NR, Rubinsztein-Dunlop H: **Optical alignment and spinning of laser-trapped microscopic particles.** *Nature* 1998; **395**:621-621.

Galajda P, Ormos P: **Complex micromachines produced and driven by light.** *Applied Physics Letters* 2001; **78**:249-251.

Galajda P, Ormos, P: **Rotors produced and driven in laser tweezers with reversed direction of rotation.** *Applied Physics Letters* 2002a; **80**:4653-4655.

Galajda P, Ormos, P: **Rotation of microscopic propellers in laser tweezers.** *Journal of Optics B: Quantum and Semiclassical Optics* 2002b; **4**:S78-S81.

Gauthier RC, Tait RN, Mende H, Pawlowicz C: **Optical selection, manipulation, trapping, and activation of a microgear structure for applications in micro-optical- electromechanical systems.** *Applied Optics* 2001; **40**:930-937.

He H, Friese MEJ, Heckenberg NR, Rubinszteindunlop H: **Direct Observation of Transfer of Angular-Momentum to Absorptive Particles from a Laser-Beam with a Phase Singularity.** *Physical Review Letters* 1995; **75**:826-829.

Higurashi E, Ukita H, Tanaka H, Ohguchi O: **Optically Induced Rotation of Anisotropic Micro-Objects Fabricated by Surface Micromachining.** *Applied Physics Letters 1994*; **64**:2209-2210.

Higurashi E, Ohguchi O, Tamamura T, Ukita H, Sawada R: **Optically induced rotation of dissymmetrically shaped fluorinated polyimide micro-objects in optical traps.** *Journal of Applied Physics* 1997; **82**:2773-2779.

Higurashi E, Sawada, R., Ito, T: **Optically induced rotation of a trapped micro-object about an axis perpendicular to the laser axis.** *Applied Physics Letters* 1998a; **72**:2951-2953.

Higurashi E, Sawada R, Ito T: **Optically induced angular alignment of birefringent micro- objects by linear polarization.** *Applied Physics Letters* 1998b; **73**:3034-3036.

Higurashi E, Sawada R, Ito T: **Optically induced angular alignment of trapped birefringent micro-objects by linearly polarized light.** *Physical Review E* 1999; **59**:3676-3681.

Luo ZP, Sun YL, An KN: **An optical spin micromotor.** *Applied Physics Letters* 2000; **76**:1779-1781.

MacDonald MP, Volke-Sepulveda K, Paterson L, Arlt J, Sibbett W, Dholakia K: **Revolving interference patterns for the rotation of optically trapped particles.** *Optics Communications* 2002; **201**:21-28.

Moothoo DN, Arlt J, Conroy RS, Akerboom F, Voit A, Dholakia K: **Beth's experiment using optical tweezers.** *American Journal of Physics* 2001; **69**:271-276.

Omori R, Shima K, Suzuki A: **Rotation of optically trapped particles in air.** *Japanese Journal of Applied Physics Part 2-Letters* 1999; **38**:L743-L745.

O'Neil AT, Padgett MJ: **Three-dimensional optical confinement of micron-sized metal particles and the decoupling of the spin and orbital angular momentum within an optical spanner.** *Optics Communications* 2000; **185**:139-143.

O'Neil AT, MacVicar I, Allen L, Padgett MJ: **Intrinsic and extrinsic nature of the orbital angular momentum of a light beam.** *Physical Review Letters* 2002a; **8805**:article no. 053601.

O'Neil AT, Padgett, M. J.: **Rotational control within optical tweezers by use of a rotating aperture.** *Optics Letters* 2002b; **27**:743-745.

Paterson L, MacDonald MP, Arlt J, Sibbett W, Bryant PE, Dholakia K: **Controlled rotation of optically trapped microscopic particles.** *Science* 2001; **292**:912-914.

Sato S, Ishigure M, Inaba H: **Optical Trapping and Rotational Manipulation of Microscopic Particles and Biological Cells Using Higher-Order Mode Nd: YAG Laser-Beams.** *Electronics Letters* 1991; **27**:1831-1832.

Sato S, Inaba H: **Optical trapping and manipulation of microscopic particles and biological cells by laser beams.** *Optical and Quantum Electronics* 1996; **28**:1-16.

Simpson NB, Allen L, Padgett MJ: **Optical tweezers and optical spanners with Laguerre-Gaussian modes.** *Journal of Modern Optics* 1996; **43**:2485-2491.

Simpson NB, Dholakia K, Allen L, Padgett MJ: **Mechanical equivalence of spin and orbital angular momentum of light: An optical spanner.** *Optics Letters* 1997; **22**:52-54.

7 Creating and rotating three dimensional structures using interference patterns between two Laguerre-Gaussian beams

7.1 Introduction

The previous chapter introduced the use of revolving interference patterns to rotate particles trapped in the pattern. Interference between a Gaussian beam and a Laguerre-Gaussian beam resulted in a spiral shaped pattern with *l* spiral arms due to the azimuthal phase index *l* of the LG beam. In this chapter we investigate the use of another family of interference patterns for the improved trapping efficiency of particles, namely LG-LG interference patterns. The interference between a Laguerre-Gaussian beam and its mirror image gives us a pattern of spots rather than spirals. The propagation of these patterns without change in form due to the identical beam propagation characteristics of the two interfering beams means that z-trapping and stacking in the bright spots is readily achieved. The pattern does not rotate in space as there is no phase difference between the two beams as the Gouy phase shift in both beams is identical. The trap sites in the pattern are spots instead of spirals because the curvature of the wavefronts of both beams match. We build on the work described in chapter six and present a new scheme for the controlled, continuous rotation of the pattern which overcomes the limitations associated with the tilting glass plate. The technique introduces a frequency shift in one of the interfering beams from less than one, to hundreds of Hertz and is applicable to inducing the slow motion of any interference pattern, creating optical conveyor belts and in the field of cold atoms where small frequency shifts are required for offset locking of the diode laser system to atomic features. The work reported in this chapter was performed by Lynn Pateson and Michael MacDonald, with additional simulations and calculations by Jochen Arlt and Karen Volke-Sepulveda.

7.2 LG-LG interference patterns

Laguerre-Gaussian beams have been discussed in previous chapters. Recall that the index *l* describes the number of 2π cycles of phase around the mode circumference, and that the pattern made by interfering an LG beam and a Gaussian beam results in a spiral shaped pattern with *l* spiral arms. This pattern consists of bright spiral arms instead of spots because of the curvature of the Gaussian wavefronts causing the pattern to exhibit marked azimuthal intensity variations as the pattern propagates away from a focus.

Furthermore, the pattern slightly rotated in space because of the mismatch in Gouy phase shift between the two beams. Interference patterns used in the following work overcome these limitations and propagate without change in form in space (apart from radial scaling due to diffraction spreading) and so allow the stacking of particles in each bright region of the pattern.

Specifically, an LG beam of index *l* is interfered with its mirror image of index *–l*, (opposite beam helicity), resulting in a spatial pattern of 2*l* spots arranged in a circle, creating multiple trapping sites (MacDonald et al., 2002). These spots do not become spiral shaped as the pattern propagates away from the focus because there is no curved Gaussian beam wavefront, and the pattern does not rotate in space because there is no phase difference between the two beams. Related patterns have been analysed in other studies (Piestun et al., 2000; Schechner et al., 1996; Tovar et al., 2000). Combining one beam of azimuthal index $l = 1$ and one with $l = -1$ results in a light pattern containing two maxima. $l = 2$ interfered with $l = -2$ results in a pattern with four bright spots arranged around a circumference.

Figure 7.1 shows the form of the interference patterns generated using LG beams of different azimuthal index *l* and interfering them with their mirror image (azimuthal index *–l*).

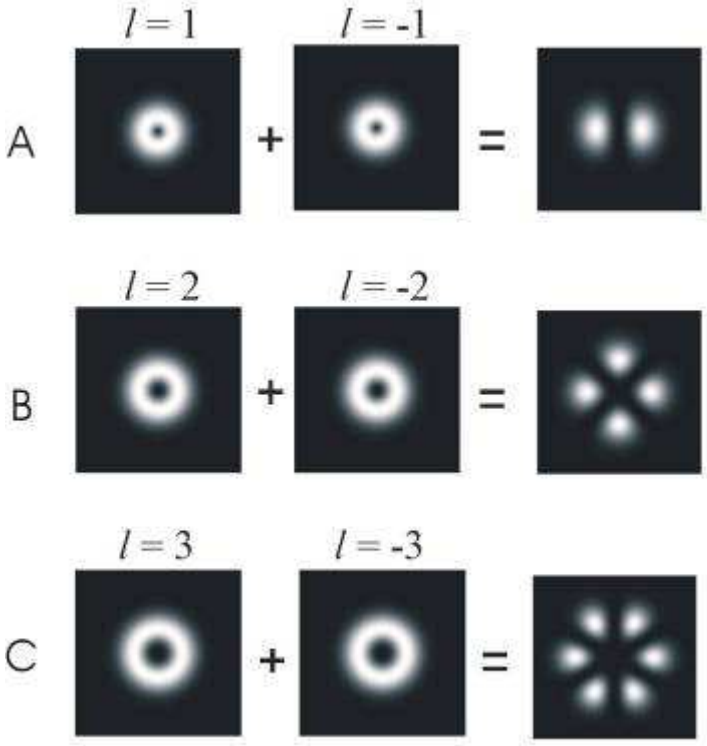

Figure 7.1: Mathematica simulations (by Michael MacDonald) of patterns generated by interference between two Laguerre-Gaussian of opposite helicity.

The general relationship between the number of trapping sites N in the interference pattern and the azimuthal index l of the two beams of opposite helicity that are interfered is:

$$N_{spots} = |l_1 - l_2| \qquad (7.1).$$

Thus we can dictate the number of spots we have in our pattern by using holograms which can produce Laguerre-Gaussian modes with the azimuthal index of our choice.

7.2.1 Propagation of LG-LG interference patterns

The intensity propagates in $|l_1 - l_2|$ columns, due to the constructive and destructive interference between the two overlapping beams which posses opposite helicity of phase. These columns of light act as separate single beam optical traps, thus making it possible to stack several trapped particles in each of the bright regions in the same manner as the stacking in a single Gaussian beam in a standard tweezers configuration described in chapter 3. Two radially adjacent spots are always π out of phase and this phase structure is crucial for the propagation characteristics of the interference pattern. Figure 7.2A shows the intensity cross-section for the case of an l = 2 and l = -2 interference pattern as it propagates from the beam waist to the far field.

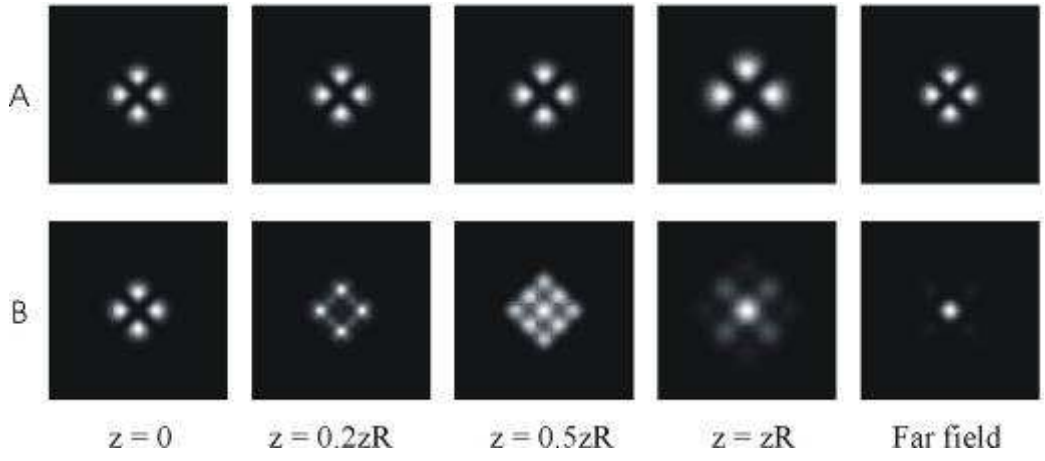

Figure 7.2: Simulation of the propagation of the laser pattern (by Jochen Arlt). A. Interference pattern between two LG beams with l = 2 and l = -2 respectively. B. Pattern with the same intensity profile but uniform phase. In the far field the pattern has completely changed. (The far field has been scaled down in A and B).

Figure 7.2B shows propagation characteristics in the case in which an aperture is imaged by illuminating it with a laser beam. In this instance the beam has the same intensity cross-section at the beam waist but a uniform phase across all the spots.

The pattern becomes distorted at a distance of $0.2z_R$ where z_R is the Rayleigh range and it has completely changed in form at a distance of z_R from the beam waist. In contrast, the interference pattern propagates to the far field without changing form, thus allowing particles to be stacked in each of the spots. If an aperture was used to create a similar pattern, stacks of particles and three-dimensional arrays could not be created. There will also be a loss of power when using an aperture to image a pattern, in contrast to using an interference pattern.

7.2.2 Experimental set-up

The experimental set-up used is similar to that used in the previous chapter but with some important modifications (figure 7.3).

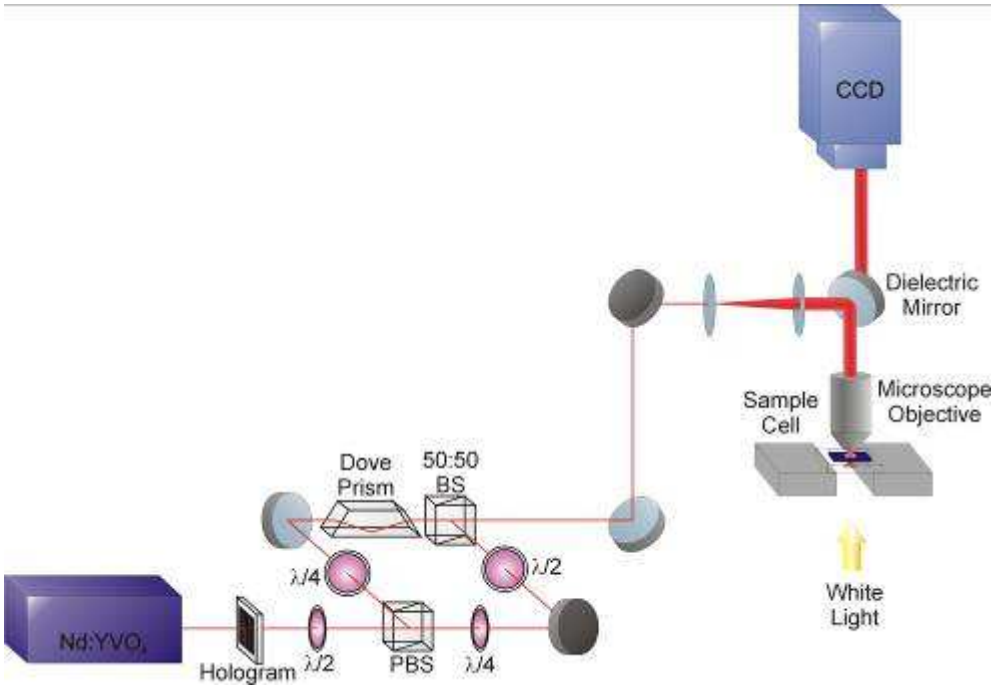

Figure 7.3: The experimental set up for creating LG-LG interference patterns.

The beam from a cw diode-pumped Nd: YVO_4 laser operating at 1064 nm is passed through a hologram creating an LG beam. The LG beam is passed through a half-

wave plate to make the beam polarised at 45° to the horizontal and is then passed through a polarising beam splitter so that the resulting orthogonally polarised beams have equal intensity in each arm of the Mach-Zender interferometer. The beams are each passed through a quarter-wave plate which makes them circularly polarised with opposite handedness ($+\hbar$ and $-\hbar$) to each other. The transmitted beam has its wavefront helicity reversed by passing it through a dove prism so that the two beams are mirror images of each other (l and $-l$). A half-wave plate in the other arm of the interferometer allows the two beams to interfere when they are recombined at a 50:50 (non polarising) beam splitter by making them the same sense of circular polarisation at the exit where they are superimposed collinearly to give the interference pattern. This pattern is then directed into an optical tweezers set-up, and focused into a sample cell consisting of a microscope slide, a 100 μm thick vinyl spacer which creates a well into which the sample is contained and a coverslip. The beam and sample are viewed from above using a CCD camera. Particles can be trapped in the bright spots of the pattern due to the gradient force of the light and the particle may be set into motion by using the method described in the previous chapter – the tilting of a glass plate in one arm of the interferometer. Another group based in Singapore have redesigned this interferometer to incorporate two holograms in a Michelson interferometer instead of using a Mach-Zender interferometer to combine LG beams of opposite helicity (Lee et al., 2003). They also interfere two LG beams of unequal azimuthal charge thus conserving orbital angular momentum in the pattern. A tilting glass plate is used to make the pattern rotate. In the following passage, we present a more elegant technique for revolving interference patterns which overcomes the limitations of tilting a glass plate in the beam and can give an unlimited number of rotations of the pattern at a stable frequency.

7.3 The angular Doppler effect

In addition to the lateral and vertical motion of the pattern, we can induce the pattern to rotate around its axis of symmetry using the angular Doppler effect (Garetz, 1981; Garetz and Arnold, 1979; Dholakia, 1998) (more generically known as the rotational

frequency shift (Bialynicki-Birula and Bialynicki-Birula, 1997)). This scheme, which Jochen Arlt initiated the use of in this context, gives us continuous and readily controlled rotation of our interference patterns and overcomes the limits associated with tilting the glass plate (low rotation number and beam displacement) and can be applied when the slow motion of an interference pattern such as those discussed above and in chapters five and six is required. It may also be used for the creation of an optical conveyer belt – a moving standing wave trap – for the transportation of atoms from a magneto-optical trap (Kuhr et al., 2001).

The angular Doppler effect is analogous to the linear Doppler effect which is observed when a moving mirror is used in one arm of a Michelson interferometer (Nichols et al., 1985). The movement of fringes at the output of a Michelson interferometer is usually explained by a difference in path length between the two beams however an equivalent explanation of the movement of the fringes is that it is due to a frequency shift experienced by one beam of $\Delta\omega=2\omega v/c$, where v is the relative velocity between the observer and the mirror, c is the speed of light and $\omega$is the frequency of the light. This is a manifestation of the linear Doppler effect (Hariharan and Ward, 1997). The direction of linear momentum is reversed by reflecting off the mirror and the frequency of the beam is changed when the velocity of the mirror $v \neq 0$.

In the angular equivalent of the linear Doppler effect, it is necessary to change the angular momentum of a beam (analogous to a mirror reversing the linear momentum of a beam) therefore a rotating E-field such as that present in circularly polarised light must be used. The angular momentum of circularly polarised light is reversed form $+\hbar$ to $-\hbar$ or vice versa by passing it through a half wave plate, thus a change in spin angular momentum of $2\hbar$ per photon occurs as the light passes through this optical element. When the half-wave plate is rotated by the torque of the light, the light produces work and loses a part of its energy and vice versa, so the frequency shift experience by light as it passes through a rotating wave plate is a result of the conservation of energy and is associated with an exchange of angular momentum (Bretenaker and Le Floch, 1990).

The frequency of circularly polarised light recorded by an observer is dependant on the rotational frequency of the incident light and in a rotating reference frame the observed frequency will be shifted by the angular frequency of that reference frame. If the half-wave plate is rotating then the observed frequency of the transmitted light in a non-rotating reference plane is shifted in frequency by twice the rotation frequency of the wave-plate either up, if the plate is rotating in the opposite sense as the incident E-field, or down if it is rotating in the same sense.

We have demonstrated the first practical application of the angular Doppler effect (MacDonald et al., 2002; Arlt et al., 2002) by introducing a difference in frequency between the two beams in the LG-LG interferometer, resulting in the rotation of the whole interference pattern of spots at a frequency of $2\Omega/|l_1 - l_2|$, where Ω is the rotation rate of the half-wave plate in one arm of the interferometer. The rotation of the pattern is a consequence of the helical wavefronts of each of the LG beams.

The angular Doppler effect is a very simple and effective way to introduce the relatively small frequency differences (from less than 1 Hz to 1 kHz) required between two light beams for the controlled rotation of an interference pattern. This difference corresponds to a frequency shift 14 orders of magnitude smaller than the frequency of the laser itself (10^{14} Hz) and the technique can be applied in any situation where slow motion of an interference pattern is desired, such as translating particles in simple linear interferometric tweezers (Chiou et al., 1997; MacDonald et al., 2001) or creating a moving 'conveyer belt' of dipole traps for the deterministic delivery of ensembles of cold atoms (Kuhr et al., 2001). The scheme can also be used for offset locking of diode laser systems to atomic features, again in the field of cold atoms. The conventional method for this makes use of acousto-optic modulators (AOMs) which can shift the frequency of a laser by tens or hundreds of MHz (1 part in 10^7) and if two AOMs are used, much smaller frequency differences of a few MHz or less can be achieved, however this is both cumbersome and expensive. If smaller frequency shifts of 1 kHz or less are required, the angular Doppler effect can realise this.

7.3.1 Frequency shift arises due to conservation of energy and angular momentum

A simple calculation, carried out by Michael MacDonald, using the conservation of energy and angular momentum of a circularly polarised photon passing through a wave-plate, shows how the frequency shift arises. Circularly polarised light has angular momentum of $+\hbar$ or $-\hbar$ per photon and when it is passed through a half-wave plate the angular momentum of the photons is reversed from $+\hbar$ to $-\hbar$ or vice versa. Conservation of angular momentum of a photon passing through a rotating half-wave plate gives,

$$\hbar + I\Omega_{rot} = -\hbar + I\Omega'_{rot} \qquad (7.2),$$

where Ω_{rot} and Ω'_{rot} are the rotation rates of the wave plate before and after the photon has passed through it, respectively, and I is the moment of inertia of the wave plate. If $L_1 = I\Omega_{rot}$ and $L_2 = I\Omega'_{rot}$ where L_1 and L_2 are the angular momenta of the wave plate before and after the beam has passed through it, the change in angular momentum is given by

$$L_2 - L_1 = 2\hbar \qquad (7.3).$$

Conservation of energy gives

$$\hbar\omega_1 + L_1^2/2I = \hbar\omega_2 + L_2^2/2I \qquad (7.4).$$

Ω_1 and Ω_2 are the frequencies of the photon before and after the photon has passed through the wave plate and the rotational kinetic energy of the wave plate is $L^2/2I$. By comparing the conservation of angular momentum and energy we find the frequency shift due to the rotating wave plate to be

$$\Delta\omega = \omega_1 - \omega_2 = 2\Omega_{rot} \qquad (7.5).$$

In our system a rotating half-wave plate is used but there is also the possibility of using an electro-optical crystal to mimic this effect which offers a system that would have no moving parts and can also achieve frequency shifts in the megahertz regime (Buhrer et al., 1962).

7.3.2 Optical beating between the two arms of the interferometer

When the input into the Mach-Zender interferometer is a Gaussian beam and the half-wave plate is stationery, the output lies on or between complete constructive or destructive interference. The interferometer is shown in figure 7.4.

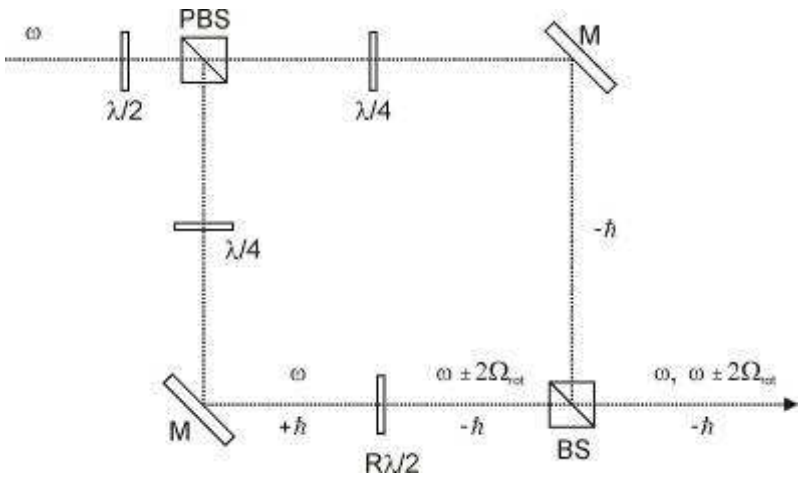

Figure 7.4: Adapted Mach-Zender interferometer for creating two co-propagating laser beams with a frequency shift between them of $2\Omega_{rot}$. PBS, polarising beam splitter; M, mirror; λ/2, half-wave plate; Rλ/2, rotating half-wave plate; BS, 50:50 beam splitter; $+\hbar$, right handed circularly polarised light; $-\hbar$, left handed circularly polarised light; Ω_{rot}, rotation frequency of half-wave plate.

As soon as the plate starts to rotate the output beats at twice the frequency of the half-wave plate rotation frequency. This is similar to the result obtained by Simon et al. from a dynamical manifestation of Berry's phase shift (Simon et al., 1988) and is used here to determine the stability of the technique. Figure 7.5 shows a beat signal as typically observed at the output of the interferometer.

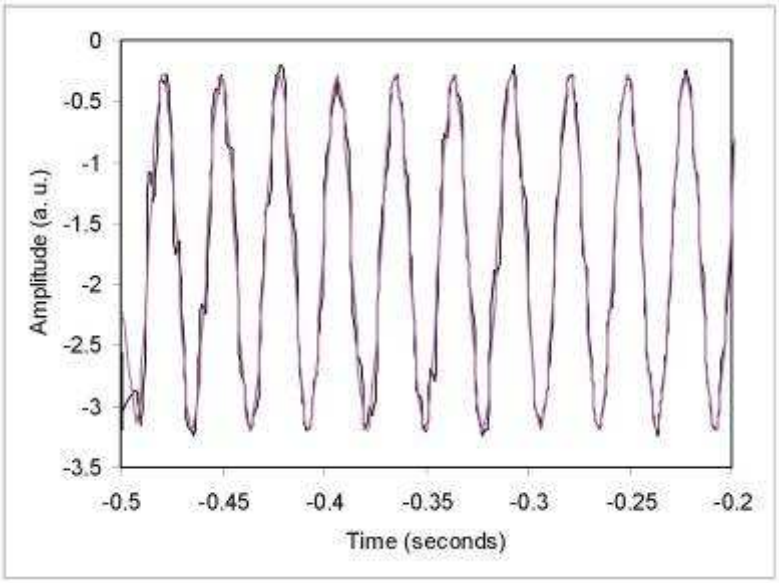

Figure 7.5: The beat signal produced by interfering two Gaussian beams separated in frequency using the angular Doppler effect with fit.

A fast Fourier-transform (FFT) analysis of this beat signal reveals a single peak at 35 Hz, exactly double the rotation rate of the half-wave plate, as expected.

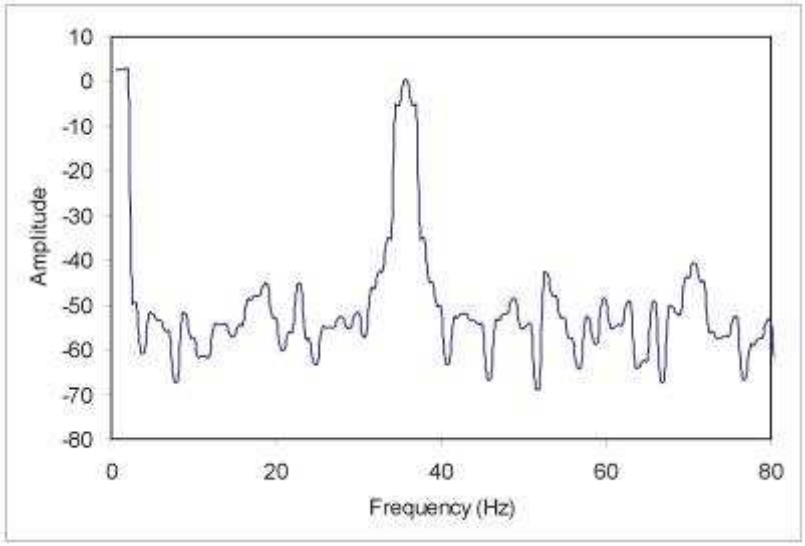

Figure 7.6: Fast Fourier transform of the beat signal shown in figure 7.5. A peak at 35 Hz is seen.

The absolute frequency stability of the laser is not crucial in this work since it is the relative frequency shift between the two interfering beams that gives the evolution in the interference pattern. However it is necessary that the laser does not suffer from longitudinal mode hops since this would lead to discontinuous jumps in the pattern. The narrow bandwidth is necessary to ensure complete constructive or destructive interference even in the presence of small inequalities in the path lengths of the two interfering beams. If the two interfering Gaussian beams are not perfectly overlapping then instead of a beat signal we get a set of linear fringes that scan from left to right and vice versa, depending on whether $\Delta\omega$is positive or negative (Arlt et al., 2002). The appearance of new fringes at the edge of the interference pattern occurs at the same frequency of the beat signal (2Ω), so that the fringes scan more slowly as the number of fringes in the pattern gets larger. These moving interference patterns can be used to trap elongated particles and translate them in a direction normal to their length in a similar fashion to the movement of interference fringes discussed in chapter 5. The following section discusses the differences between the interference patterns between an LG beam and a Gaussian beam introduced in chapter 6, and an LG-LG interference pattern which has been the basis of this chapter, and the rotation of these patterns.

7.4 Comparison of LG-LG patterns and LG-Gaussian beam patterns

For the case of two interfering Laguerre-Gaussian beams with opposite helicities the number of spots in the resulting interference pattern is given by $|l_1 - l_2|$ and the rate of rotation of the pattern is given by $2\Omega/|l_1 - l_2|$, where Ω is the rotation rate of the half-wave plate and the frequency difference between the two arms of the interferometer is 2Ω. On the other hand, in the case of the interference pattern between an LG beam of azimuthal index *l* and a Gaussian beam, the number of spiral arms (or spots at the focus) is *l*, and the rotation rate of the pattern is $2\Omega/l$. The

interference patterns that we have created using Gaussian beams and various Laguerre-Gaussian beams are illustrated in figure 7.7. Figure 7.7.1 shows the interference of two Gaussian beams which results in a pattern of fringes when the two beams are not co-linear, but interfering at a slight angle. Figure 7.7 (2 and 3) show the interference of a Gaussian beam with a Laguerre-Gaussian beam and the actual pattern generated, and figures 7.7 (4-6) show the interference of two Laguerre-Gaussian beams of opposite helicity. This opposite helicity results in identical beam propagation characteristics, thus the propagation of the resulting interference pattern.

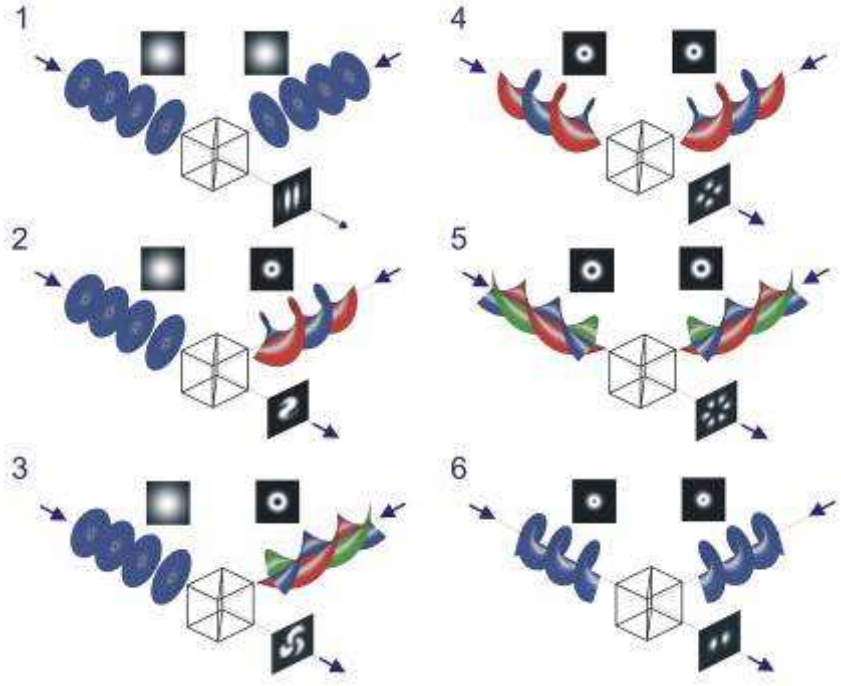

Figure 7.7: Interference patterns which we have created and used to manipulate various particles. 1. The pattern of linear fringes made when two Gaussian beams are interfered at a slight angle. 2. A two armed spiral pattern results from the interference of a Gaussian beam with an l = 2 LG beam. 3. A three armed spiral pattern results from the interference of a Gaussian beam with an l = 3 LG beam. 4. Interfering an l = 2 and an l = -2 LG beam results in a four spot pattern. 5. An l = 3

interfered with an l = -3 LG beam gives a six spot pattern. 6. Interfering an l = 1 with an l = -1 LG beam results in a two spot pattern.

It is worth noting that the rotation rate of a two spot pattern created by interfering an l = 1 and an l = -1 LG beam is Ω, while for a two armed spiral pattern created using a Gaussian beam and an l = 2 LG beam we find that the rotation rate is also Ω (calculated by Karen Volke-Sepulveda). It follows that for a given number of tweezing sites (spots or spiral arms) the rotation rate will be the same if the pattern was created by interfering a Gaussian and LG beam or an LG and LG beam, even though the expressions for the rotation rates are different in each case. The sense of rotation of the pattern is simply reversed by reversing the sense of rotation of the wave plate (shifting the frequency down rather than up).

The antinodes of an interference pattern between an LG beam and its mirror image result in more efficient trapping sites, with which to z-trap or stack particles, than by interfering an LG beam with a Gaussian beam. Continuous rotation of either of these groups of patterns at a stable frequency using the angular Doppler effect is much better than the tilting of a glass plate, however, for alignment purposes or slight rotation, the tilting plate method suffices.

7.5 Results

Different versions of the interference pattern between two LG beams of opposite helicity have been used on various groups of trapped particles. The pattern is directed into a sample cell containing particles to be manipulated and the experimental set up is shown in figure 7.3 above. A two spot pattern formed by superimposing an l = 1 beam and an l = -1 beam has been used to tweeze and rotate groups of 1μm silica spheres and several rod-like particles, including chromosomes.

The rotation of the pattern and therefore the trapped particles using the angular Doppler shift is continuous and of a uniform speed, in contrast to using a tilting glass plate in one of the beams as described in chapter 6. The sense and speed of pattern

and particle rotation can be easily controlled by manipulating the sense and rotation rate of the half-wave plate.

Various groups of 1 μm spheres have been trapped in the same interference pattern with stacking of the spheres occurring in one or both of the bright spots. The structure of spots can be rotated and translated in either the x, y or z direction simultaneously. The z-trapping of a rotating structure is a result which cannot be realised using an LG-Gaussian interference pattern, or by imaging an aperture. This is because the propagation of the trapping sites which occurs in an LG-LG interference pattern is crucial to the stacking and z-trapping of the trapped particles. As previously mentioned, the propagation of the beam and the resulting propagation of the separate trapping sites are due to the lack of mismatch in Gouy phase shift between the two interfering beams.

Figure 7.8 shows a group of four 1 μm silica spheres trapped in the $l = 1$, $l = -1$ interference pattern with two spheres in each of the two spots.

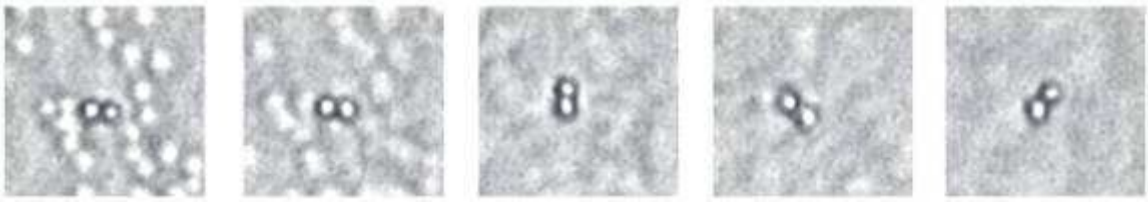

Figure 7.8: A group of four 1 μm diameter silica spheres that is tweezed and lifted vertically whilst simultaneously being rotated through the sample cell. The interference pattern used is an ($l = 1$) + ($l = -1$) pattern of two spots. Only the top two spheres are visible as the structure is viewed from above.

The microstructure is tweezed and lifted vertically whilst being rotated through the sample cell, with only the top two spheres being visible in the picture. Figure 7.9 shows a cubic structure of eight 1 μm spheres assembled and rotated in a four spot, $l = 2$, $l = -2$ interference pattern.

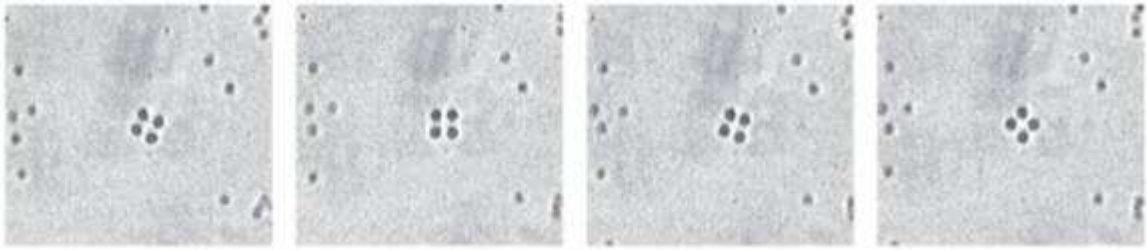

Figure 7.9: The rotation of a cubic structure consisting of eight 1 μm diameter spheres. The interference pattern is that of an (l = 2) and an (l = -2) Laguerre-Gaussian beam which has four spots. The structure is rotated using the angular Doppler effect at rates up to 2 Hz.

Figure 7.10 shows the same structure collapsing as the laser beam is blocked, revealing the eight constituent spheres.

Figure 7.10: The same cubic structure is seen to collapse, revealing the eight constituent spheres as the trapping laser beam is blocked.

A cartoon of the eight spheres held in the l = 2 + l = -2 interference pattern can be seen in figure 7.11 to illustrate the trapping.

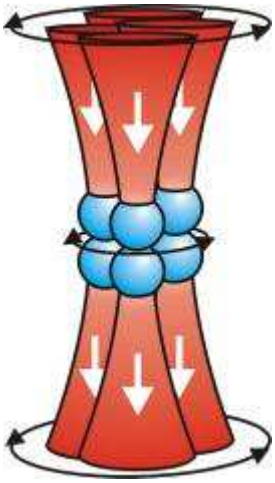

Figure 7.11: The trapping of eight silica spheres in a four spot interference pattern (two spots stacked in each spot) to create a cubic structure.

By controlling the number of spheres trapped in each bright region, we can create asymmetric 3D structures. Figure 7.12 below shows some of the structures which we have created in our optical traps. The long chains of stacked particles are those discussed in chapter 3. Future possibilities for structures are shown in the bottom right corner of the diagram using patterns which he have not yet used to trap particles. Also shown are some of the structures which we created in the LG-LG interference pattern optical traps.

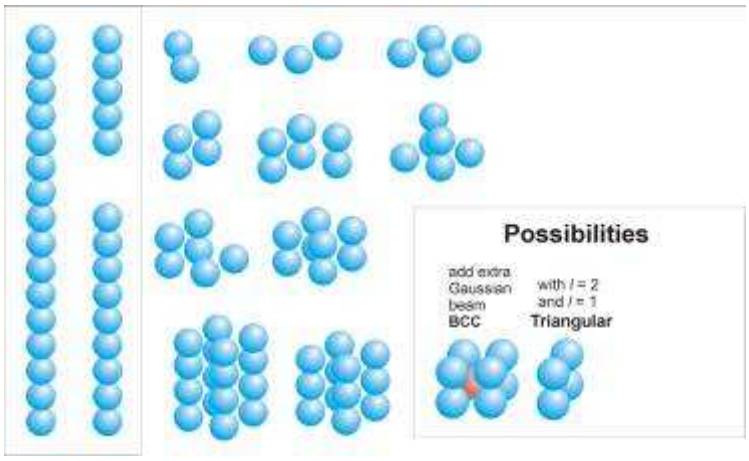

Figure 7.12: Structures that have been created and future possibilities.

Our ensemble of trapped particles can act as a predetermined nucleus for subsequent growth of novel crystalline structures by self-assembly, or the patterns can be used to rotate micromachine elements such as the microfabricated cog shown in figure 7.13.

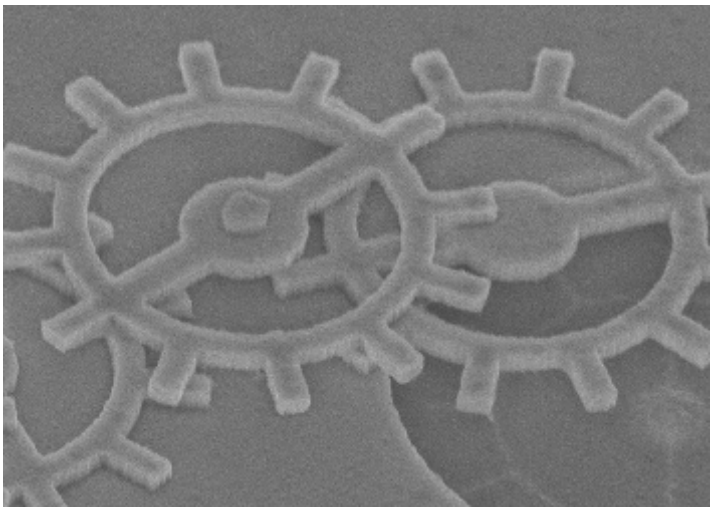

Figure 7.13: Microfabricated cogs created by Steve Neale at the University of St Andrews.

The propagating interference patterns we have generated could be retro reflected to form a standing wave which could offer discrete trapping sites in the axial direction (Burns et al., 1990). The creation and manipulation of artificial structures at or below the micrometer level is of current interest in colloid physics. A further use for our interference pattern is the aligning or rotation of particles in each distinct trap site as the pattern itself rotates as a whole (Paterson et al., 2002).

7.6 The alignment or rotation of trapped birefringent particles in a polarised, revolving interference pattern

The following work was performed by Lynn Paterson. The technique combines two methods of rotation; firstly the use of linearly or circularly polarised light and

secondly the rotation of the interference pattern. This technique may assist in driving large arrays of micromachines, or in microfluidic studies.

7.6.1 Experimental setup

The experimental set-up used is shown in figure 7.14 and the output from the interferometer is circularly polarised, so that any birefringent particle in a trap site will spin due to the transfer of angular momentum from the beam to the particle. Crushed fragments of calcite or mercury (I) chloride (Hg_2Cl_2) were used as particles to be trapped in this work as they are both birefringent.

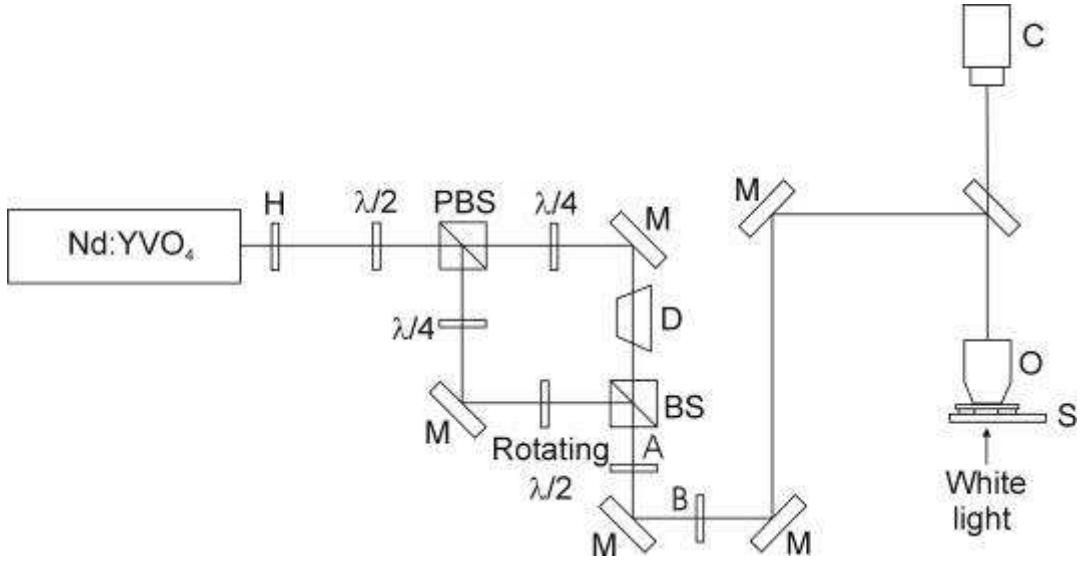

Figure 7.14: Experimental set-up to use the polarisation of light and a rotating interference pattern together to spin birefringent particles. H, hologram; λ/2, half-wave plate; PBS, polarising beam splitter; λ/4, quarter-wave plate; M, mirror; D, dove prism; BS, 50;50 beam splitter; A, position of quarter-wave plate used to make beam linearly polarised; B, position of half-wave plate used to rotate the plane of vibration of the linearly polarised light; L, lens; O, microscope objective; S, sample chamber; CAM, CCD camera.

7.6.2 Spinning and orbiting of a birefringent particle in a circularly polarised, revolving light pattern

Figure 7.15 shows a fragment of mercury (I) chloride trapped in one of the spots of the $l = 1$, $l = -1$ interference pattern. Both spots in the rotating pattern are circularly polarised and the particle spins continuously around its own axis a rate of tens of Hertz with 100 mW of incident power.

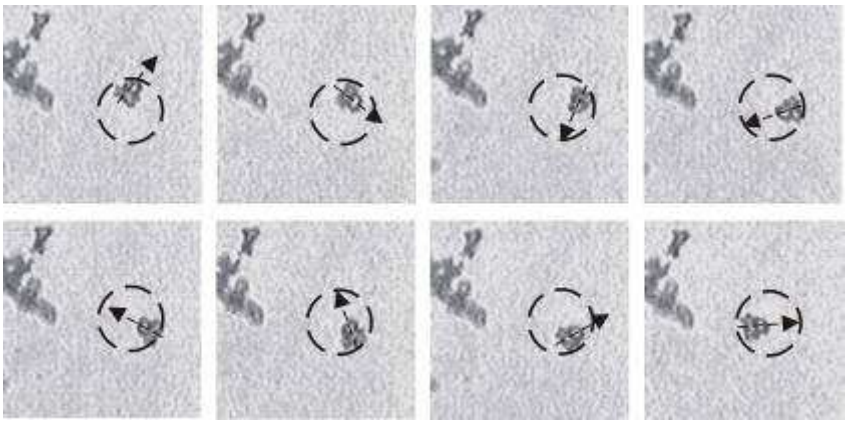

Figure 7.15: Fragment of mercury (I) chloride spins around its own axis in a clockwise direction (shown by changing direction of arrow) and orbits in the x-y plane of the sample in a clockwise direction (shown by circle) both at the same time.

The rate of rotation of the particle around its axis can be lowered by reducing the power of the laser or by making the trapping beam elliptically polarised. This rotation of the fragments around their own axis (due to the transfer of spin angular momentum) can be followed by looking at the arrow which shows the direction of alignment of the fragment of mercury (I) chloride in figure 7.15. As the interference pattern is rotated in a clockwise direction using the angular Doppler effect (inside the dashed circle) the trapped, spinning particles follow the rotation of the pattern. The pattern orbits with a period of one second.

By inserting a quarter-wave plate into the beam at the position marked ‘A’ in figure 7.14 we convert the polarisation of the beam from circular to linear. The fast axis of

a trapped birefringent particle will align with the plane of polarisation of the light field causing the particle to orient itself. If we can rotate the vibration axis of the E-field we can also make the particle rotate controllably. This is done by inserting a half-wave plate at the position marked 'B' in figure 7.14 and rotating it. The half-wave plate changes the axis of linear polarisation by 2θ where θ is the angle between the axis of polarisation of the light and the fast axis of the half-wave plate. Rotating the half-wave plate results in the rotation of the axis of vibration of the electric field of the beam and the trapped particle follows this rotation, as it remains aligned with the changing axis of polarisation. This can be seen in figure 7.16A where a fragment of crushed calcite is trapped in one spot of the interference pattern.

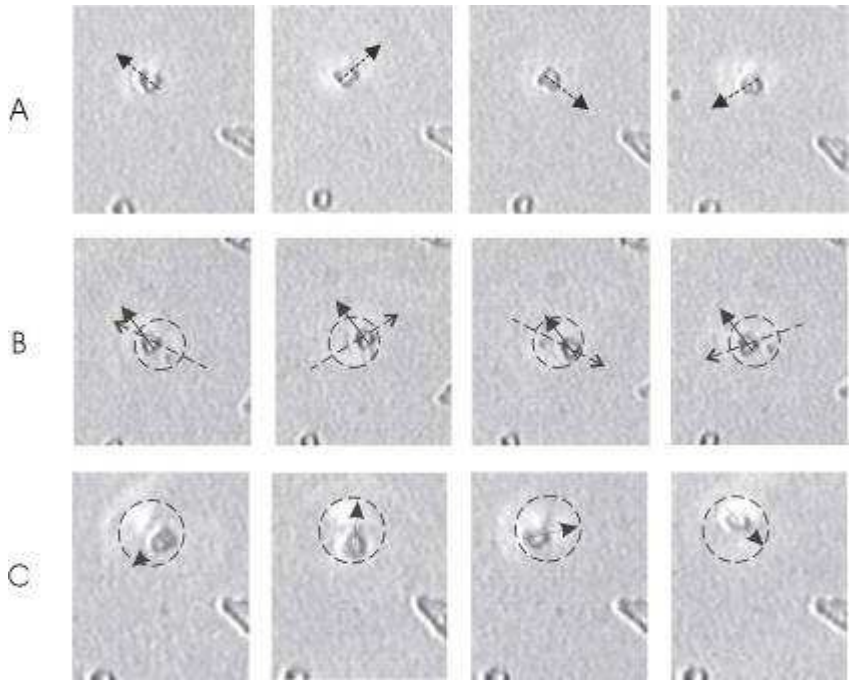

Figure 7.16: Rotating a birefringent particle in a linearly polarised light beam. A. A fragment of crushed calcite is trapped in one spot of the interference pattern. It stays in the same location because the interference pattern doesn't move, but it rotates about its axis in a clockwise direction (shown by arrow). The fragment is continuously realigning with the changing axis of linear polarisation of the trapping laser. B. The fragment follows the clockwise rotation of the interference pattern

(shown by dashed circle, large dashed arrow passes through the centre of the two maxima). It remains aligned in one direction only (shown by small arrow) because the linear polarisation of the beam remains unchanged. C. The same fragment spins around its own axis and orbits in the x-y plane simultaneously due to the axis of linear polarisation of the trapping beam constantly rotating and the interference pattern also rotating.

The interference pattern is stationary so when the half-wave plate is rotated in the beam the particle will rotate around its own axis (in this case in a clock-wise direction) but remain in the same position. Figure 7.16B shows the fragment following the rotation of the interference pattern (circle) but remaining aligned in the same direction (small arrow) because the beam is linearly polarised and the plane of polarisation is not being rotated. Combining the rotation of the interference pattern in the x-y plane and the rotation of the plane of polarisation of the beam we achieve the results shown in figure 7.16C. The same calcite fragment in figures 7.16A and B rotates around its own axis (the changing alignment shown by the arrow) and at the same time follows the revolving interference pattern (circle marks the outer limits of the pattern). The speed of pattern rotation, thus the orbiting of the particle is controlled by the angular Doppler effect. The speed of the trapped particle rotating about its own axis (which is typically less than 1 Hertz) is determined by the rate of rotation of the half-wave plate at position ‘B’ in figure 7.14. Figure 7.17 shows four fragments of calcite, each trapped in a bright spot of an $l = 2$, $l = -2$ interference pattern.

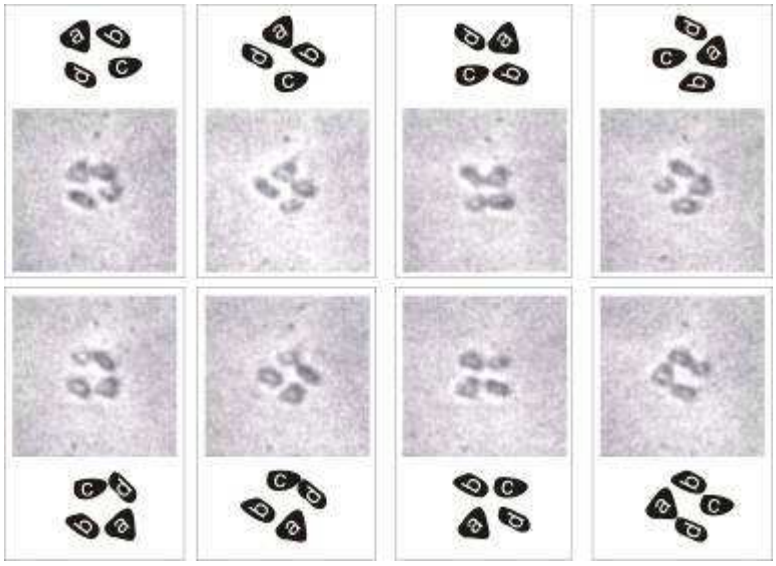

Figure 7.17: Top panel from left to right then bottom panel from left to right shows four fragments of calcite (marked a, b, c and d) aligned in the bright spots of a $l = 2$, $l = -2$ interference pattern. The pattern is rotated in a clockwise direction while the fragments remain aligned with the axis of linear polarisation which does not change.

In this case the beam is also linearly polarised with the quarter-wave plate at position A and half-wave plate at position B.

The interference pattern and the trapped particles can be moved laterally or rotationally, with the trapped particles remaining aligned to the axis of vibration of the electric field as they are moved. The figures marked a, b, c and d show more clearly that the particles remain aligned in the same direction as they follow the motion of the interference pattern.

7.7 Discussion

In this chapter we have built on work described in the previous chapter to improve trapping in interference patterns but we have also presented a new ability which has not been previously possible, the continuous, controlled motion of an interference pattern.

By interfering two Laguerre-Gaussian beams of opposite helicity, an interference pattern of spots around a circumference is created, each bright spot acting as a separate trap site which propagates without change in structure. This leads to the ability to stack and z-trap particles that are trapped in the pattern, which was not achieved using an LG-Gaussian interference pattern and would be unlikely if an imaged aperture was used. Various 3D structures can be created by using beams of different azimuthal index *l* to create the pattern, and these structures can be rotated by using the angular Doppler shift, a technique which utilises a rotating half-wave plate for generating a frequency shift in one of the arms of the interferometer. The assembly and manipulation of these structures is of interest in colloid physics plus the groups of trapped particles can act as a predetermined nucleus for the self-assembly of novel crystalline structures.

The interference patterns may also be used in combination with a standing wave trap to create discrete trapping sites in the axial direction (Burns et al., 1990) or with spatial light modulators (SLMs) (Curtis et al., 2002) to create large arrays of micro-machines over three-dimensions.

The applications of these rotating patterns and rotating structures will no doubt lead to enhanced microfluidic studies, for example they may act as all-optically driven pumps or stirrers in microfluidic devices, with microscopic volumes of fluid being uniformly stirred over their entire volume by three dimensional arrays of rotating optically trapped structures. As optical traps are non contact, friction will not occur as readily and samples can remain completely sterile. In biology this technique may be applied to the measurement of torsional properties of molecules such as rotary motor proteins or biopolymers or to viscosity measurements of microscopic volumes, for example inside cells. The optical rotator may become an indispensable piece of kit for lab-on-a-chip experiments.

References

Arlt J, MacDonald M, Paterson L, Sibbett W, Dholakia K, Volke-Sepulveda K: **Moving interference patterns created using the angular Doppler-effect.** *Optics Express* 2002; **10**:844-852.

Bialynicki-Birula I, Bialynicki-Birula Z: **Rotational frequency shift.** *Physical Review Letters* 1997; **78**:2539-2542.

Bretenaker F, Le Floch A: **Energy exchange between a rotating retardation plate and a laser beam.** *Physical Review Letters* 1990; **65**:2316.

Buhrer CF, Baird D, Conwell EM: **Optical frequency shifting by electro-optic effect.** *Applied Physics Letters* 1962; **1**:46-49.

Burns MM, Fournier JM, Golovchenko JA: **Optical Matter - Crystallization and Binding in Intense Optical-Fields.** *Science* 1990; **249**:749-754.

Chiou AE, Wang W, Sonek GJ, Hong J, Berns MW: **Interferometric optical tweezers.** *Optics Communications* 1997; **133**:7-10.

Curtis JE, Koss BA, Grier DG: **Dynamic holographic optical tweezers.** *Optics Communications* 2002; **207**:169-175.

Dholakia K: **An experiment to demonstrate the angular Doppler effect on laser light.** *American Journal of Physics* 1998; **66**:1007-1010.

Garetz BA, Arnold S: **Variable frequency shifting of circularly polarised laser radiation via a rotating half-wave retardation plate.** *Optics Communications* 1979; **31**:1-3.

Garetz BA: **Angular Doppler-Effect.** *Journal of the Optical Society of America* 1981; **71**:609-611.

Hariharan P, Ward B: **Interferometery and the Doppler effct: An experimental verification.** *Journal of Modern Optics* 1997; **44**:221-223.

Kuhr S, Alt W, Schrader D, Muller M, Gomer V, Meschede D: **Deterministic delivery of a single atom.** *Science* 2001; **293**:278-280.

Lee WM, Yuan X-C, Tang DY: **Optical tweezers with multiple optical forces using double-hologram interference.** *Optics Express* 2003; **11**:199-207.

MacDonald MP, Paterson L, Sibbett W, Dholakia K, Bryant PE: **Trapping and manipulation of low-index particles in a two- dimensional interferometric optical trap.** *Optics Letters* 2001; **26**:863-865.

MacDonald MP, Paterson L, Volke-Sepulveda K, Arlt J, Sibbett W, Dholakia K: **Creation and manipulation of three-dimensional optically trapped structures.** *Science* 2002; **296**:1101-1103.

Nichols TD, Harrison DC, Alpert SS: **Simple laboratory demonstration of the Doppler shift of laser light.** *American Journal of Physics* 1985; **53**:657-660.

Paterson L, MacDonald M, Arlt J, Dultz W, Schmitzer H, Sibbett W, Dholakia K: **Controlled simultaneous rotation of multiple optically trapped particles.** *Journal of Modern Optics* 2002; **50**:1591-1599.

Piestun R, Schechner YY, Shamir J: **Propagation-invariant wave fields with finite energy.** *Journal of the Optical Society of America A-Optics Image Science and Vision* 2000; **17**:294-303.

Schechner YY, Piestun R, Shamir S: **Wave propagation with rotating intensity distributions.** *Physical Review E* 1996; **54**:R50-R53.

Simon R, Kimble HJ, Sudarshan ECG: **Evolving geometric phase and its dynamical manifestation as a frequency shift: An optical experiment.** *Physical Review Letters* 1988; **61**:19-22.

Tovar AA: **Propagation of Laguerre-Bessel-Gaussian beams.** *Journal of the Optical Society of America A-Optics Image Science and Vision* 2000; **17**:2010-2018.

8 Introduction to the generation of Fluorescent *in situ* Hybridisation (FISH) chromosome probes and their application to chromatid break studies

8.1 Introduction

We wish to create small, fluorescent chromosome probes in order to detect any change in the chromosomes (such as deletions, duplications, translocations or inversions) in the region adjacent to chromatid breaks. This chapter contains a review of how chromosome probes similar to those we wish to create have been generated with more detail of the materials and methods in appendix A. Chromatid breaks are also described, as are how they are thought to come about in a chromosome as a result of DNA damage. Finally, we summarise how we plan to generate chromosome probes using optical techniques.

8.2 Polymerase Chain Reaction

The polymerase chain reaction (PCR) was invented in 1985 and it is an incredibly simple but powerful technique in which any piece of DNA can be copied many times in vitro. A typical PCR reaction follows a three step cycle of denaturation, annealing of primers and elongation. The DNA double helix melts at high temperature (94°C) and specifically designed primers will anneal to the single stranded DNA molecule at a lower temperature. Primers need to be 18-30 nucleotides long and have a similar G and C content so that they anneal to their complementary sequences at similar temperatures. They are designed to anneal to opposite strands of the target sequence so that they will be extended toward each other by addition of nucleotides to their 3' end. If the target DNA sequence is not known but some amino acid information is known degenerate primers can be designed using the genetic code. The enzyme DNA polymerase is used by cells for DNA replication (it reads the DNA sequence of nucleotides and makes a complementary sequence in the presence

of Mg^{2+}). For PCR a thermally stable enzyme called Taq DNA polymerase, originally found in *Thermus aquaticus* is used along with primers and an equal mix of bases, and works optimally at a temperature of 72°C. Taq polymerase however is known to introduce errors into newly synthesised sequences due to its lack of 3' to 5' proofreading exonuclease activity (one nucleotide per 250 nucleotides polymerised). The sensitivity of the reaction means that any piece of DNA in the mixture will be amplified so care must be taken to avoid contamination. If the reaction is not optimal a smear of products can be seen on a gel, and parameters such as the Mg^{2+} concentration and the annealing temperature should be changed. Mg^{2+} concentration required varies with each sequence and is usually between 1 and 4 mM, and too low an annealing temperature favours mispairing. If a PCR reaction is 100% efficient one molecule would become 2^n after n cycles, with 20-40 cycles commonly used.

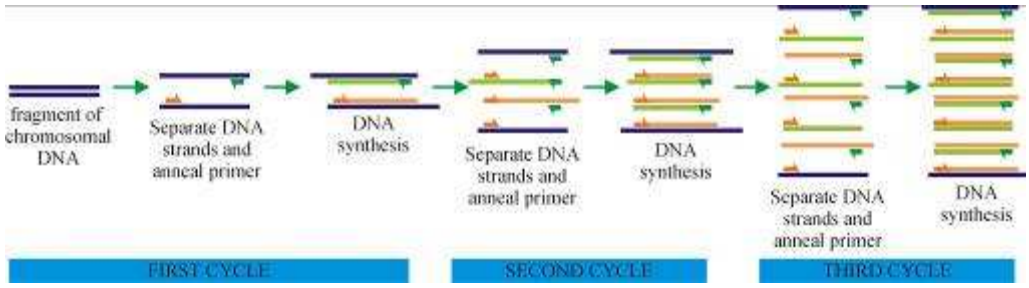

Figure 8.1: The polymerase chain reaction. The DNA is briefly heated to separate the strands of the double helix and then cooled to allow primers to bind by hydrogen bonding. The DNA polymerase extends the primers by adding nucleotides (bases) using the longer DNA strand as a template and the amount of target DNA doubles with each cycle performed.

8.3 Previous methods of making whole chromosome or region specific FISH probes

Fluorescent *in situ* hybridisation is one of the main advances in cytogenetics which has led to the greater understanding of the molecular basis of human disease as well the structure, function and evolution of chromosomes.

Flow cytometry, which was originally developed for cell analysis and separation, is now used also for sorting chromosomes (Langlois et al., 1982). Fluorescent activated cell (or chromosome) sorters (FACS) measure DNA content of chromosomes and also the base pair composition. Dyes that bind preferentially to A-T pairs (such as Hoechst 33258) or to G-C pairs (chromomycin A3) are used and are made to fluoresce by the dual laser flow cytometer, each chromosome emitting a different signal and chromosomes can be collected or discarded. These flow sorted chromosomes are often used as a template for general amplification of DNA, or in other words multiple loci in these sequences are amplified simultaneously, in order to create whole chromosome paints for FISH. For general amplification of DNA, primers based on repetitive sequences within the genome can be used (Nelson et al., 1989), such as the *Alu* repeat in human DNA of which there are 900,000 in the haploid genome giving a spacing of 3-4 kb. This type of PCR is called interspersed repetitive sequence PCR (IRS-PCR), however it has limitations such as repeats not being uniformly distributed and is only applicable to species where abundant repeat families have been identified. Linker Adapter PCR (LA-PCR) is another useful technique for general amplification of DNA in which microdissected chromosome bands or flow sorted chromosomes are digested with a frequently cutting restriction enzyme (Ludecke et al., 1989, Saunders et al., 1989). The resulting fragments are ligated to short oligonucleotides which serve as priming sites for PCR.

8.3.1 DOP-PCR allows more general amplification

Degenerate oligonucleotide-primed (DOP) PCR allows more general amplification than IRS-PCR or LA-PCR and has been performed on specific flow sorted

chromosomes or microdissected chromosomes or chromosome fragments for various cytogenetic applications including creating probes for fluorescent *in situ* hybridisation (FISH). DOP-PCR was designed and described in 1992 in three papers by a group at the University of Cambridge. First published was the paper entitled 'Cytogenetic Analysis by Chromosome Painting Using DOP-PCR Amplified Flow-Sorted Chromosomes' by Telenius et al. (Telenius et al., 1992a). The template for DOP-PCR in this case was hundreds of flow sorted human chromosomes with a translocation (chromosomes were sorted by passing a suspension through a dual-laser sorter, in which the two lasers excited the dyes which stained the chromosomes and could analyze them according to size and base-pair composition). The degenerate primer 6-MW 5'CCG ACT CGA GNN NNN NAT GTG G-3' was used and the DOP-PCR was carried out in the presence of $MgCl_2$, KCl, Tris-HCl, dNTPs and Taq polymerase. Concentrations of reagents and thermal cycles performed are detailed in the appendix section but, importantly five cycles using a low annealing temperature of 30°C were used prior to 35 cycles using a standard annealing temperature of 62°C. A secondary labelling reaction using 25 cycles with the higher annealing temperature was carried out using an aliquot of the primary reaction product using a lower dTTP concentration and adding biotin-11-dUTP. The resulting probe was ethanol precipitated with 3 μg of competitor DNA (Cot-1) and resuspended in 15 ml hybridisation buffer and used for FISH. Target metaphase chromosomes (normal, as opposed to the flow sorted chromosomes which had translocations) that were fixed on a microscope slide were denatured prior to the hybridisation. The probes were also denatured and preannealed with Cot-1 DNA to suppress repeated sequences before application to the slides. Hybridisation was carried out in a humidified box for 16 hours at 42°C. The slides were then washed and the probe was visualised by the two layer avadin-fluorescein isothiocyanate (FITC) detection system which produces a fluorescent signal at the site of biotinylated probe hybridisation. Metaphases were counter stained with DAPI or propidium iodide and the translocations could be characterised. The authors suggest that this method could be used for 'isolating unknown marker chromosomes for analysis by chromosome painting and hence determining their

origin. This should have relevance to the field of clinical cytogenetics, in cases where specific chromosome aberrations are shown to have prognostic value.'

In this publication it is stated that at a sufficiently low annealing temperature only the six specific bases of the 3' end of the oligonucleotide will prime the reaction, theoretically priming every 4^6(~4kbp) base pairs along the starting DNA thus at a frequency allowing a highly diverse amplification to take place. The DOP-primer consists of three parts (figure 8.2), six specific bases at the 3' end, the middle section contains six nucleotides of degenerate sequence and the 5' end has a recognition sequence for a restriction enzyme that cuts rarely within the genome (*Xho*I). The low annealing temperature of the first cycle allows the partially degenerate 3' end to anneal to the template material (8.2A). In the following low-temperature cycles fragments are generated which contain the full length of the primer at one end and its complementary sequence on the other end (8.2B). All the products from the first five cycles will contain the full length primer sequence so the annealing temperature can be raised from 30°C to 62°C (8.2C). The middle section will in practice anneal to a partially mismatched sequence because of its degeneracy, but apparently without any adverse effect on the reaction. This DOP-PCR primer and protocol should enable the amplification of DNA sources ranging in size from 2.4 kb up to complete genomes.

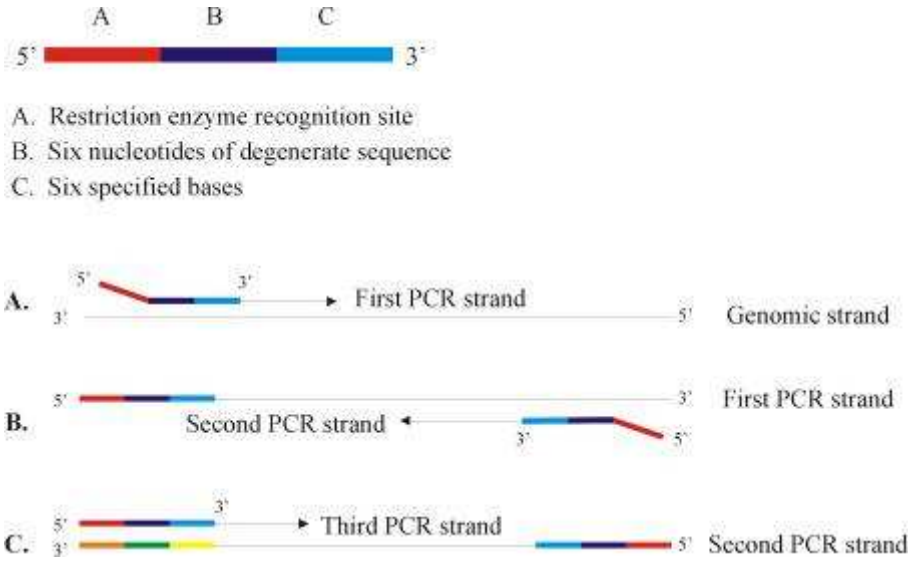

Figure 8.2: Degenerate oligonucleotide primer and DOP-PCR. A. At a low annealing temperature the six specific bases and the adjacent six degenerate bases will anneal to the template material. B. A few more low-annealing temperature cycles allow the generation of fragments containing the primer sequence at one end and its complimentary sequence at the other end. C. A higher annealing temperature allows only the full length of the primers to anneal to the fragments already created (taken from Telenius, H., A. H. Pelmear, et al. (1992). "Cytogenetic analysis by chromosome painting using DOP-PCR amplified flow-sorted chromosomes." *Genes, chromosomes and cancer* 4: 257-263).

Another of the papers by this group is 'Degenerate Oligonucleotide-Primed PCR: General Amplification of Target DNA by a Single Degenerate Primer' (Telenius et al., 1992b), in which two degenerate primers (6-M 5' AAGTCGCGGCCGCNNNNNNATG 3'and 6-MW 5' CCGACTCGAGNNNNNNATGTGG 3') and one non-degenerate primer (5' GCAATGAGATGCAACAGAGCA 3') were designed. Comparing PCR on genomic DNA using primer 6-M with three specific bases at the 3' end and 6-MW with six specified 3' nucleotides, it was found that 6-MW gave more efficient amplification, possibly reflecting more efficient annealing of that primer. Details of the methods used can be found in the appendix. The authors investigated the

optimal working conditions of DOP-PCR using the 6-MW primer by using it on genomic and cosmid DNA under different concentrations of $MgCl_2$, primer and Taq polymerase as well as with two different buffer types. The resulting product concentration was found to be dependent mainly on Taq polymerase concentration but also proportional to the primer concentration. It is important to note is that at very high polymerase concentrations (6.5 U/ 50 µl), primer related products were seen in negative controls. It was found that for both buffers used, optimal concentrations of reagents were 2-4 µM primer and 1.25-4 U Taq in 50 µl reaction containing 2 mM $MgCl_2$. From the data published (the products detected by ethidium bromide on an agarose gel) it seems that 3.75 U of Taq and 4 µM of primer produces the highest product yield. Of course the aim of DOP-PCR is to amplify as many sites as possible in contrast to conventional single-locus PCR, so primers and Taq will be depleted much quicker than in conventional PCR and instead of exponential amplification, linear amplification is observed, so for 35 cycles only 35 times the original concentration of template (n) will be present ($35n$, rather than n^{35}). Doubling the concentration of polymerase should double the product yield but as mentioned above, primer related products are seen in the negative controls when high Taq concentrations are used. DOP-PCR was used to amplify DNA of different species and complexity. PCRed genomic DNA from human, mouse and fruit fly all showed up as smears in the gel, cosmid DNA was amplified as discrete bands. FISH was carried out to compare the product from PCR using the partially degenerate primers, and the product from using two different *Alu*-specific primers. It was found that DOP-PCR produced brighter, more even and uniform paints than the paints made from IRS-PCR products. It is concluded that DOP-PCR relies on two basic requirements, firstly the initial low annealing temperature cycles which allow the primer to initiate PCR from short target sequences and secondly, primer degeneracy. The six degenerate nucleotides mean that there are 4^6 different sequences that the primers can anneal to, as opposed to a non-degenerate primer which may only anneal to one sequence.

8.3.2 DOP-PCR of needle microdissected chromosomes

Also published in 1992 was a paper by Meltzer et al. titled 'Rapid generation of region specific probes by chromosome microdissection and their application' (Meltzer et al., 1992). DOP-PCR was used to create region specific, fluorescent chromosome probes. The whole procedure is named Micro-FISH due to the microdissection and subsequent fluorescence *in situ* hybridisation reaction and it is stated that the method presented is rapid enough for the worker to create one or more paint probes in one day. This paper describes microdissecting abnormal metaphase chromosomes instead of normal chromosomes to create the probes, so that one may microdissect a known region of unidentifiable translocation, create a probe for that region and hybridise with normal metaphases to find out from which chromosome the translocated region originated. Metaphase chromosome fragments were dissected using microneedles and the desired number of scrapings (25-50) were transferred to a collection drop and amplified by DOP-PCR, details of which, and the rest of the process, can be found in appendix A. The authors speak of the potential value of these probes for detecting deletions as well as translocations, and how the probes will facilitate diagnosis of specific genetic diseases by enabling the analysis of previously unidentifiable translocations.

One year later in 1993 the same authors published a modified strategy for the generation of regional paint probes in 'Generation of band-specific painting probes from a single microdissected chromosome' (Guan et al., 1993). Chromosome fragments are pretreated before PCR with Topoisomerase I which dramatically increases the efficiency of amplification, and reduces the number of dissected DNA fragments required to generate probes. Topoisomerase I catalyses the relaxation of supercoiled DNA by producing single strand breaks in the double stranded DNA and it was thought that because DNA in metaphase chromosomes is highly condensed and the higher order structure of supercoiled DNA may limit the access of primers and polymerase to the template. PCR products from the Topo I pretreated dissected DNA appear as a smear ranging from 200-650 base pairs, however the PCR products which were not pretreated with Topo I remained below the sensitivity of ethidium

bromide staining, which suggests that Topo I treatment increases the yield of the PCR reaction. It is also noted that even though quantities of DNA were detected by ethidium bromide after being generated in a secondary PCR labelling reaction, no useful fluorescent signals were observed using probes generated without Topo I treatment. The introduction of preamplification with T7 DNA polymerase also results in increased efficiency of amplification and fluorescence intensity, because the lower reaction temperature promotes successful priming at shorter stretches of primer annealing. One to five copies of a targeted chromosome region were dissected and transferred into a collection buffer and subsequently amplified by DOP-PCR, fluorescently labelled and successfully hybridised to the target chromosome (see appendix A for method).

In 1996 and 1997 there were a few papers published which describe DOP-PCR of microdissected chromosomes to create chromosomal region specific micro clone libraries and chromosomal paint probes. Zimmer et al. amplified 15 to 20 of the same chromosome scraped off coverslips with glass microneedles to construct microclone libraries (Zimmer et al., 1997). The tips of the needles with the scraped chromosomes were dropped into a collection buffer and the DNA is amplified. This paper had some helpful hints such as sterilizing equipment with UV radiation before use and using stringent negative controls to reduce contamination which does occur often. It also suggests that using freshly prepared chromosome spreads for scraping and using acetic acid: methanol fixative in a ratio of 1: 5 instead of the standard 1: 3 in order to reduce the possibility of DNA damage due to excessive acid conditions.

Thalhammer et al. established probes for sub regions of the human genome by using DOP-PCR amplification of AFM (atomic force microscope) cantilever-dissected chromosome regions (Thalhammer et al., 1997). The AFM cantilever acted as a needle and cut through the chromosomal area of interest and the DNA that adhered to the tip was transferred to a collection tube. These authors found that less than 1 pg of microdissected DNA could be amplified in this way.

A recently published article in Biotechniques by Julio S. Masabanda and Darren K. Griffin (Masabanda and Griffin, 2003) describes a method for increasing the specificity and the signal of FISH probes made from microdissected chromosomes.

In the paper they tried to combat the problems that I also encountered using DOP-PCR of microdissected chromosomes, such as non-specific weak signals which have been attributed to co-amplification of non-target DNA and the formation of primer concatamers during the PCR. They state that the problem is exacerbated when lower numbers of templates are used and that 10-20 isolated chromosomes represent the limit of an experiment, and the problem is worsened when further amplifications are made from the original DOP-PCR product.

Their solution for enriching the sequences in the region of interest was to carry out a primary DOP-PCR and a secondary labelling DOP-PCR as normal (labelling with biotin 16-dUTP). This biotinylated product was then co-hybridised with fragmented (200-800 bp) genomic hamster DNA which had a linker arm ligated to it.

The DOP-PCR product and the linkered genomic DNA were combined and allowed to re-anneal overnight. The biotinylated DNA was captured by streptavadin coated paramagnetic beads and the annealed Genomic DNA was amplified by using a specific primer complementary to the attached liker arm.

The results of FISH show that the paint material is brighter and more specific using this purification protocol, and another advantage is that the probes produced in this manner do not require the inclusion of cot-1 DNA in the hybridisation mixture as contaminating repetitive sequences are removed by cot-1 DNA at an earlier stage. They summarise by saying they 'can take poor quality chromosome paints and generate bright, specific ones free from repetitive elements, contaminating DNA, primer artefacts, and non-specific background.'

8.4 Laser microdissection

The following passage describes the used of optical scissors to cut chromosomes directly, or to cut around film which the chromosomes of interest are attached to. This is of particular interest as we wish to create narrow band FISH probes using lasers to cut the chromosomes. In 1997, He et al. examined whether laser microsurgery, or needle microdissection in combination with laser pick-up, or in combination with optical trapping can be applied to DNA cloning to improve

existing techniques (He et al., 1997). The system used was a two beam optical trap and single beam optical scissors combined with a laser scanning confocal microscope and is termed CATS (confocal ablation trapping system). The trapping laser was an argon ion laser pumped cw Ti: Sapphire laser with an adjustable wavelength range from 700 nm to 1000 nm. The beam from this laser was split into two trapping beams and each of the three beams were manipulated by using computer controlled joysticks that control scanning mirrors. For chromosome microdissection, a frequency doubled, Q-switched Nd: YAG laser which produces a beam at 532 nm was used. The focused spot of this laser was 0.5 μm in diameter. A chromosomal region of interest in a metaphase spread was isolated for needle collection by ablating the surrounding material and then scraping the region of interest which was left behind with a sterile needle. Twenty fragments were used for each PCR in this case. Needle microdissection was performed by directly scratching the chromosome fragments from the slide and placing them in a PCR tube containing buffer. Seven fragments were collected in this case. Chromosomes in suspension were trapped by using the two trapping beams, one holding each end of the chromosome in a horizontal position, and the cutting laser was moved across the desired chromosomal region. The fragment was then moved from the dissecting well to the collecting well through a zigzag channel using one of the trapping beams, but it is not discussed if these fragments are actually amplified or how they are removed from the collection chamber. It is concluded that laser-cut fragments can be subjected to successful PCR and DNA libraries can be generated. The laser technique is said to provide more accurate chromosome regional targeting. Also compared were laser microdissected fragments which were exposed to 10 minutes of trapping laser radiation. The fragments were collected using a needle and amplified successfully.

The group who used the AFM for microdissection also published a paper in 1999 entitled 'Laser microdissection and laser pressure catapulting for the generation of chromosome specific paint probes' (Schermelleh et al., 1999). Metaphases were spread on a 1.35 μm thick piece of polyethylene naphthalate (PEN) or polyester-based (NYLA) membrane taped onto a microscope slide. By using a commercially

available ‘UV-laser microbeam microdissection in combination with laser pressure catapulting’, single chromosomes were collected and amplified by DOP-PCR. The basics of this technique are mounting the chromosomes on ultrathin membranes, the laser ablation of any unwanted genetic material adjacent to the target chromosome, isolation of target chromosome by laser dissection of the membrane around the chromosome and collection of the chromosome stuck to the membrane by laser pressure catapulting. The system used was the Robot-Microbeam, made by P.A.L.M. Microlaser Technologies in Germany which consists of a 337 nm nitrogen laser focused through an inverted microscope, and a computer controlled stage and micromanipulator. 0.2-0.3 μJ/pulse was used for ablation and 0.5-0.6 μJ/pulse was used for membrane dissection and results in a cutting width of around 3 μm. The chromosome attached to the dissected membrane was catapulted into a collection device 1 mm above the slide by focusing the laser slightly below the membrane and using a single laser pulse of 1-2 μJ/pulse. The collection device was a small piece of glass heat sealed to a pipette tip with a drop of glycerol on it to facilitate adherence of the chromosome. Collection of the chromosome could be monitored by focusing an objective onto the glass. The glass particle was then transferred to a microfuge tube and centrifuge so that the glycerol with the chromosome in it would go to the bottom of the tube and the glass could be removed. DOP-PCR was carried out and following that the probe was labelled and FISH was performed. The probe showed specific hybridisation over the entire length of the captured chromosome, even if only a single copy of a chromosome was used as a template however, background hybridisation is often seen due to debris from the ablated chromosomes on the membrane being amplified along with the target chromosome. The authors make some suggestions for creating smaller, chromosome region specific probes, such as ablating all unwanted genetic material adjacent to the target region before dissecting the membrane, or finding a membrane which requires less energy to cut it, making the cutting width finer, as 3 μm is too large to microdissect fragments.

Nanodissection of human chromosomes has been performed using near-infrared femtosecond laser pulses (Koenig et al., 2001). Pulses from an 80 MHz femtosecond laser source at 800 nm with a mean power of 15-100 mW, 170 fs pulse

width and millisecond beam dwell time was used to cut holes in chromosomes which were 100 nm FWHM which is below the diffraction limited spot size. Chromosomes were also dissected with FWHM cut sizes below 200 nm. The authors suggest that high-repetition-frequency femtosecond lasers at a low mean power focused by a high numerical aperture can be used as 'novel ultraprecise non-invasive nanosurgery tools with a precision below the diffraction-limited spot size without visible collateral damage' and that the non-invasive inactivation of chromosomal regions within living cells is possible.

8.4.1 Commercially available laser capture microdissection tools

The first commercial laser capture microdissection apparatus The PixCell was developed in 1996 and later the PixCell II at the National Institutes of Health and was brought to market by Acturus Engineering of California. A microscope slide containing a dissected tissue sample is placed on an inverted microscope and a microfuge cap with film attached is placed above the sample. A focused 810 nm HeNe laser melts the film onto the target area of tissue containing cells of interest which is plucked from the rest of the sample when the cap and the attached film is removed. Tissue samples have to be completely dehydrated and the set up is not so good for irregularly shaped samples and only really punches out circles, with the user not having much control over their size. However it has the advantage of the user being able to visualise fluorescence while using the laser and the dissected product can also be easily visualised.

A competitor of this system is the P.A.L.M. (*p*ositioning and *a*blation with *l*aser *m*icrobeams) Robot-Microbeam, mentioned previously, which is made by P.A.L.M. Micro Technologies of Germany. A UV 337 nm nitrogen laser is used for laser microbeam microdissection (LMM) and laser pressure catapulting (LPC). An area of interest within the tissue is circumscribed by the laser which has a focus of less than 1 μm. The sample can be collected by using a glass microneedle to pick up the excised region or the laser can be refocused below the target region which ejects the

cells into a microfuge cap placed immediately above the sample. In the paper described above a film is used which was provided by the manufacturers and it was also used to isolate single chromosomes instead of single cells. The beam can also be used to ablate any unwanted material. The SL μCUT is another system from MMI AG of Switzerland. A 332 nm nitrogen laser is used. Tissue samples are placed on a microscope slide and are covered by a thin membrane. The laser circumscribes the membrane which is removed along with the tissue by sticking to an adhesive-lined microfuge cap.

Leica Microsystems of Germany make the AS LMD which uses a 332 nm laser to ablate tissue as well as membrane. The tissue sample adheres to a membrane coated slide and is place upside down on an upright microscope. When the area is excised it falls due to gravity into a microfuge cap. This system is good for irregularly shaped samples as you can trace the area you wish to dissect on a computer screen using a mouse.

A more recent system is the Clonis made by BioRad's Microscopy division in the UK. The film to which the cells adhere is in a Petri dish and a 780 nm IR laser cuts the film and welds it to an underlying substrate. The welded film and cells stay behind while the remaining film and the unwanted cells are lifted away. This was developed to be used for sterile tissue culture but can also be used for archival tissue.

The prices of these systems start around $100,000 (Roberts, 2002) and they are often used in conjunction with other tools such as micromanipulators and optical tweezers, and some groups have realised their potential for isolating whole chromosomes, however the technique is not intricate enough to dissect structures as small as chromosomes themselves.

In summary methods used for the isolation of chromosome fragments for enzymatic amplification are

- **Needle microdissection** (Meltzer et al., 1992; Guan et al., 1993; Zimmer et al., 1997)
- **AFM cantilever tip microdissection** (Thalhammer et al., 1997)
- **Laser ablation of unwanted material and needle pick-up of remaining fragment** (He et al., 1997)

- **Laser ablation of surrounding membrane and laser catapulting of chromosome-membrane stack** (Schermelleh et al., 1999)
- **Laser microdissection and optical tweezing of fragment** (demonstrated separately but not together (He et al., 1997)

Now that we have explored how to create a fluorescent chromosome probe, we now discuss the application of FISH probes to the investigation of chromatid breaks.

8.5 Mammalian DNA and chromosomes

The genetic information of living organisms is stored in its deoxyribonucleic acid (DNA) which is a long, unbranched linear polymer in the shape of a double helix which contains many millions of nucleotides (also called bases). Each base pair is 0.34 nm apart and the double helix is 2 nm wide. The human genome contains 3 x 10^9 nucleotide pairs which consist of 35, 000 genes. DNA is associated with proteins and the DNA-protein complex is called chromatin. During interphase, when genes are expressed, the chromatin fibres are usually highly extended and tangled. As the cell prepares for mitosis, the chromatin coils and folds up (condenses) to form a number of short, thick, discrete metaphase chromosomes that can be visualised under a light microscope. Different species have different sizes and numbers of chromosomes within their cells. The typical packaging of DNA into mammalian metaphase chromosome can be seen in figure 8.3.

A 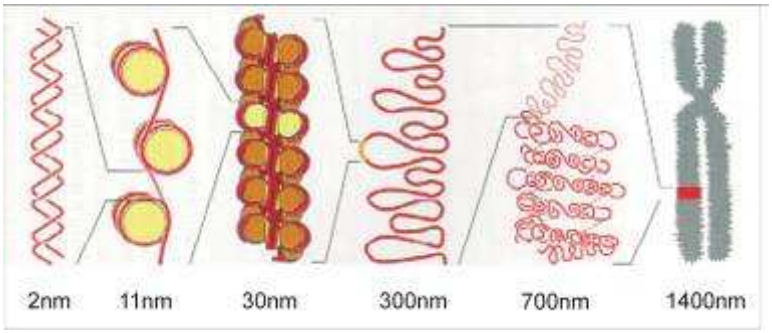

B 

Figure 8.3: Levels of chromatin packaging in a mammalian metaphase chromosome. A. The 2 nm wide DNA double helix forms 'beads on a string' in association with protein complexes called nucleosomes. The 30 nm chromatin fibre is a tightly wound coil. These fibres form looped domains 300 nm wide. A metaphase chromosome has all its DNA highly condensed into a compact structure which can be seen in B. (both taken from Alberts et al., Molecular Biology of the Cell).

8.5.1 Chromosome aberrations

Some metaphase chromosomes of cells which have been treated with chemicals or irradiation show aberrations (UKEMS, 1983). A discontinuity in the DNA such as a break is one type of aberration, visible using the light microscope to view metaphase chromosomes, and chromosomal numerical changes within the cell are also classed as aberrations. Malignant cells are usually chromosomally abnormal. Any drastic changes in the chromosomes such as numerical changes are usually lethal to the cell so there is no danger to the organism however, subtle changes in chromosomal structure, such as translocations, inversions, duplications and deletions, are more hazardous to the organism as they may not be lethal to the cell.

Chromosomal structural aberrations can be of the chromosome type (figure 8.4) where the damage occurs in G0 or G1 before the chromosome has replicated and the aberrations can be seen in both chromatids at metaphase, or the chromatid type

(figure 8.5) which involves only one chromatid of the damaged chromosome, due to the damage occurring after replication.

Chromosome type aberrations can be classed as gaps or breaks which involve only one chromosome, or exchanges, with interchanges occurring between chromosomes, and intrachanges occurring within a chromosome. A gap (or achromatic lesion) is classified as being smaller than the width of a chromatid with both chromatids involved at identical loci and the distal region is always aligned with the proximal region. A break or terminal deletion is so called because the gap is larger than the width of a chromatid and the two regions may not be aligned. Interchanges are exchanges involving two or more lesion in the same or different chromosomes and results from an exchange between two chromosomes in G1. Intrachanges occur within a chromosome and the exchange can be between arms (interarm intrachange) and result in a centric ring with an accompanying fragment, or within an arm (intraarm intrachange) which results in an acentric ring (the result of an interstitial deletion) accompanying the chromosome. These chromosome type aberrations can be seen in figure 8.2.

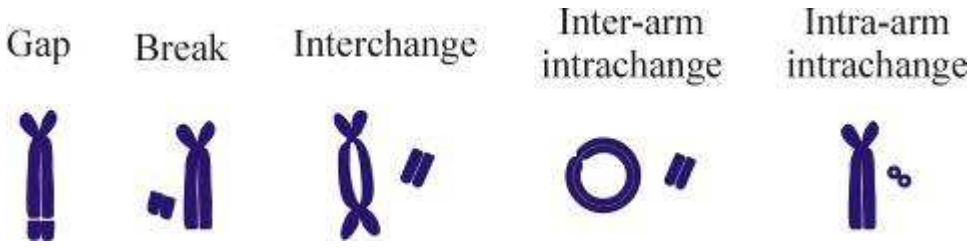

Figure 8.4: Chromosome type aberrations.

Chromatid type aberrations usually involve only one chromatid of each chromosome except for isochromatid breaks, which are due to damage occurring after the chromosome has replicated. These aberrations can also be classed as gaps, where the gap (which occurs in only one chromatid of the chromosome) is smaller than the width of a chromatid, a chromatid break or deletion where the gap in one chromatid is larger than chromatid width and the fragment usually remains aligned with the parent chromatid and if it is displaced it is usually associated with the chromosome

of origin. Isochromatid breaks or deletions are another class of chromatid type aberrations in which the broken ends are rejoined either proximally, distally or at both ends. Exchanges are seen between chromosomes (interchange) which are asymmetrical if rejoining is completed and results in a dicentric and accompanying fragment sometimes called a quadriradial, or symmetrical which only leads to a dicentric chromatid or a fragment if rejoining is incomplete. Exchanges also occur within a chromosome (intrachanges) either between arms (interarm interchange) or within an arm (intraarm interchange). An interarm intrachange will result in an asymmetrical structure with a fragment produced if rejoining is incomplete or a symmetrical structure with no fragment if rejoining is complete. An intraarm intrachange results in a minute or interstitial deletion that remains associated with the chromosome of origin. Isochromatid interchanges are another class of chromatid type aberrations with a dicentric and a fragment formed or a monocentric triradial is formed with no fragment if rejoining is complete. Examples of chromatid type aberrations are illustrated in figure 8.5.

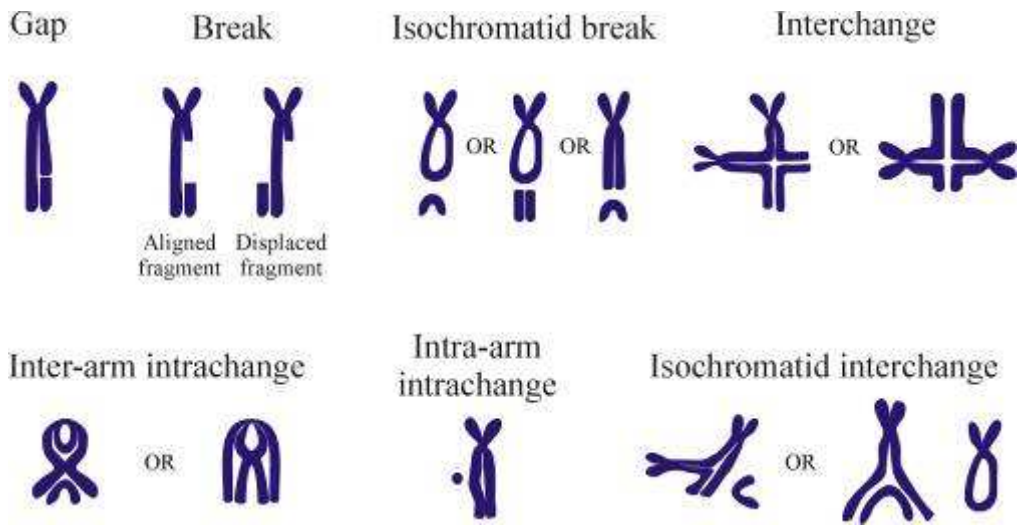

Figure 8.5: Chromatid type aberrations.

8.5.2 Chromatid breaks

On average chromatid breaks occur more frequently in cells from cancer patients than in normal control individuals indicating that a higher proportion of cancer patients may be more radiosensitive than normal. 42% of a group of breast cancer cases studied showed elevated lymphocyte chromatid radiosensitivity compared with only 9% of a group of normal controls (Scott et al., 1994, Scott et al., 1999).

One of the most intriguing questions in radiobiology is the relationship between primary DNA damage and the aforementioned visible chromosomal aberrations. Sometimes a single dsb (double strand break) in the cell created by ionizing radiation (X and γ rays) during the G2 phase of the cell division cycle can result in a break in the sister chromatid when it is viewed through the microscope during metaphase when the chromosomes have condensed prior to cell division. It is puzzling that a single dsb can lead to the apparent loss of such a large section of chromosome (sometimes up to 30% of a sister chromatid arm). The precise mechanism by which this occurs is not clear, although several models have been proposed.

Sax proposed in 1940 that a lesion in the DNA resulted in a break in the chromatid, or if two chromatids were involved in an exchange then this would be the result of two lesions in the DNA (Sax, 1940). The breakage first model proposed by Bender et al. in 1974 (Bender et al., 1974) follows on from this and states that the initial lesion is the visible chromatid break itself, however, assuming a dsb is the initiating lesion, the ends of the dsb would either have to shrink (but there is never dense staining at the ends to indicate this) or have been digested by an exonuclease (but it is known that mammalian cells do not significantly degrade their DNA even after high doses of radiation). Another proposal is that two dsbs create a segment which is lost, hence the gap, however the doses used (0.2-1 Gy) are too low to create two dsbs in one chromosome. A dose of 0.25 Gy should make one dsb per four chromosomes per diploid cell and in addition the dose-effect curve for chromatid breaks is linear (Bryant, 1998a). Furthermore, it has been reported that one single

double strand break is sufficient to create a chromatid break (Rogers-Bald et al., 2000).

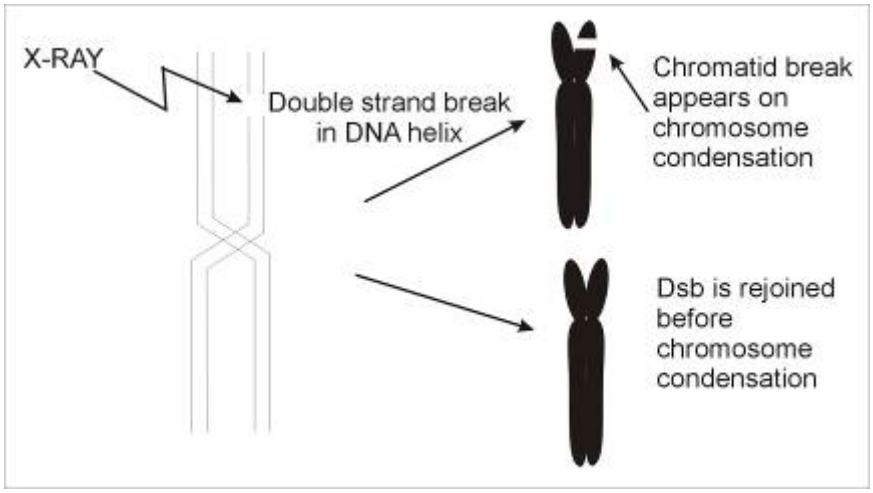

Figure 8.6: The breakage first model according to Bender et al. (1974). The initial lesion in the DNA double helix (which would result in the loss of 0-4 bases) is the visible chromatid break. However the chromatid break viewed under the microscope is an apparent loss of up to 40 mega bases.

The Revell Exchange model (Revell, 1959) proposed that an exchange occurs between the sites of an unspecified type of damage at the necks of looped chromatin domains, but the chances of two such lesions occurring close together at the necks of the loops is again very low for the dose range used in the G2 experiments. In addition, as mentioned above there is a linear relationship between breaks and dose (Bryant, 1998a) – for two lesions a quadratic relationship would be required.

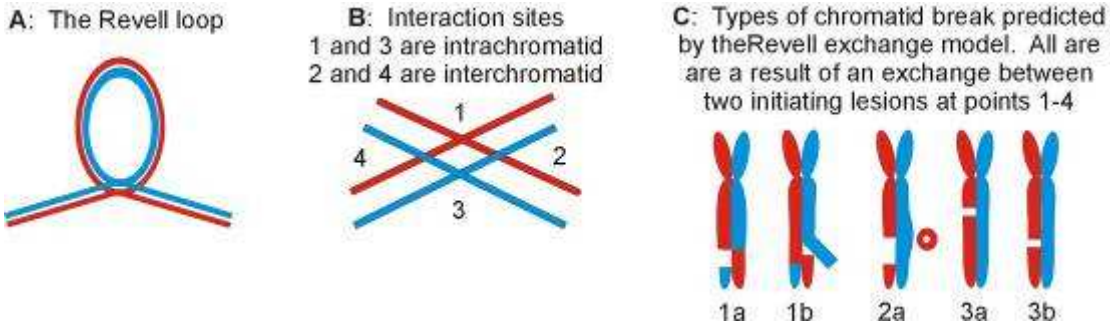

Figure 8.7: The Revell exchange model (Revell, 1959). Exchange occurs at neck of loop where damage occurs. Exchanges that involve both sister chromatids (exchanges at point 2 or 4 in B) result in colour-switches of type 1a or 1b in C when chromosomes are harlequin stained. Intrachromatid exchanges involving only one sister chromatid (at lesions in point 1 or 3, in B) result in a non colour-switch break of type 2a, 3a or 3b in C.

Nevertheless the exchange model does make some predictions which are supported by observation, for example the exchanges involving both sister chromatids which result in a switch of strands at the break point (figure 8.8). A proportion of chromatid breaks (between 10-20% depending on cell line) are formed by a mechanism involving such sister chromatid rearrangements around the break site. These are detected by the presence of a colour-switch at the break point in harlequin (FPG - fluorescence plus Giemsa staining) - stained chromosomes. The remainder of the (non colour-switch) breaks may be formed by chromatin rearrangements but only involving one sister chromatid.

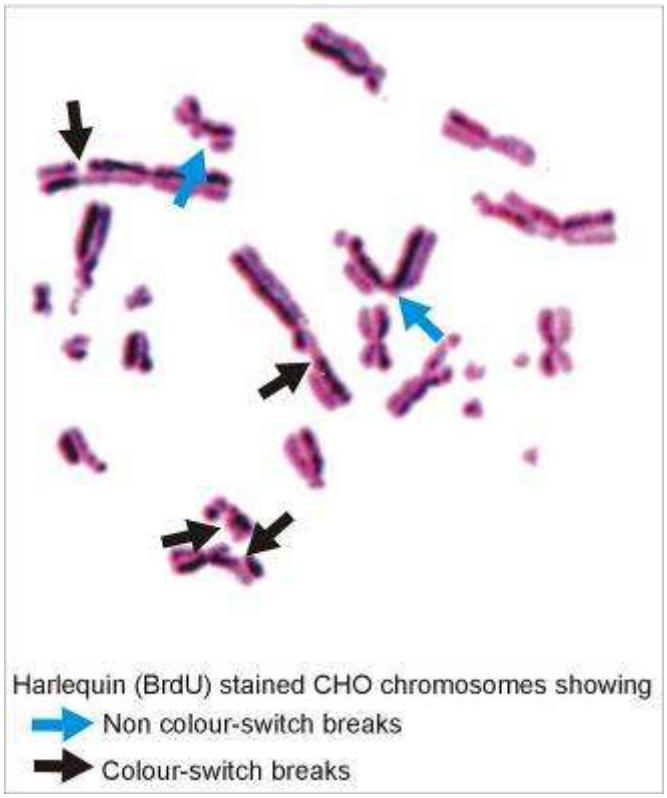

Figure 8.8: Harlequin stained Chinese hamster chromosomes (using 5-bromo-2'-deoxyuridine [BrdU]). The lighter sister chromatid is the most recently synthesised. Colour-switch breaks (black arrows) and non colour-switch breaks (blue arrows) can be seen (taken from Bryant, 1998a).

8.5.3 Chromatid breaks are formed by a single-event mechanism

Many experiments have shown that a single dsb is sufficient to induce such a chromatid break which represents an apparent loss of up to 40Mb of DNA. Chromatid breaks are induced by X and γ rays as a linear function of dose (Bryant, 1998a, Bryant et al., 1998, Terzoudi et al., 2000) which suggest that chromatid breaks are formed by a single-event mechanism. Using a genetically engineered CHO cell line containing a single I-SceI site that can be cut enzymatically to yield a unique genomic dsb by treatment of streptolysin-O porated cells with I-SceI endonuclease (Meganuclease), it was shown that a single dsb suffices to induce

either a colour-switch or non colour-switch chromatid break, in a similar ratio to that of γ rays (Rogers-Bald et al., 2000). The dsbs induced by the endonuclease appear to mimic radiation induced dsbs as they trigger the phosphorylation of histone H2AX over mega-base sized chromatin domains surrounding the dsb (Rogakou et al., 1999). The function of γ-H2AX is thought to be the signalling and recruitment of DNA processing enzymes involved in the rejoining of the dsb and also preparation of the chromatin prior to repair. Chromatid breaks have also been induced in Chinese hamster cells by exposure to ultrasoft carbon K-shell X rays (Bryant et al., 2003). The energy of these X rays is not sufficient for the secondary electrons to span more than one DNA double helix (Michalik, 1994) so only single dsbs are created, and it was found that around 10% of the carbon K-shell X-ray induced chromatid breaks have associated colour-switches at breakpoints, indicating that they arise through sister chromatid rearrangements.

8.6 The Signal Model

The Bryant signal model (Bryant, 1998a, Bryant, 1998b) proposes that a single dsb in a loop of DNA (perhaps comprising one or a few transcription factory domains (Iborra et al., 1997)) in the chromosome signals to the cell to make some kind of recombinational exchange at the loop neck. Chromatin is cut (perhaps by DNA processing enzymes located in the transcription factories) and loops (presumably containing the repaired initiating damage) are illegitimately recombined, perhaps leading to deletion, duplication or inversion of a section of DNA and a visible break is seen if time does not allow for the recombinational exchange to be completed.

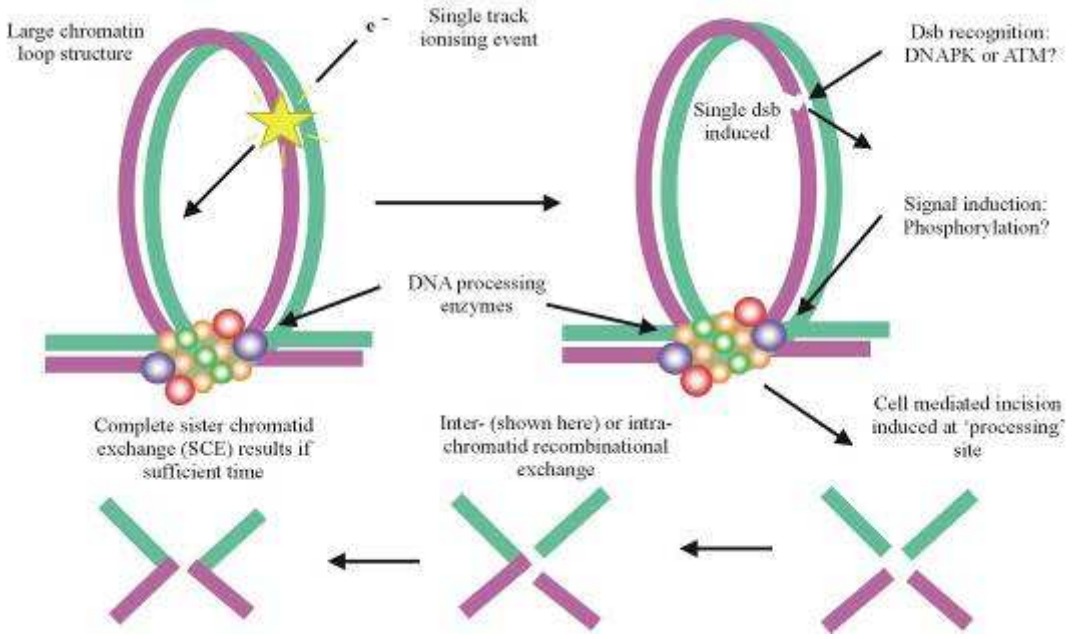

Figure 8.9: The Signal Model (Bryant, 1998a). Large looped domain structures in the chromosome are thought to consist of one or a few transcription factory domains, perhaps containing DNA processing enzymes. The double strand break (dsb) signals the cell to make an exchange at the neck of the loop, resulting in an inter- or intra-chromatid recombinational exchange, perhaps leading to excision of the loop. If time does not allow for exchange to be completed, a chromatid break is visible.

Chromatid breaks involving interchromatid exchanges (those between sister chromatids) show colour-switches at break points in harlequin stained cells, whereas intrachromatid breaks show no colour-switches but may involve a small inversion at the break point or the excision of a small chromatin ring. The exchanges are of the same type as those predicted by Revell but the model differs in that only one single double strand break is required to initiate the recombinational exchange instead of two unspecified lesions required by Revell's model. Furthermore, the model does not predict that the aberration types would be equally likely, with the intra chromatid types (figure 8.11) appearing to be the predominant form.

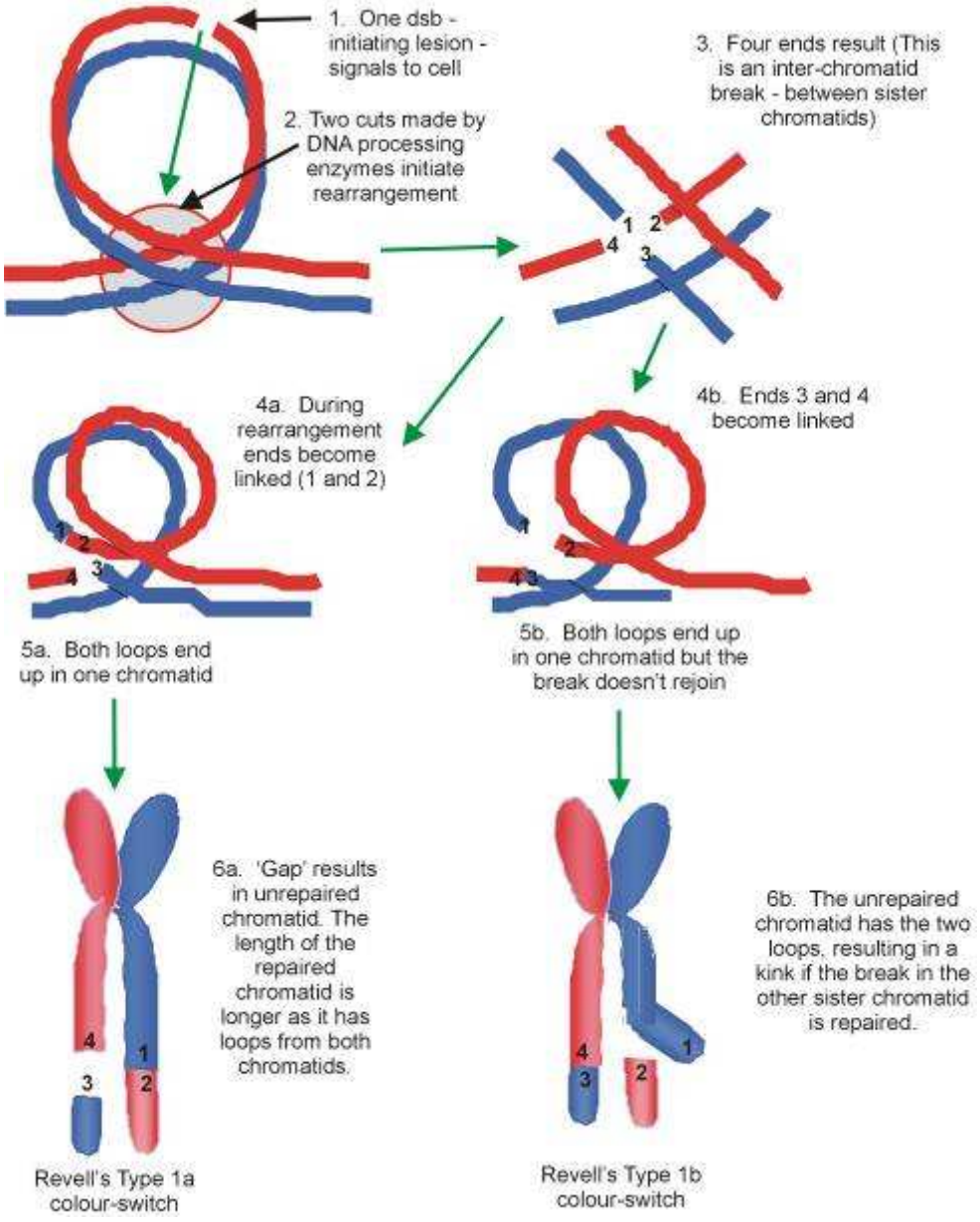

Figure 8.10: Possible mechanisms for a colour-switch rearrangement. The two sister chromatids are recombined such that one of them gets the loop belonging to the other – hence the break in the chromatid at the colour-switch site.

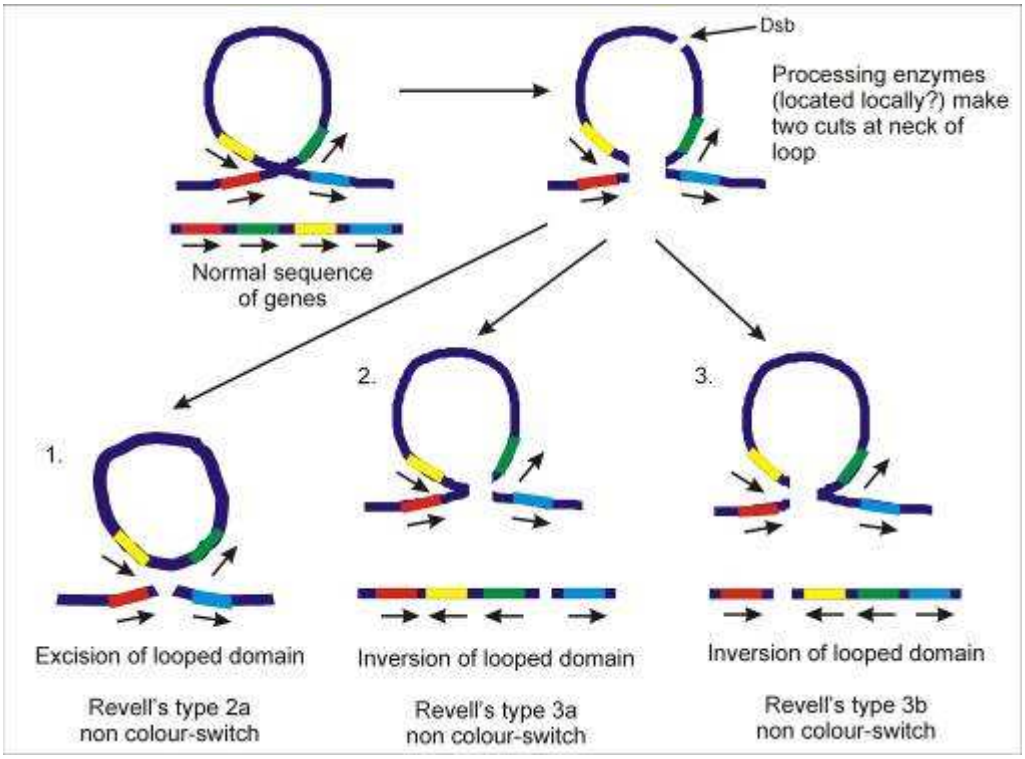

Figure 8.11: Non colour-switch break rearrangements (due to intra-chromatid breaks) can lead to excision of a chromatin ring (1) or genomic inversions (2, 3).

The chromatid breaks disappear with time of sampling after irradiation, and it was thought that perhaps this is due to the DNA repair enzymes having more time to act, but it also supports the idea of recombination, giving the cell more time to complete the exchange process. Thus according to the signal model, disappearance of chromatid breaks represents completion of the recombinational rearrangement.

As mentioned above, cancer patients (30-40% of them) show higher mean radiosensitivity than controls (i.e. more chromatid breaks per cell for the same dose of radiation), and it is know that abnormal chromosomes are often present in cancer cells. Also, changes in the nucleotide sequence of DNA are known to lead to cancer. Inversions and excisions of DNA sequence which can occur as a result of recombinational rearrangements, predicted by the signal model could be causing proto-oncogenes to be expressed as oncogenes, or could delete tumour suppressor genes, or creating fusion proteins that could disrupt the cell cycle control

mechanisms. Thus, formation of some types of chromatid break may be potentially oncogenic.

Why the cell makes such chromatin rearrangements at sites of damage is unclear. Perhaps it is an attempt by the cell to excise the damaged region of DNA at first division, making the daughter cell with the damage die, but allowing the other daughter cell to survive, or it could be that the whole rearrangement process is a deleterious by-product of radiation induced damage to the DNA, and cellular machinery used for other purposes within the cell is triggered to make dramatic structural changes by the presence of the dsb.

8.7 Methods to investigate the Signal Model

Several cell lines of Chinese hamster ovary cells or Muntjac cells have already been created which carry a transfected site, the sequence of which is recognised by the endonuclease I-SceI. These cell lines have also been engineered to contain an inducible expression system involving the I-SceI gene and the enzyme is expressed endogenously in the presence of the insect ecdysone analogue Ponasterone A. The I-SceI endonuclease will cut the chromosome at one specific point in each cell always at the same location on the same chromosome where the recognition sequence has integrated.

Colcemid is added to the cells shortly after endonuclease induction and this chemical blocks the cell division cycle at metaphase by preventing the polymerisation of microtubules on the mitotic spindle (by binding to tubulin). The cells are then fixed, stained and mounted onto a microscope slide and chromatid breaks are sought by examining the metaphases using a microscope.

One of the aims of my research was to create FISH (fluorescent *in situ* hybridisation) probes to detect the putative inversions in non colour-switch breakpoints mentioned above. A series of narrow band fluorescent chromosome FISH probes for the regions adjacent to the chromatid break could help detect translocations or inversions in that area and test the signal model.

The FISH probes were to be generated using optical tweezers and scissors, by microdissecting chromosome fragments using a cutting laser, and manipulating the cut fragment with optical tweezers. The isolated fragments could then be amplified by DOP-PCR (degenerate oligonucleotide primed - polymerase chain reaction) and fluorescently labelled. The paint probes (say red, yellow, and green), are hybridised to target metaphases with induced double strand breaks and viewed under fluorescence and compared to normal metaphases. Opposite sequences of coloured probes at the break sites in chromatids from those in normal chromatids would prove the existence of inversions and support the signal model. This scheme can be seen in figure 8.12.

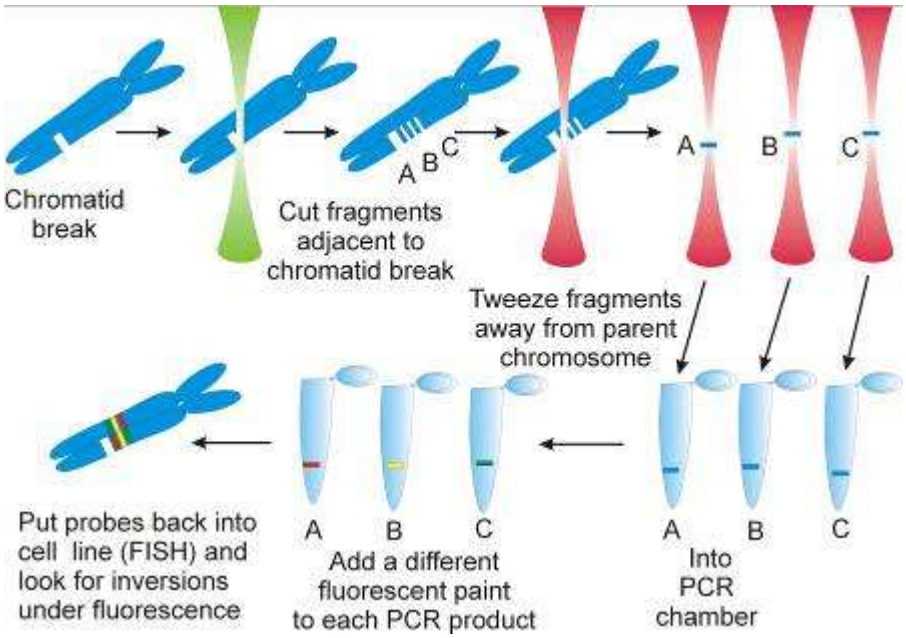

Figure 8.12: Method for creating narrow band chromosome FISH probes.

An alternative scheme would be to make many narrow band paint probes from over one entire chromosome. The FISH probes would be added to the target metaphases (both irradiated with induced chromosome breaks and normal), and chromosomes examined for inversions at break sites of the irradiated chromosomes.

8.8 Summary

Degenerate oligonucleotide primed - polymerase chain reaction (DOP-PCR) is an existing technique used for the general amplification of microdissected chromosomal material. Chromosome paint probes have been successfully created within various groups by performing this technique on FACS sorted, whole chromosomes or on needle or optically microdissected and manipulated chromosomal material.

In this work we aim to use DOP-PCR to create fine FISH probes from laser microdissected, optically tweezed chromosomal fragments. The FISH probes will have applications in cytogenetics and cytometry, and in particular will be useful for the detection of chromosomal inversions which are thought to be found in association with single, double strand break (dsb)-induced chromatid breaks. The search for these putative inversions using narrow band chromosome FISH probes created in this way will test the signal model, which states that chromatid breaks are induced by a single dsb and that there is a recombinational event within the chromosome which results in a chromatid gap and perhaps deletions, duplications or inversions in the DNA.

References

Bender MA, Griggs HG, Bedford JS: **Mechanisms of chromosomal aberration production, III. Chemicals and ionising radiation.** *Mutation Research* 1974; **23**:197-212.

Bryant PE: **The signal model: a possible explanation for the conversion of DNA double-strand breaks into chromatid breaks.** *International Journal of Radiation Biology* 1998a; **73**:243-251.

Bryant PE: **Mechanisms of radiation-induced chromatid breaks.** *Mutation Research-Fundamental and Molecular Mechanisms of Mutagenesis* 1998b; **404**:107-111.

Bryant PE, Finnegan C, Swaffield L, Mozdarani H: **G2 chromatid breaks in murine scid cells.** *Mutagenesis* 1998; **13**:481-485.

Bryant PE, Jones C, Armstrong G, Frankenberg-Schwger M, Frankenberg D: **Induction of chromatid breaks by carbon K-shell ultrasoft X rays.** *Radiation Research* 2003; **159**:247-250.

Guan X, Trent JM, Meltzer PS: **Generation of band-specific painting probes from a single microdissected chromosome.** *Human Molecular Genetics* 1993; **2**:1117-1121.

He W, Liu Y, Smith M, Berns MW: **Laser microdissection for generation of a human chromosome region-specific library.** *Microscopy and Microanalysis* 1997; **3**:47-52.

Iborra FJ, Pombo A, Jackson DA, Cook PR: **Active RNA polymerases are localized within discrete transcription 'factories' in human nuclei.** *Journal of Cell Science* 1997; **109**:1427-1436.

Koenig K, Riemann I, Fritzsche W: **Nanodissection of human chromosomes with near-infrared femtosecond laser pulses.** *Optics Letters* 2001; **26**:819-821.

Langlois RG, Yu LC, Gray JW, Carrano AV: **Quantitative karyotyping of human chromosomes by dual beam flow cytometry.** *Proceedings of the National Academy of Science USA* 1982; **79**:7876-7880.

Ludecke HJ, Senger G, Claussen U, Horsthemke B: **Cloning defined regions of the human genome by microdissection of banded chromosomes and enzymatic amplification.** *Nature* 1989; **338**:348-350.

Masabanda JS, Griffin DK: **Generation of chromosome paints: Approach for increasing specificity and intensity of signals.** *Biotechniques* 2003; **34**.

Meltzer PS, Guan X, Burgess A, Trent JM: **Rapid generation of region specific probes by chromosome microdissection and their application.** *Nature Genetics* 1992; **1**:24-28.

Michalik V: **Distance distributions for energy deposition clusters in different particle tracks.** *Radiat. Prot. Dosim.* 1994; **52**:245-248.

Nelson DL, Ledbetter SA, Corbo L, Victoria MF, Ramirez-Solis R, Webster TD, Ledbetter DH, Caskey CT: **Alu polymerase chain reaction: A method for rapid isolation of human-specific sequences for complex DNA sources.** *Proceedings of the National Academy of Science USA* 1989; **86**:6686-6690.

Revell SH: **The accurate estimation of chromatid breakage and its relevance to a new interpretation of chromatid abberations by ionizing radiations.** *Proceedings of the Royal Society of London B* 1959; **150**:563-589.

Roberts JP: **The cutting edge in laser microdissection.** *Biophotonics International* April 2002:50-53.

Rogakou E, Boon C, Redon C, Bonner WM: **Megabase chromatin domains involved in DNA double-strand breaks in vivo.** *Journal of Cell Biology* 1999; **146**:905-915.

Rogers-Bald M, Sargent RG, Bryant PE: **Production of chromatid breaks by single dsb: evidence supporting the signal model.** *International Journal of Radiation Biology* 2000; **76**:23-29.

Saunders RD, Glover DM, Ashburner M, Siden-Kiamos I, Louis C, Monastirioti M, Savakis C, Kafatos F: **PCR amplification of DNA microdissected from a single polytene band: a comparison with conventional microcloning.** *Nucleic Acids Research* 1989; **17**:9027-9037.

Sax K: **An analysis of X-ray induced chromosomal abberations in Tradescantia.** *Genetics* 1940; **25**:41-68.

Schermelleh L, Thalhammer S, Heckl W, Posl H, Cremer T, Schutze K, Cremer M: **Laser microdissection and laser pressure catapulting for the generation of chromosome specific paint probes.** *Biotechniques* 1999; **27**:362-367.

Scott D, Spreadborough A, Levine E, Roberts SA: **Genetic predisposition to breast cancer.** *Lancet* 1994; **344**:1444.

Scott D, Barber JBP, Spreadborough AR, Burrill AR, Roberts SA: **Increased radiosensitivity in breast cancer patients: A comparison of two assays.** *International Journal of Radiation Biology* 1999; **75**:1-10.

Telenius H, Pelmear AH, Tunnacliffe A, Carter NP, Behmel A, Ferguson-Smith MA, Nordenskjold M, Pfragner R, Ponder BAJ: **Cytogenetic analysis by chromosome painting using DOP-PCR amplified flow-sorted chromosomes.** *Genes, chromosomes and cancer* 1992a; **4**:257-263.

Telenius H, Carter NP, Bebb CE, Nordenskjold M, Ponder BAJ, Tunnacliffe A: **Degenerate oligonucleotide-primed PCR: General amplification of target DNA by a single degenerate primer.** *Genomics* 1992b; **13**:718-725.

Terzoudi GI, Jung T, Hain J, Vrouvas J, Margaritis K, Donta-Bakoyiannis C, Markropoulos V, Angelakis PH, Pantelias GE: **Increased G2 chromosomal radiosensitivity in cancer patients: The role of cdk/cyclin-B activity level in the mechanisms involved.** *International Journal of Radiation Biology* 2000; **76**:607-615.

Thalhammer S, Stark RW, Muller S, Wienberg J, Heckl WM: **The atomic force microscope as a new microdissecting tool for the generation of genetic probes.** *Journal of Structural Biology* 1997; **119**:232-237.

UKEMS: The United Kingdom Environmental Mutagen Society: **Report of the UKEMS sub-committee on guidelines for mutagenicity testing Part 1.** *The United Kingdom branch of the European Environmental Mutagen Society* 1983; **1**:43-61.

Zimmer R, Haberfeld A, Verrinder Gibbens AM: **Microisolation of the chicken Z chromosome and construction of microclone libraries.** *Genome* 1997; **40**:865-872.

9 Investigation of various methods to isolate and amplify chromosomes and chromosomal fragments

9.1 Introduction

This chapter describes the process of creating chromosome probes. Materials and equipment used are listed in the appendix and this chapter details the experimental procedures undertaken and results are also described.

We aimed to create narrow band chromosome FISH (fluorescent *in situ* hybridisation) probes in order to detect inversions or any change in the DNA sequence of chromatids around a break point on the chromatid. The break point would be produced using an endogenously expressed endonuclease or by irradiation.

The use of optical tweezers was the major approach taken to isolate single chromosomes and laser microdissected fragments, although various other methods were attempted. This isolated chromosomal DNA was enzymatically amplified using degenerate oligonucleotide primed polymerase chain reaction (DOP-PCR), although another amplification method using a kit named Genomiphi was also used in the later stages of work. The downstream application of the amplified chromosome fragments was to create a series of very small FISH probes, with which putative inversions in the DNA of chromatids may be detected. Previously, other groups have successfully performed DOP-PCR on hundreds of flow sorted chromosomes (Telenius et al., 1992a) or tens of needle microdissected chromosomes (Meltzer et al., 1992, Zimmer et al., 1997). Only two groups have claimed to amplify a single chromosome, one group have amplified various single copy, microdissected, chromosome fragments using DOP-PCR (Guan et al., 1993). More recently, another group have used optical tweezers to manipulate a whole chromosome into a capillary tube and the chromosome was subsequently amplified (Wang et al., 2003). However, the authors do not give the details of the PCR and the results of any FISH reactions performed are not published, so it is not known how efficient this method is.

Using the optical tweezers technique we aimed to create a narrow band FISH probe from a single optically microdissected chromosomal fragment. The creation of whole chromosome FISH probes generated from amplification of single, isolated, whole chromosomes was also attempted. All the work described in this chapter was performed by Lynn Paterson, with the exception of the ecdysone response expression system.

Whole cell DNA is also amplified and used to label chromosomes with biotin so that streptavidin coated microspheres may be attached to the chromosomes via biotin-streptavadin bonding. The attached spheres act as 'handles' with which to manipulate the chromosomes in an optical trap. Focused laser light can trap spheres more readily than the chromosomes due to less light being scattered by the sphere and more light being refracted through it, resulting in enhanced optical manipulation.

9.2 Cell lines and chromosomes

9.2.1 Cell lines used in experiments

Wild type Chinese hamster ovary (CHO) cells and wild type Muntjac cells provided us with chromosomes which were used for optical cutting and tweezing. CHO GS1943, CHO G2H3 and Muntjac RG1Z2H1 cell lines have been transfected using the Ecdysone-Inducible Mammalian Expression System (Invitrogen). A gene of interest (in this case I-SceI endonuclease) is endogenously expressed in response to the presence of Ponasterone A. The expressed I-SceI protein cuts DNA at a specific, transfected, recognition site, resulting in a cohesive ended double strand break with a 3' 4 bp overhang.

The cut is generated as follows. The ecdysone receptor (VgEcR) and the retinoid X receptor (RXR) are expressed from the pVgEcR plasmid vector and associate to form a heterodimer which binds to a hybrid ecdysone response element (E/GRE) in the presence of Ponasterone A, a synthetic analogue of the insect hormone ecdysone. The hybrid ecdysone response element (E/GRE) is incorporated into the inducible expression vector of the system and will induce expression of our gene of interest

when the heterodimer binds to it. Our gene of interest (I-SceI) was ligated into the inducible expression vector and is expressed, thus makes the cut, in the presence of Ponasterone A, when the RXR/VgEcR heterodimer binds to the hybrid ecdysone response element (E/GRE). An overview of this system can be seen in figure 9.1.

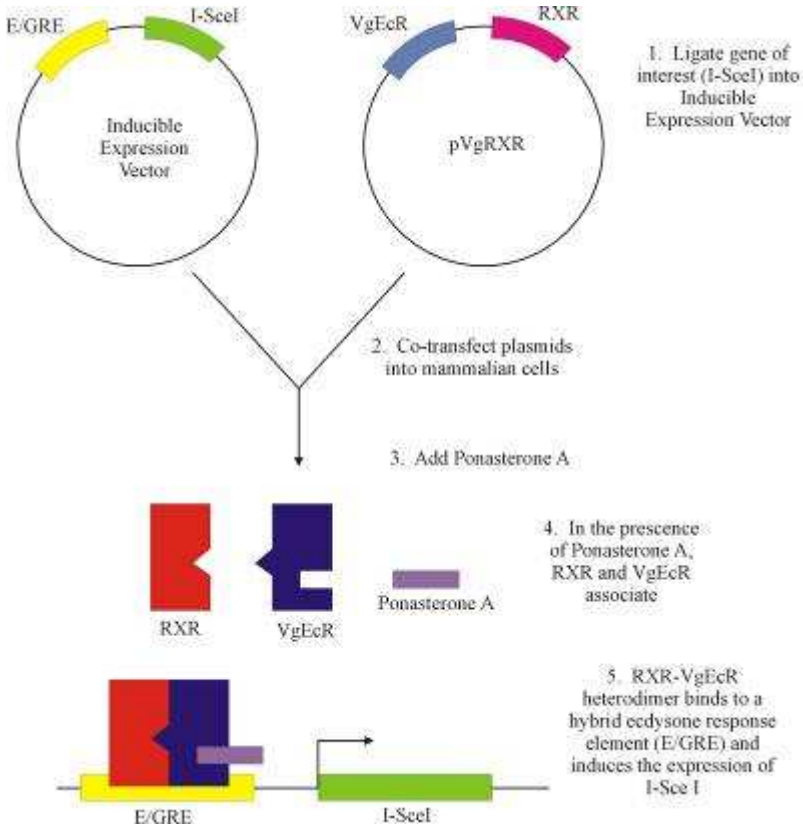

Figure 9.1: Overview of the ecdysone response system used to induce expression of I-SceI in mammalian cells.

9.2.2 Chromosome Preparation

9.2.2.1 Preparation of cells

2-3 x 10^5 Chinese Hamster Ovary cells were grown for 3-4 days until they became confluent in 10 ml MEM FCS, flushed with an air and CO_2 mixture, at a temperature

of 37˚C. (At least 5 x 10^5 Muntjac cells were grown in each flask containing 10 ml MEM FCS for 3-4 days until confluent).

Cells were trypsinised and counted using a Coulter counter and between 10^7 and 2 x 10^7 cells were put into a roller bottle containing 100 ml MEM FCS. The bottles were flushed with air and CO_2 mixture and put on rollers at 37˚C. The CHO cells were incubated for two days and the Muntjac cells for three days.

9.2.2.2 Isolating the mitotic cells

Colcemid was added to the medium in the roller bottles (final concentration 0.1 μg/ml) and the bottles were left for a further 2-3 hours at 37°C. This treatment blocks the cell division cycle at metaphase by preventing polymerisation of microtubules on the mitotic spindle. In the roller bottles the growing cells adhere to the plastic inner wall of the bottles but during mitosis the cells round up and adhere less strongly to the surface and can be shaken into the medium by rapidly rotating the roller bottles using an in-house made shaker. The medium containing the mitotic cells was collected and replaced by 100 ml fresh medium containing a final colcemid concentration of 0.1 μg/ml and the process was repeated.

9.2.2.3 Preparation of chromosomes

The medium containing the cells was centrifuged for 10 minutes at 1200 rpm. The medium was removed leaving a pellet of cells in the centrifuge tube. Cells were then pooled in hypotonic solution (HYP 2 - 1:1, 0.075M KCl: dH_2O) for 20 minutes allowing them to swell. The cells were centrifuged again for 10 minutes at 1200 rpm, the supernatant removed and the pellet of cells resuspended in fixative (1:3, acetic acid: methanol). Centrifugation and resuspension in fixative was repeated twice and finally the sample was dispensed into 1 ml eppendorfs tubes and stored (1 ml of cells in fixative for every half roller bottle used).

9.3 Methods of isolation of whole chromosomes and chromosomal fragments

9.3.1 Isolating a single chromosome or chromosomal fragment using optical tweezers

Several methods were tested to isolate chromosomes or fragments and transfer them to a sterile container in which PCR could be performed and they are described in the following passage. Chromosomes are microdissected and micromanipulated using optical tweezers initially and later needles or pipette tips were used to isolate single chromosomes for amplification.

9.3.1.1 Preparing chromosomes for optical tweezing

Cells in fixative were passed through a 25g needle and syringe ten times to lyse the swollen cells. The sample was then centrifuged for 10 minutes at 1200 rpm. The fixative was removed and chromosomes were resuspended in 200 µl Phosphate Buffered Saline (PBS). Centrifugation and resuspension in PBS was repeated.

To stain the chromosomes for tweezing Dif Quik staining was used. 20 µl of the sample was added into an 80 µm deep, 1 cm wide, vinyl spacer that was adhered to a large cover glass. 5 µl of Dif Quik was added to the sample. This dye stains any DNA present thus the CHO chromosomes can be viewed on a monitor. The large cover glasses (22 x 50 mm) were coated in a hydrophobic substance called Sigmacote, which prevents chromosomes sticking to the bottom of the sample cell by binding to glass and forming a hydrophobic surface.

9.3.1.2 Tweezing chromosomes

Chromosomes in suspension were prepared as described in section 9.3.1.1. A diode running at 780 nm or Nd: YAG laser operating at a wavelength of 1064 nm was directed into a sample cell from above (standard tweezers) and chromosomes in the

local vicinity of the beam were pulled into the focal region due to the gradient force of the laser. Chromosomes tend to align with the beam in the direction of beam propagation and can be manipulated in three dimensions. Figure 9.2 shows a CHO chromosome approximately 7μm in length, stained with Diff Quik, which has not aligned with the beam, being tweezed laterally along the bottom of the sample cell. In an inverted set-up the chromosomes were levitated upwards through the sample cell by the radiation pressure of the laser coming into the sample from below.

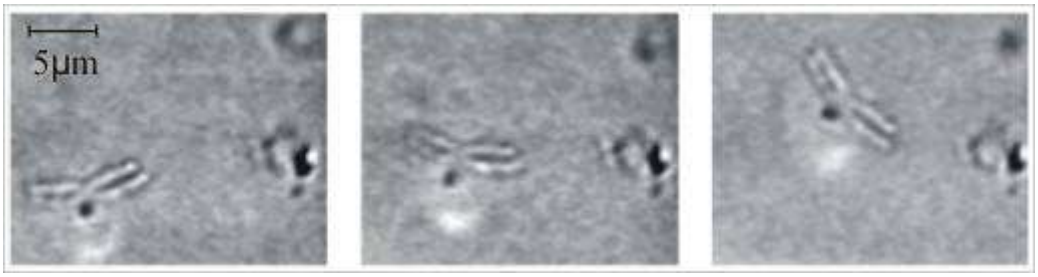

Figure 9.2: Tweezing of a CHO chromosome.

9.3.1.3 Cutting chromosomes

Laser light at a wavelength of 1064 nm does not damage the genetic material, however, a pulsed laser at a wavelength of 532 nm will cause heating in the chromosome and will cut through the material. A Q-switched, frequency doubled Nd: YAG laser with a wavelength of 532 nm and 10 mW of average power per pulse was used as optical scissors to cut chromosomes into fragments with which fluorescent probes could be generated by amplification and labelling of the amplified product. Figure 9.3 shows a 10 μm long Muntjac chromosome being cut into fragments using this laser. The chromosome was stuck to the bottom of a sample cell and the microscope stage was translated so that the chromosome crossed the optical path at the beam focus and was cut due to heating (opticuted).

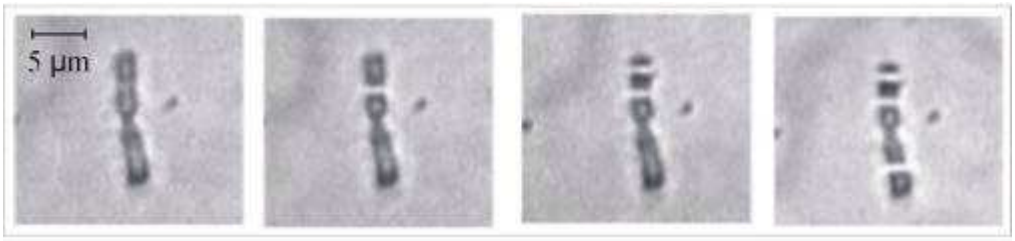

Figure 9.3: Optical microdissection of a Muntjac chromosome.

The optical tweezer and scissors are combined in a system illustrated in figure 9.4, which shows the tweezing beam directed into a sample cell from below and a cutting laser coming from above. This set up allows us to guide whole chromosomes or laser microdissected fragments away from other chromosomes and debris in the sample cell by levitation caused by the radiation pressure from the laser. These whole chromosomes or fragments are then used as template DNA with which chromosome FISH probes can be created.

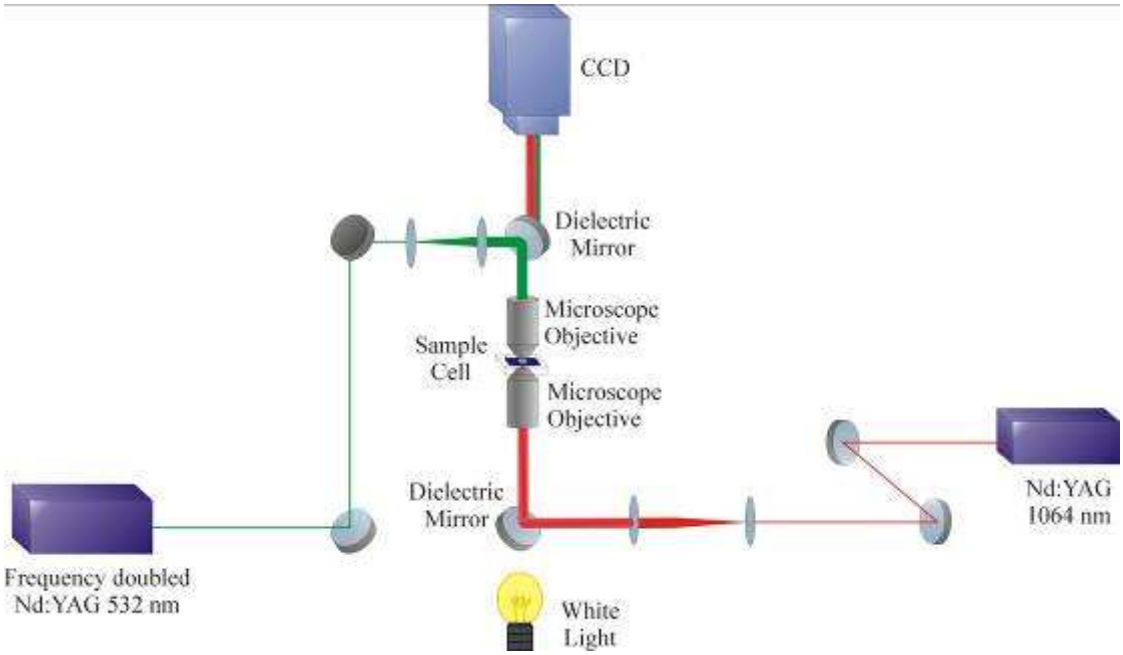

Figure 9.4: Schematic of chromosome microdissection and manipulation system.

Chromosomes which had settled on the bottom of the sample cell were cut and then levitated upwards through the sample cell, away from the rest of the chromosomes. Whole chromosomes were also levitated in this manner.

9.3.1.4 Chromosome levitation

One method explored with which to isolate a chromosome or a laser microdissected chromosomal fragment using optical tweezers is described as follows. A chromosome was guided to the top of the sample cell where it stuck to the coverslip and the remaining chromosomes in the suspension were left to sink due to gravity and stick to the bottom of the sample cell. The coverslip with the single attached chromosome or fragment was then removed, cut and placed in a microfuge tube, to which the PCR regents were added. This technique is illustrated in figure 9.5 and captured frames of a chromosome being levitated in this manner are shown in figure 9.6.

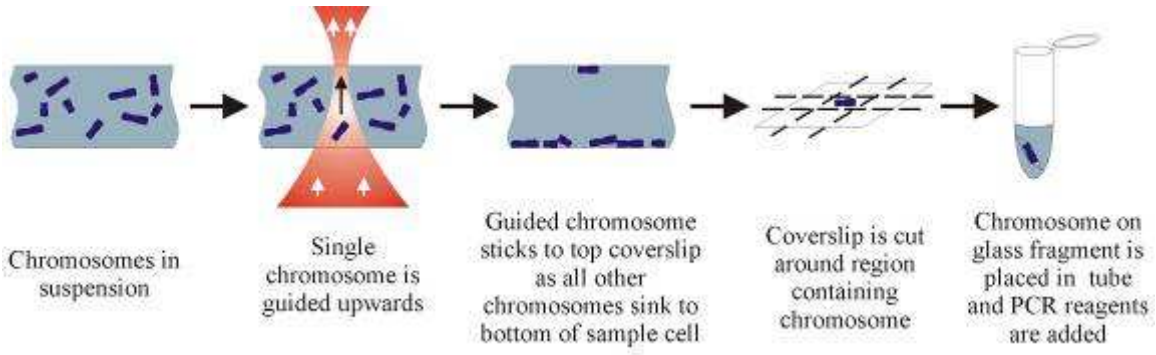

Figure 9.5: Attachment of chromosome to coverslip using optical tweezers.

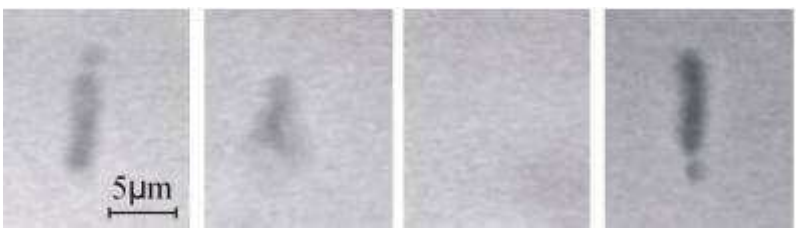

Figure 9.6: Chromosome levitation.

The first frame shows a Muntjac chromosome which has settled near the bottom surface of the sample chamber and the second frame shows the chromosome beginning levitation as the laser, coming into the sample from below, is switched on. The third image is hat of the bottom of the sample chamber with the chromosome gone and the fourth frame is that of the same chromosome having been guided to the top coverslip of the sample chamber.

In another experiment a chromosome was guided such that it stuck to the top coverslip in the sample cell and then the whole coverslip was removed with the spacer attached to it and was itself used as a chamber in which PCR was performed.

9.3.2 Mechanical isolation of chromosomes (scraping off glass)

Due to lack of success in generating FISH probes from the aforementioned techniques of chromosome isolation, the follow methods were attempted.

9.3.2.1 Preparation of chromosomes fixed on slide for scraping

Ice cold slides are flooded with 50% ice cold acetic acid and 20 µl of cells in fixative (1: 3, acetic acid: methanol) are dropped onto the slide. Excess acetic acid is tapped off and slides are left to air dry slowly overnight.

9.3.2.2 Needle/Pipette tip micromanipulation of chromosomes

Single chromosomes fixed on a microscope slide were found under the phase contrast microscope. These chromosomes were scraped off the cover glass using a 25g needle and transferred into a collection buffer within a PCR tube. The chromosomes could also be removed from the cover glass by pipetting 1 µl of sterile water onto the site and scraping the chromosome off the glass with the pipette tip,

and then transferring the water and chromosome off the glass and into a PCR tube. This method is illustrated in figure number 9.7.

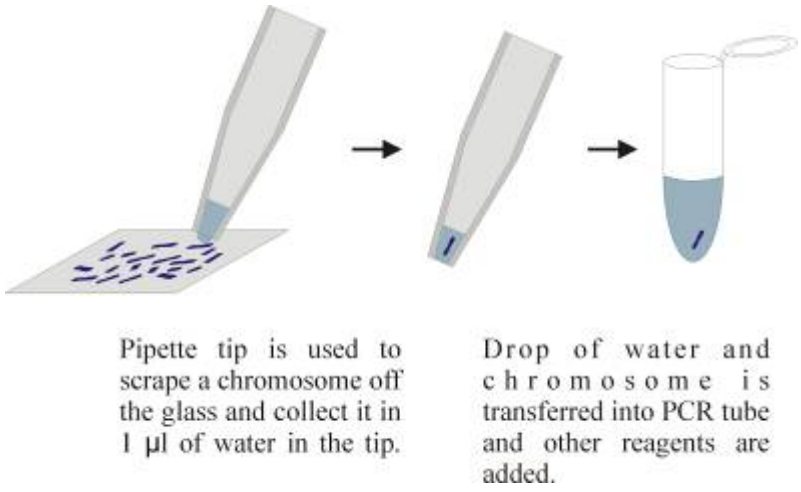

Figure 9.7: Chromosomes are scraped off a cover glass and resuspended in a small volume of water then transferred to PCR tube.

9.4 Generating a chromosome FISH probe from isolated chromosomal material

9.4.1 Degenerate Oligonucleotide Primed Polymerase Chain Reaction (DOP-PCR)

9.4.1.1 Primary DOP-PCR

The primary PCR of chromosomes or of the positive controls (using fragmented, genomic DNA or many chromosomes in suspension) and of a negative control with no DNA template is performed in a final volume of 50 µl. The final concentrations of reagents is 1x PCR buffer, 2 mM $MgCl_2$, 4 µM degenerate oligonucleotide primers of sequence 5'– CCGACTCGAGNNNNNNATGTGG -3', 0.2 mM dNTP mix, 0.05% W-1 and 2 units of Taq polymerase. The mixture is made up to 50 µl

with sterile H_20. PCR is performed on a thermal cycler (Techne) and cycles used in the following work have included;

1 cycle	95°C	3 minutes
30 cycles	94°C	1 min
	50°C	1 min
	72°C	2 mins
1 cycle	72°C	8 mins.

Also used was;

1 cycle	94°C	9 mins
8 cycles	94°C	1 min
(25°C)	30°C	1.5 mins (three minute transition from 30°C to 72°C)
	72°C	3 mins
25 (30) cycles	94°C	1 min
(50°C)	62°C	1 min
	72°C	1.5 mins
1 cycle	72°C	8 mins

9.4.1.2 ReadyMix Taq

Primary amplification was also carried out using ReadyMix Taq (Sigma) which, as the name suggests, is a ready made master mix of all the reagents needed for the PCR, excluding DNA template and primers. The advantage of using this method is that it saves preparation time and reduces the risk of contamination. 25µl of the Ready mix was used for each amplification reaction with 4 µM of degenerate oligonucleotide primer (DOP) and DNA template, with the total volume being made up to 50 µl with H_2O. The final concentrations of the reagents in the ReadyMix Taq were 10 mM Tris-HCl, 50 mM KCl, 1.5 mM $MgCl_2$, 0.001% gelatin, 0.02 mM dNTP and 1.5 units of Taq polymerase. The cycling parameters used were the same as described above.

9.4.1.3 Alternative protocol for chromosome amplification

Chromosome fragments have been pretreated before PCR with Topoisomerase I which is used to increase the efficiency of amplification (Guan et al., 1993). Topoisomerase I catalyses the relaxation of supercoiled DNA by producing single strand breaks in the double stranded DNA. DNA in metaphase chromosomes is highly condensed and the higher order structure of supercoiled DNA may limit the access of primers and polymerase to the template, so enzymatically producing nicks in the DNA should allow primers more access to template.

Two units of Topoisomerase I is added to the chromosome in collection buffer and incubated for 30 minutes at 30 °C, and the enzyme is inactivated by incubating at 94 °C for ten minutes. Collection buffer was either 5 µl of 10 x PCR buffer and 4 µl 25mM $MgCl_2$ (the reagents of the PCR reaction described above, excluding Taq, dNTPs and primer, which would be denatured by heating or by enzyme action), or TAPS buffer used by Telenius (Telenius et al., 1992b) and Thalhammer (Thalhammer et al., 1997) which consisted of final volumes of 25 mM TAPS (N-tris (hydroxymethyl) methyl-3-amiopropanesulfonic acid) pH 9.3, 50 mM KCl, 1 mM DDT, 2 mM $MgCl_2$ and 0.05% W-1 or the collection buffer used by Zimmer et al. (Zimmer et al., 1997) which contains 40 mM Tris-HCl (pH 7.5), 20 mM $MgCl_2$, 50 mM NaCl.

Proteinase K may also be added to the collection buffer containing the chromosomal material to digest any proteins associated with the chromatin which may inhibit PCR. 50 µg/µl is added and incubated at 37 °C for one hour and then inactivated by incubating at 95 °C for ten minutes.

9.4.1.4 Secondary Polymerase Chain Reaction

A secondary labelling reaction of the primary product is performed to incorporate biotin 16-dUTP into the PCR product or directly fluorescently label the product with spectrum Green-dUTP. The labelling reaction is carried out in a volume of 50 µl,

containing final concentrations of 1 x PCR buffer, 2 mM $MgCl_2$, 4 µM degenerate oligonucleotide primers, 0.05 µM of dATP, dCTP and dGTP and 0.04µM of dTTP and 0.01 µM of biotin 16-dUTP or Spectrum Green-dUTP, 0.05% W-1, 2 units of Taq polymerase and 10 µl of the primary reaction product. The mix is made up to 50 µl with sterile H_2O and the cycle used is as follows:

1 cycle	94°C	9 mins
25 (30) cycles	94°C	1 min
	62°C	1 min
	72°C	1.5 mins
1 cycle	72°C	8 mins.

ReadyMix Taq is also used in some secondary labelling reactions, however the concentration of dTTP cannot not be reduced, and labelling with dUTP may not be as efficient.

9.4.2 Fluorescent in situ hybridisation (FISH) techniques

9.4.2.1 Precipitating Probe

To prepare the probe mix, 10µl of biotin or Spectrum Green labelled secondary PCR product is combined with 0.1 volume (1 µl) of 3M sodium acetate and in some instances Cot-1 DNA is also added at this stage. 2.5 volumes (25µl) of ice cold absolute ethanol are added to the mix to precipitate the DNA. The mixture is briefly mixed and left at minus 20°C for two hours and then centrifuged at 13,000 rpm in a mini centrifuge for thirty minutes to pellet the DNA. The supernatant is removed and the pellet is air dried for fifteen minutes. The DNA pellet is resuspended in 3 µl H_2O and 7 µl hybridisation buffer and left for thirty minutes to dissolve. Before hybridising the probe to target metaphases on a slide the probe and the metaphases must be denatured, either separately or together. The probe can be denatured by heating the probe mix for five minutes in a 73°C water bath.

9.4.2.2 Preparation of microscope slides with target metaphases

Ice cold slides are flooded with 50% ice cold acetic acid and 20 µl of cells in fixative (1: 3, acetic acid: methanol) are dropped onto the slide. Excess acetic acid is tapped off and slides are left to air dry slowly overnight. Before hybridisation with the probe the target metaphases on the slides can be denatured by immersing slides for five minutes in denaturation solution at 73°C. Slides are then dehydrated by placing in 70% ethanol solution for one minute, followed by one minute in 85% ethanol solution, and one minute in a 100% ethanol solution. The ethanol is allowed to evaporate before 10µl of the denatured probe and in some instances Cot 1-DNA is dropped onto the slide and a coverslip is placed on top and sealed with rubber cement. The slide is placed in a humidified box (HYBrite) at 37°C for at least sixteen hours.

The target metaphases and probe may be denatured together by dropping the probe (not denatured) and in some experiments Cot-1 DNA, onto the slide (not denatured), putting a coverslip on top and sealing with rubber cement and then denaturing by heating in the HYBrite to 73°C for five minutes and then hybridising at 37°C for at least sixteen hours.

9.4.2.3 Spectrum Green-dUTP labelled probe

Following hybridisation with the Spectrum Green-dUTP labelled probe, the rubber cement and coverslip are removed from the slide and the slide is washed in a solution of 0.4 x SSC/0.3% NP-40 at 74°C by agitating for 1-3 seconds then left to stand in the solution for 2 minutes. The slide is then immersed in a wash solution containing 2 x SSC/0.1% NP-40 at ambient temperature and is again agitated for 1-3 seconds and left to stand in the solution for no more than one minute. Following washing, the slides are left to air dry in darkness and once they have dried 20 µl of

DAPI counter stain is added to each slide, a coverslip is placed on top and is sealed using nail polish.

Slides are viewed using a fluorescent microscope and the optical filters used are DAPI to view the DAPI counter stain and FITC to view the Spectrum Green-dUTP labelled probe. The triple band pass filter allows both signals to be seen simultaneously.

9.4.2.4 Biotin-avadin Cy3 probe

Metaphases that have been hybridised with a biotin 16-dUTP labelled probe are washed as above by placing in 0.4 x SSC/0.3% NP-40 at 74°C for two minutes and then in 2 x SSC/ 0.1% NP-40 at ambient temperature for no more than one minute. The slide is left to air dry and is then incubated with 100 µl of blocking buffer (BSA blocking buffer, TNB blocking buffer, or non fat dairy milk blocking buffer with a large coverslip placed on top) for 30 minutes at room temperature in a humidified box. After this incubation any excess blocking buffer is tapped off and 100 µl of a 1:300 solution of avadin-Cy3 in blocking buffer is added to each slide. A large coverslip is placed on top and the slide is incubated in the dark for thirty minutes at 37°C in a humidified box. Slides are then washed either three times for five minutes each time in washing buffer (50% formamide in 2 x SSC) and then rinsed three times in dH_2O and air dried or, alternatively, washed three times in TNT washing buffer for five minutes each wash and then air dried. Finally 20 µl of DAPI counter stain is added onto the slide, a coverslip is placed on top, sealed and the slide is viewed under fluorescence. The DAPI filter is used to view the blue signal from the DAPI counterstain and the rhodamine filter is used to view the red signal of the Cy3 signal. Again a triple band pass filter can be used to view the two signals together.

9.4.3 Other methods used for the generation of chromosome FISH probes

9.4.3.1 Purifying genomic DNA

Fragmented genomic DNA is used as a template for PCR in positive control reactions and it is generated as follows.

1-2 x 10^7 CHO cells are grown over two days in one roller bottle until confluent when the cells are trypsinised and collected in a pellet by centrifugation. Digestion buffer (400 mM NaCl, 100 mM Tris HCl (pH 8.5), 50 mM EDTA and 0.5% SDS) and RNase (at a final concentration of 40 μg/ml) are added to the pellet and the sample is incubated for one hour at 37 °C. Following that, an equal volume of digestion buffer containing proteinase K (for final concentration 100 μg/ml) is added and the mixture is incubated overnight at 50 °C. The sample is combined with a double volume of isopropanol and the sample is gently mixed for approximately one hour until the DNA has precipitated. The DNA is collected using a pipette tip and transferred into a fresh tube where it is rinsed with 70% ethanol by centrifugation at 2000 rpm for 2 minutes in a 20 cm diameter rotor. The pellet is air dried and resuspended in TE of pH 8 and is ready for use.

Alternatively, a Genomic DNA Purification (Promega) kit may be used. 1-2 x 10^6 CHO cells are used to give a yield of 6-7 μg of DNA. Cells are harvested by trypsinisation and centrifuged to pellet the cells. The supernatant is removed and the pellet is washed in PBS by centrifugation, the supernatant is removed and the pellet is vortexed vigorously. Nuclei Lysis solution is added to the pellet and pipetted until the cells are lysed and there are no clumps remaining. 3 μl of RNase Solution is added and mixed into the nuclear lysate. The mixture is incubated for 15-30 minutes at 37°C then cooled to room temperature, and 200 μl of Protein Precipitation Solution is added and the mixture is vortexed vigorously. The sample is chilled on

ice for ten minutes and centrifuged to precipitate the protein into a tight white pellet. The supernatant containing the DNA is removed and transferred to a fresh tube containing 600 µl of isopropanol at ambient temperature, leaving the precipitated protein behind. The solution is mixed until white thread-like strands of DNA form a visible mass and then centrifuged until the DNA forms a small visible pellet. The supernatant is removed and 600 µl of 70% ethanol is added to wash the DNA and the sample is centrifuged then the supernatant is removed. The DNA pellet is dried and 100 µl of DNA Rehydration Solution is added and incubated at 65°C for one hour or at 4 °C at room temperature.

The DNA can be fragmented by sonication and the size of fragments can be checked by running an aliquot of the sample on an agarose gel. The concentration of the DNA is measured using the Gene Quant and can reduced by diluting with TE.

9.4.3.2 Preparing Cot-1 DNA

Cot-1 DNA is made as follows. Genomic hamster DNA is isolated from CHO cells as described above and is sonicated to produce fragments between 500-2000 bp. The DNA is diluted to 0.25 µg/µl in S1 nuclease reaction buffer and denatured in boiling water for fifteen minutes. Repetitive sequences are allowed to reanneal at 63°C for 22 minutes and then cooled to 37°C and the remaining single stranded unique sequences are digested with S1 nuclease (0.8 units per µg of DNA) and incubated for two minutes at 37°C. The reaction is stopped by adding 0.1 volume of 0.5M EDTA. The digested DNA and proteins are removed by a phenol chloroform extraction. An equal volume of phenol is added to the mixture and is vortexed for one minute and then centrifuged at 12,000 rpm in a micro centrifuge for two minutes. The top (aqueous) layer containing the DNA is transferred to a fresh tube and the size of the generated Cot DNA should be in the range 100-500 bp.

Alternatively, commercially available mouse or human Cot-1 DNA is used in hybridisation experiments (Vysis, Invitrogen).

9.5 Results of enzymatic amplification of isolated chromosomes and fragments to make chromosome FISH probes

9.5.1 DOP-PCR of a previously DOP-PCRed, needle microdissected, chromosome fragment

Needle microdissection of the CHO X chromosome and DOP-PCR of the microdissected fragments was carried out by another group at another location and an initial experiment was the amplification and labelling of this primary product in a secondary DOP-PCR reaction. The reagents used in this amplification were 1x PCR buffer, 2 mM $MgCl_2$, 4 μM degenerate oligonucleotide primers, 0.5 mM of dATP, dGTP, dCTP, 0.4 mM dTTP, 0.1 mM of biotin 16-dUTP, 0.05% W-1 and 2 units of Taq polymerase. The mixture was made up to 50 μl with sterile H_20. Cycling parameters were

1 cycle	95°C	3 minutes
30 cycles	94°C	1 min
	50°C	1 min
	72°C	2 mins
1 cycle	72°C	8 mins.

FISH was performed on CHO metaphases following the protocol detailed in the methods section and the resulting hybridisation results are shown in figure 9.8.

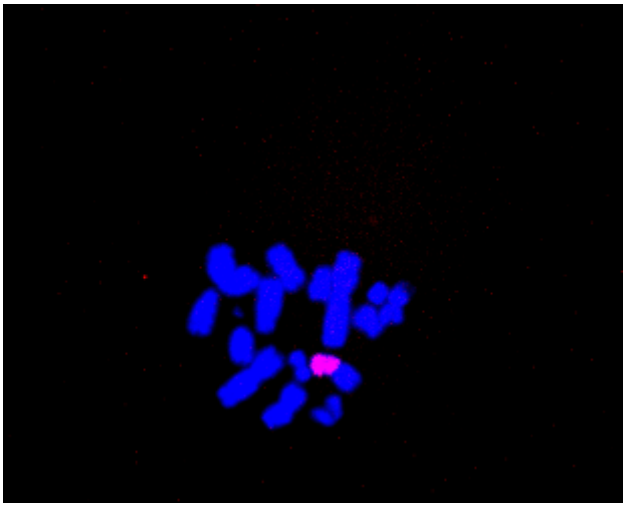

Figure 9.8: Red region is paint probe generated by DOP-PCR of a microdissected chromosome.

9.5.2 DOP-PCR of isolated chromosomes or fragments

9.5.2.1 Optically levitated chromosomes or fragments stuck to glass

Whole chromosomes and laser microdissected chromosome fragments were guided in a sample cell using inverted optical tweezers in the set up illustrated in figure number 9.4 above. As described above, the chromosome was guided to the top of the sample cell where it stuck to the coverslip and the other chromosomes and cellular debris in the sample were allowed to sink to the bottom of the sample cell. The coverslip was then carefully removed and cut around the region where the chromosome adhered. This glass fragment with the chromosome or chromosomal fragment attached to it was transferred into a microfuge tube, and PCR reagents were added. This method is illustrated in figure number 9.5 above. The DNA was subjected to a PCR reaction which is described in the methods section as is the second round, labelling reaction, precipitation of the probe and the hybridisation reaction. An alternative method which was tested was to use the top coverslip, with

vinyl spacer attached, as a well in which to perform PCR. The tweezed chromosome remains stuck to the glass and the PCR reagents is added to the well created by the spacer. Another coverslip is placed on top to seal the chamber and PCR cycles are performed on a heating block.

9.5.2.2 Micromanipulation using a pipette tip

Another method used to isolate single chromosomes, or a few chromosomes for subsequent amplification makes use of a 2 µl pipette tip. Chromosomes fixed on a glass coverslip or slide can be scraped off by re-suspending a single chromosome of interest in a micro-litre volume of sterile water and making use of the plastic pipette tip to free the chromosome from its attachment to the glass. The micro-litre of water with the chromosome suspended in it may then be transferred to a Microfuge tube and PCR can be performed. This method is illustrated in figure number 9.7.

9.5.2.3 DOP-PCR

The degenerate oligonucleotide primer of sequence 5'CCG ACT CGA GNN NNN NAT GTG G-3' consists of three parts; six specific bases at the 3’ end, the middle section contains six nucleotides of degenerate sequence and the 5’ end is a specific sequence of ten bases. The low annealing temperature of the first cycle allows the partially degenerate 3’ end to anneal to the template material. In the following low temperature cycles, fragments are generated which contain the full length of the primer at one end and its complementary sequence on the other end. All the products from these first low-annealing temperature cycles will contain the full length primer sequence so the annealing temperature can be raised from 30°C to 62°C and these long nucleotide sequences can be amplified further.

If the PCR is performed using the following cycles:

1 cycle	95 °C	3 minutes
30 cycles	94 °C	1 min
	50 °C	1 min
	72 °C	2 mins
1 cycle	72 °C	8 mins.

A product for the positive control (containing genomic DNA or many chromosomes suspended in water) is observed when an aliquot of the PCR product is run on a 2% agarose gel, and no product is seen for the negative control (which is the same as the positive but contains no template DNA). However, when the cycles used are

1 cycle	94 °C	9 mins
8 cycles	94 °C	1 min
(25 °C)	30 °C	1.5 mins (three minute transition from 30°C to 72°C)
	72 °C	3 mins
25 (30) cycles	94 °C	1 min
(50 °C)	62 °C	1 min
	72 °C	1.5 mins
1 cycle	72 °C	8 mins,

as recommended in the literature for degenerate oligonucleotide primed - polymerase chain reaction, a product in the negative control is always created.

Reagents used in the PCR of positive controls and of microdissected, tweezed chromosomes and of single scraped chromosomes are detailed in the methods section. DNA template used as a positive control was either fragmented, genomic DNA or many hundreds of metaphase chromosomes resuspended in PBS, TE or water. To create a probe that does not label every chromosome in the cell, either fragments of chromosomes, whole single chromosomes or a few chromosomes (up to half the chromosomes in a metaphase cell) are used as template DNA. For the negative control, sterile water is added in place of template DNA.

An experiment was performed to determine if attachment of chromosomes to a glass substrate inhibits amplification of the DNA. Serial dilutions of chromosomes in

water are dropped onto a fragment of cover glass and allowed to dry, and the same dilutions of chromosomes in suspension are PCRed using the following; one cycle at 95 °C for 3 minutes, 30 cycles of 94 °C for 1 min, 50 °C for 1 minute and 72 °C for 2 minutes and finally one cycle at 72 °C for 8 minutes. Chromosomes in water were counted using a haemocytometer and dilutions contained approximately 250, 25 and 2.5 chromosomes and a negative control containing water only was also performed. An aliquot of the products were run on a 2% agarose gel and typically showed a bright smear for the amplification product of 250 chromosomes in suspension and very feint smears for the other products.

PCR was performed on chromosomes in suspension that were either not stained or stained with Giemsa or with Diff Quik to determine if the stain (which is required to visualise the chromosomes when optical tweezing) has any adverse effect of FISH, and it was discovered that neither Giemsa staining or Dif Quik staining inhibited FISH. Chromosomes were brightly labelled in all cases and the negative control which was run in parallel showed no labelling.

9.5.3 DOP-PCR of optically levitated chromosomes

PCRs were performed using a positive control, single whole chromosomes that had been tweezed onto a glass coverslip and placed into a PCR tube (initially laser microdissected fragments were used, however when this failed to produce results single whole chromosomes were used), and a negative control. A typical result can be seen in figure 9.9. The target metaphases of the positive control are labelled with Spectrum Green (9.9A), the negative is very faintly labelled (9.9G) and the single whole chromosome probes are label all of the chromosomes of target metaphases at an intensity in between that of the positive and the negative controls (9.9B-F).

A 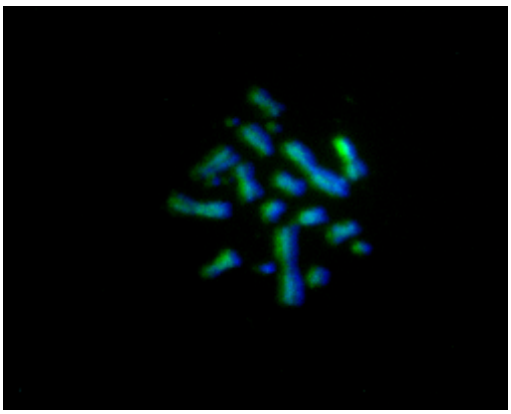

B 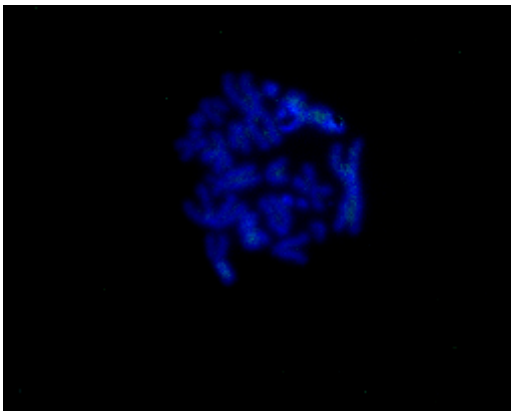

C 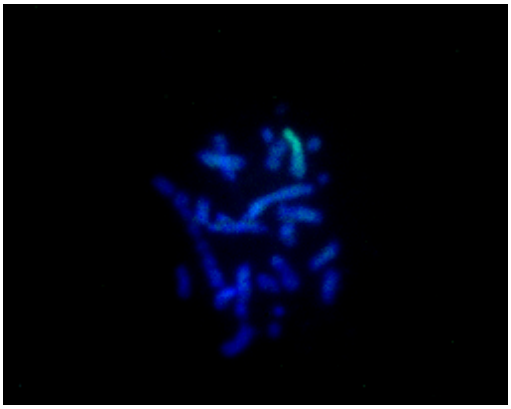

D 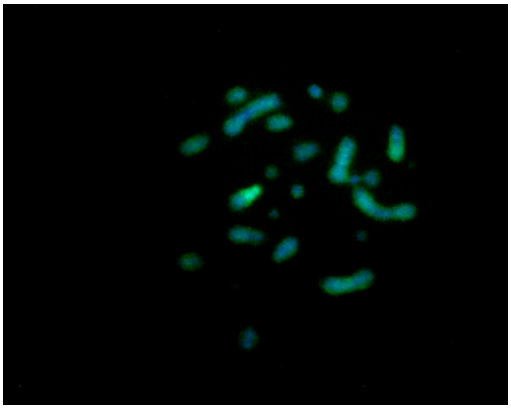

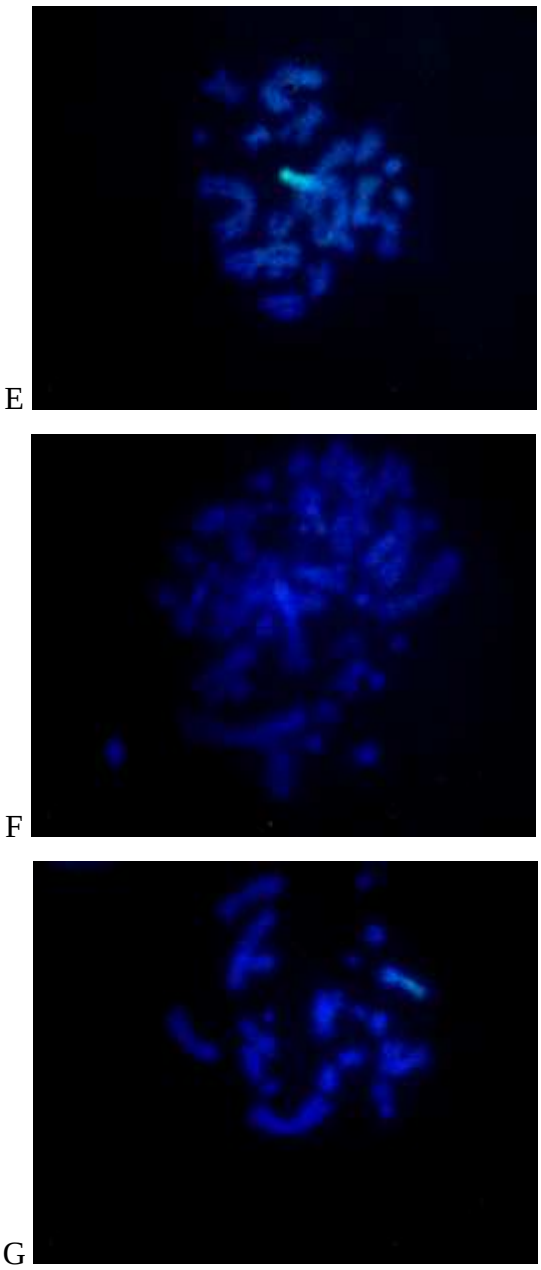

Figure 9.9: FISH slides of A. positive control, B. probe 1, C. probe 2, D. probe 3, E. probe 4, F. probe 5, G. negative control.

In many of the DOP-PCRs carried out there was some labelling of chromosomes in the negative control. This was initially thought to be contamination, and efforts went into getting rid of any contamination, by using flow hoods to prepare samples,

UV sterilising tubes, tips and water, and using filter tips to stop any splash back of reagents into the pipette.

9.5.3.1 DOP-PCR using ReadyMix Taq

In order to combat contamination Readymix Taq was introduced in place of Taq, buffer, dNTPs, detergent and $MgCl_2$. This meant that contamination due to repeated pipetting is reduced and all that needs to be added to the mix is primer, template and water. It was also discovered that, at the low annealing temperature used for DOP-PCR a product in the negative control is always produced, thought to be concatenation and then extension of the primers themselves. As a result of this, a fresh negative control was set up for every secondary reaction performed, and at the last stage of the experiment – the FISH slide – this resulted in no labelling of the target chromosomes. This can be explained as the annealing temperature used in the secondary reactions is higher, so primer dimers and contatamers are not produced so are not available to be amplified by Taq polymerase.

Positive and negative controls were working as desired with all chromosomes being labelled by FISH in the positive control, which used genomic DNA or chromosomes suspended in water as template material, and chromosomes not being labelled in the negative reaction. However, it seemed that the amplified and labelled product from a tweezed whole chromosome or fragment resulted in the labelling of the same region of chromosome each time FISH was performed, regardless of the chromosome that was tweezed. This happened in the case of both CHO chromosomes and Muntjac chromosomes (figure 9.10).

A 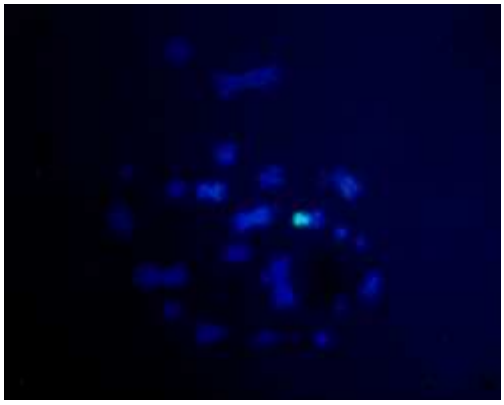 B 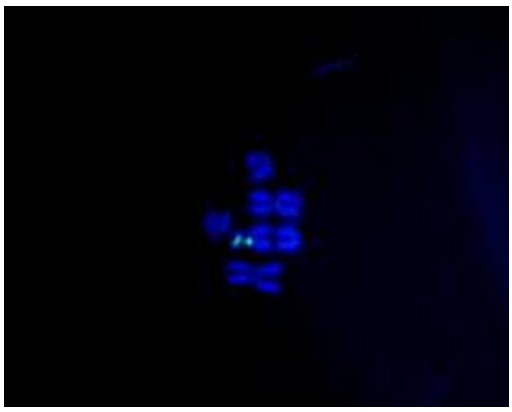

Figure 9.10: In each FISH performed, the same region of chromosome was labelled in A. CHO metaphases and B. Muntjac metaphases.

On first appearance this could be thought of as an actual FISH probe which could be utilised in chromatid inversion studies, but after many amplification experiments on different chromosomes it was concluded that this fluorescence is labelling of repetitive sequences in the DNA. To prevent this from happening again, Cot-1 DNA was preannealed with probe or target metaphases to suppress the labelling of repetitive sequences. At this juncture optically tweezed chromosomes and chromosomal fragments were substituted with chromosomes scraped off a microscope slide using either a needle or a pipette tip as the micromanipulator.

9.5.4 DOP-PCR following published protocols

Various protocols, described in the literature and discovered from personal communications with Julio Masabanda, were followed in order to create a specific and strong probe. Single whole chromosomes, or in some cases a few chromosomes, were collected using the scraping method described above and transferred to a tube containing PCR buffer, $MgCl_2$ and W-1. Topoisomerase I was added to the sample and then the mixture was incubated for 30 minutes at 37 °C for the enzyme to create single strand cuts in the DNA to relax the tightly coiled double stranded DNA of the fragment. Proteinase K was then added to the sample and incubated for a further 30

minutes at 37 °C to digest any protein in the sample. The enzyme was then denatured by incubating at 95 °C for 10 minutes. Finally, the DOP primers, dNTPs and Taq polymerase are added and PCR is performed according to the low annealing temperature protocol described above. Various other collection buffers are used to incubate the chromosomes with or without Topoisomerase I. Telenius et al., in the original DOP-PCR paper (Telenius et al., 1992b), performed the amplification of genomic DNA using two different buffers, named A and B. Buffer A consisted of 10 mM Tris HCl, 1.5 mM $MgCl_2$ and 50 mM KCl and buffer B consisted of 25 mM TAPS, 2 mM $MgCl_2$, 50 mM KCl, 1 mM DDT and 0.05% W-1. The positive and negative controls, and the single scraped chromosomes in the collection buffers were incubated with Topoisomerase I, and after the denaturation step the remaining reagents were added to the mixture (2 μM DOP primer, 0.2 mM dNTPs, 1.5 units of Taq polymerase in buffer A and 2.5 units in buffer B). As described in the methods section, the primary amplification used the low annealing temperature cycles and the secondary labelling reaction used the higher annealing temperature cycles. Unfortunately the FISH probes generated in this way did not label target metaphases well. The positive controls for sample A and B were slightly speckled with probe but not brightly labelled, the whole chromosome probe for both methods A and B also did not label a single chromosome only, but speckles of probe could be seen on all chromosomes and background and the negative control was similar. Two other buffers were used in experiments, taken from two other papers, one by Zimmer et al. (Zimmer et al., 1997) which consisted of 40 mM Tris-HCl (pH 7.5), 20 mM $MgCl_2$, 50 mM NaCl and 0.5 mg/ml Proteinase K and another by Thalhammer et al. (Thalhammer et al., 1997) which contained 25 mM TAPS, 50 mM KCl, 1 mM DTT, 2 mM $MgCl_2$ and 0.05% W-1 which is the same as Telenius' buffer B. Positive controls, negative controls and single chromosomes scraped off a cover glass were incubated with Topoisomerase I prior to amplification in order to increase the amount of PCR product. Cycles with the initial low annealing temperature were used in the primary amplification reaction, as described above. Aliquots of the sample were run on a gel and showed no products for any of the reactions, not even a smear for the positive control, thus a secondary reaction was not performed.

9.5.5 A further DOP-PCR method

Another scheme was attempted using the reagents 1 x PCR buffer, 2 mM $MgCl_2$, 1 μM DOP primers, 0.2 mM dNTP, 0.05% W-1, 2.5 units of Taq polymerase and made up to 25 μl with sterile water. A positive and a negative control were of course performed and two samples containing single chromosomes were also used to create a whole chromosome paint probe. This amplification was carried out in parallel with an experiment in which the samples were incubated with 3.5 units of Topoisomerase I at 37 °C for 30 minutes and then the enzyme was denatured for ten minutes by heating to 95 °C. The cycles used were:

1 cycle	94°C	9 mins
8 cycles	94°C	1 min
	30°C	1.5 mins (three minute transition from 30°C to 72°C)
	72°C	3 mins
25 cycles	94°C	1 min
	62°C	1 min
	72°C	1.5 mins
1 cycle	72°C	8 mins.

An aliquot of the products were run on a gel which showed only a feint smear for the positive control without Topo I added. A secondary reaction was performed using either 10 μl of primary product as template with 25 μl of Ready mix Taq, 2 μM DOP primers and made up to 50 μl with sterile water, or using 10 μl primary product, 1 x PCR buffer, 2 mM $MgCl_2$, 2 mM DOP primers, 0.2 mM dATP, dGTP, dCTP, 0.18 mM dTTP, 20 μM Spectrum Green-dUTP, 0.05% W-1, 5 units of Taq polymerase and made up to 50 μl with sterile water. The cycles used in the secondary PCR were:

1 cycle	94°C	9 mins
25 cycles	94°C	1 min
	62°C	1 min
	72°C	1.5 mins

1 cycle 72°C 8 mins.

The gel of the secondary reaction always showed a smear for each product. However, the FISH image showed faint labelling of all target metaphases for both Topo I treated and untreated positive controls of amplified CHO fragmented, genomic DNA. The fresh negative control would show no labelling, the negative control that was carried across from the primary negative showed speckling of probe in the background and on the target metaphases. The amplified single chromosome probes showed similar labelling to the secondary negative with slight speckled labelling of probe on all target metaphases and in the background. These results were typical of many DOP-PCRs attempted and typical results can be seen in figure 9.11. In this experiment the technique described directly above was used and resulted in the all the target metaphases of the positive control probe and of one of the whole chromosome probes being slightly labelled 9.11 (A and C) and the other whole chromosome probe, the secondary negative and the primary negative not being labelled 9.11 (B, D and E respectively).

A 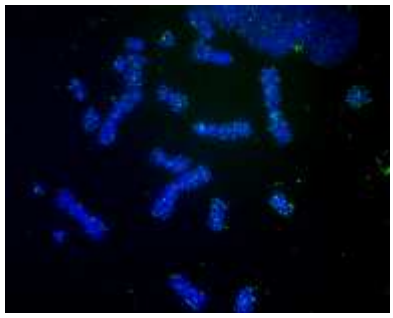

B 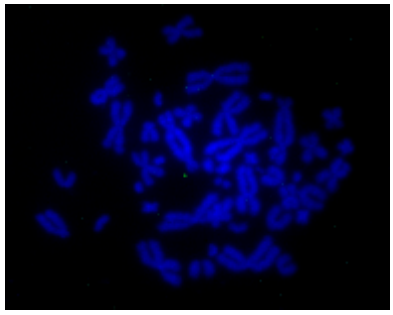

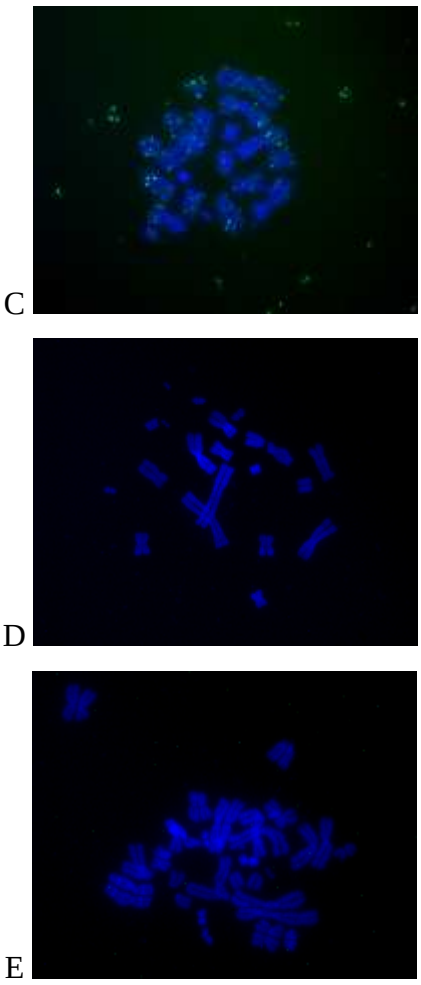

Figure 9.11: Typical DOP-PCR results. A. positive control, B. probe 1, C. probe 2, D. secondary negative control, E. primary negative control.

Due to the continuing problem of obtaining results of FISH similar to that described above, we decided to try making chromosome paint probes via another method, discovered through a personal communication with Julio Masabanda and a subsequently published piece of work (Masabanda and Griffin, 2003), which claimed to create paint probes that were brighter and more specific.

9.5.6 Linker Adaptor PCR

9.5.6.1 Method

A technique that has been used to create a brighter, more specific paint probe uses streptavidin coated paramagnetic spheres to isolate biotinylated PCR product. The biotinylated DNA is hybridised with fragmented genomic DNA with adaptors linked to the fragments which are a template for PCR primers to anneal to, and PCR is performed using these specific primers. This method was developed by Masabanda and Griffin and published in Biotechniques (Masabanda and Griffin, 2003) and an overview of the technique is illustrated in figure 9.12.

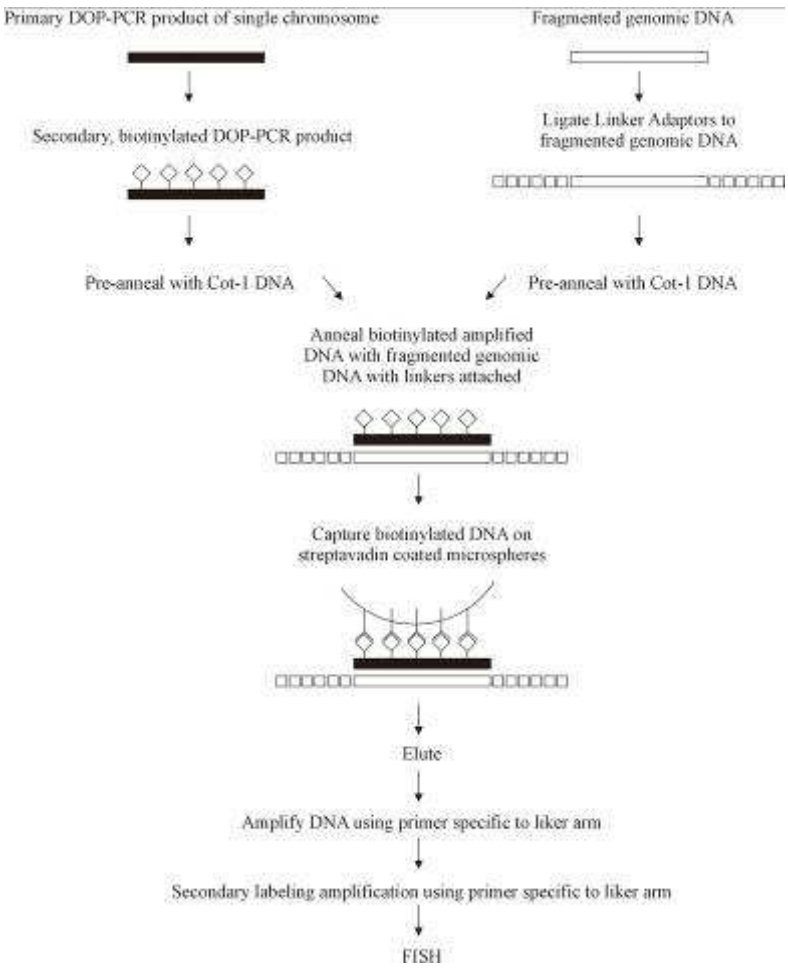

Figure 9.12: Overview of PCR using linker adaptors.

Genomic CHO DNA is isolated as described above and fragmented by sonication. Two oligonucleotides (Invitrogen) of complementary sequence (5'-CCT CTG AAG GTT CCA GAA TCG ATA GGT CGA CCG-3' and 5'-CGG TCG ACC TAT CGA TTC TGG AAC CTT CAG AGG TTT-3') are annealed to make the double stranded adaptor prior to ligation in a final volume of 100 µl containing final concentrations of 10nmol of both oligonucleotides, 1 x annealing buffer (100 nM Tris-HCl (pH 7.5), 1 M NaCl, 10 mM EDTA) and made up to 100 µl with dH_2O. The solution was held at 65 °C for 10 minutes allowed to cool slowly to room temperature. Adaptors are ligated onto the sonicated CHO DNA using T4 DNA ligase (Promega) with a 1: 3 molar ratio of genomic DNA: adaptor. 200 ng of genomic DNA, 20 ng of adaptor, 1 x ligase buffer and 1 unit of T4 DNA ligase are combined in a final volume of 10 µl and the reaction is incubated for eighteen hours at 15 °C.

Chromosomal DNA is amplified using one of the above mentioned methods and in the second amplification reaction the DNA is labelled with biotin 16-dUTP. The probe is precipitated as detailed above. The genomic DNA with the linker adaptors attached and the labelled probe are heated for 10 minutes at 75 °C to separate the double stranded DNA and they are both separately reannealed with Cot-1 DNA at 37 °C for 3 hours. The two samples are mixed together and allowed to reanneal at 37 °C for sixteen hours then cooled to ambient temperature.

Streptavidin coated paramagnetic microspheres are prepared by washing prior to adding the entire contents of the annealing reaction. The spheres and DNA are incubated for 10 minutes at ambient room temperature and gently mixed by inverting. The beads with attached DNA (due to streptavidin-biotin bonding) are captured using a magnetic stand and the supernatant is carefully removed without disturbing the pellet. The spheres are washed and finally the DNA is eluted and used as a template for two further PCR reactions. A primer of sequence 5'-CCT CTG AAG GTT CCA GAA TCG ATA G-3' (complementary to one of the linked adaptors) is used at a final concentration of 0.5 µM in a volume of 50 µl which also included 1 x PCR buffer, 2 mM $MgCl_2$, 0.05% W-1, 0.2 mM dNTP, 5 units of Taq and 20 µl of the eluted DNA. The cycles used for this PCR are:

1 cycle	94°C	5 mins
35 cycles	94°C	1 min
	60°C	1 min
	72°C	2 mins
1 cycle	72°C	8 mins.

A second reaction which uses these cycles in which the DNA is labelled with biotin 16-dUTP is carried out as described in the section above as is the *in situ* hybridisation reaction in which the probe is annealed to target metaphases.

9.5.6.2 Results of chromosome amplification using Linker Adaptor PCR

DOP-PCR was performed as described in the methods section on single chromosomes scraped off a microscope slide using the pipette tip method, and a secondary amplification was performed in which the product was labelled with biotin 16-dUTP. The method described immediately above was followed and a gel of the products of the first PCR reaction using a primer specific to the Linker Adaptor showed no smears on the gel for the positive control, the negative control or for the two samples which both contained a single scraped chromosome at the beginning of the process. However, a gel of the products from the secondary reaction using the specific primer (the fourth amplification in all) showed discrete bands for the positive control and the two whole chromosome probes but not for the negative control. This could indicate that fragments of genomic DNA with the linker adaptors attached of different size have been pulled out of the sample at the stage of biotin-streptavidin attachment and have been subsequently amplified.

Probe precipitation and FISH was performed and the slides showed that the positive control had indeed labelled all target metaphase well, the negative control had not labelled any of the target chromosomes which was a good result, however one of the whole chromosome probes had labelled all of the target chromosomes quite brightly,

and the other paint probe had labelled some chromosomes quite faintly, but not others, although it was unfortunately not uniform labelling of specific chromosomes for each metaphase. At this juncture another amplification method, which does not utilise degenerate oligonucleotide primers but makes use of a kit that contains random hexamer primers for general amplification of DNA, was attempted.

9.5.7 Genomiphi PCR

9.5.7.1 Method

After many unsuccessful attempts to create chromosomal probes from chromosomal fragments or whole single chromosomes using degenerate oligonucleotide primers (DOP-PCR) a further attempt was made in which a commercially available DNA amplification kit, named Genomiphi (Amersham Biosciences) was used. The manufacturers claim was that any DNA present in the reaction would be primed at multiple sites by random hexamers and the reaction would produce large quantities of DNA. The kit uses random hexamers which anneal to template DNA at multiple sites and non-specifically prime polymerisation catalysed by bacteriophage Phi29 DNA polymerase. Phi29 DNA polymerase initiates replication simultaneously at the multiple sites on denatured double stranded DNA. The reaction does not require thermal cycling and is performed overnight at 30 °C, the optimal temperature for the enzyme to replicate DNA. As new single stranded DNA is synthesised additional primers bind to the newly replicated and displaced strands and subsequently, large quantities of high molecular weight, double stranded DNA is produced.

1 µl of template DNA is added to 9 µl of sample buffer which contains the random hexamers. The sample is heated to 95°C for 3 minutes to denature the template DNA then cooled to 4 °C on ice. This mixture of denatured template and random hexamers is combined, on ice, with 9 µl of reaction buffer (which contains salts and deoxynucleotides, and is adjusted to a pH that is optimal for Phi29 DNA polymerase-catalysed synthesis) and 1 µl enzyme mix, and incubated at 30°C

overnight. After amplification Phi29 DNA polymerase is heat-inactivated by incubating for ten minutes at 65°C. The biotinylated probe is precipitated and *in situ* hybridisation is performed as described above.

9.5.7.2 Results of Genomiphi PCR

To create paint probes, 1 µl of sterile water with a few resuspended chromosomes scraped off a cover glass is used and no DNA is added to the negative control. Template DNA used for one positive control was lambda DNA which comes with the kit and another positive control uses genomic CHO DNA. Large smears can be seen when an aliquot of the products (even the negative control) is run in a 2% agarose gel, except in one of the samples which is the product of the amplification of a few chromosomes. A secondary labelling reaction with Spectrum Green-dUTP was performed using DOP primers and the low annealing temperature cycle described above, and the FISH probes were created. The positive control worked well and labelled all the target metaphase chromosomes brightly however, probe 1, 2 and the negative control all showed only 'speckling' on chromosomes and in the background. The secondary labelling reaction was repeated with biotin 16-dUTP using the Genomiphi kit rather than DOP-PCR however, the gel of the product showed a bright smear in the negative lane, as well as less bright smears in the lanes for the positive controls and the two probes. FISH of the positive control probe showed good labelling of all the target metaphases, the first probe showed labelling around the outside of all chromosomes, the second probe was also slightly speckled with probe but not quite as much and the negative control also appeared slightly labelled.

In summary, many attempts were made to generate either a whole chromosome paint probe or a narrow band paint probe using DOP-PCR (and Genomiphi PCR) of a single chromosome or chromosomal fragment as template DNA for the reaction. This proved to be unsuccessful resulting in either indiscriminate labelling of all chromosomes or no labelling at all, instead of labelling on a specific chromosome, or chromosomal region.

A completely different approach was then taken in which a whole cell paint probe from one species was used as a FISH probe for a related species. If this resulted in banding patterns on the chromosomes the probe could be useful for studies of chromatid rearrangements caused by irradiation induced breaks in the DNA.

9.5.8 Whole cell paint probe hybridised to metaphases of another cell line

A paint probe created by amplifying genomic DNA of one cell line was hybridised with target metaphases of another cell line. It was expected that this would result in banding patterns on the chromosomes due to conserved sequences of the genomes, and these large bands could be useful in the search for putative chromosomal inversions. Muntjac chromosomes were amplified and labelled in the method previously described and the resulting paint probe was hybridised with CHO metaphases which were fixed on slides. The resulting labelling was similar to that which was seen earlier when repetitive sequences were labelled on the same region of each metaphase no matter which chromosome had been amplified. A picture of such a CHO metaphase labelled with a paint probe generated from Muntjac DNA can be seen in figure 9.13. Again the same region of repetitive DNA can be seen to be labelled by this probe as can be seen in figure 9.10A.

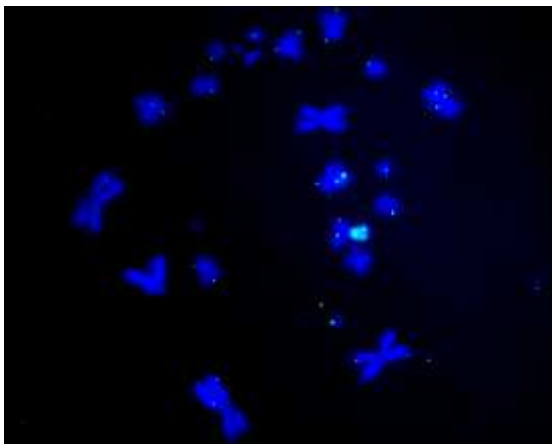

Figure 9.13: CHO metaphases labelled with a whole cell Muntjac paint probe.

CHO genomic DNA was used to create a chromosomal paint probe for FISH with target Muntjac metaphase chromosomes. The probe was created by the standard method described in the methods section and hybridised to Muntjac metaphases fixed onto slides. Two attempts were made at labelling the Muntjac metaphases with a CHO whole cell paint probe. Initially the probe labels the repetitive DNA region on the chromosome (figure 9.14A) as seen in figure 9.10B. However, when the experiment was repeated at a later stage the Muntjac chromosomes were labelled with the probe in small spots rather than large bands (9.14B) and it was difficult to determine if the speckling was uniform for every metaphase.

A 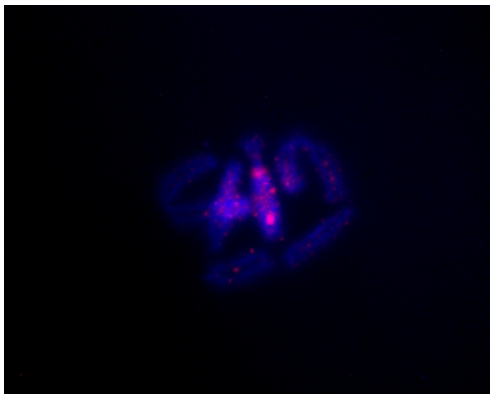 B 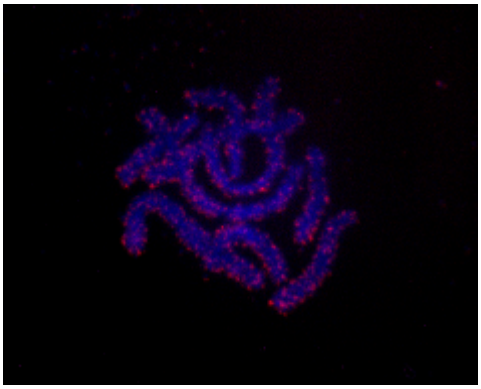

Figure 9.14: CHO whole cell paint probe hybridised to Muntjac chromosomes.

As the label was spotted across the chromosomes rather than bands across the chromosome, it was concluded that these probes would not have a use in the search for putative chromatid inversions associated with radiation induced chromatid breaks.

9.6 Attachment of streptavidin coated microspheres to chromosomes

Another set of experiments which involved the attachment of microspheres to whole chromosomes via biotin-streptavadin bonding in order to facilitate the manipulation of chromosomes in an optical trap are describe in the following section. Chromosomes scatter much of the focused laser light, whereas transparent spheres

will readily refract the trapping light and scatter it less hence the spheres will be trapped more strongly than chromosomes themselves.

9.6.1 Attaching microspheres to CHO chromosomes

Two general methods have been used to attach microspheres to chromosomes, both making use of the bonding between streptavidin and biotin. Streptavidin coated microspheres (either 1 μm or 5 μm in diameter) are used (from Bangs laboratories) and CHO genomic DNA is amplified and labelled with biotin 16-dUTP by DOP-PCR as described above. In one technique a probe-sphere conjugate is made prior to hybridising with metaphase chromosomes and the other technique consists of hybridising the probe to the chromosomes and then incubating the microspheres with the biotinylated chromosomes.

9.6.1.1 Hybridising a probe-sphere conjugate to chromosomes

100 μl of stock solution of streptavidin coated microspheres is washed twice by centrifugation (1200 rpm in a 20 cm diameter rotor for 10 minutes) in PBS and finally resuspended in 200 μl of PBS. 10 μl of these spheres in PBS are added to the biotinylated probe in hybridisation buffer (see above for how probe was made), and incubated for fifteen minutes at ambient temperature while gently mixing. The sphere-probe mixture is then washed three times in 100 μl wash solution by centrifugation (1200 rpm in a 20 cm diameter rotor for 10 minutes) and is finally resuspended in 100 μl of hybridisation buffer. The hybridisation buffer containing the probe-sphere conjugate is then added to a pellet of metaphase chromosomes, and the mixture is denatured by heating at 73°C for five minutes and then hybridised to the chromosomes by incubating for sixteen hours at 37 °C.

The pellet of metaphase CHO chromosomes is made by passing mitosis blocked cells in fixative through a 25g needle and syringe ten times to rupture the cell

membrane and release the metaphase chromosomes. The sample is then washed twice in PBS by centrifugation for 10 minutes at 1200 rpm in a 20 cm diameter rotor with all the supernatant being removed in the last step leaving a pellet of chromosomes.

After hybridisation with the probe-sphere conjugate, the chromosomes are washed to remove unbound spheres and probe three times in 100 µl fresh wash solution by centrifugation (1200 rpm in a 20 cm diameter rotor for 10 minutes each wash), and the chromosomes with spheres attached are finally resuspended in 80 µl PBS.

9.6.1.2 Attaching microspheres to biotinylated chromosomes

10 µl biotinylated probe in hybridisation buffer is added to a pellet of metaphase chromosomes and the mixture is denatured by heating to 73°C for five minute and hybridised by incubating at 37 °C for sixteen hours. Chromosomes are washed twice in 200 µl of high stringency buffer (50% formamide in 2 x SSC) by centrifugation each time at 1200 rpm in a 20 cm diameter rotor for 10 minutes, and then washed once more in 100 µl of wash solution by centrifuging at 1200rpm for 10 minutes in the same rotor. The sample is incubated for thirty minutes with 100 µl of blocking buffer (non fat dairy milk) and then centrifuged out of the blocking buffer (1200 rpm for 10 minutes). The supernatant is aspirated and 10 µl of streptavidin coated microspheres (which had been washed twice and resuspended in PBS as above) in 50 µl blocking buffer is added then incubated for thirty minutes at ambient temperature. Chromosomes were washed three times by centrifugation in 100 µl wash solution at 1200 rpm for 10 minutes to remove unbound beads and chromosomes were resuspended in 80 µl PBS.

9.6.2 Results of attaching microspheres to whole chromosomes

Both 1 μm and 5 μm diameter spheres were attached to chromosomes. When 5 μm spheres were added to previously biotinylated chromosomes, approximately 5 or 6 spheres would attach to the chromosomes, and when the probe-sphere conjugate was added to chromosomes between zero and two spheres would attach to each chromosome. Typical examples of these results can be seen in figure 9.15.

A 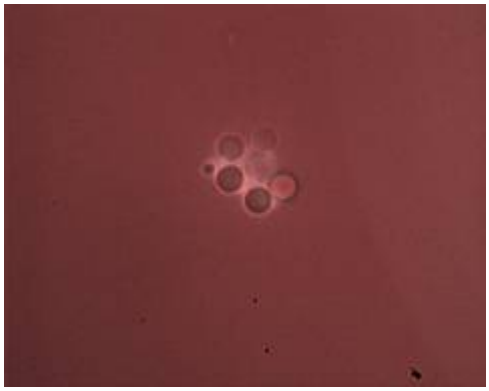 B 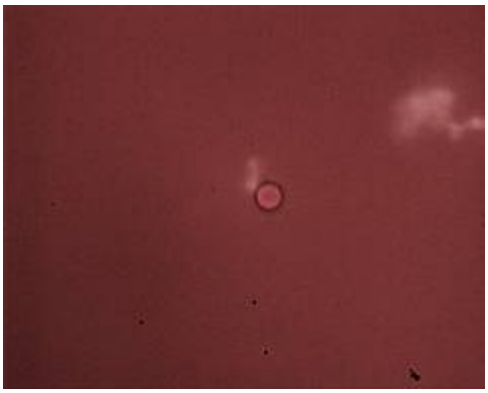

Figure 9.15: A. Five 5 μm diameter spheres attached to a DAPI stained chromosome by incubating streptavadin coated microspheres to biotinylated chromosomes, B. A single 5 μm diameter sphere attached to a chromosome by hybridising probe-sphere conjugates with chromosomes.

One micron diameter spheres were also attached to chromosome using the same two methods. If the spheres were added to biotinylated chromosomes approximately twenty spheres would attach to a chromosome, and if the probe-sphere conjugate method was used, between zero and four spheres would attach to each chromosome. Examples of the results of these experiments can be observed in figure 9.16.

A 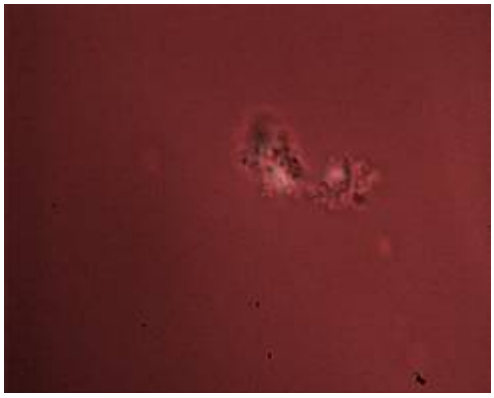 B 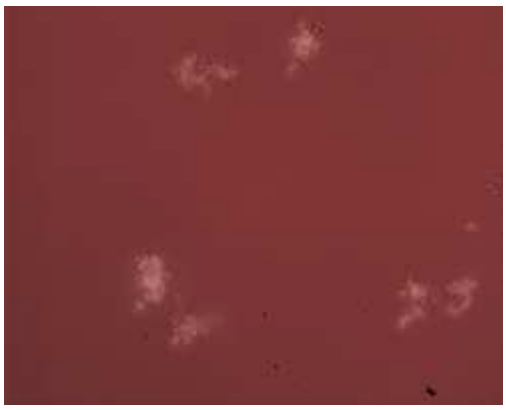

Figure 9.16: A. Many 1 μm spheres attached to chromosomes, B. Few 1 μm spheres attached to chromosomes, using the two methods described in the text.

Interestingly, if excess spheres were added to the biotinylated chromosomes, the surface of each chromosome becomes saturated with spheres, and this can be seen in figure 9.17.

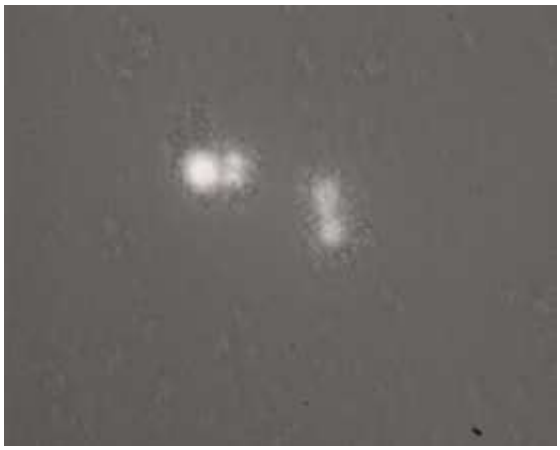

Figure 9.17: Many 1 μm streptavadin coated spheres attached to chromosomes after incubating them in excess with biotinylated chromosomes.

9.6.3 Optical micromanipulation of chromosomes with microspheres attached

These samples of chromosomes with beads attached can be tweezed in a Bessel beam, with the sphere attachments used as handles with which the focused laser light traps more strongly than the chromosome itself.

Bessel beams were introduced in chapter 2. They have an intensity cross section that does not change as they propagate and are termed 'non-diffracting' beams because the beam centre does not spread. The Bessel beam offers a narrow beam of light which is equivalent to an enhanced depth of focus for a light beam and this provides good two dimensional localisation when guiding particles through a sample cell compared to using a Gaussian beam. It is illustrated in figure 9.18 that guiding with a Gaussian beam provides good localisation either at the initial capture area (a) or at the final destination for the particle (b) where the diffracting Gaussian beam is focused, but the central maximum of a Bessel beam provides good localisation throughout the sample cell.

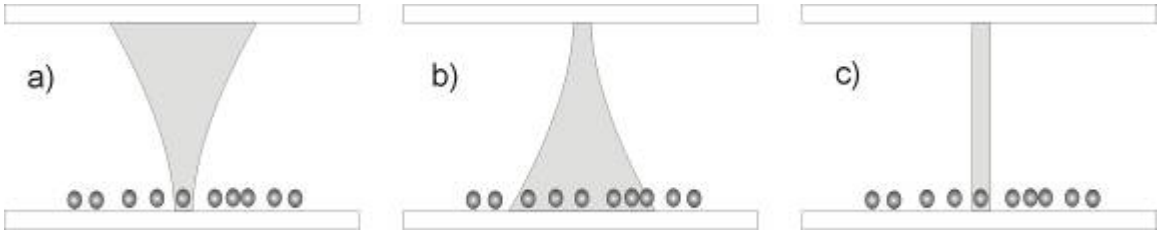

Figure 9.18: Comparison of Gaussian and Bessel beam guiding.

As discussed in chapter 2, passing a Gaussian beam through a conical shaped optical element called an axicon offers the most efficient way to generate an approximation to a Bessel beam.

Microscopic particles can be guided horizontally along such beams, and data of guiding various objects (a 3 μm diameter sphere, a 5 μm diameter sphere and a single CHO chromosome) can be seen in 9.19.

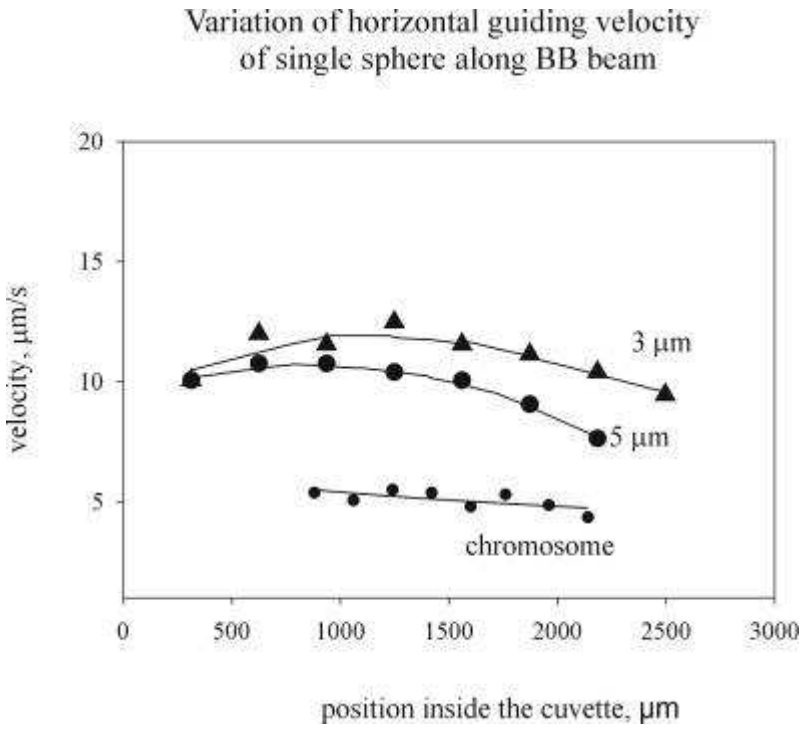

Figure 9.19: Guiding velocities of a 3 μm sphere, a 5 μm sphere and a chromosome in a Bessel beam.

It can be seen that larger objects are guided at slower velocities. The velocities of many CHO chromosomes with 1 μm spheres attached via the biotin-streptavadin bond were measured, and the distribution of velocities is shown in figure 9.20.

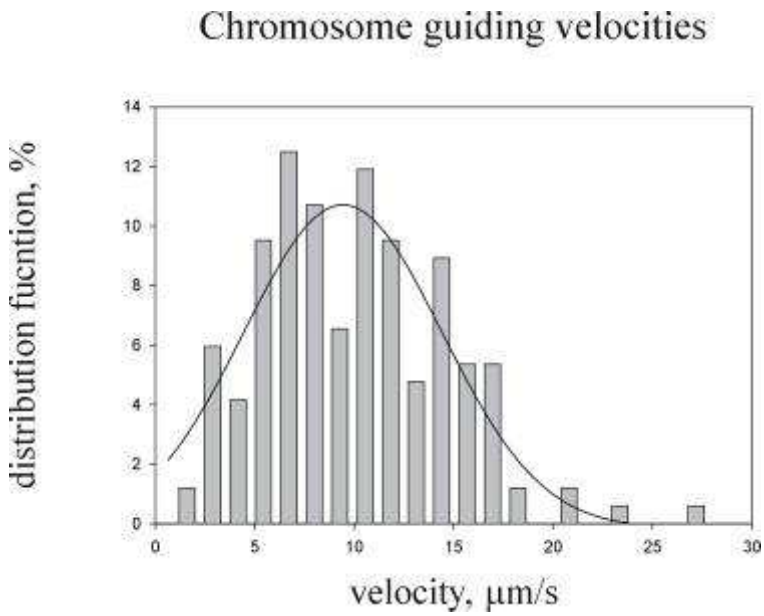

Figure 9.20: Chromosomal guiding velocities along a Bessel beam.

The lower velocities in this graph are attributed to the larger of the CHO chromosomes with smaller chromosomes and unattached spheres have higher velocities. This method of attachment of spheres to act as handles with which to ease manipulation of chromosomes also has huge implications in chromosome sorting, and may differentiate between chromosomes by mass, or by velocity measurements, differences in which are determined by the mass of the chromosome. Chromosomes can also be transported in a tilted washboard potential in a manner analogous to the unidirectional motion of a molecular motor along a polarised linear substrate (Tatarkova et al., 2003a, Tatarkova et al. *To be submitted* 2003b).

9.7 Discussion

Several methods have been used in the work described in this chapter in an attempt to create a fine chromosome FISH probe. Initially, laser microdissected, optically tweezed chromosomal fragments were used as a template with which to amplify using DOP-PCR, label and make into a probe. At a later stage, single whole, tweezed chromosomes were used as template material, and then whole chromosomes

or a few chromosomes scraped off a cover glass. DOP-PCR has been widely used to amplify FACS sorted chromosomes or many copies of a needle microdissected chromosome fragment. In our work, amplification of only single copies of a chromosome or fragment was attempted unlike multiple copies in other work. This is perhaps one of the reasons we were unsuccessful in creating a fine probe or even a single chromosome probe. In theory amplification of a single piece of template should work but it may be that the nature of the degenerate primers results in concatenation of the primers which compete with the chromosomal material and take over as the main template.

Whole cell paint probes have applications in the search for chromosome inversions, for instance a whole cell paint probe from one species may be hybridised with chromosomes of another species, resulting in a distinct banding pattern along the chromosomes, however when this was tried using a CHO probe on Muntjac chromosomes and vice versa the resulting pattern was spotted throughout the chromosomes. Perhaps if a species more similar was used the labelled area would be larger and appear as bands across the chromosome. Whole cell probe has also been used to biotinylate chromosomes, and attach streptavadin coated microspheres to the chromosomes via biotin-streptavadin bonding.

The use of optical tweezers to isolate single chromosomes and laser microdissection to create fragments has huge potential if the tweezed chromosomal material can remain sterile and free from other contaminating DNA, and if DOP-PCR can be optimised. In fact a paper has recently been published by another group which has used DOP-PCR to amplify an optically tweezed chromosome (Wang et al., 2003) and the work carried out for my PhD came close to achieving similar results.

References

Guan X, Trent JM, Meltzer PS: **Generation of band-specific painting probes from a single microdissected chromosome**. *Human Molecular Genetics* 1993; **2**:1117-1121.

Masabanda JS, Griffin DK: **Generation of chromosome paints: Approach for increasing specificity and intensity of signals**. *Biotechniques* 2003; **34**.

Meltzer PS, Guan X, Burgess A, Trent JM: **Rapid generation of region specific probes by chromosome microdissection and their application**. *Nature Genetics* 1992; **1**:24-28.

Tatarkova SA, Sibbett W, Dholakia K: **Brownian particle in an optical potential of the washboard type**. *Physical Review Letters* 2003; **91**:article no. 038101.

Tatarkova SA, Paterson L, Carruthers AE, Bryant PE, Dholakia K: **Chromosome transport in an optical washboard potential**. *To be submitted* 2003.

Telenius H, Pelmear AH, Tunnacliffe A, Carter NP, Behmel A, Ferguson-Smith MA, Nordenskjold M, Pfragner R, Ponder BAJ: **Cytogenetic analysis by chromosome painting using DOP-PCR amplified flow-sorted chromosomes**. *Genes, chromosomes and cancer* 1992a; **4**:257-263.

Telenius H, Carter NP, Bebb CE, Nordenskjold M, Ponder BAJ, Tunnacliffe A: **Degenerate oligonucleotide-primed PCR: General amplification of target DNA by a single degenerate primer**. *Genomics* 1992b; **13**:718-725.

Thalhammer S, Stark RW, Muller S, Wienberg J, Heckl WM: **The atomic force microscope as a new microdissecting tool for the generation of genetic probes**. *Journal of Structural Biology* 1997; **119**:232-237.

Wang H, Liu X, Li Y, Han B, Lou L, Wang K: **Isolation of a single rice chromosome by optical micromanipulation**. *Journal of Optics A: Pure and Applied Optics* 2003; **6**:89-93.

Zimmer R, Haberfeld A, Verrinder Gibbens AM: **Microisolation of the chicken Z chromosome and construction of microclone libraries**. *Genome* 1997; **40**:865-872.

10 Final Conclusions

10.1 Summary of Thesis

This thesis reports novel optical techniques used for the enhanced micromanipulation of particles in optical tweezers. A single beam, optical gradient force trap was discovered in 1986 by Arthur Ashkin and has since become an important tool in many aspects of biology, chemistry and physics. Novel laser beams have been developed in order to manipulate particles which could not previously be trapped in optical tweezers and in my work we have used annular shaped Laguerre-Gaussian beams which posses orbital angular momentum and 'non-diffracting' Bessel beams as well as the most commonly used TEM_{00} mode Gaussian beam.

After introducing optical tweezers, novel laser beams and biological uses of optical tweezers in chapter 2, experimental work performed using a Gaussian in both a standard and an inverted configuration is described in chapter 3. Silica spheres were aligned along the axis of beam propagation, using z-trapping in the standard configuration, with maximum stacks of three spheres. In the inverted set up radiation pressure is used to stack particles, resulting in stacks of sixteen spheres at most. The critical horizontal velocities of stacks are measured in order to determine their stability. Critical velocities in both the lateral and axial directions are also measured and described in chapter 4. In this case, silica spheres are trapped in a Laguerre-Gaussian beam and the velocities are used to calculate the *Q* value (or trap efficiency) of the optical tweezer. The use of a Laguerre-Gaussian beam is reported to improve axial trapping efficiency due to the lack of on-axis rays which do not contribute to the transverse trapping force and in a standard configuration are detrimental to axial trapping due radiation pressure caused by scattering.
We have also demonstrated a novel method to align rod-shaped particles in the sample plane as opposed to the beam propagation axis and translate them in two dimensions using an interference pattern between two Gaussian beams. The pattern

consists of a sequence of bright and dark fringes and arrays of rods can be created by trapping them parallel to the bright fringes. We also show the trapping and creation of arrays of low refractive index particles (bubbles), and arrays of high and low refractive index particles. The creation of an interference pattern for novel trapping experiments leads us to the following chapters where Laguerre-Gaussian beams have been used to generate interference patterns. Using these patterns we can create, translate and rotate optically trapped structures.

Spiral interference patterns were created by combining a Gaussian beam and a Laguerre-Gaussian beam. A particle could be trapped in each of the spiral arms of the pattern so that structures could be created and rotated by setting the pattern into rotation. This was achieved by changing the optical path length in one arm of the interferometer by simply tilting a glass plate in the beam path. The following chapter builds on the Gaussian Laguerre-Gaussian work but also introduces new abilities which were not previously possible. A Laguerre-Gaussian beam is interfered with its mirror image (of opposite helicity) to create a pattern of spots rather than spirals. In this work pattern and particle rotation is induced using the angular Doppler effect – a technique developed during the course of my PhD – which introduces a frequency shift between the two interfering beams by passing one arm of the interferometer through a rotating half-wave plate. This frequency shift between two beams ranges from less than one Hertz to hundreds of Hertz is applicable not only to this work but for moving any interference pattern in many fields, including optics and atomic physics.

The following two chapters describe the background and experimental work performed in order to create fluorescent chromosome probes. Chapter eight describes chromatid aberrations and proposed mechanisms as to how the come about and how we plan to study these breaks in the chromosome. The technique of degenerate oligonucleotide - polymerase chain reaction (DOP-PCR) is described and this is the major method used in chapter nine for the amplification of optically microdissected and manipulated chromosomal fragments. We also describe additional experimental work performed in the physics – biology interface such as the guiding of chromosomes in a Bessel beam, using spheres attached to the

chromosomes as handles, and also the fluorescence of stained chromosomes using a newly available blue diode laser.
In summary, novel laser beams have been used to improve the optical trapping of a range of particles from silica spheres, glass cylinders, bubbles and chromosomes and in particular we can build three dimensional structures using optical scaffolding (an interference pattern) and furthermore rotate these structures.

10.2 Future work

This work will lead to many exciting avenues of research but the areas which I believe hold most intrigue are the manipulation of chromosomes and other biological particles in optical tweezers, microfluidic studies using the aforementioned rotation techniques and the building of three dimensional structures using optical scaffolding.

The ability to isolate a single whole chromosome or a chromosomal fragment could mean the rapid and inexpensive generation of fluorescent *in situ* hybridisation (FISH) chromosome paint probes. At this present time there are only a few groups worldwide who report on generating their own probes for whole chromosomes or specific regions on the chromosome, and this is accomplished by using FACS or needle microdissection, with DOP-PCR performed on many copies of the chromosomal material. Commercially available whole chromosome paints are expensive (approximately £300 for 10 assays) and are limited to only human chromosomes. Recent work published by researchers in China has reported the amplification of a single optically tweezed rice chromosome, which will have very important implications for the generation of FISH probes. The future could see FISH probes of very narrow sections of any chromosome made to order, using optical scissors and tweezers in combination with molecular methods, within a day, for use in translocation studies or for the investigation of chromatid breaks at St Andrews University School of Biology.

Interference patterns such as those described in chapters 5, 6 and 7 will no doubt be used in future applications not only in optical tweezers but in the investigation of novel modes such as the Laguerre-Gaussian beams. Patterns similar to those we have created can be used for creating lock-and-key assemblies of particles for example, in the construction of a predetermined nucleus for the subsequent growth of self assembling, novel crystalline structures. The angular Doppler effect which we have used for the motion of our interference patterns may find many applications where there is a need for frequency shifts in the region of less than 1 Hertz to kHz, for example in atomic physics.

The rotation of interference patterns in a controlled and continuous fashion paves the way for rotational devices in lab-on-a –chip ensembles, such as valves and pumps to control the flow of volumes in the microlitre to millilitre range, and for torsional control, to viscosity measurements in a small volume of fluid, for example in different regions within biological cells.

To summarise, novel laser beams can be used to create tailored beams for use in optical tweezers for the enhancement of non-contact, all-optical micromanipulation. In the future such optical traps may be found incorporated into labs-on-a-chip. They could be used in biological assays for either controlling the flow of fluid by means of turning valves and cogs or by using the optical toolkit directly on biological specimens. Cutting, guiding, rotating or tweezing of samples is possible using the array of optical tools available in the kit.

Appendix A

DOP-PCR protocols

A.1 Introduction

The following is a review of previously used methods for DOP-PCR of chromosomal material. The methods of transferring the chromosomes to a collection PCR tube is described in chapter 9 and this section details the experimental methods used for DOP-PCR and FISH published by other groups.

A.2 Review of DOP-PCR methods

A.2.1 Telenius et al. 'Cytogenetic analysis by chromosome painting using DOP-PCR amplified flow-sorted chromosomes', 1992a.

Hundreds of flow-sorted chromosomes were used as a template for DOP-PCR. The degenerate primer 6-MW 5'CCG ACT CGA GNN NNN NAT GTG G-3' was used and the DOP-PCR was carried out in a 50 µl reaction volume containing 2 mM $MgCl_2$, 50 mM KCl, 10 mM Tris-HCl (pH 8.4), 0.1 mg/ml gelatine, 200 µ of each dNTP, 2 µM of primer and 1.25 units of Taq polymerase. Cycles for the primary reaction were 10 minutes at 94 °C, follower by five cycles of one minute at 94 °C, 1.5 minutes at 30 °C, a three minute transition from 30 °C to 72 °C, and three minutes extension at 72 °C. This was immediately followed by 35 cycles of one minute at 94 °C, one minute at 62 °C and three minutes at 72 °C with an addition of one second per cycle to the extension step. The final extension was increased to ten minutes. A secondary labelling reaction was carried out as above using 5 µl of the primary reaction product and the following amendments. The dTTP concentration was lowered to 80 µM and 200 µM of biotin -11-dUTP was added. Only 25 thermal

cycles were performed and the cycles using the lower annealing temperature were omitted. The resulting concentration was typically found to be 30 ng/ µl and 200 ng of probe was used for each hybridisation. The probe was ethanol precipitated with 3 µg of competitor DNA (Cot-1) and resuspended in 15 ml hybridisation buffer (50% formamide, 10% dextran sulphate, 2 x SSC, 0.5 mM Tris-HCl (pH 7.6), 0.1 mM EDTA, 0.1 µg/ µl sonicated salmon sperm DNA). Target metaphase chromosomes (normal, as opposed to the flow-sorted chromosomes with a translocation which acted as a template for DOP-PCR) that were fixed on microscope slides were denatured in 70% formamide, 2 x SSC at 65 °C for 2 minutes prior to the hybridisation. The probes were also denatured at 65 °C for ten minutes and preannealed with Cot-1 DNA at 37 °C for a minimum of 30 minutes in order to suppress repeated sequences before application to the target metaphases. Hybridisation was carried out in a humidified box for 16 hours at 42 °C. Following that the slides were stringently washed twice in 50% formamide, 2 x SSC at 42 °C for 5 minutes. The probe was visualised by the two layer avadin-fluorescein isothiocyanate (FITC) detection system which produces a fluorescent signal at the site of biotinylated probe hybridisation. Metaphases were counterstained with DAPI or propidium iodide and the translocations could be characterised.

A.2.2. Telenius et al. 'Degenerate oligonucleotide primed PCR: General amplification of target DNA by a single degenerate primer', 1992b.

Reactions were carried out 50 µl containing 10 mM Tris-HCl (pH 8.4), 2 mM $MgCl_2$, 50 mM KCl, 2 µM primer, 0.2 mM dNTPs and 1.25 U Taq DNA polymerase, and products were analysed by electrophoretic separation on a 1% agarose gel. Cycling conditions were 5 minutes at 95°C, followed by 5 low annealing temperature cycles of 1 minute at 94°C, 1.5 minutes at 30°C, a 3 minute transition from 30 to 72°C and 3 minutes of extension at 72°C. This was followed by 25-35 cycles of 1 minute at 94°C, 1 minute at 62°C and 3 minutes at 72°C with an additional 1 second per cycle to the extension step and a final extension of 10

minutes. If the five low annealing temperature cycles were omitted there was no amplification. Cosmid DNA was used as template DNA to compare the non-degenerate primer with 6-MW primer, and it was shown that more priming sites are available to a partially degenerate primer than to a unique primer. Two buffers were used. Buffer A was as described above, buffer B contained 25 mM N-tris(hydroxymethyl)methyl-3-aminopropanesulphonic acid (TAPS) (pH 9.3), 50 mM KCl, 1 mM dithiothreitol (DTT) and 0.05% polyoxyethylene ether (W1). Product yields up to 7 µg in 50µl were achieved under optimal conditions. 5 µl of primary product was labelled with biotin-11-dUTP in a secondary amplification reaction for 25 cycles excluding the low annealing temperature cycles. The final reaction mixture was as described above but with the addition of 300 µM biotin-11-dUTP. 150 ng of biotinylated probe was used for each in situ hybridisation. The probes were ethanol precipitated with 3 µg of Cot-1 competitor DNA resuspended in 15 µl hybridisation mixture containing 50% formamide, 10% dextran sulphate, 2 x SSC, 0.5 mM Tris-HCl (pH 7.6), 0.1 mM EDTA and 0.1µg/µl sonicated salmon sperm DNA. Probes were denatured at 65°C for 10 minutes then preannealed at 37°C for 1 hour. FISH was carried out as described in 'Cytogenetic Analysis by Chromosome Painting Using DOP-PCR Amplified Flow-Sorted Chromosomes'.

A.2.3. Meltzer et al. 'Rapid generation of region specific probes by chromosome microdissection and their application', 1992.

25-50 microdissected chromosomes are transferred into a collection drop containing 50 µg/ml proteinase K. The collection drop was incubated at 37°C for 1 hour and then at 90°C for 10 minutes to denature the proteinase K. The final reaction volume for PCR was 50 µl and the mixture contained 1.5 µM primer, 200 µM of each dNTP, 2 mM $MgCl_2$, 50 mM KCl, 10 mM Tris-HCl (pH 8.4), 0.1 mg/ml gelatine and 2.5 U Taq polymerase. The cycles were an initial denaturation at 93°C for 4 minutes followed by 8 cycles at 94°C for 1 minute, 30°C for 1 minute, and 72°C for 3 minutes, then 28 cycles at 94°C for 1 minute, 56°C for 1 minute and 72°C for 3

minutes with a final extension at 72°C for 10 minutes. 2 μl of the primary reaction product was labelled in a secondary reaction identical to the first except the dTTP concentration was reduced to 100 μM and 100 μM biotin-11-dUTP was added and 28 cycles were performed at 94°C for 1 minute, 56°C for 1 minute and 72°C for 3 minutes with a final extension at 72°C for 10 minutes. 10ng/μl of probe was used for FISH in a 20 μl hybridisation mixture also containing 50% formamide, 10% dextran sulphate, 1 x SSC and 3 μg Cot-1 DNA. This hybridisation mixture was added to metaphase slides which had been denatured by heating in 72°C 70% formamide, 2 x SSC for 2 minutes and dehydrated through an alcohol series and air dried. Slides were incubated at 37°C overnight in a moist chamber. After hybridisation slides were washed three times in 2 x SSC, 50% formamide at 42°C for 3 minutes, then rinsed for 3 minutes in 2 x SSC at room temperature. For probe detection the slides were washed in 0.1 M sodium phosphate, 0.1 % NP-40 (pH 8.0) at 45°C for 15 minutes and 2 minutes at room temperature then incubated at room temperature for 20 minutes in a bath containing 5 μg/ml fluorescien conjugated avadin in 0.1 % NP-40 with 5% nonfat dairy milk and 0.02% sodium azide. The slides were washed twice in 0.1 % NP-40 for 2 minutes each time and the signal was amplified by incubation with 5 μg/ml biotinylated anti-avadin in PN with 5% nonfat dairy milk and 0.02% sodium azide for 20 minutes at room temperature. The slides were washed twice in PN for 2 minutes each time and the incubation in fluorescein conjugated avadin was repeated. Metaphases are then mounted by adding 10 μl fluorescein antifade solution (10 mg/ml p-phenylamine dihydrochloride in 90% glycerol (pH 8.0)) containing 0.2 μg/ml propidium iodide.

A.2.4. Guan et al. 'Generation of band-specific painting probes from a single microdissected chromosome', 1993.

One to five copies of a targeted chromosome region were dissected and transferred into a collection buffer containing 40 mM Tris-HCl (pH 7.5), 20 mM $MgCl_2$, 50 mM NaCl, 200 μM of each dNTP, 1 U Topo I and 5 pM of primer and was incubated at 37 °C for 30 minutes, followed by an incubation at 96°C for 10 minutes. They

found that treating microdissections with or without Proteinase K had no apparent effect on probe quality. An initial eight cycles of PCR at 94°C for 1 minute, 30°C for 2 minutes and 37°C for 2 minutes were carried out by adding fresh 0.3 units of T7 DNA polymerase at each cycle. This preamplification was followed by a conventional PCR reaction in 50 µl of reaction volume containing 10 mM Tris-HCl (pH 8.4), 2 mM $MgCl_2$, 50 mM KCl, 0.1 mg/ml gelatine, 200 µM of each dNTP, and 2 units of Taq DNA polymerase. The initial denaturation was at 95°C for 3 minutes followed by 35 cycles at 94°C for 1 minute, 56°C for 1 minute ad 72°C for 2 minutes with a final extension of 5 minutes at 72°C. 2 µl of the primary PCR product was labeled with biotin-16-dUTP in a secondary PCR reaction identical to the first except for the addition of 20 µM biotin-16-dUTP, and only 12-16 cycles of 1 minute at 94°C, 1 minute at 56°C and 2 minutes at 72°C with a 5 minute final extension at 72°C. The PCR products were then purified using a Centricon 30 filter and used for FISH. For each hybridisation 100 ng of probe was added to 10 µl hybridisation mixture containing 55% formamide, 2 x SSC and 1 µg human Cot-1 DNA and denatured at 75°C for 5 minutes. The metaphase slides were denatured in 70% formamide, 2 x SSC at 70°C for 2 minutes and hybridised with probes at 37°C in a moist chamber overnight. Slides were washed three times in 50% formamide, 2 x SSC at 45°C for 3 minutes each. The probe was detected by two layers of FITC-conjugated avadin and amplified with one layer of anti-avadin antibody and slides were counter stained with 0.5 µg/ml propidium iodide in an antifade solution.

A.2.5. Zimmer et al. 'Microisolation of the chicken Z chromosome and construction of microclone libraries', 1997.

Fifteen to twenty copies of the same chromosome scraped off coverslips with glass microneedles are amplified to construct microclone libraries. The tips of the needles with the scraped chromosomes were dropped into 10 µl of a collection buffer consisting of 40 mM Tris-HCl (pH 7.5), 20 mM $MgCl_2$, 50 mM NaCl, plus 0.5 mg/ml proteinase K. 1 U of topoisomerase and 50 µg/µl of proteinase K were then

added to the buffer, the topoisomerase 1 to create single strand nicks in the DNA to relax the tightly coiled DNA allowing the primers access to the template DNA. The proteinase K digests any proteins present in the chromatin. A drop of mineral oil was added on top and then the solution was incubated at 37°C for 1 hour. The enzymes were inactivated by incubating at 95°C for 10 minutes. DOP-PCR was carried out in 50 μl containing 10 mM Tris-HCL (pH 8.3), 50 mM KCl, 1.5 mM $MgCl_2$, 0.01% gelatin, 200 μM of each dNTP, 2 μM of DOP primer and 50 U/ml Taq polymerase. The DNA was amplified for 8 cycles of 94°C for 1 minute, 30°C for 1 minute, and 72°C for 3 minutes and then for 30 cycles of 94°C for 1 minute, 56°C for 1 minute and then 72°C for 3 minutes. A 10 μl aliquot of the primary reaction product was subjected to a secondary DOP-PCR as before but without the 8 preliminary cycles, and this was not a labeling round as the aim was not to create fluorescent chromosome paints, but to clone the secondary PCR products.

A.2.6. Thalhammer et al. 'The atomic force microscope as a new microdissecting tool for the generation of genetic probes', 1997.

Chromosomes are microdissected using an atomic force microscope (AFM) needle and the whole cantilever is transferred to a collection buffer containing 25 mM N-tris(hydroxymethyl) methyl-3-aminopropanesulphonic acid (TAPS) (pH 9.3), 50 mM KCl, 1 mM DTT, 2 mM $MgCl_2$, 0.05% W1 detergent. Topoisomerase 1 was added to a final concentration of 2 U and incubated for 30 minutes at 37°C. Inactivation of the topoisomerase 1 was performed by incubating at 95°C for 10 minutes.

The DNA was amplified in a 25 μl final reaction volume containing 25 mM TAPS (pH 9.3), 50 mM KCl, 1 mM DTT, 2 mM $MgCl_2$, 0.05% W1 detergent, 200 μM of each dNTP, 4 μM of DOP primer and 5 U of Taq polymerase. The primary cycling conditions consisted of an initial denaturation for 8 minutes at 94°C followed by eight low annealing temperature cycles each of 94°C for 1 minute, 30°C for 1.5 minutes, a ramp to 72°C over 3 minutes then 72°C for 3 minutes. These cycles were followed immediately by 25 cycles each of 94°C for 1 minute, 62°C for 1 minute

and 72°C for 1.5 minutes with a time increment of 10 seconds. In the final cycle the last step was extended to 8 minutes. 2 pg of the primary reaction product was labeled for FISH in a secondary DOP-PCR reaction. The dTTP was reduced to 100 μM and biotin-16-dUTP was added to a concentration of 100 μM. The cycling conditions were 5 minutes at 94°C followed by 30 cycles of 94°C for 1 minute, 62°C for 1 minute and 72°C for 1.5 minutes. In the final cycle the last step was extended to 8 minutes. An aliquot of this secondary PCR product was taken to make the FISH probe and was co precipitated with the same amount of cot-1 DNA (5 μl of probe, 5 μg cot-1 DNA), salmon sperm DNA, 3M sodium acetate, and 2.5 volumes of EtOH. The DNA was precipitated overnight at -20°C and the pellet was resuspended in 15 ml hybridisation buffer consisting of 50% deionised formamide, 10% dextran sulphate,0.5 M NaH_2PO_4, 0.5 M Na_2HPO_4, 2 x SSC and ddH_2O. The probes were denatured at 68°C for 7 minutes with 30 minutes preannealing at 37°C. The target metaphase spreads were denatured in a hybridisation solution containing 2 x SSC and 70 % formamide for 1 minute at 68°C. The probe was added to the target metaphases and they were hybridised together in a humidified box overnight at 37°C. The slides were washed twice in 2 x SSC, 50% formamide at 45°C, and twice in 2 x SSC at 45°C. Slides were washed in 4 x SSC/Tween solution at room temperature and incubated with 3% bovine serum albumin (BSA) dissolved in 4 x SSC/Tween for 30 minutes at 37°C to avoid non-specific binding of the antibody. The biotinylated probes were detected using avadin coupled with fluorocein isothiocyanate (FITC). 100 μl of avadin-FITC diluted 1:200 in 4 x SSC/Tween/3% BSA was dropped on the slides and incubated for 45 minutes at 37°C. Slides were washed three times in 4 x SSC/Tween at 42°C for 5 minutes each wash and then counterstained with DAPI.

A.2.7. Masabada et al. ‘Generation of chromosome paints: Approach for increasing specificity and intensity of signals’, 2003.

A method for enhancing the specificity and signal of FISH probes is to perform the primary DOP-PCR and a secondary labeling DOP-PCR as normal (labeling with

biotin 16-dUTP). This biotinylated product was then co-hybridised with fragmented (200-800 bp) genomic hamster DNA which had a linker arm ligated to it using T4 DNA ligase. The sequence of the linker arm used here was

5'-CCTCTGAAGGTTCCAGAATCGATAGGTCGACCG-3'
3'-TTTGGAGACTTCCAAGGTCTTAGCTATCCAGCTGGC-5'.

Both the biotinylated PCR product (100 ng) and the genomic fragments with attached linker arms (1 μg) were pre annealed with hamster cot-1 DNA. Double stranded DNA was separated at 75°C for 10 minutes and then re-annealed at 37°C for 3 hours, following that both the DOP-PCR product and the linkered genomic DNA were combined and allowed to re-anneal overnight. The biotinylated DNA was captured by streptavadin coated paramagnetic beads and the annealed Genomic DNA was amplified by using a specific primer complementary to the attached liker arm
(5'-CCTCTGAAGGTTCCAGAATCGATAG-3'). The products were checked using an agarose gel, and a further PCR incorporating biotin 16-dUPT was performed using 2 μl of product.

A.2.8. Schermelleh et al. 'Laser microdissection and laser pressure catapulting for the generation of chromosome specific paint probes', 1999.

Laser microdissected chromosomes were amplified in 25 μl containing 60 mM Tris-HCl (pH 8.5), 15 mM $(NH_4)_2SO_4$, 3.5 mM $MgCl_2$, 0.05% W1 detergent, 200 μM each dNTP, 1.5 μM 6MW primer and 1.5 U Taq. Cycles were an initial denaturation at 96°C for 3 minutes and 8 low stringency cycles of 96°C for 1 minute, 30°C for 1 minute, a three minute transition from 30 to 72°C and 72°C for 2 minutes, followed by 35 high-stringency cycles of 94°C for 1 minute, 56°C for 1 minute, 72°C for 2 minutes and a final extension of 5 minutes at 72°C. 2 μl of the primary reaction product were labeled with digoxigenin or biotin in a secondary PCR in a 50 μl volume containing 10 mM Tris-HCl (pH 8.3), 2 mM $MgCl_2$, 50 mM KCl, 200 μM each dNTP, except dTTP which was at a concentration of 160 μM, 40 μM

Digoxigenin-11-dUTP or biotin-16-dUTP, 1.5 μM 6MW primer and 2 U Taq. Cycles were initial denaturation at 94°C for 3 minutes, 20 cycles of 94°C for 1 minute, 56°C for 1 minute, 72°C for 30 seconds and a final extension at 72°C for 3 minutes. Probe size was measured on a 1% agarose gel and was found to range from 300-800 bp. 50 ng/μl of the labeled probe was hybridised with 1 μg/μl of Cot-1 onto metaphase chromosomes and resulted in the specific hybridisation over the entire length of the captured chromosome.

References

Guan X, Trent JM, Meltzer PS: **Generation of band-specific painting probes from a single microdissected chromosome.** *Human Molecular Genetics* 1993; **2**:1117-1121.

Masabanda JS, Griffin DK: **Generation of chromosome paints: Approach for increasing specificity and intensity of signals.** *Biotechniques* 2003; **34**.

Meltzer PS, Guan X, Burgess A, Trent JM: **Rapid generation of region specific probes by chromosome microdissection and their application.** *Nature Genetics* 1992; **1**:24-28.

Schermelleh L, Thalhammer S, Heckl W, Posl H, Cremer T, Schutze K, Cremer M: **Laser microdissection and laser pressure catapulting for the generation of chromosome specific paint probes.** *Biotechniques* 1999; **27**:362-367.

Telenius H, Pelmear AH, Tunnacliffe A, Carter NP, Behmel A, Ferguson-Smith MA, Nordenskjold M, Pfragner R, Ponder BAJ: **Cytogenetic analysis by chromosome painting using DOP-PCR amplified flow-sorted chromosomes.** *Genes, chromosomes and cancer* 1992a; **4**:257-263.

Telenius H, Carter NP, Bebb CE, Nordenskjold M, Ponder BAJ, Tunnacliffe A: **Degenerate oligonucleotide-primed PCR: General amplification of target DNA by a single degenerate primer.** *Genomics* 1992b; **13**:718-725.

Thalhammer S, Stark RW, Muller S, Wienberg J, Heckl WM: **The atomic force microscope as a new microdissecting tool for the generation of genetic probes.** *Journal of Structural Biology* 1997; **119**:232-237.

Zimmer R, Haberfeld A, Verrinder Gibbens AM: **Microisolation of the chicken Z chromosome and construction of microclone libraries.** *Genome* 1997; **40**:865-872.

Appendix B

Materials

Product	Supplier

B.1. Reagents

B.1.1. Antibiotics

Zeocin	Invitrogen
Hygromycin	Invitrogen

B.1.2. Chemicals

10 x Phosphate Buffered Saline (PBS)	Gibco
Acetic Acid	BDH AnalR
Bovine Serum Albumin	Sigma
Colcemid	Invitrogen
Dithiothreitol (DDT)	Sigma
Dextran Sulphate	Sigma
Diff Quik	Sigma
EDTA (Ethylenediamine Tetraacetic Acid)	Sigma
Ethanol	BDH AnalR
Ethidium Bromide	Sigma
Formamide	BDH AnalR
Hydrochloric Acid (HCl)	BDH AnalR
Isopropanol	BDH AnalR
Isoton	Coulter electronics
Magnesium chloride ($MgCl_2$) (25 mM)	Promega

Methanol	BDH AnalR
Nonident-P40	Sigma
Potassium Chloride (KCl)	BDH AnalR
Sigmacote	Sigma
Sodium Acetate	BDH AnalR
Sodium Chloride (NaCl)	BDH AnalR
Sodium Dodecyl Sulphate (SDS)	BDH AnalR
TAPS) buffer (pH 9.3)	Sigma
(N-tris(hydroxymethyl) methyl-3-amiopropanesulfonic acid	
Tris ((hydroxymethyl)methylamine)	BDH AnalR
Tween 20	Sigma

B.1.3. Enzymes

Proteinase K	Sigma
Readymix Taq (0.06U/µl)	Sigma
RNase	Sigma
S1 nuclease (100U/µl)	Fermentas
T4 DNA Ligase (100U/µl)	Promega
Taq polymerase (in storage buffer B) (100U/µl)	Promega
Topoisomerase I (5-15U/µl)	Invitrogen
Trypsin	Difco

B.1.4. Other PCR/ ligation/ hybridisation reagents

10 x PCR buffer	Promega
1 kb DNA ladder	Promega
Avadin-Cy3	Vysis
Biotin 16 dUTP (1 mM)	Roche
DAPI counterstain	Vysis

DOP primers (84 nmol)	Sigma-Genosyis
dNTPs (10 mM)	Promega
HindIII/lambda DNA ladder	Promega
Human Cot-1 DNA	Vysis
Lambda DNA/ HindIII ladder	Promega
Ligase buffer	Promega
Linker adaptors (50 nmol)	Invitrogen
$MgCl_2$ (25 mM)	Promega
Mouse Cot-1 DNA	Invitrogen
Primer for adaptors (50 nmol)	Invitrogen
S1 nuclease buffer	Fermentas
Spectrum Green dUTP (1 mM)	Vysis
Spectrum Orange dUTP (1 mM)	Vysis
Streptavidin coated microspheres	Bangs
Streptavidin Magnasphere Paramagnetic Particles	Promega
W-1	Life Technologies/Gibco

B.1.5. Kits

Genomiphi DNA Amplification kit	Amersham
Wizard Genomic DNA purification kit	Promega

B.2. Equipment

B.2.1. Centrifugation

Centrifuge (Function line)	Heraeus
Microfuge (microcentaus/ force 7)	MSE/Labnet

B.2.2. Electrophoresis

Gel rig	made in house
Electrophoresis power supply (SL-3654)	Scotlab

B.2.3. Glassware

Slides	BDH
Coverslips	BDH

B.2.4. Microscopy

Fluorescence microscope (Axioskope)	Zeiss
Olympus Microscope	Olympus
Software	Smart Capture VP

B.2.5. Plastic ware

Culture flasks (T75cm2)	Nunclon
Roller bottles (850 ml)	Griener
Centrifuge tubes (50 ml, 15 ml)	TTP
Microfuge tubes (1.5 ml, 0.6 ml, 0.2 ml)	Axygen Scientific
Petri dishes (30 mm)	Nunclon

B.2.6. Others

Gene Quant	Pharmacia
Slide warmer (HYBrite)	Vysis
Incubator for cell culture	Heraeus Instruments
Magnetic Separation Stand	Promega
Particle Counter	Coulter Electronics
Pipette tips (10 µl, 20 µl)	Thistle laboratories
Roller bottle shaker	made in house

Slide shaker	Scotlab
Thermal cycler (Techgene/GeneE)	Techne
Water bath	Grant

B.3. Formulation of frequently used solutions

B.3.1. Solutions for chromosome preparation

Fixative

1: 3, Acetic acid: Methanol

Hypotonic solution (HYP)

0.075 M KCl

Trypsin

25% trypsin

0.02% PBS/EDTA

B.3.2. Collection buffers for PCR

TAPS collection buffer

TAPS (N-tris (hydroxymethyl) methyl-3-amiopropanesulfonic acid) buffer (pH 9.3)

50 mM KCl

1 mM DDT

2 mM $MgCl_2$

0.05% W-1

Zimmer collection buffer

40 mM Tris-HCl (pH 7.5)

20 mM $MgCl_2$

50 mM NaCl

B.3.3. Solution for agarose gel

Tris-EDTA
1mM EDTA
10 mM Tris (pH 7.6)

2% agarose gel
2% agarose
Tris-EDTA

B.3.4. Solutions for FISH

Denaturation solution (pH 7.0-7.5)
70% formamide
2 x SSC

Hybridisation buffer
50% formamide
10% Dextran Sulphate
2 x SSC

B.3.5. Solutions for washing slides after FISH

Wash solution
4 x SSC
0.05% Tween 20

High stringency washing buffer (HSB)
50% formamide in 2 x SSC

73 °C wash solution

0.4 x SSC

0.3% Nonident P-40

Room temperature wash solution

2 x SSC

0.1% Nonident P-40

TNT Washing Buffer

0.1 M Tris-HCl

0.15 M NaCl

0.05% Tween 20

B.3.6. Blocking buffers used prior to labelling with avadin-Cy3

BSA blocking buffer

4 x SSC

0.05% Tween 20

3% bovine serum albumin (BSA)

Non fat dairy milk (NFDM) blocking buffer

TNB blocking buffer

0.1M Tris HCl (pH 7.5)

0.15 M NaCl

0.5% blocking reagent (i.e. BSA)

Appendix C

Publications and publicity

C.1. Publications

C.1.1. Publications (Refereed)

Tatarkova SA, Paterson L, Carruthers AE, Bryant PE, Dholakia K: **Chromosome transport in an optical washboard potential**. *To be submitted* 2003.

Lake TK, Carruthers AE, Paterson L, Taylor M, Gunn-Moore F, Allen JW, Sibbett W, Dholakia K: **An optical trapping apparatus incorporating violet diode laser and extended cavity surface emitting laser systems**. *To be submitted* 2003.

L. Paterson L, M. P. MacDonald MP, J. Arlt J, W. Dultz W, H. Schmitzer H, W. Sibbett W and K. Dholakia K: **Simultaneous rotation of multiple optically trapped particles.** *Journal of Modern Optics* 2003; **50**:1591-1599.

Arlt J, MacDonald M, Paterson L, Sibbett W, Dholakia K, Volke-Sepulveda K: **Moving interference patterns created using the angular Doppler-effect**. *Optics Express* 2002; **10**:844-852.

MacDonald MP, Paterson L, Volke-Sepulveda K, Arlt J, Sibbett W, Dholakia K: ***Creation and manipulation of three-dimensional optically trapped structures****. Science 2002;* ***296****:1101-1103.*

MacDonald MP, Volke-Sepulveda K, Paterson L, Arlt J, Sibbett W, Dholakia K: **Revolving interference patterns for the rotation of optically trapped particles**. *Optics Communications* 2002; **201**:21-28.

MacDonald MP, Paterson L, Sibbett W, Dholakia K, Bryant PE: **Trapping and manipulation of low-index particles in a two- dimensional interferometric optical trap**. *Optics Letters* 2001; **26**:863-865.

Paterson L, MacDonald MP, Arlt J, Sibbett W, Bryant PE, Dholakia K: ***Controlled rotation of optically trapped microscopic particles****. Science 2001;* ***292****:912-914.*

C.1.2. Publications (Not refereed)

Paterson L, MacDonald MP, Volke-Sepulveda K, Arlt J, Sibbett W and Dholakia K: **Continuous motion of interference patterns using the angular Doppler-effect.** Proceedings of SPIE vol. 5121, pp. 98-102 (2003).

MacDonald MP**,** Paterson L, Armstrong G, Arlt J, Bryant P, Sibbett W and Dholakia K: **Laguerre-Gaussian laser modes for biophotonics and micromanipulation.** Proceedings of SPIE (2003).

C.2. Conference papers

C.2.1. Conference papers (Refereed)

MacDonald MP**,** Paterson L, Armstrong G, Arlt J, Bryant P, Sibbett W and Dholakia K: **Laguerre-Gaussian laser modes for biophotonics and micromanipulation**: Advanced Laser Technologies 02, Adelboden, Switzerland, September 2002.

Paterson L, MacDonald MP, Volke-Sepulveda K, Arlt J, Sibbett W and Dholakia K: **Continuous motion of interference patterns using the angular Doppler-effect.** LAT 2002, Moscow, June 2002.

Dholakia K, Paterson L, MacDonald MP, Arlt J, Sibbett W and Bryant PE: ***Optical Micro-rotator.*** *The Royal Society Summer Science Exhibition July 2002.*

MacDonald MP, Paterson L, Arlt J, Sibbett W and Dholakia K: **Controlled construction, rotation and translation of 3-dimensional, optically trapped structures.** Conference on Lasers and Electro-Optics 2002 May 19-24, Long Beach, California, paper CFC3.

MacDonald MP, Paterson L, Arlt J, Volke-Sepulveda K, Bryant PE, Sibbett W and Dholakia K: **Controlled rotation of optically trapped particles.** Quantum Electronics and Photonics 15 September 3-6 2001, Glasgow, Scotland.

Paterson L, MacDonald MP, Arlt J, Sibbett W and Dholakia K: **Optical trapping of low-index spheres in an interference pattern.** Quantum Electronics and Photonics 15 September 3-6 2001, Glasgow, Scotland.

Paterson L, MacDonald MP, Arlt J, Volke-Sepulveda K, Bryant PE, Sibbett W and Dholakia K: ***Controlled rotation of trapped particles in a spiral interference pattern.*** *Conference on Lasers and Electro-Optics 2001 May 6-11, Baltimore, Maryland, postdeadline paper CPD27-1.*

MacDonald MP, Paterson L, Sibbett W, Bryant P and Dholakia K: **Optical tweezing of rod-like particles and hollow spheres in an interference pattern.** Conference on Lasers and Electro-Optics 2001 May 6-11, Baltimore, Maryland, paper CWN4.

C.2.2. Conference papers (not refereed)

Paterson L, MacDonald MP, Arlt J, Sibbett W, Bryant PE, Dholakia K: **Controlled Rotation of Trapped Microscopic Particles in an Interference Pattern.** SET (Science, Engineering and Technology) for Britain, March 2001, House of Commons, London, UK.

Paterson L: **Novel optical manipulation techniques**. Postgraduate Conference, June 2001, School of Physics and Astronomy, St Andrews University, St Andrews, UK.

Armstrong GN, Dholakia K, Bryant PE, Sibbett W, Paterson L, Gray L, Garces-Chavez V, MacDonald MP: **Studies of chromatid inversions using novel optical micro-manipulation techniques**. Postgraduate Conference June 2002, School of Physics and Astronomy, St Andrews University, St Andrews, UK.

Paterson L: **Novel optical tweezers for bioscience**. LEOS (Lasers and Electro-Optics Society) meeting, June 2003, St Andrews University, St Andrews, UK.

C.3. Publicity

- Numerous local, national and international newspaper articles when 'Controlled rotation of optically trapped microscopic particles' was published in Science in May 2001.

- Exhibited the 'optical micro-rotator' at the Royal Society Summer 2002 Exhibition.

- Exhibited optical tweezers at the BBC Tomorrow's World Road show, summer 2002 (in London and Glasgow).

- BBC Radio 4 'Frontiers' programme on Optical Tweezers Technology reported on the chromosome cutting aspect of our work.